# Design of Smart Chemical Sensor Arrays: an Approach Based on Source Separation Methods

Leonardo Tomazeli Duarte

**INSTITUT POLYTECHNIQUE DE GRENOBLE**

N° attribué par la bibliothèque:

***THÈSE***

pour obtenir le grade de

**DOCTEUR de L'Institut Polytechnique de Grenoble**

**Spécialité: Signal, Image, Parole, Télécoms**

préparée au laboratoire

**Grenoble Images Signal Parole et Automatique (GIPSA-lab)**

dans le cadre de l'École Doctorale

**Électronique, Électrotechnique, Automatique et Traitement du Signal**

présentée et soutenue publiquement par

**Leonardo TOMAZELI DUARTE**

le 17 novembre 2009

# Design of Smart Chemical Sensor Arrays: an Approach Based on Source Separation Methods

**Directeur de thèse:**

Christian JUTTEN

**JURY**

M. Jacques FOULETIER, Président
M. Yannick DEVILLE, Rapporteur
M. Ali MOHAMMAD-DJAFARI, Rapporteur
M. Christian JUTTEN, Directeur de thèse
M. Saïd MOUSSAOUI, Examinateur
M. Pierre TEMPLE-BOYER, Examinateur

# Acknowledgments

First of all, I want to express my gratitude to my supervisor, Prof. Christian Jutten, for his support, availability and kindness. His passion for science and teaching, and his devotion to his students were really inspiring and helped me to grow as a researcher and as a person.

I wish to thank my thesis committee members: the president of the jury, Prof. Jacques Fouletier, and the reviewers, Prof. Yannick Deville and Prof. Ali Mohammad-Djafari, for their careful reading and suggestions. I am grateful to Prof. Pierre Temple-Boyer for their suggestions and for receiving me at the LAAS laboratory. Finally, I wish to thank Prof. Saïd Moussaoui for his careful reading, insightful ideas, and for his collaboration.

I am grateful to the National Council for Scientific and Technological Development (CNPq-Brazil) for funding my thesis. I also thank the Région Rhône-Alpes for providing me a research fellowship.

I wish to thank all the people I met at the Gipsa-lab for providing a stimulating and friendly environment. I am especially grateful to Cédric Gouy-Pailler, Ladan Amini, Reza Sameni and Sophie Achard. I am indebted to Bertrand Rivet for the discussions and collaboration.

It is difficult to overstate my gratitude to Romis Attux, Ricardo Suyama and João Marcos Travassos Romano for their support and for their guidance since my first steps as a researcher. I would also like to thank my colleagues from the DSPCom laboratory for their support.

I am grateful to all researchers with whom I discussed some technical points. In particular, I wish to thank Shahram Hosseini. I am grateful to Ahmed Benyahia and Jérôme Launay for their support during my stay at the LAAS laboratory.

I would like to thank all my friends, the long-standing ones and the ones I met at Grenoble, for their support. I am indebted to the voluntary members of the Alliance Française de Grenoble for their kindness and for helping me during my studies in French language.

I would like to thank my uncle Luiz, my aunt Sueli and my cousins Alexandre and Bruno for their love and encouragement. I also thank my parents-in-law, Agenor and Yara, my sister-in-law, Alexandra, and my relatives for their support.

I cannot find words to thank my parents, Aparecida and Sebastião, for their love and continual support throughout my studies. Without their help this thesis would not have been possible. I also thank my brother, Ronaldo, for his friendship, love and for being an example to me.

Lastly, but most importantly, I would like to thank my dear wife, Camila, for her love, unconditional support, encouragement, patience and for joining me in this adventure. To her, I dedicate this thesis.

# Résumé

L'une des principales difficultés dans l'utilisation de capteurs chimiques concerne le manque de sélectivité inhérent à ces dispositifs. La stratégie classique pour faire face à ce problème est fondée sur le développement de nouvelles membranes qui conduisent à des capteurs plus sélectifs. Toutefois, plus récemment, on a démontré que ce problème peut également être traité par une autre approche, dans laquelle l'acquisition de données est effectuée par un réseau de capteurs qui ne sont pas forcément sélectifs. Ainsi, dans une deuxième étape, les informations pertinentes sont récupérées à l'aide des outils de traitement de signal. L'un des bénéfices le plus remarquable dans cette démarche concerne la flexibilité du système de mesure : le même réseau de capteurs peut être utilisé pour réaliser différents types d'analyse.

Dans cette thèse, nous étudions l'utilisation de réseaux de capteurs dans le problème de l'analyse chimique quantitative. Cependant, contrairement à la grande majorité des travaux dans cette ligne, notre approche envisage des solutions non-supervisées, n'ayant pas besoin d'une étape d'étalonnage. Cette situation peut être formulée comme un problème de séparation aveugle de sources. Puisque les capteurs chimiques considérés dans cette recherche présentent des réponses non-linéaires, le processus de mélange sous-jacent au réseau de capteurs est non-linéaire, ce qui rend le problème difficile.

Les principales contributions de cette recherche sont liées justement au développement de méthodes de séparation des mélanges non-linéaires sur mesure pour les réseaux d'électrodes sélectives potentiométriques. Nous considérons des solutions fondées sur l'analyse en composantes indépendantes, mais également sur d'autres stratégies qui nous permettent de prendre en compte des connaissances *a priori* typiques dans l'application ciblée dans cette recherche, comme la positivité des activités chimiques.

# Abstract

Chemical sensors usually lack selectivity, that is, they may respond to interfering species other than the target one. The conventional strategy to cope with this problem is based on the development of new sensitive membranes that lead to more selective sensors. More recently, however, much attention has been given to an alternative approach, in which the data acquisition is conducted through an array of sensors that are not necessarily selective. Then, in a second stage, signal processing tools are employed to extract the relevant information from the acquired data. Among the benefits brought by this approach, is the flexibility inherent in a sensor array, which allows one to consider different analytes, or even different types of analysis, by using the same measuring system.

In this thesis, we study the problem of quantitative chemical analysis through sensor arrays. However, unlike the majority of the works in this line, we consider an unsupervised approach in which the adjustment of the signal processing method does not require a set of training (or calibration) points. This situation can be formulated as a Blind Source Separation (BSS) problem. The difficulty here lies in the fact that the chemical sensors considered in this research are clearly nonlinear devices, thus resulting in nonlinear mixing models.

The main contributions of this research are related to the development of nonlinear BSS methods tailor-made for arrays of ion-selective electrodes. We consider a paradigm based upon the Independent Component Analysis (ICA) but also upon other strategies that allow us to incorporate some information typical of the application considered in this research, like positivity of chemical activities.

# Contents

# List of Figures

# List of Tables

# List of abbreviations

| | |
|---|---|
| ANN | Artificial Neural Networks |
| BSS | Blind Source Separation |
| CLT | Central Limit Theorem |
| CT | Clifford-Touma |
| ECG | Electrocardiogram |
| EEG | Electroencephalogram |
| ICA | Independent Component Analysis |
| ISFET | Ion-Sensitive Field-Effect Transistor |
| LOD | Limit of Detection |
| LQ | Linear-Quadratic |
| LS | Least Squares |
| MAP | Maximum *a posteriori* |
| MCMC | Markov Chain Monte Carlo |
| MDCT | Modified Discrete Cosine Transform |
| MIMO | Multiple-Input Multiple-Output |
| MISO | Multiple-Input Single-Output |
| MLP | Multilayer Perceptron |
| MMSE | Minimum Mean Square Error |
| NE | Nicolsky-Eisenman |
| NMF | Non-negative Matrix Factorization |
| pdf | Probability density function |
| PNL | Post-Non Linear |
| SCA | Sparse Component Analysis |
| SISO | Single-Input Single-Output |
| SNR | Signal-to-Noise Ratio |
| SOM | Self-organizing Maps |
| SSA | Smart Sensor Array |
| SVM | Support Vector Machines |
| VOC | Volatile Organic Component |

# Introduction

One of the most relevant problems in chemical sensing is related to the difficulty in building sensors that respond exclusively to a given target chemical species. Considerable effort has been devoted to finding new materials that result in more selective sensors. This first strategy to deal with interference problems is very popular among chemists and has been providing impressive results. More recently, however, it has been shown that the lack of selectivity of chemical sensors can also be treated via an alternative concept, quite widespread among the signal processing community. Instead of relying on a single highly selective sensor, this alternative idea advocates the use of a set of sensors that are not necessarily selective. Then, the relevant information is found by applying signal processing methods. An interesting aspect of such a strategy, commonly named Smart Sensor Arrays (SSA), concerns its similarity to the principles that govern the sensory systems of living organisms like us; in many situations our imperfect sensory units are compensated by sophisticated mechanisms based on diversity.

The advances on multichannel data processing have been paving the way for efficient chemical SSAs. Valuable tools like artificial neural networks (ANN) and support vector machines (SVM) have been providing very good results in a multitude of applications involving quantitative and qualitative chemical analysis. One can even find commercial solutions making use of these methods [125]. However, despite all this success, there are still some limitations in the chemical SSAs developed to date. In particular, they are mostly based on supervised data processing methods, which means that, before their effective use, the user should perform a learning stage to adjust their parameters. The problem here is that such training procedure requires a set of calibration points, and, in some situations, the acquisition of such points is not simple. For instance, if the sensors suffer from drift, one must perform a calibration whenever the array is used.

Considering again the analogy between a chemical SSA and organic sensory systems, it is well-known that mammals, by exploiting the sensing diversity in a very efficient way, can deal with a given information even in the absence of reference signals. What if a similar scheme could be set for a chemical SSA? Certainly, a move toward total unsupervised solutions would be a tremendous breakthrough in chemical sensing. For example, this new approach could result in *plug-and-measure* chemical analyzers, in which no calibration procedures are needed.

The interesting perspectives in the use of unsupervised systems have been constantly evoked in the literature of chemical SSAs. However, interestingly enough, this is still a little studied topic. Although some progress has been achieved in unsupervised qualitative methods, the first

studies on unsupervised quantitative analysis are quite recent. Of course, this problem is far from being trivial and, at first glance, it seems unfeasible. Nonetheless, the signal processing community, among others, has been studying over the last two decades a problem, which is called Blind Source Separation (BSS), whose formulation suits perfectly the case of unsupervised quantitative analysis via chemical SSAs. Indeed, the goal in BSS is to search for a set of unknown signals (sources) by using only a set of signals (mixtures) that correspond to mixed versions of the sources. In the case of chemical arrays, the sources would represent the concentrations of the chemical species under analysis, whereas the mixtures would be the array outputs.

The first BSS methods addressed linear mixing models and were based on the concept of Independent Component Analysis (ICA). The assumption of a linear mixing model has led to very efficient algorithms. Moreover, the combination of ICA and linear models has been proved to be quite useful in many domains. Examples of problems in which BSS methods were applied encompass analysis of physiological signals such as brain and cardiac signals, audio separation, wireless communications, and image processing.

However, the main difficulty in obtaining a BSS-based chemical SSA is related to the nature of the resulting mixing process. As chemical sensors are (very often) nonlinear devices, the outputs of the sensor array correspond to a nonlinear mapping of the concentrations to be measured. Therefore, the application of the standard linear BSS methods in these cases is at best questionable. The challenging aspect here is that many problems (theoretical and practical ones), which are absent in linear BSS, appear when the more general problem of nonlinear BSS is considered. In particular, because of their high degree of flexibility, nonlinear models are much more susceptible to overfitting than linear ones. This characteristic points out that care must be taken in the extension of linear BSS methods to the nonlinear case. For example, the application of ICA in a nonlinear scenario does not necessarily give good estimations of the original sources. In view of this constant risk of overfitting in nonlinear models, theoretical advances advocate that, instead of searching for general solutions, nonlinear BSS should be rather studied on a case-by-case basis. Actually, it has been shown that, although the same ideas that allow source separation in linear models cannot be employed in a general nonlinear framework, they may still be valid in restricted classes of nonlinear models. These results are by no means negligible as they assure that the nonlinear BSS problem can be tackled, at least, in some cases.

In this thesis, our goal is to study several aspects related to the use of nonlinear BSS methods for performing unsupervised quantitative chemical analysis. Our analysis encompasses both theoretical and practical points. More specifically, **we aim at developing and analyzing nonlinear BSS methods tailored for chemical sensor arrays and at their validation through actual data**. Special attention is given to the problem of how incorporating prior information that are typical in chemical analysis. Concerning the type of chemical sensor considered in this work, our focus is on ion-selective electrodes (ISE), which have been intensively applied for measuring ionic concentration. Moreover, as a minor contribution, we also consider a BSS solution that can be used in a particular kind of gas sensor array.

## Organization of the manuscript

In Chapter 1, we provide a brief review on the two topics of interest in this thesis; in a first moment, we discuss some points related to chemical sensors, notably the interference phenomenon that is typical of these devices. Then, we discuss the source separation problem, with a special attention to its nonlinear instance.

In Chapter 2, we describe a set experiments conducted with ISE arrays. These experiments were conducted at the Laboratoire d'Analyse et d'Architecture des Systèmes (LAAS/CNRS, France) with the aim of providing actual data to validate some of the methods proposed in this thesis.

We begin, in Chapter 3, to present our contributions related to nonlinear source separation methods. In this context, we consider the case in which the ions under analysis have different valences. This situation results in a class of nonlinear models characterized by the presence of power terms. To deal with this problem, we develop a source separation method based on a recursive separating system whose parameters are adjusted through an ICA algorithm.

In Chapter 4, we consider the problem of how to take advantage of some information that may be available in our problem. In a first contribution, we show that, by considering that one of the sources is inactive during a certain time window, the class of mixing models considered in Chapter 3 can be simplified. In a second contribution, we deal with the class of post-nonlinear (PNL) models, which is important in context of ions with equal valences. In this situation, we show that, when the sources are bandlimited signals —a concept that is closely related to slowly-varying signals—then it becomes possible to set a two-stage algorithm in which the nonlinear and linear stages of the PNL mixing model can be estimated separately.

In Chapter 5, we continue our discussion on the use of prior information but now by relying on a Bayesian approach, which is more suitable for considering certain types of prior knowledge, like, for instance, the non-negativity of the sources. The algorithm developed in this chapter is based on MCMC sampling methods and can be applied to ISE arrays. We also introduce a Bayesian solution to perform BSS of linear-quadratic (LQ) mixtures, which are relevant in the context of gas sensors arrays.

In Chapter 6, we discuss some issues related to the practical application of BSS methods to actual problems.

The thesis is closed with a chapter that presents our conclusions and comments about some relevant problems that demand future investigation.

There are also other points that are left as appendixes. In particular, we call the reader's attention to Appendix C, in which we describe a novel linear BSS method that can extract smooth signals in a very efficient manner. Although not entirely in the scope of this thesis, this method can be applied, for instance, in conjunction with the PNL two-stage solution developed in Chapter 4.

# Chapter 1

# State of the art

## 1.1 Introduction

In this chapter, we present a brief introduction to the chemical sensors considered in this work. Special attention is devoted to ion-selective electrodes (ISE) and to the interference phenomenon that takes place in these sensors. We also discuss how this interference problem can be approached by means of smart sensor arrays (SSA). In a second part of this chapter, we introduce the blind source separation (BSS) problem. The standard solutions designed for operating in linear models are briefly reviewed. Then, some theoretical and practical aspects regarding the nonlinear case are discussed. Finally, this chapter is closed with a discussion on the use of BSS techniques in chemical sensor arrays.

## 1.2 Chemical sensors

According to the current IUPAC's[1] definition [89], a chemical sensor is *a device that transforms chemical information, ranging from the concentration of a specific sample component to total composition analysis, into an analytically useful signal.* The nature of this resulting signal can be used to classify a chemical sensor [66] into, at least, three distinct categories: optical, mass variation, and electrochemical devices. The sensors that are considered in this thesis belong to this last category, in which the transducer mechanism relates a chemical signal with an electrical signal. In contrast to optical and mass variation sensors, electrochemical sensors are typically simple devices, and their use does not involve sophisticated laboratory procedures. This feature is certainly the main reason why electrochemical sensors are so widespread in industrial applications [66], or, more generally, whenever a rapid analysis is required.

Electrochemical sensors can be divided into three groups: potentiometric, amperiometric and conductometric sensors. Again, the criterion for this classification is related to the transduction stage. A variation in the chemical species under analysis may induce a variation in the electrical potential (potentiometric sensors), in the current (amperiometric sensors), and in the resistance/conductance (conductometric sensors). This thesis focus on a well-studied potentiometric

[1] International Union of Pure and Applied Chemistry.

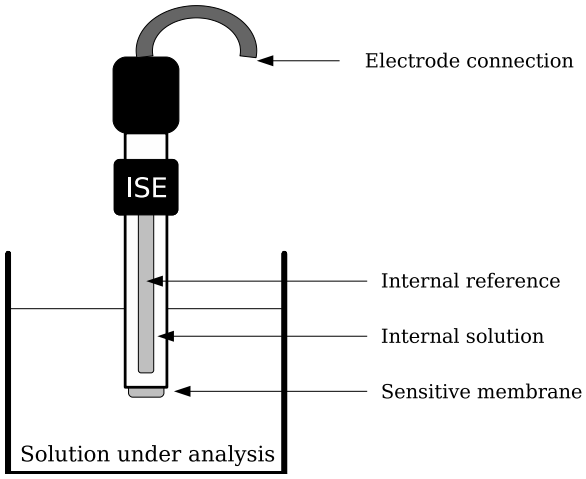


Figure 1.1: Simplified diagram of an ion-selective electrode.

sensor: the ion-selective electrode. As a secondary topic, we also consider a particular type of conductometric sensors used for measuring gas concentrations: the tin oxide electrode. In the following sections, a brief description of these two types of chemical sensors will be provided.

### 1.2.1 Ion-selective electrodes

Despite its long history —it dates back to the beginning of 20th century [6] —the ISE is still one of the most used chemical sensor. Among the reasons for this success are the simplicity of the ISE and the fact that such a device measures chemical species in their ionic forms, which is important in the majority of applications. The oldest ISE, the glass electrode, is still an ubiquitous device for measuring the pH[2] and is by far the most successful chemical sensor in commercial terms. Still, the existence of applications in which the analysis of other ions are needed motivated the development of new ISEs for ions such as ammonium and potassium.

An ISE is basically composed of an internal solution, an internal reference electrode and a sensitive membrane. A simplified diagram of the ISE is shown in Figure 1.1. The very core of the ISE transduction mechanism is the sensitive membrane. Briefly speaking, the generated electrical potential in this membrane is usually a result of the electrochemical equilibrium associated with the exchange of ions between the analyzed solution and the internal reference solution[3]. The nature of these exchanged ions depends on the chemical composition of the ISE membrane. For example, if pH estimation is desired, then the sensitive membrane should favor the hydrogen ion exchange, which, in this case, can be achieved through a membrane composed of a specific glass (from where the denomination glass electrode). There are also membranes constituted of different materials such as polymers and crystals.

The mathematical description of the transduction mechanism of potentiometric sensors like

[2]The pH is the negative logarithm of the hydrogen ion activity.

[3]Actually, the transducer mechanism is a very complicated subject and it is still object of study. The following references discuss this topic in more details [66, 19, 6].

the ISE is based on the Nernst equation [145], which, under the assumption that the concentration of the ISE internal solution is constant, states that the equilibrium membrane potential $E$ is given by

$$E = E_0 + \frac{RT}{zF} \log a, \tag{1.1}$$

where $a$ denotes the activity[4] of the target ion, whose valence is represented by $z$. The other parameters in this equation are physical constants; $R$ is the gas constant, $T$ the temperature in Kelvin, and $F$ the Faraday constant. Finally, $E_0$ is a reference potential, which is also constant.

In addition to indicating a linear relation between the membrane potential and the logarithm of the ionic activity, the Nernst equation predicts the sensitivity[5] of a potentiometric sensor. Indeed, for a room temperature and considering a monovalent ion, the term multiplying the logarithm ($RT/zF$) in Equation (1.1) takes approximately 59mV, i.e. the expected sensitivity is 59mV per decade. Electrodes with such a sensitivity are said to present a Nernstian response. Due to causes such as the electrode aging and the fabrication process, one can observe deviations from the Nernst sensitivity. If a larger sensitivity is observed, then one has a super-Nernstian response. Conversely, one has a sub-Nernstian response whenever the sensitivity is smaller.

*Applications*

After this brief description of the ISE, let us mention some applications of this device. Certainly, the most important ones are found in the domain of clinical analysis [6, 145, 126, 113]. Indeed, ISEs fit perfectly in this kind of application as their ability to provide prompt chemical analyzes allows the conduction of rapid diagnoses. In this domain, for instance, ISEs are used for estimating the activities of the blood electrolytes —for example sodium ($Na^+$), potassium ($K^+$), calcium ($Ca^{2+}$), magnesium ($Mg^{2+}$), lithium ($Li^+$) and the hydrogen ion (pH) —and also of the urine electrolytes $Na^+$ and $K^+$ [6].

Another important domain of application of ISEs is water quality control [142, 144]. Some of the ions of interest in this case are ammonium, potassium, calcium and magnesium. The sum

[4]The activity $a$ of an ion, whose valence is $z$, can be seen as measure of effective concentration and is given by

$$a = f \cdot c,$$

where $c$ is the ionic concentration. The dimensionless activity coefficient $f$ depends on the ionic strength $I$ and can be calculated according to the Debye-Hückel equation [145], which can be approximated by

$$-\log(f) = A \cdot z^2 \cdot \sqrt{I},$$

where $A$ is a constant [145, 76] that is approximately 0.5. Finally the ionic strength $I$ is a function of the concentration of all ions (represented by $c_1, c_2, \ldots, c_N$) within the solution and of their valences (represented by $z_1, z_2, \ldots, z_N$):

$$I = \sum_i c_i \cdot z_i^2.$$

For high diluted solutions, the ionic strength tends to zero, which gives an activity coefficient $f$ close to one. Therefore, in these cases, the activity becomes equal to the concentration. However, this is not true for high concentrated solutions because $f < 1$ in these cases.

[5]We refer the reader to [43] for a mathematical definition of the sensitivity of a sensor.

of these two last species gives the water total hardness, an important parameter that must be controlled in industrial applications as hard water may damage water pipes and other industrial structures.

There are many other applications in which ISEs play an important role. To cite some examples, these devices have been applied in beverage quality control [107], biodiesel analysis [38], environmental monitoring [6] (including soil analysis and detection of trace metals). This list is not exhaustive, and a brief review on the literature of the area indicates many other applications of ISEs.

### 1.2.2 Gas sensors

The tin oxide ($SnO_2$) sensor is another example of chemical device that has been drawing a lot of attention in both scientific community and industry. Since its origin, which dates back to the 1960s [5], the tin oxide sensor has been an important instrument for measuring gas concentration. Some advantages in using tin oxide sensors include: low cost, relative simplicity, and real-time operation [34]. These particular characteristics make the tin oxide sensors one of the most important gas sensors in commercial terms.

The transduction mechanism in a tin oxide sensor is a result of the interaction between the gas under analysis and the oxygen adsorbates, i.e. oxygen species which are accumulated on the sensor surface [111, 158]. This interaction takes place in the form of oxidation or reduction reactions, that is, the interaction between the gas under analysis and the adsorbed oxygen is characterized by an exchange of electrons. The key point here is that the number of free electrons in the sensor surface is associated with its electrical resistance (or equivalently with its conductance). Therefore, by measuring this resistance one can determine the concentration of the analyte, which makes the tin oxide sensor a typical example of a conductometric device.

A last remark on the transduction mechanism of tin oxide sensors is that an acceptable degree of sensitivity is achieved only when the sensor is submitted to high temperatures, usually greater than 200°C. This requirement is attained by incorporating a heater element into the sensor structure [5, 161]. Several works [155, 133] have shown that, by modulating the temperature of operation of a tin oxide electrode, its selectivity can be increased. Moreover, by considering such dynamical configuration, one can ease the problem related to the long time needed by a tin oxide sensor to achieve a steady state response.

*Applications*

Notable applications of tin oxide sensors are found in toxic gases monitoring systems [5, 121]. For example, they are used to detect the presence of carbon monoxide, an odorless gas well-known for its harmfulness to some living organisms, including human beings. Other examples of hazardous gases that can be detected through tin oxide sensors include [92, 121] ammonia, ozone and hydrogen sulfide. Tin oxide gas sensors are also useful in many industrial applications [121] as, for instance, for monitoring leakages of flammable gases, and in control systems of combustion engines.

The development of tin oxide sensors able to detect volatile organic components (VOC) [109, 34] has increased the range of applications of these devices over the last years. Indeed, they are now an important tool in food control and classification. Moreover, they can be used for detecting VOCs that are important in the diagnosis of certain diseases [141].

### 1.2.3 Selectivity of chemical sensors

Ideally, a sensor should be totally selective toward the target analyte, i.e. it should not respond to other chemical components present in the substance under analysis. In practice, however, it is very difficult to develop a total selective transducer mechanism. For example, the two types of chemical sensors described above suffer from lack of selectivity and, thus, their responses may also be influenced by interfering species. While in some situations this interference process can be negligible, there are other cases in which this problem seems to be more accentuated and, if no care is taken, the measurements obtained in these situations may become uncertain.

Much effort has been employed to understand why and how the interference process takes place in a chemical sensor. Not surprisingly, the "why" question requires a deep knowledge of the physiochemical aspects underlying the transducer mechanism. To make a long story short[6], the interference problem comes from a possible interaction between the sensitive material and chemical species presenting the same properties of the target species. For example, in the context of ISEs, interference may be caused by ions having radii close to that of the target ion [42].

The "how" question, which is the most important for the present study, is usually approached through empirical models. Certainly, the derivation of sound physiochemical models for the sensors contacting surface has been providing a more accurate description of the interference process [111, 20]. Yet, because of their simplicity, the first empirical models are still the most used both among the scientific community and practitioners.

In chemical systems, one can find several phenomena that are typically of nonlinear nature. For example, the description of process such as saturation, inhibition, and hysteresis, is strongly based on nonlinear models. This is also true for the interference phenomenon. Indeed, a common point that the most successful empirical and theoretical interference models share is that they are nonlinear and, therefore, a consistent mathematical description of the interference phenomenon in ISEs and in tin oxide sensors can only be achieved when nonlinear elements are considered therein.

#### 1.2.3.1 Interference in ISEs

The Nicolsky-Eisenman (NE) equation is the most widespread model describing the interference in ISEs. The NE equation, which dates back to 1937 [66], can be seen as an empirical extension of the Nernst equation. Assuming that $a_i$ and $a_j$ denote the activities of the target and interfering ions, respectively, and $z_i$ and $z_j$ their respective valences, then, according to the NE equation,

[6] This subject has been intensively studied in the fields of chemistry, physics and material sciences. For a more detailed description of the chemical sensors working principles, we refer the reader to [66, 76, 5].

the membrane potential is given by:

$$E = E_0 + d_i \log\left(a_i + \sum_{j,j\neq i} K_{i,j} a_j^{z_i/z_j}\right), \tag{1.2}$$

where $d_i = RT/z_iF$. $K_{i,j}$, which is called the selectivity coefficient, gives an idea about the degree of interference between the ions $i$ and $j$. This coefficient is expected to be positive as interference in ISEs is not an inhibitory process. There are mainly three chemical protocols [153] for calculating $K_{i,j}$. While the *fixed interference* and *separation solution* methods are explicitly based on the NE equation, a more analytical approach, the *matched potential* method, estimates $K_{i,j}$ by relying only on the membrane potentials obtained during an experiment where the concentration of the interfering ion is gradually increased. The advantage of this strategy is that the selectivity coefficients give good indications of the existing interference level even in situations for which the NE equation is not accurate.

According to the NE equation, the interference phenomenon breaks the linearity, predicted by the Nernst equation, between the membrane potential and the logarithm of the ionic activity. To illustrate this point, let us suppose a $Na^+$-ISE whose selective coefficients toward the ions $K^+$, $Li^+$, and $NH_4^+$, are given by 0.1, 0.01, and 0.001, respectively. In Fig. 1.2, we show the response of this $Na^+$-ISE in the presence of a solution containing $Na^+$ plus a single interfering ion of activity 0.1M. We also plot its response when no interfering ion is present, i.e. the ideal Nernstian response. Note that the interference phenomenon causes a decrease in the limit of detection[7] (LOD) of the electrode. For example, in the presence of $Li^+$, the ISE gives very bad measurements for the $Na^+$ activities below 0.001M.

Although widely used, the NE model presents several limitations. First, it neglects the fact that the selectivity coefficient may depend on the temperature and on the concentration of the ions within the solutions [42, 153]. This is even more problematic when this dependence is nonlinear, like in the electrodes studied in [42].

Another limitation of the NE model is that it predicts the same sensitivity (the slope $RT/z_iF$) for both target and interfering ions, which is not true in some situations. In [153], for instance, measurements provided by a $Ca^{2+}$-ISE gave a Nernstian slope of 29mV per decade for $Ca^{2+}$, but sub-Nernstian slopes of 24mV and 8mV per decade for the Strontium ($Sr^{2+}$) and Barium ($Ba^{2+}$) ions, respectively. However, from the NE equation standpoint, all these sensitivities would be incorrectly modeled as 29mV per decade.

Finally, as pointed out in several works (see [153, 120, 124, 20], for instance), if the ions have different valences, there may be ranges of concentration for which the NE model is unacceptable. This limitation has motivated the derivation of new interference models having a stronger theoretical foundation. For instance, by relying on the phase boundary potential model, [124] provided a new model that outperforms the NE formalism, especially when the interference is weak.

[7] The limit of detection (LOD) can be defined as the value below which the sensor is not able to detect changes in the concentration of the analyte.

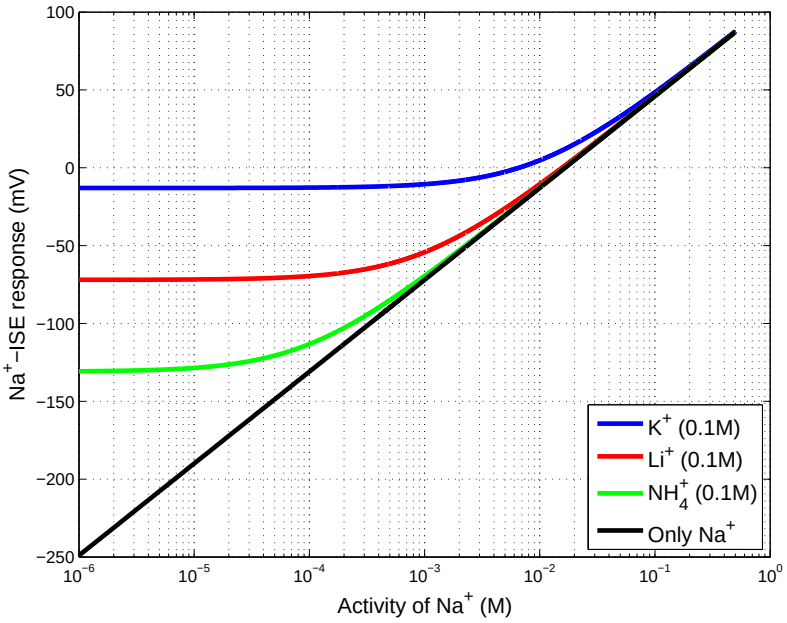


Figure 1.2: Responses of an $Na^+$-ISE in the presence of $Na^+$ plus a monovalent interfering ion.

#### 1.2.3.2 Interference in gas sensors

In tin oxide gas sensors, interference takes place in an additive form, as in ISEs, but can also result in an inhibitory process [110]. In other words, the effects of the target analyte upon the sensor may be attenuated in the presence of interfering gases. Therefore, one may end up with measurements indicating a lower concentration than the actual one. This characteristic is particularly incompatible with the main applications of tin oxide which, as discussed before, are related to the detection of toxic gases.

Several models have been proposed for a steady-state description of the interference phenomenon in tin oxide sensors. Among these contributions, the most popular is the work developed by Clifford and Touma, which proposed an empirical model based on the power law theory [162]. The Clifford-Touma (CT) equation suggests that if a tin oxide sensor is in contact with two gases of concentrations $a_1$ and $a_2$, then its electrical conductance $G$ is given by[8]:

$$G = G_0 + K_1 a_1^{r_1} + K_2 a_2^{r_2} + K_{12} a_1^{r_1} a_2^{r_2}, \tag{1.3}$$

where $G_0$, $K_1$, $K_2$, $K_{12}$, $r_1$ and $r_2$ are physical quantities depending on the temperature of operation. More specifically, $G_0$ is the sensor conductance measured in the absence of analytes. $K_1$ and $K_2$ correspond to the sensitivity toward the two gases under analysis, while $K_{12}$ is the selectivity coefficient related to these two gases. These three parameters can be either positive or negative. Finally, the value of the power terms $r_1$ and $r_2$ depends on the degree of interaction between each gas and the sensor. According to [111], these parameters usually lie in the interval $[0.3, 0.9]$.

[8]This equation can also be extended to the cases involving more than two gases [111].

### 1.2.4 Dealing with the interference: the sensor array approach

The interference problem has been a recurrent topic of study in the analytical chemistry community as it is certainly one of the most important shortcomings of chemical sensors such as the ones described in the last sections. A first natural strategy to overcome this problem is to tackle its origin: the sensitive mechanism. Indeed, a lot of effort has been devoted to the conception of new materials that result in more selective sensors [5]. However, this approach has the inconvenient of being somewhat specific, in the sense that the design of a new sensor has, as starting point, a particular ion as target. Therefore, if a different application, with a different target ion, is envisaged, then novel research efforts must be conducted for this new particular case. Moreover, the search for a more selective membrane may culminate on a rather expensive sensor, thus loosing the benefit of cost that is typical of devices like ISEs and tin-oxide sensors.

In the case of ISEs, a second strategy to circumvent the interference problem involves adding a solution that interacts with the interfering ions. For example, the added solution can be chosen so its reaction with the interfering ions results in a precipitate [145]. Although popular among chemists, this approach presents two major problems. First, it requires the conduction of laboratory procedures thus restricting its application in the field. Second, the specification of the added solution requires a precise knowledge about the composition of the solution under analysis.

Recently, it has been shown that the interference problem can be dealt with via an approach that, differently from the ones discussed in last paragraphs, does not work in a chemical basis. Rather, it is based on a conjunction very popular in the signal processing community. Instead of a highly selective sensor, this new idea suggests the use of an array of sensors that are not necessarily selective —actually, low-selective sensors are usually adopted in this context. As a consequence, the acquired data in this case are expected to be quite corrupted as they correspond now to a kind of mixtures of the concentrations of the chemical species. To compensate for that, the analysis of such data is conducted by signal processing tools that, by exploiting the diversity provided by the array, are able to extract the relevant information. This concept, which is called smart sensors array (SSA), became quite widespread in many applications notably because of the progress in digital processors technology and the achieved developments on multivariate data processing methods.

In Figure 1.3, the main elements of a SSA are depicted. The very core of this structure is the signal processing block. Actually, the term “smart” makes reference to the adaptive character of this block, which allows the SSA to operate in different situations through minor, and often automatic, changes. For example, a SSA that is set to identify a given element can be easily reconfigured to identify a different element. Besides this remarkable adaptability, there are other features that have been contributing to the success of SSAs. A first one is related to its robustness. In fact, even when one sensor within array fails, it may be still possible to proceed the analysis by using the information collected by the others electrodes [76]. A second interesting feature of SSAs regards the possibility of using different types of chemical sensors. This can be done by incorporating data fusion methods into the signal processing block.

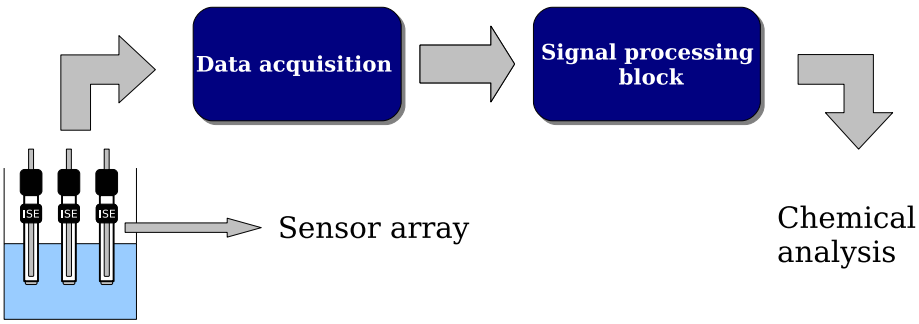


Figure 1.3: Diagram of a smart sensor array.

In the literature of chemical sensors, SSAs developed for analyzing gases and liquids are also called electronic nose [125] and electronic tongue [156], respectively. This comes from the analogy between these SSAs and the functioning of the olfactory and taste systems. Interestingly, one can also find an underlying interference phenomenon in these organic systems as their millions of sensor units respond differently to a same substance. Electronic noses and tongues are now major topics of research in chemical sensing. In particular, much attention has been given to the choice of the SSA signal processing block. In the following, we shall discuss some of the advances in this subject.

#### 1.2.4.1 Signal processing methods for smart chemical sensors arrays

The signal processing techniques used in SSAs can be classified based on two attributes. The first one concerns the nature of the envisaged task. In *qualitative analysis*, the signal processing should assign classes for the array outputs. For example, in some medical diagnosis applications, the outcome of the data processing block is a binary variable indicating whether a patient suffers (or not) from a given disease. In mathematical terms, this classification task can be seen as a mapping taking elements from an infinite set (in our case, the measurements taken by the sensors) to a finite set, in which the elements represent the classes.

In the case of *quantitative analysis*, the problematic can be put as follows: given the measurements taken by the sensor array, which were the values of concentration that resulted in these measurements? In this situation, the data processing technique must be able to somehow "invert" the effects introduced by the interference phenomenon into the transducer stage. In contrast to qualitative analysis, both the measurements taken by an array and the outputs of the signal processing block are real numbers in quantitative analysis, that is, we have now a mathematical mapping between two infinite sets.

A second attribute used in the classification of signal processing methods is related to the way that these methods are adjusted. In *supervised methods*, the parameters of the processing system are adjusted by considering a set of training (or calibration) data. Therefore, in a stage (training stage) that precedes the effective use of the array, one should provide to the signal

processing block an exhaustive collection of measurements taken by the array together with the desired output for that measurements (a given class in the qualitative case and the actual concentrations in quantitative analysis). Conversely, if no training stage is conducted and the parameters of the processing system are adjusted by only means of the array outputs, then the method is said to be *unsupervised* or *blind*.

Each combination of the two attributes described in the last two paragraph leads to different signal processing tasks. For instance, supervised qualitative chemical analysis is a clear example of (supervised) pattern classification, which, for instance, can be dealt with through particular machine learning techniques, such as multilayer perceptron (MLP) neural networks, support vector machines and hybrid neural-fuzzy systems. Another important data processing task in the context of supervised qualitative analysis is feature extraction, which is commonly employed as a preprocessing stage searching for hidden patterns in the acquired data. Besides, feature extraction is an important tool for reducing the dimension of the analyzed data. Very often, the incorporation of a feature extraction stage into the pattern recognition system makes it simpler and enhances the rate of correct classification.

In the case of supervised quantitative analysis through sensor arrays, one ends up with a multivariate regression problem[9]. This subject has been a major area of study in many different domains. In particular, the advent of techniques such as artificial neural networks has stimulated the research on regression in nonlinear models. Among the studied topics in this area, much attention has been given to the design of regressors that are flexible enough to capture nonlinear effects but, at the same time, are robust to overfitting [81].

Many electronic tongues and noses available to date work in a supervised fashion. However, one can find a growing number of works that consider chemical unsupervised qualitative analysis. In this particular situation, the classes are not known beforehand; they are found based on the degree of similarity between the elements of the data set. In other words, two elements belong to the same class if they are similar in some sense. For example, elements that present a small Euclidean distance can be considered similar. This task of grouping elements based on their similarities is also known as clustering analysis and can be approached through algorithms like k-means and self-organizing maps (SOM) [62].

The three signal processing tasks that we have discussed so far (supervised and unsupervised qualitative analysis, and supervised quantitative analysis) are now familiar to the community of chemical SSAs[10]. A non-exhaustive list of works that considered each of these tasks are presented in Table 1.1. In this same table, we also highlight the situation addressed in the present thesis: unsupervised quantitative chemical analysis. This particular case is a typical example of a blind source separation problem. In contrast to the other three situations shown in Table 1.1, the development of BSS-based smart chemical sensor arrays is still in its infancy and is faced with a big challenge: the more standard BSS techniques cannot be (directly) applied in systems such as electronic tongues and noses. The implications of this problem will be discussed in more details in the second half of this chapter, which will introduce the BSS problem.

[9] It can be also formulated as an inversion problem.

[10] The branch of chemistry that studies this type of problem is known as chemometrics.

Table 1.1: Examples of data processing methods used in chemical SSAs.

| | Qualitative analysis | Quantitative analysis |
|---|---|---|
| Supervised | **Supervised pattern classification** | **Multivariate regression** |
| | Discriminating function analysis [79] | Partial-least squares [107, 144] |
| | Neural networks [32] | Neural networks [22, 107, 10, 131] |
| | Support vector machines [132] | Support vector machines [77] |
| | Efficient feature extraction [70] | Evolutionary computation [80] |
| Unsupervised | **Clustering analysis** | **Blind source separation** |
| | K-means [67] | Independent component analysis |
| | Self-organizing map [156] | [23, 28] |
| | Principal component analysis [157] | |

## 1.3 Blind source separation

Blind Source Separation (BSS) aims at retrieving an ensemble of signals (sources) that underwent a mixing process. The term "blind" is employed because this separation process is conducted based on a minimum amount of information about the sources: one does not have access to training samples and to any statistical modeling for the sources. One of the most interesting aspects in BSS concerns the generality of its formulation; one can find BSS problems in a great diversity of domains: from astronomical imaging to biosignal processing (see the textbooks [94, 90] for some examples of BSS applications). Even the human brain is usually faced with problems close to BSS: we are able to understand our interlocutor(s) even in the presence of music and other people talking. This ability is known as cocktail-party effect [83] and has been constantly evoked in the literature to illustrate the goal of BSS.

Despite its simple formulation, BSS is a complicated problem and its resolution demanded a breakthrough in signal processing. Indeed, the seminal work of Ans, Hérault and Jutten [84] indicated that a formulation based on second-order statistics, which was the standard approach in statistical signal processing at that time, was not appropriate for a BSS context. This result, together with the advances in blind deconvolution [82], pointed out the importance of somehow incorporating higher-order statistics into the resolution of unsupervised signal processing problems. This has eventually led to the idea of independent component analysis [39], an important (and still most used) tool for tackling the BSS problem. In the sequel we will provide a mathematical formulation of the BSS problem and show how ICA and other more recent strategies can be used therein.

### 1.3.1 Mathematical formulation

Let the vectors $\mathbf{s}(t) = [s_1(t), s_2(t), \ldots, s_{n_s}(t)]^T$ and $\mathbf{x}(t) = [x_1(t), x_2(t), \ldots, x_{n_m}(t)]^T$ represent sets of $n_s$ sources and $n_m$ mixtures, respectively. The mixing process that relates these two vectors can be expressed through a mathematical mapping $\mathcal{F}(\cdot)$, i.e.

$$\mathbf{x}(t) = \mathcal{F}(\mathbf{s}(t)). \tag{1.4}$$

Then, the goal of BSS is to provide estimates of the sources $\mathbf{s}(t)$ based only on the observations $\mathbf{x}(t)$, that is, neither the mixing mapping $\mathcal{F}(\cdot)$ is known nor strong prior information about the sources are available. Note that, in the context of chemical sensor arrays, the sources represent the concentrations of the chemical species under analysis whereas the mixtures comprise the responses of each sensor within the array.

The characteristics of the mixing system $\mathcal{F}(\cdot)$ can be used for defining the following "BSS taxonomy": 1) *linear BSS* concerns the cases where $\mathcal{F}(\cdot)$ is a linear mapping. Otherwise, one ends up with a *nonlinear BSS* problem. 2) When $\mathcal{F}(\cdot)$ is a static (memoryless) system, it is said that the resulting model is an *instantaneous* one; otherwise one has a *dynamical* model. 3) Finally, the relation between the number of sources $n_s$ and the number of mixtures $n_m$ is also used to classify BSS problems: BSS is said to be *underdetermined*, *determined* and *overdetermined* when the number of mixtures is, respectively, smaller, equal and greater than the number of sources.

In Figure 1.4, the general scheme of BSS is illustrated. The retrieved sources[11], represented by the vector $\mathbf{y}(t) = [y_1(t), y_2(t), \ldots, y_{n_s}(t)]^T$, are given by

$$\mathbf{y}(t) = \mathcal{G}(\mathbf{x}(t)), \tag{1.5}$$

where $\mathcal{G}(\cdot)$ corresponds to the separating mapping. Of particular interest in BSS methods is how to define a separation criterion, that is, a strategy to adjust the parameters of $\mathcal{G}(\cdot)$. The difficulty here is that the lack of information renders the general BSS formulation a typical example of ill-posed problem[12], and, thus, every separation criterion defined in a such general scenario would be useless. Still, this problem can be overcome by considering further information about the sources. For example, let us imagine that the sources present a known mathematical property that is lost after mixing. Then, a straightforward idea for building a separation criterion would be to adjust $\mathcal{G}(\cdot)$ so that it gives estimations $\mathbf{y}(t)$ having the same mathematical property observed in $\mathbf{s}(t)$. The idea here is that the recovery of such original characteristic is enough to guarantee that $\mathcal{G}(\cdot)$ perfectly inverts $\mathcal{F}(\cdot)$.

Putting the idea presented in the last paragraph in a more rigorous formulation, a separation criterion can be defined through the following principle: given a property of $\mathbf{s}(t)$, the mapping $\mathcal{G}(\cdot)$ must be chosen so that such property be invariant under the transformation $\mathbf{y}(t) = \mathcal{G} \circ \mathcal{F}(\mathbf{s}(t))$ if, and only if, $\mathcal{G} \circ \mathcal{F}$ is the identity transformation or, at least, a mapping that does not mix the signals $\mathbf{s}(t)$. Evidently, the challenging point in this idea concerns the practical definition of the sources' characteristic acting as invariant. On the one hand, a very broad characteristic may lead to an ill-posed problem since it may act as invariant even when $\mathcal{G} \circ \mathcal{F}$ has a non-diagonal Jacobian, i.e. when it is still mixing the sources. However, on the other hand, if one makes use of a very detailed characteristic of the sources to define a separation criterion,

[11] In some applications, there is no need to retrieve all the sources, i.e. only the extraction of one or of a few sources is desired. The resulting problem in these cases is called Blind Source Extraction (BSE).

[12] Indeed, we can have an intuition on the ill-posedness of the more general BSS problem by looking at it as a representation problem, in which one searches for both $\mathbf{s}(t)$ and $\mathcal{F}(\cdot)$ (or equally $\mathcal{G}^{-1}(\cdot)$ in the determined case) that originated the observations $\mathbf{x}(t)$. Evidently, if no further information is incorporated into the described representation problem, then it may admit non-unique solutions. We shall return to this point later.

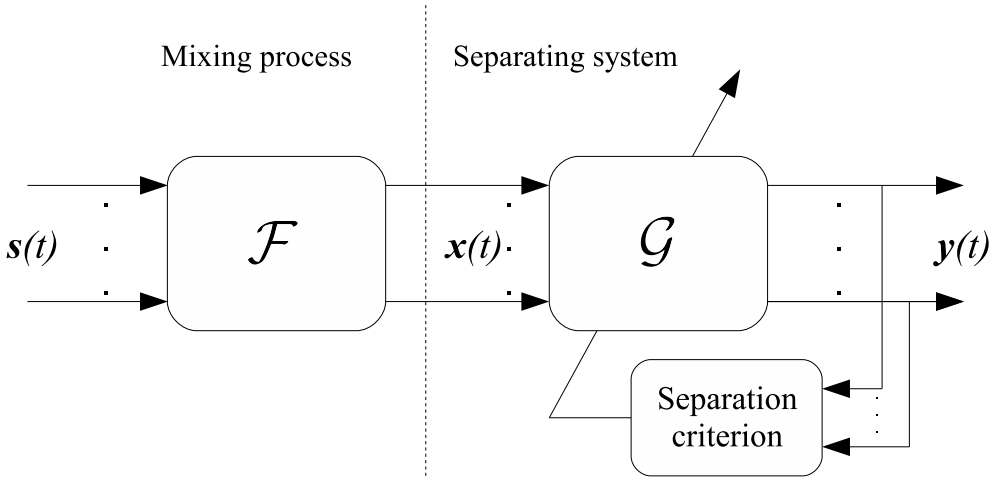


Figure 1.4: BSS basic setup: mixing and separating systems.

then one is definitely in a context that is not blind anymore. This discussion summarizes the main questions underlying the viability of BSS methods, namely: are there properties that can characterize whole classes of signals (especially the classes found in practical problems) and that, at the same time, are invariant only for non-mixing mappings? In the following, we discuss how this question is approached in the classical BSS formulation of linear instantaneous mixing models.

### 1.3.2 Linear instantaneous models

The most common BSS set-up considers mixing models[13] that are linear, instantaneous and determined (or possibly overdetermined). Besides its simplicity, this linear configuration provides acceptable descriptions in various practical problems. For example, in BSS of physiological signals such as the electrocardiogram (ECG) or the electroencephalogram (EEG), the corresponding mixing models can be well described by linear models [143, 90].

In linear BSS, the mixing process described in Equation (1.4) becomes[14]

$$\mathbf{x}(t) = \mathbf{A}\mathbf{s}(t), \tag{1.6}$$

that is, the mixing process in now represented by a $n_m \times n_s$ matrix $\mathbf{A}$. Moreover the separating system of Equation (1.5) should be defined linear and, thus, the recovered signals are given by

$$\mathbf{y}(t) = \mathbf{W}\mathbf{x}(t), \tag{1.7}$$

[13] In this thesis, neither dynamical nor underdetermined models are considered. Therefore, we will only emphasize whether the mixing system is linear or nonlinear, given that all cases discussed from now on are instantaneous and determined (or possibly overdetermined).

[14] For matter of clarity, sometimes we will omit the temporal index $t$ used in the description of the sources and mixtures.

where $\mathbf{W}$ is the $n_s \times n_m$ separating matrix.

In the spirit of the discussion presented in the Subsection 1.3.1, a separation criterion for finding $\mathbf{W}$ could be obtained by exploiting a known characteristic of the sources. For example, let us assume that the sources can be modeled as uncorrelated centered random variables of variances given by $\sigma_1, \ldots, \sigma_{n_s}$. In this situation the correlation matrix $\mathbf{R_s}$ of the vector containing the sources is given by[15]

$$\mathbf{R_s} = E\{\mathbf{s}\mathbf{s}^T\} = \text{diag}(\sigma_1, \ldots, \sigma_{n_s}), \tag{1.8}$$

where $\text{diag}(\sigma_1, \ldots, \sigma_{n_s})$ denotes a diagonal matrix whose diagonal entries are $\sigma_1, \ldots, \sigma_{n_s}$.

As a result of the mixing process, the elements of the vector $\mathbf{x}$ become correlated. Therefore, the correlation matrix of $\mathbf{x}$ is not diagonal anymore and, more specifically, it is given by

$$\mathbf{R_x} = \mathbf{A}E\{\mathbf{s}\mathbf{s}^T\}\mathbf{A^T} = \mathbf{A}\text{diag}(\sigma_1, \ldots, \sigma_{n_s})\mathbf{A^T}. \tag{1.9}$$

We thus had a property (mutually uncorrelated sources) that was lost after the mixing process. Hence, we could now try to perform source separation by retrieving this lost property. In this context, to have a sound separation criterion, every $\mathbf{W}$ giving a set of mutually uncorrelated signals should result in a product $\mathbf{WA}$ that is a non-mixing matrix, given by the product of a diagonal matrix $\mathbf{D}$ and a permutation matrix[16] $\mathbf{P}$. Unfortunately, this is not true for the described correlation-based approach.

It can be easily demonstrated that there are matrices $\mathbf{W}$ that provide uncorrelated estimated sources but also result in a product $\mathbf{WA}$ that is still a mixing matrix. A simple way to check this result is by firstly considering the ideal separating matrix which is given $\mathbf{W}_{ideal} = \mathbf{A}^{-1}$. Obviously, this matrix solves the source separation problem because $\mathbf{y} = \mathbf{s}$ in this case. That said, let us suppose a new situation in which the separating matrix is now given by $\mathbf{W} = \mathbf{Q}\mathbf{W}_{ideal}$, where $\mathbf{Q}$ can be any orthogonal matrix. The correlation matrix of $\mathbf{y}$ in this situation is given by

$$\mathbf{R_y} = \mathbf{Q}\mathbf{W_{ideal}}\mathbf{A}\text{diag}(\sigma_1, \ldots, \sigma_{n_s})\mathbf{A}^T\mathbf{W}_{ideal}^T\mathbf{Q}^T = \text{diag}(\sigma_1, \ldots, \sigma_{n_s}). \tag{1.10}$$

That is, because $\mathbf{Q}\mathbf{Q}^T = \mathbf{I}$ (this comes from the orthogonality of $\mathbf{Q}$) $\mathbf{R_y}$ is a diagonal matrix no matter the orthogonal matrix $\mathbf{Q}$. In other words, we end up with uncorrelated estimated sources $\mathbf{y}$ which are given by

$$\mathbf{y} = \mathbf{Q}\mathbf{W}_{ideal}\mathbf{x} = \mathbf{Q}\mathbf{s},$$

and, thus, are still mixed versions of the sources.

The procedure of transforming a correlated random vector into an uncorrelated vector (with correlation matrix equal to identity) is commonly called spatial whitening[17]. Therefore, from the discussion presented in this section, it became clear that whitening does not assure BSS as

[15] We omit the time index since we are considering here that each source corresponds to a white random process.

[16] Note that, a permutation matrix $\mathbf{P}$ in the solution means that the original order of the sources cannot be recovered. Equivalently, by accepting diagonal matrices $\mathbf{D}$ other than the identity matrix in our solution, we cannot retrieve the correct scales of the sources. These permutation and scale ambiguities are typical of unsupervised methods and their resolution can be achieved only when further information, like the variances of the original sources, is available.

[17] Whitening can be performed by methods of principal components analysis (PCA)

it can provide, at the best, an orthogonal transformation (rotation) of the actual sources. The breakthrough idea in BSS is exactly related to that limitation of whitening. In fact, the first works on BSS indicated that source separation can be indeed achieved by a procedure close to the one discussed in the last paragraphs. However, an important modification is necessary: one must take into account an information "stronger" than the correlation as, for instance, the concept of statistical independence[18]. This eventually resulted in the notion of independent component analysis.

#### 1.3.2.1 Independent component analysis

Although ICA first appeared as a solution to the BSS problem, it rapidly became an important methodology in signal processing and machine learning problems other than the source separation one. For example, ICA can be also useful in problems like feature extraction, efficient coding and prediction. In this thesis, we limit our discussion to the application of ICA to BSS. The interested reader is referred to [40, 94, 90] for further information on other aspects associated with ICA.

The application of ICA to the linear BSS problem is possible when the following conditions hold [39]

- The sources are statistically mutually independent;
- There is, at most, one Gaussian source;
- The mixing matrix $\mathbf{A}$ has full rank.

Based on the Darmois-Skitovich theorem, Comon [39] derived the fundamental result of ICA, namely: given the assumptions described above, the retrieved signals $\mathbf{y}$ are statistically mutually independent if, and only if, $\mathbf{WA} = \mathbf{PD}$, where $\mathbf{P}$ is permutation matrix and $\mathbf{D}$ a diagonal matrix. Put differently, under some conditions, the recovery of the sources, up to order and scale ambiguities, can be achieved by searching for independent components $\mathbf{y}$.

The practical implementation of ICA is accomplished through the formulation of an optimization problem, in which the cost function should be able to measure the statistical independence. In the BSS literature, this particular cost function is usually termed contrast function and its maximum value is attained only when a given random vector $\mathbf{y}$ is mutually independent. From this discussion, it follows that, in the application of ICA to linear BSS, the retrieved sources are given by

$$\mathbf{y} = \tilde{\mathbf{W}}\mathbf{x}, \quad \tilde{\mathbf{W}} = \arg\max_{\mathbf{W}} \mathcal{C}(\mathbf{W}\mathbf{x}), \tag{1.11}$$

where $\mathcal{C}(\cdot)$ corresponds to a contrast function.

A first natural candidate to build a contrast function is the opposite of the mutual information of a random vector $\mathbf{y} = [y_1, \ldots, y_{n_s}]^T$. The mutual information is defined as the Kullback-Leibler

[18] The random variables $z_1, z_2, \ldots, z_N$ are statistically mutually independent if, and only if, the joint distribution $p(z_1, z_2, \ldots, z_N)$ can be expressed as the product of the marginal distributions $p(z_1)$,$p(z_2)$,...,$p(z_N)$. A noteworthy property resulting from this definition is that variables that are statistical independent are always uncorrelated but there may be uncorrelated variables that are not independent.

divergence between the joint and the product of marginal distributions of the vector $\mathbf{y}$ [41], that is

$$I(\mathbf{y}) = \int p(\mathbf{y}) \log \left( \frac{p(\mathbf{y})}{\prod_{i=1}^{n_s} p(y_i)} \right) d\mathbf{y}, \tag{1.12}$$

where $p(\mathbf{y})$ is the joint distribution of $\mathbf{y}$ while $p(y_i)$ represents the marginal distribution of $y_i$. It can be shown that $I(\mathbf{y}) \geq 0$ and that the equality here occurs if, and only if, the elements of $\mathbf{y}$ are mutually independent. Therefore, this property allows one to solve the ICA by defining a contrast function given by $\mathcal{C}(\mathbf{y}) = -I(\mathbf{y})$ [39].

For the case of mutual information, the resolution of the problem expressed in (1.11) via a gradient-based optimization technique results in the following update rule

$$\mathbf{W} \leftarrow \mathbf{W} - \mu \frac{\partial I(\mathbf{W}\mathbf{x})}{\partial \mathbf{W}}, \tag{1.13}$$

where $\mu$ corresponds to the positive step size. The calculation of the gradient $\partial I(\mathbf{W}\mathbf{x})/\partial \mathbf{W}$ can be accomplished by resorting to a simple mathematical manipulation involving the definition of mutual information. Actually, Equation (1.12) can be equally written as [41]

$$I(\mathbf{y}) = \sum_{i=1}^{n_s} H(y_i) - H(\mathbf{y}), \tag{1.14}$$

where $H(\cdot)$ denotes the Shannon's differential entropy. Based on the fact that $\mathbf{y} = \mathbf{W}\mathbf{x}$ in our case, we can rewrite (if $\mathbf{W}$ is invertible) the joint entropy $H(\mathbf{y})$ as [41, 90]

$$H(\mathbf{y}) = H(\mathbf{x}) + \log |\det \mathbf{W}|.$$

Since $H(\mathbf{x})$ does not depend on $\mathbf{W}$, this joint entropy term can be omitted from the gradient calculation, that is

$$\frac{\partial I(\mathbf{W}\mathbf{x})}{\partial \mathbf{W}} = \frac{\partial}{\partial \mathbf{W}} \sum_{i=1}^{n_s} H(y_i) - \frac{\partial \log |\det \mathbf{W}|}{\partial \mathbf{W}}.$$

A further development of this equation (see [15] for instance) shows that the learning rule presented in (1.13) can be rewritten as

$$\mathbf{W} \leftarrow \mathbf{W} - \mu \left( E\{\Psi(\mathbf{y})\mathbf{x}^T\} - \mathbf{W}^{-T} \right), \tag{1.15}$$

where $\Psi(\mathbf{y}) = [\psi(y_1), \psi(y_2), \ldots, \psi(y_{n_s})]$ corresponds to the vector of score functions, where each element is defined by $\psi(y_i) = -p(y_i)'/p(y_i)$. Note that, since $\mathbf{y} = \mathbf{W}\mathbf{x}$, Equation (1.15) can also be written as

$$\mathbf{W} \leftarrow \mathbf{W} - \mu \left[ \left( E\{\Psi(\mathbf{y})\mathbf{y}^T\} - \mathbf{I} \right) \mathbf{W}^{-T} \right].$$

It is noteworthy that Equation (1.15), which give us a route for calculating the independent components, depends on the distributions $p(y_i)$ through the associated score functions. This means that, unlike the whitening approach, which only considers second-order statistics, the learning rule (1.15) considers a complete statistical characterization of the random variables $y_i$. On the other hand, the exploitation of all statistics in this case requires the estimation of score functions, which is usually a cumbersome task. Therefore, the computational burden associated

with the ICA-based algorithm (1.15) is expected to be much heavier than the one associated with whitening algorithms. Therefore, although in perfect harmony with the theoretical idea of ICA, the mutual information approach does not provide a simple practical implementation of ICA.

Fortunately, ICA can be performed in a simpler manner by defining contrast functions that are not based directly on probability density functions (pdf) but rather on some higher-order moments. One interesting example in this context concerns the contrast function based on the kurtosis, a statistic closely related to the fourth-order cumulant of a random variable [102]. The utility of the kurtosis in ICA is related to the so-called non-gaussianity maximization approach [90, 40], which is based on the observation that the mixtures are always "more Gaussian" than the sources (this result stems from the central limit theorem (CLT)). Thus, in view of this result, the non-gaussianity maximization approach searches for components that are as far as possible from Gaussian variables (again, we are trying to recover an original property of the sources). This can be done by maximizing their kurtosis, since this statistic is a natural measure of the "gaussianity" of a random variable [130]. It can be proved that, if the mixtures are whitened in a pre-processing stage, the non-gaussianity maximization principle provides independent components [90, 40].

There are several approaches that also lead to simple ICA algorithms. Examples include

- Infomax [25];
- Maximum likelihood approach [35, 137];
- Nonlinear decorrelation methods [36];
- Nonlinear PCA [97];
- Cumulant-based approaches [39].

Since the literature on BSS and ICA methods is very abundant, the presentation of these approaches is beyond the scope of this chapter and we refer the interested reader to [40, 90] for an introduction to this subject. Still, we close our brief introduction to ICA with two important remarks on this topic. First, there are strong connections between the above-mentioned ICA approaches; they can be described through an equivalent theoretical framework [90, 97, 106] and, thus, result in similar algorithms. For example, the Infomax principle provides a learning rule almost equal to the one presented in Equation (1.15). The only modification concerns the nonlinear function $\psi(\cdot)$: instead of the score functions of $y_i$, fixed nonlinear functions, that should be defined beforehand, are considered in the Infomax method.

Finally, we remark that, besides the achievements in the definition of separation criteria, the study on ICA has been also dealt with the application of optimization tools other than the ordinary gradient-descent method. Examples in this line of research include: the concepts of natural and relative gradient [36, 8], the utilization of fixed-point methods (the well known FastICA [90] algorithm follows this approach), and the formulation of ICA as a task of joint diagonalization of higher-order cumulants (this is the idea underlying the JADE algorithm [37]).

#### 1.3.2.2 Second-order methods

ICA is not the only way to perform BSS; alternatives to ICA can be obtained by exploiting prior information that are usually available in real problems. For example, in ICA the sources are regarded as i.i.d. random process, i.e. such methodology does not make use of the fact that, very often in real applications, the sources have a clear temporal structure. By taking into account such an information, it becomes possible to derive efficient BSS algorithms founded on second-order statistics (the methods exploiting such an idea are usually called second-order BSS methods[19]). In this approach, there are basically two formulations that can be considered. While the first one is based on the assumption that each source is a time-correlated stationary process [26], the second considers that the sources are non-stationary signals [136].

According to the discussion of Section 1.3.2, a simple diagonalization of the correlation matrix $R_{\mathbf{x}}(0) = E\{\mathbf{x}(t)\mathbf{x}(t)^T\}$ is not enough to assure source separation. Yet, under the condition that the sources are mutually uncorrelated and that each one has a different temporal structure (or equivalently a different spectral content), it is possible to achieve source separation by jointly diagonalizing $R_{\mathbf{x}}(0)$ and one (or several) lagged covariance matrices, given by $R_{\mathbf{x}}(\tau) = E\{\mathbf{x}(t-\tau)\mathbf{x}(t)^T\}, \tau \neq 0$ [151, 26, 40].

The formulation of BSS as a problem of joint diagonalization of correlation matrices permits the utilization of relevant theoretical insights and established methods developed in linear algebra. For example, the SOBI algorithm [26], which is based on the diagonalization of several correlation matrices[20], makes use of a diagonalization method based on Givens rotations.

#### 1.3.2.3 Sparse component analysis

In the last few years, there is a clear trend toward approaches that make use of other types of prior information that are usually less general than the ones considered by ICA and second-order methods[21]. In this context, much attention has been paid to the use of Sparse Component Analysis (SCA) [74, 71], which works with the assumption that the sources can be represented by sparse signals, i.e. their variances are null (almost null in practice) in most of the time[22]. SCA is a useful tool notably for solving underdetermined BSS problems and has been intensively studied in the context of audio signal separation.

The basic principle behind SCA can be understood through Figure 1.5, which refers to a BSS problem with three sources and two mixtures. The left column of this figure corresponds to a situation in which the sources are not sparse. As can be seen in the bottom of this column, the scatter plot of the mixtures does not give us any particular information about the mixing

[19]Some authors also consider second-order BSS methods as ICA methods. However, as these two approaches are based on distinct formulations and work under different assumptions, we believe that they should be classified into different groups.

[20]This is done for overcoming problems that appears when the correlation matrices to be diagonalized possess degenerate eigenvalues

[21]The term "semi-blind" is usually employed to classify these types of methods since they usually consider stronger prior information than the ones considered in ICA. However, some care must be taken given that "semi-blind" is also used for classifying methods that work with a very reduced set of reference signals.

[22]It is thus an extreme case of non-stationary sources.

process. Conversely, when the sources are sparse (right column of Figure 1.5), the directions given by the columns of the mixing matrix become visible in the scatter plot of the mixtures. In such a case, therefore, source separation can be carried out by firstly identifying the columns of **A** with, for example, a clustering approach [74]. After that, one ends up with a sparse inverse problem for which several efficient techniques are available [74, 71].

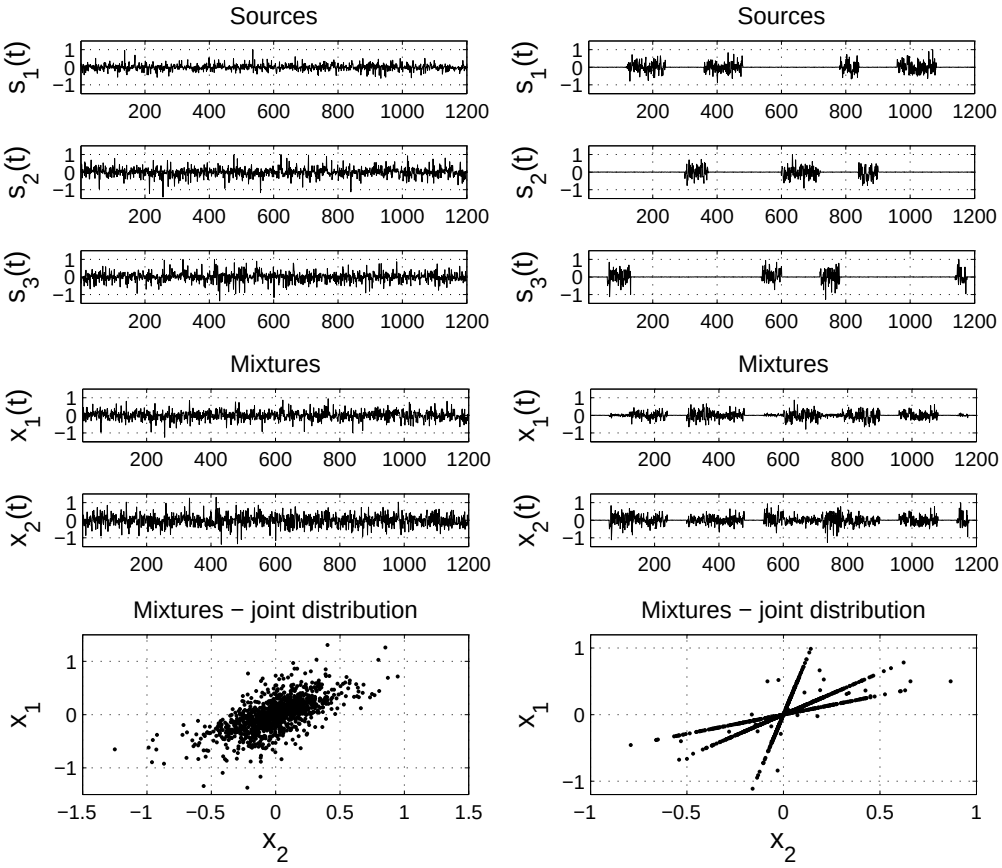


Figure 1.5: Example illustrating the application of SCA to an underdetermined source separation (3 sources and 2 mixtures). The left column presents the sources, mixtures and the scatter plot of the mixtures for a case when the sources are not sparse. In the right column, the same figures are presented but now for the case of sparse sources. The sparsity of the sources results in mixtures whose joint plot is aligned with the directions given by the columns of the mixing matrix **A**.

In the example illustrated by Figure 1.5, which was firstly presented in [73], the sources were sparse in time. However, SCA can be also applied for signals that are sparse in representations other than the temporal one. This can be achieved by considering the source separation problem in a transformed domain[23]. For example, audio sources may not be sparse in time but may become sparse after the application of, for instance, the modified discrete cosine transform (MDCT) [68]. One important question in SCA is how to find good sparse representations for a given class of signals, i.e. it is important to define a "dictionary" of signals that allows one to

[23]This can be done under the condition that the mixing process be also linear in the transformed domain.

write the signals of interest as a linear combination of the elements of the dictionary being the coefficients of such combination sparse.

#### 1.3.2.4 Non-negative matrix factorization

The goal of non-negative matrix factorization [129, 104] (NMF)[24] methods is to factorize a given matrix into the product of two matrices, both of them having non-negative elements. Mathematically speaking, given a matrix $\mathbf{X}$ one searches two positive matrices, say $\mathbf{A}$ and $\mathbf{S}$ (with $a_{ij} \geq 0$ and $s_{jk} \geq 0$), that give a good representation of $\mathbf{X}$, i.e. $\mathbf{X} \approx \mathbf{AS}$. Hence the formulation of NMF is convenient to linear source separation problems in which both the sources and the mixing coefficients take non-negative values. For example, this is usually the case in chemical analysis given that the sources are related to concentrations [122].

Because NMF is not unique [57, 123], source separation methods based on this approach must resort to regularization terms. In this spirit, some NMF extensions work with the assumption that the sources, besides positive, are also sparse [88]. Another type of regularization that has been proposed is to consider that the sources are actually smooth signals [164]. Finally, it is also possible to define a constrained NMF framework when one has access to a reference signal with a shape close to the one of the desired sources [108].

#### 1.3.2.5 Other approaches

In the literature, one can find BSS methods based on strategies that were not discussed so far. Examples include:

- BSS based on Bayesian approach[25] [119, 100];
- Constrained ICA [112];
- Methods based on time-frequency representations [27, 52].

### 1.3.3 Nonlinear models

In some practical cases, the linear approximation does not give a good enough description of the interference model. For example, we mentioned in Section 1.2.3 that devices like ISEs and tin oxide gas sensors can be well described only when nonlinear models are considered. Also, in many applications, the presence of amplification stages may introduce nonlinear distortions. In such cases, the mixing process underlying the sensor array becomes nonlinear, and, thus, cannot be approached by linear BSS models anymore.

The first approaches to the nonlinear instance of BSS appeared in [33, 93]. However, it was only after the works [91, 150] that it became possible to have an idea about some fundamental problems involving nonlinear mixtures. For example, by relying on the Darmois' theorem, [91] showed that for a given random vector —which could represent the mixtures —it is always

[24] Also known as positive matrix factorization.

[25] We provided a brief introduction to Bayesian source separation methods in Chapter 5.

possible to find a nonlinear transformation that results in a vector whose elements are statistically independent. Moreover, they showed that such transformation is not unique; it thus became clear that a simple extension of the ICA principle to the nonlinear case was not enough to assure BSS in a general context. Yet, Taleb and Jutten [150] showed that an ICA-based solution assures source separation in a class of constrained models called post-nonlinear (PNL) models. This work was fundamental to indicate that, even though nonlinear BSS is an ill-posed problem in its general formulation, we can find some particular classes of nonlinear models in which source separation is still possible. This point will be discussed in more details latter.

Besides the non-uniqueness question, there are other limitations that make nonlinear BSS a complicated problem. First, many of the ideas and methods applied in the linear case are based on a linear-algebraic framework —for example, the second-order methods for linear BSS exploit, in a very efficient way, the temporal structure of the sources by jointly diagonalizing correlation matrices —and, thus, are not appropriate to a nonlinear context. Second, as we discussed before, the simplicity inherent in ICA-based linear BSS methods is much due to possibility of obtaining independent components through quantities simpler than the "exact" measures of independence such as the mutual information. Conversely, in nonlinear models, care must be taken in the utilization of such simplified measures of independence. For example, we saw that kurtosis-based contrast functions are associated with the non-gaussianity maximization principle, which, in a nonlinear context, becomes meaningless. A third problem in nonlinear BSS is that, in certain nonlinear models, it may be difficult to define an adequate separating model. The trade off here is that very flexible structures may lead to non-unique solutions whereas simpler systems may not be enough to totally invert the nonlinear mapping. Finally, as nonlinear functions usually amplify the effects of noise, nonlinear BSS algorithms are much more sensitive to noise than the linear ones. More details and a review on nonlinear BSS can be found in [96, 7].

#### 1.3.3.1 ICA, separability conditions and constrained models

Briefly, a mixing model is said to be *separable*[26] if the application of ICA assures that the resulting mapping from the sources to their estimated versions has a diagonal Jacobian, which means that the composition of the mixing and separating mappings results in a non-mixing mapping. For example, under the conditions described in 1.3.2.1, the linear model is separable. On the other hand, as discussed before, the works [91, 150] revealed that nonlinear models are, as rule, not separable.

Intuitively speaking, the lack of separability in nonlinear models comes from their high degree of flexibility and, thus, nonlinear BSS may be feasible only in constrained situations. However, the problem of how to impose such constraints is hard and, sometimes, may be very tricky. For example, an apparent logical solution to cope with the lack of separability would be to constrain the separating system to be a smooth mapping[27]. However, it can be shown that even smooth models are able to mix the sources while keeping their independence [15].

[26] A formal definition of separability can be found elsewhere [65].

[27] Here, the notion of smoothness means a mapping that is not too flexible.

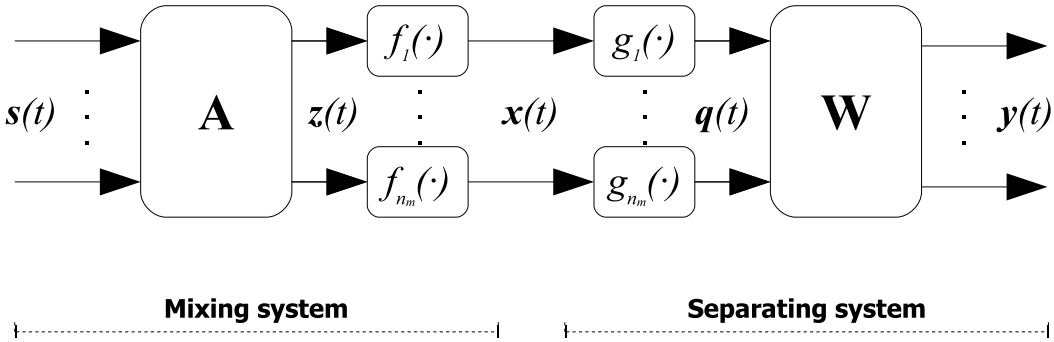


Figure 1.6: PNL mixing and separating systems.

The example presented above is interesting as it points out that a more prudent approach is to work in situations for which structural constraints are imposed on both the mixing and the separating systems. Of course such approach does not always work. Yet, it has been fundamental in the search for separable models. In the sequel, we discuss some examples of constrained models.

#### 1.3.3.2 Post-nonlinear models

The basic structure of a post-nonlinear (PNL) model[28], which was introduced [150], is shown in Figure 1.6. The mixing process is composed of a mixing matrix $\mathbf{A}$ which is followed by component-wise functions, represented by the vector of functions $\mathbf{f}(\cdot) = [f_1(\cdot), f_2(\cdot), \ldots, f_{n_m}(\cdot)]^T$. Thus, a given mixture $x_i(t)$ can be written as

$$x_i(t) = f_i\left(\sum_{j=1}^{n_s} a_{ij} s_j(t)\right),$$

and the mixing process can be represented through the following vectorial notation

$$\mathbf{x}(t) = \mathbf{f}(\mathbf{A}\mathbf{s}(t)). \tag{1.16}$$

As shown in Figure 1.6, the PNL separating system is basically a mirrored version of the mixing system and, thus, the estimated sources are given by

$$\mathbf{y}(t) = \mathbf{W}\mathbf{g}(\mathbf{x}(t)), \tag{1.17}$$

where $\mathbf{g}(\cdot) = [g_1(\cdot), g_2(\cdot), \ldots, g_{n_m}(\cdot)]^T$ is a set of nonlinear functions that must be adjusted to invert the action of $\mathbf{f}(\cdot)$, and $\mathbf{W}$ corresponds to the linear separating matrix.

The separability of PNL models was addressed in several works [150, 15, 2] and requires the following conditions:

[28]The PNL model is inspired by sensor arrays where the amplifying stages introduce some nonlinear distortion [150].

- The sources are statistically mutually independent;
- There is, at most, one Gaussian source;
- The mixing matrix has full rank and must actually mix the signals, that is, each row and column of $\mathbf{A}$ should contain two elements that are not null;
- The functions $f_i(\cdot)$ and $g_i(\cdot)$ must be monotonic.

Note that, as the PNL model comprises a linear model, the same conditions required for the separability of linear models also show up in PNL models. Moreover, in PNL models, the sources can be recovered up to the same ambiguities present in the linear case plus a DC ambiguity —even if the sources are centered, the retrieved sources may have a DC level. Finally, the structural relation between PNL and linear models has been taken into account by the works [150, 15, 2] that addressed the separability of PNL models under the mentioned conditions. In fact, the separability of PNL models can be proved by showing that, under the typical hypotheses of ICA, the statistical independence of $\mathbf{y}$ results in the linearity of the composition $f_i \circ g_i \ \forall i$. Having proved that, the resulting model becomes linear and, thus, one can complete the proof by making use of the separability result of linear models [39].

*ICA-based approaches*

The separability of PNL models provides the theoretical foundations for the derivation of ICA-based techniques in this case. In this context, a natural approach is to set a method based on the mutual information, whose opposite is also a contrast for PNL models. In this case, the parameters of the separating system can be found by resolving the following optimization problem

$$\min_{\mathbf{W},\mathbf{g}(\cdot)} I\left(\mathbf{y}(t)\right) \equiv \min_{\mathbf{W},\mathbf{g}(\cdot)} \sum\nolimits_i H(y_i(t)) - H(\mathbf{y}(t)) \tag{1.18}$$

According to the entropy transformation law [90, 41], $H(\mathbf{y}(t))$ can be rewritten as a function of the joint entropy of the mixtures, $H(\mathbf{x}(t))$, which allows one to rewrite (1.18) as follows

$$\min_{\mathbf{W},\mathbf{g}(\cdot)} \sum\nolimits_i H(y_i(t)) - H(\mathbf{x}(t)) - \log\left|\det \mathbf{W}\right| - E\left\{\log \prod\nolimits_i \left|g_i'(x_i(t))\right|\right\}. \tag{1.19}$$

As $H(\mathbf{x}(t))$ does not depend on the separating system parameters, the optimization problem expressed in Equation (1.19) is equivalent to the following one

$$\min_{\mathbf{W},\mathbf{g}(\cdot)} C\left(\mathbf{y}(t)\right) = \sum\nolimits_i H(y_i(t)) - \log\left|\det \mathbf{W}\right| - E\left\{\log \prod\nolimits_i \left|g_i'(x_i(t))\right|\right\}. \tag{1.20}$$

This "trick" is important in a practical standpoint because it avoids the estimation of multidimensional quantities.

In [150], the derivation of a gradient descent algorithm for optimizing (1.19) was proposed. By considering that the $i$-th nonlinear separating function $g_i$ is parametrized by the vector $\Theta_i$,

the following learning rule was obtained

$$\mathbf{W} \leftarrow \mathbf{W} - \mu_{\mathbf{W}} \left( E\{\Psi(\mathbf{y})\mathbf{q}^T\} - \mathbf{W}^{-T} \right) = \mathbf{W} - \mu_{\mathbf{W}} \left( E\{\Psi(\mathbf{y})\mathbf{y}^T\} - \mathbf{I} \right) \mathbf{W}^{-T} \quad (1.21)$$

$$\Theta_i \leftarrow \Theta_i - \mu_{\mathbf{\Theta}_i} \left( -E\left\{ \frac{\partial \log |g_i'(\mathbf{\Theta}_i, x_i)|}{\partial \mathbf{\Theta}_i} \right\} + E\left\{ \Big( \sum_{k=1}^{n_s} \psi(y_k) w_{ki} \Big) \frac{\partial g_i(\mathbf{\Theta}_i, x_i)}{\partial \mathbf{\Theta}_i} \right\} \right) \quad (1.22)$$

where $\mu_{\mathbf{W}}$ and $\mu_{\mathbf{\Theta}_i}$ correspond to the learning rates.

Like in the linear case (Equation (1.15)), the learning rules derived for the PNL model also depend on the score functions $\Psi(\mathbf{y}) = [\psi(y_1), \psi(y_2), \ldots, \psi(y_{n_s})]^T$. We mentioned before that, in the linear case, it is possible to avoid the estimation of score functions by defining simpler criteria that also lead to statistical independence. However, in the PNL case, a rough estimation of the score functions leads to poor results and, consequently, score function estimation becomes a central point in this problem. Classical examples of methods to carry out this task of estimation include: techniques founded on the Gram-Charlier expansion [150] and kernel methods [150, 15]. More recently, Pham [134] proposed a very efficient kernel-based method for estimating score functions. His approach differs from the classical ones in two points: the estimation is done over a regular grid and a cardinal spline is used as kernel function.

An alternative way for obtaining an ICA method for PNL mixtures is based on the notion of the differential of the mutual information [18, 15]. Briefly speaking, this idea, which can be used in any problem involving mutual information optimization, differs from [150] in considering the cost function (1.19) instead of the one presented in (1.20). As demonstrated in [4], although equivalent in a theoretical standpoint, these expressions may lead to different practical algorithms [16] due to the different statistical properties of the associated estimators.

We close this subsection by mentioning some works that also dealt with ICA algorithms for PNL mixtures. In [3], the authors derived a method based on a measure of statistical independence called quadratic dependence. The motivation for this approach resided in the fact that there may be a large bias in the estimators associated with the mutual information approach. Other important topics in the PNL-ICA framework concerns the definition of appropriate parametrizations for $g_i(\mathbf{\Theta}_i, \cdot)$. The difficulty here is to find flexible functions that do not violate the monotonicity requirement to the model's separability. This matter has been studied, for instance, in [135].

*Two-stage solutions*

The PNL methods mentioned so far work in an one-stage basis, in which the two parts (linear and nonlinear) of a PNL model are adjusted at the same time to minimize a measure of independence between the estimated sources. Despite the theoretical soundness of this one-stage approach, there are several drawbacks regarding its applicability. For example, when the mutual information is considered as separation criterion, it becomes necessary to estimate marginal entropies (or their derivatives), which is costly in computational terms. Moreover, in one-stage methods, it is complicated to define MISO (multiple-input single-output) contrasts and, thus, to design a source extraction algorithm for searching only for a set of the original

sources.

An alternative approach to one-stage methods is motivated by the peculiar structure of the PNL mixture; its clear division between the linear and the nonlinear sections suggests that one could treat each stage separately. The major benefit brought by this formulation (known as the two-stage approach) is that linear BSS can be used to adapt $\mathbf{W}$. Actually, after canceling the nonlinear distortion introduced by the functions $f_i(\cdot)$ in a first moment, the problem is reduced to the one of linear BSS. The main difficulty in developing a PNL two-stage solution concerns the definition of a criterion for adjusting $g_i(\cdot)$ so it inverts $f_i(\cdot)$. Note that every attempt based on independence criteria becomes meaningless in this case.

The first two-stage PNL method was obtained through a geometric approach [17]. To illustrate how this method works, let us consider an example of two PNL mixtures obtained from two sources that are mutually independent and uniformly distributed. In Figure 1.7, we present the scatter plots of these sources, as well as the outputs of the linear and of the nonlinear mixing stages. Initially, one has a rectangular joint plot that, due to linear mixing, becomes a parallelogram that is not rectangular anymore. Then, the nonlinear functions $\mathbf{f}(\cdot)$ transform this parallelogram into a nonlinear form. Based on this observation, [17] shows that is possible to invert the action of $\mathbf{f}(\cdot)$ by searching for $\mathbf{g}(\cdot)$ that give again a scatter plot in the form of a parallelogram.

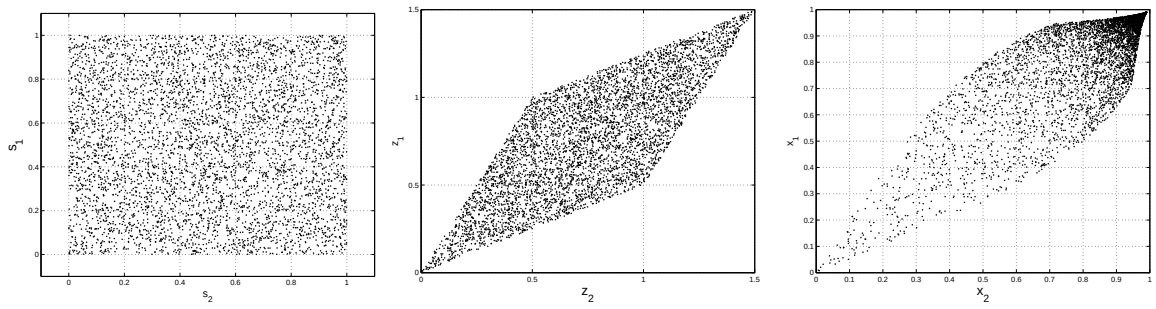


Figure 1.7: Illustration of the geometrical approach for PNL mixtures: sources (left), outputs of the linear mixing stage (center) and mixtures (rigtht).

Another two-stage PNL method exploits the relations between gaussianity and nonlinear functions [147, 165]. According to the central limit theorem, the outputs of the linear mixing stage, $\mathbf{z}(t)$ tend toward Gaussian distributions. However the nonlinear functions $f_i(\cdot)$ destroy the Gaussian aspect of $z_i(t)$. In view of this observation, [147, 165] suggest that $\mathbf{g}(\cdot)$ can be adjusted in order to provide signals $\mathbf{q}(t)$ that are as most Gaussian as possible. Unfortunately, this approach does not assure a perfect inversion of $\mathbf{f}(\cdot)$ because it is based on an asymptotic result, and, consequently, the distributions of $z_i(t)$ are close to Gaussian only when there is a great number of sources. Still, this approach has been proved to be a valuable initialization scheme for other PNL algorithms.

Finally, we cite the work of Lee at al [105] which developed a two-stage approach in which the estimations of the nonlinear functions are done through a dimensionality reduction technique.

#### 1.3.3.3 Linear-quadratic models

It is common to draw analogies between multiple-input multiple-output (MIMO) and single-input single-output (SISO) systems. For example, the linear BSS model is usually associated with SISO filters [13, 14]. By resorting to this analogy, the linear-quadratic (LQ) mixing model can be regarded as an extension of second-order Volterra filters [127], since both models are characterized by the presence of quadratic-terms. Indeed, in its more general form, the LQ model is given by

$$x_i(t) = \sum_{j=1}^{n_s} a_{ij} s_j(t) + \sum_{1 \leq j < k \leq n_s} b_{ijk} s_j(t) s_k(t), \quad \forall i \in 1, \ldots, n_m, \forall t \in 1, \ldots, n_d, \tag{1.23}$$

where $a_{ij}$ et $b_{ijk}$ correspond to the mixing parameters.

Source separation of LQ mixtures was firstly reported in [101, 1]. In both works, the LQ model was approached through linear methods. However, such an approach is feasible only when the very restrictive class of circular sources are considered.

More general BSS algorithms for LQ mixtures were proposed in [86, 87]. In these works, special attention was paid to the problem of how defining a proper structure for the separating system. Indeed, in contrast to linear, or even PNL mixtures, it is quite difficult to find a parametric separating system able to perfectly invert the LQ model[29]. This task requires calculating the analytical form of the inverse mapping associated with (1.23), i.e. it is necessary to express the sources as a function of the mixtures. This is difficult in LQ models because it is associated with the inversion of polynomial functions [86]. Moreover, even when it is possible to conduct this inversion —for example, in the case having two sources and two mixtures —the resulting separating system may assume a complex form that renders difficult the derivation of a training algorithm.

In [86], it has been shown that recurrent systems provide an interesting way to define the LQ separating model. To understand the basic motivation behind such an approach, let us consider an example with two mixtures and two sources, i.e.

$$x_1(t) = s_1(t) + a_{12} s_2(t) + b_{112} s_1(t) s_2(t) \tag{1.24}$$

$$x_2(t) = s_2(t) + a_{21} s_1(t) + b_{212} s_1(t) s_2(t). \tag{1.25}$$

Now, let us represent the samples of the mixtures at a given instant $T$ by $x_i(T)$. In order to retrieve $s_i(T)$ from the mixtures $x_i(T)$, the recurrent system shown in Fig. 1.8 can be used [86]. Mathematically speaking, this system is given by

$$y_1(n) = x_1(T) + w_{12} y_2(n-1) + t_{112} y_1(n-1) y_2(n-1), \tag{1.26}$$

$$y_2(n) = x_2(T) + w_{21} y_1(n-1) + t_{121} y_1(n-1) y_2(n-1). \tag{1.27}$$

[29] One could think of powerful nonlinear structures, such as MLP neural networks, to perform the inversion of LQ models. However, as discussed before, the use of too flexible structures could lead to identifiability problems. Moreover, the better a MLP network can do is to give an approximate inverse mapping.

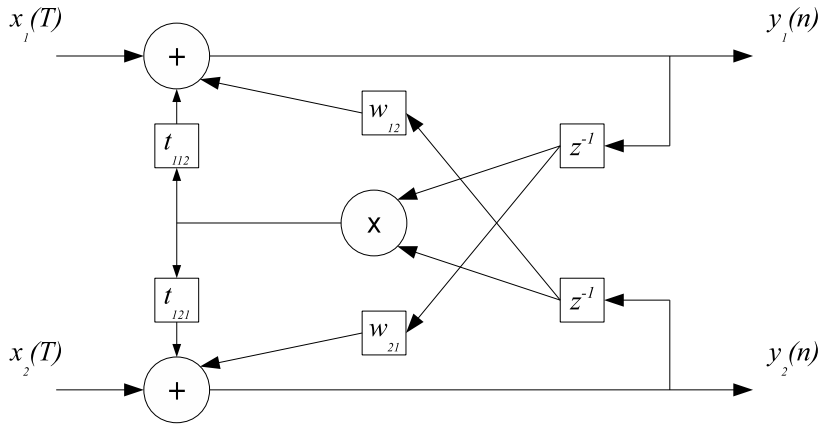


Figure 1.8: The recurrent LQ separating system proposed in [86].

It is easy to show that, when $w_{ij} = -a_{ij}$ and $t_{ijk} = -b_{ijk}$, this dynamical system admits $y_1 = s_1(T)$ and $y_2 = s_2(T)$ as fixed points[30]. That is, this recurrent network allows one to invert the action of the LQ mixing system in an implicit manner.

An important issue that was discussed in [86] concerns the stability of the recurrent system (1.27). Indeed, for this strategy to work, the sources and mixing coefficients should satisfy the local stability condition derived in [86]. More recently, in order to overcome this limitation, [50] proposed an alternative recurrent system that eases the stability problem.

Concerning the adjustment of the recurrent network, a first approach [86] considered an ICA learning rule based on a nonlinear decorrelation approach. Then, the same authors derived a more rigorous technique through a maximum likelihood framework [87], which can also be obtained through the minimization of the mutual information between the outputs of the recurrent system.

Curiously enough, although ICA strategies are usually adopted in LQ models, the separability of this model has never been proved. Yet, there are some evidences suggesting separability, at least for the case of two sources and two mixtures. Firstly, to the best of our knowledge, there are no counterexamples against the separability. Moreover, the reported performance of ICA-LQ methods does not point out any particular problem that would be related to a possible lack of separability. Finally, the separability indeed holds for two sources and two mixtures in the particular case $a_{12} = 2b_{112}$ and $a_{21} = 2b_{121}$. Indeed the resulting model in this case becomes an example of a class of models —the models satisfying the addition theorem (AT) —for which the separability has already been proved [64].

[30] These fixed points are calculated by solving equations (1.26) and (1.27) in $y_i$ after setting $y_i(n) = y_i(n-1) = y_i$.

## 1.4 Application of BSS techniques to chemical sensor arrays

The application of BSS methods to chemical sensor arrays is a relative new topic and was considered in a small number of papers. The first contributions in this area were made by Sergio Bermejo and collaborators [29, 28]. In these works, linear source separation was employed to process the data obtained by an array of ion-sensitive field-effect transistors[31] (ISFET). In [63], a linear BSS method was also considered but now in the context of gas sensor arrays.

As discussed in Section 1.2, ISEs and tin-oxide sensors are clearly nonlinear devices and, thus, arrays of such sensors culminate in nonlinear BSS problems. For instance, in the case of ISEs, when the ions under analysis have the same valences, the NE model becomes an example of PNL model. Moreover, assuming that $r_i$ is known in the CT equation (1.3), the mixing process associated with a tin oxide sensor array can be described by means of the LQ model. These two facts were firstly observed in [23]. This work investigated the application of the PNL method proposed in [150] to ISFET arrays and the application of the LQ methods [86, 87] to arrays of tin oxide sensors.

## 1.5 Conclusion

In the first part of this chapter, we briefly introduced the chemical sensors that will be considered in the following chapters. Special attention was devoted to the interference problem and to how solve it through sensor arrays. In a second part, we turned our attention to the blind source separation. We provided a brief introduction to the classical linear BSS solutions. Then, we discussed some aspects related to the nonlinear instance of the BSS problem. In particular, we saw that unsupervised chemical quantitative analysis via chemical sensor arrays leads to a nonlinear BSS problem.

[31] ISFETs and ISEs have the same principle of operation. However, ISFETs are miniaturized devices built on a MOSFET by replacing the metallic gate with a membrane sensitive to the ion of interest. The ISFET modeling is also based on the NE equation and, thus, the source separation methods developed for ISEs are also valid for ISFETs.

# Chapter 2

# Experiments with ISE arrays

## 2.1 Introduction

This chapter describes a set of experiments conducted with ion-selective electrodes arrays. In a first moment, the experimental set-up is detailed. Then, we try to identify the scenarios in which the interference process is considerable and also to quantify the errors resulting from a modeling based on the Nicoslky-Eisenman equation. Although the primary goal of the present thesis is the analysis of unsupervised sensor arrays, the acquired data can also be useful in the design of supervised smart arrays.

The experiments described in this section were done in a cooperation with Dr. P. Temple-Boyer (Laboratoire d'Analyse et d'Architecture des Systèmes - LAAS/CNRS, Toulouse France) and his team. The datasets obtained in the performed experiments are public available at www.gipsa-lab.inpg.fr/isea.

## 2.2 Experimental

The objective of the conducted experiments is to acquire a dataset having the following entries: 1) temporal evolution of the activity of the ions under analysis (sources) and 2) the steady-state response of each ISE within the array (mixtures). A first step to attain such goal is to define an experimental set-up in which the concentrations of ionic solutions within a beaker vary in time. In the sequel, we will detail how this can be achieved.

### 2.2.1 Materials

Manufactured ISEs (Consort©) were used in the experiments. Two titrators Dosimat 765 (Metrohm©) were responsible for injecting solutions in the beaker containing the analytes. The solution under analysis was stirred through a Fisher Bioblock© magnetic stirrer. The acquisition block was composed of a Consort© C835 desktop analyzer and of an acquisition software developed by researchers of the LAAS laboratory. Finally, all solutions were prepared using deionized water and, in contrast to common practice, no buffer solution to keep the pH fixed

was used. The motivation for working in such a crude situation is related to the benefits brought by unsupervised SSAs, which reside exactly in the simplification of laboratory procedures.

### 2.2.2 Scenarios

Experiments were conducted in each of the following situations:

1. Analysis of a solution containing $NH_4Cl$ and KCl using one $NH_4^+$-ISE and one $K^+$-ISE ;
2. Analysis of a solution containing NaCl and KCl using two $Na^+$-ISE , one $K^+$-ISE and one $Cl^-$-ISE ;
3. Analysis of a solution containing NaCl and $CaCl_2$ using two $Na^+$-ISE and one $Ca^{2+}$-ISE .

The first scenario concerns a well-known example of interference in the ISE context: the potassium and ammonium ions. This case is relevant in applications like water quality monitoring. In the second scenario, we also address the analysis of two monovalent ions (sodium and potassium) but now the ISE array is composed of four electrodes, including a $Cl^-$-ISE and an additional sodium electrode. One of the motivations for performing this second scenario is to check whether a possible variability between two electrodes of the same type can be exploited by a BSS method. Finally, in the third scenario, we analyze the situation in the ions have different valences (calcium and sodium). As it will be discussed in Chapter 3, this third case results in a very challenging mixing model.

### 2.2.3 Experimental details and data set organization

In Figure 2.1, a picture of the experimental set-up is shown. The diagram presented in Figure 2.2 illustrates how the experiments took place. Basically, there were two titrators responsible for injecting salt solutions. The parameters of these titrators, such as the total volume of injected solution and the injection period, were controlled via software. Concerning the data acquisition, the ISEs were connected to a desktop meter which in turn communicated with a personal computer through the RS232 port. The precision of the desktop meter was 1mV and the measurements were recorded every 5 seconds.

As discussed in the scenarios definition, two chloride salt solutions were analyzed; we shall represent these solutions by $S_1Cl$ and $S_2Cl$, where $S_1$ and $S_2$ denote the cations associated with the chlorine anion. The concentrations of these cations were varied according to the following injection scheme:

1. Initially, the beaker contained a solution of $S_1Cl$ with concentration $C_i$ and volume $v = 50mL$;
2. In a first period of approximately one hour, only the first titrator was active and it injected the salt solution $S_2Cl$ (concentration $C = 10^{-1}M$) with an injection period of 30s. The total injected volume was 5mL;

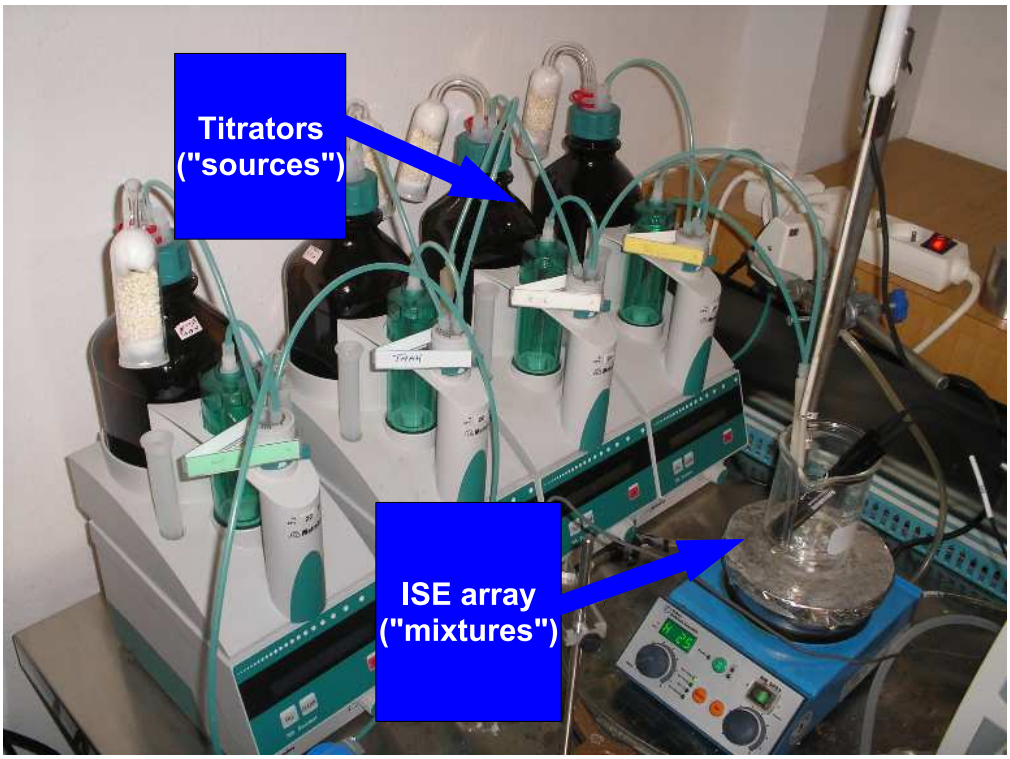


Figure 2.1: Experimental set-up. In a blind source separation context, the sources are related to the titrators given that these devices are responsible for varying the ionic concentrations. The mixtures are obtained from the ISE array.

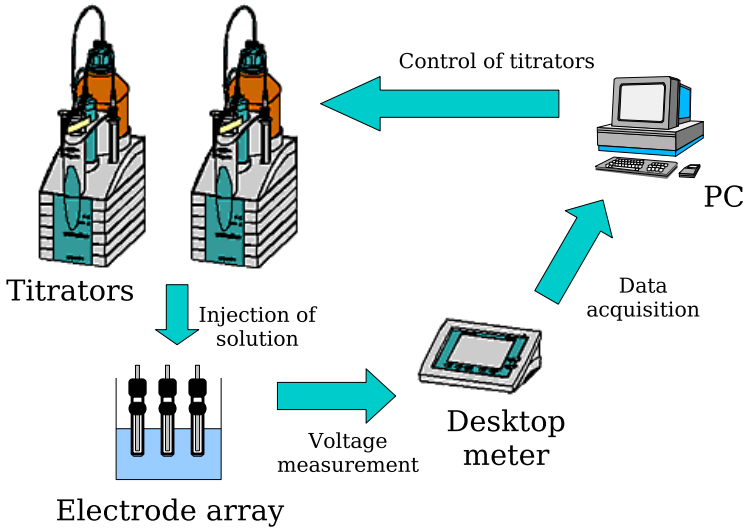


Figure 2.2: Diagram illustrating the experimental set-up.

3. In a second period of approximately one hour, the first titrator was deactivated and the second titrator started the injection of the salt solution $S_2Cl$ (concentration $C = 10^{-1}$M)

but now the total injected volume was 110mL with an injection period of 30s.

As a result of this injection scheme, the concentrations of the cations $S_1$ and $S_2$ vary in the range $10^{-4} - 10^{-1}$M. In Figure 2.3, the temporal evolution of these concentrations, for one experiment, is shown (these are the source signals in our problem). Given that a linear injection scheme (same amount of solution at each injection) was considered, it became necessary to define two injection periods (steps 2 and 3) in order to obtain measurements in the concentration range $10^{-4} - 10^{-3}$M. This explains why only 5mL of solution is injected during the first hour of the experiment.

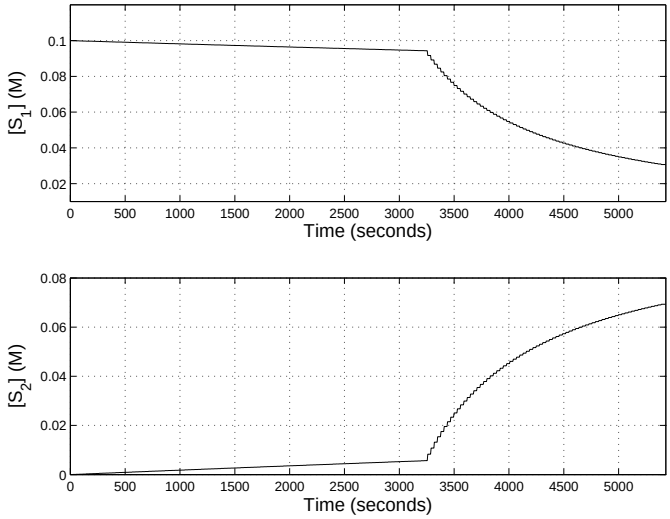


Figure 2.3: Temporal evolution of the concentrations of the cations $S_1$ and $S_2$.

In each scenario, the same injection procedure was performed eight times (each realization took approximately two hours). The difference between these realizations was the initial concentration $C_i$ of the salt solution $S_1Cl$. We considered concentrations close to $C_i = 10^{-i}$M, $i = 1, \ldots, 4$. At the end of these four experiments, we repeated the same procedure but with an inversion of salt solutions, i.e., we started with an initial volume of solution $S_2Cl$ and then an injection of solution $S_1Cl$ took place. Finally, the electrodes were rinsed with distilled water between each experiment.

The following notation was defined in order to identify each experiment: $SAS_110^{-C}S_2$, where A, $S_1$, $C$ and $S_2$ refer to the scenario number, the initial salt solution present in the beaker, its (approximate) concentration, and the injected solution, respectively. For example, $S1NH_410^{-1}K$ refers to an experiment of the first scenario where an initial solution of $NH_4Cl$ with concentration of approximately $10^{-1}$M was set, and where KCl was injected by the two titrators according to the procedure described above. Therefore, the first scenario is composed of the following eight experiments: $S1NH_410^{-i}K$ for $i = 1, \ldots, 4$ and $S1K10^{-i}NH_4$ for $i = 1, \ldots, 4$. Finally, the activities were estimated according to the Debye-Hückel formalism (see Section 1.2.1).

## 2.3 Data analysis

The characterization of ISEs is commonly performed via the conduction of some chemical protocols. For instance, as we mentioned in Section 1.2.3.1, the selectivity coefficients of the NE equation can be estimated, for instance, through the matched potential method. These chemicals protocols are very useful in practice as they provide selectivity coefficients offering a good indication of the degree of interference. However, our focus will be on a regression approach. In fact, as the ultimate goal of the present work concerns the application of BSS methods, we are mainly interested in assessing the goodness of fit of the considered mixing model.

In our study, we will focus on a data modeling based on the NE equation. The model parameters $E_0$, $d_i$ and $K_{i,j}$ will be estimated through a non-linear least square (LS), i.e. by resolving the following optimization problem[1]:

$$\min_{E_0,d_i,K_{i,j}} \frac{1}{N}\sum_{t=1}^{T}\left[E(t)-\left(E_0+d_i\log\left(a_i(t)+\sum_{j,j\neq i}K_{i,j}a_j(t)^{z_i/z_j}\right)\right)\right]^2, \tag{2.1}$$

where $T$ is number of samples, $a_j(t)$ is the activity of the $j$-th ion, and $E(t)$ denotes the actual response of the electrode at the instant and $t$. As it will be discussed later, we also consider alternative models to the NE equation and a LS regression approach is also conducted for these cases.

The goodness of fit of the NE model will be checked through the signal-to-noise ratio (SNR), which, for a logarithmic decibel scale, is defined as

$$\mathrm{SNR} = 10\log\frac{\sigma_E^2}{\sigma_e^2}, \tag{2.2}$$

where, $\sigma_E^2$ and $\sigma_e^2$ denote the variance of the actual sensor response and the variance of the regression error, respectively. Besides yielding a relative measure of model fitness, the SNR gives us a more direct way for estimating the amount of noise present in the mixed signals.

### 2.3.1 First scenario

The modeling of the potassium and ammonium electrodes through the NE equation has led to the results shown in Tables 2.1 and 2.2, respectively. A first point that merits some discussion concerns the difference between the SNR obtained when considering each experiment separately and when considering four or eight experiments altogether. This discrepancy is a clear indicator that the NE equation could only provide a proper local description of the data. Actually, modeling the whole data is difficult because of the lack of repeatability; we observed that the simple fact of immersing the electrodes in a new solution may cause a considerable drift in the measurements. Interestingly enough, while this lack of repeatability poses serious problems in a supervised context (it may result in a model with poor generalization capability), it can be used as an argument for unsupervised approaches.

[1]This was done through the Matlab's function *nlinfit* which is based on the Gauss-Newton algorithm.

Table 2.1: First scenario: modeling the $K^+$-ISE through the NE equation.

| **Experiment** | $E_0$(mV) | $d$(mV) | $K_{K^+,NH_4^+}$ | SNR(dB) |
|---|---|---|---|---|
| $S1NH_410^{-i}K$<br>$S1K10^{-i}NH_4$<br>$i = 1, \ldots, 4$ | 115.08 | 38.94 | 0.0314 | 8.91 |
| $S1NH_410^{-i}K$<br>$i = 1, \ldots, 4$ | 123.82 | 43.83 | 0.0093 | 12.46 |
| $S1K10^{-i}NH_4$<br>$i = 1, \ldots, 4$ | 114.36 | 37.25 | 0.0655 | 10.9 |
| $S1NH_410^{-1}K$ | 174.95 | 81.46 | 0.0680 | 30.3 |
| $S1NH_410^{-2}K$ | 144.85 | 57.48 | 0.0739 | 35.7 |
| $S1NH_410^{-3}K$ | 129.91 | 46.10 | 0.2420 | 26.5 |
| $S1NH_410^{-4}K$ | 128.90 | 45.18 | 3.0158 | 23.8 |

Table 2.2: First scenario: modeling the $NH_4^+$-ISE through the NE equation.

| **Experiment** | $E_0$(mV) | $d$(mV) | $K_{NH_4^+,K^+}$ | SNR(dB) |
|---|---|---|---|---|
| $S1NH_410^{-i}K$<br>$S1K10^{-i}NH_4$<br>$i = 1, \ldots, 4$ | 125.53 | 44.05 | 0.0976 | 14.3 |
| $S1NH_410^{-i}K$<br>$i = 1, \ldots, 4$ | 125.18 | 42.38 | 0.0761 | 15.0 |
| $S1K10^{-i}NH_4$<br>$i = 1, \ldots, 4$ | 128.67 | 47.51 | 0.1157 | 15.9 |
| $S1K10^{-1}NH_4$ | 184.11 | 89.63 | 0.2293 | 31.2 |
| $S1K10^{-2}NH_4$ | 149.95 | 61.78 | 0.2769 | 30.0 |
| $S1K10^{-3}NH_4$ | 148.36 | 59.62 | 1.3782 | 30.1 |
| $S1K10^{-4}NH_4$ | 135.16 | 51.68 | 2.3373 | 22.7 |

Still in Tables 2.1 and 2.2, one may observe that the estimated slopes $d_i$ are of the same order of magnitude as the theoretical Nernstian slopes (59mV). Concerning the selectivity coefficients, the greater values obtained in the regression of the $NH_4$-ISE suggests that such electrode is more sensitive to $K^+$ than the other way around.

Besides the values of the estimated $K_{i,j}$, another way to check the interference phenomenon can be achieved by plotting, for each experiment, the response of the electrode as a function of the activity of its respective target ion. For example, one can note in Figure 2.4 that the $NH_4^+$-ISE presents an almost linear (with respect to the logarithm of the activity) response when the activity of $K^+$ is smaller. On the other hand, the ammonium electrode does not provide good measurements for activities below 0.01M when the activity of $K^+$ is high (experiment $S1K10^{-1}NH_4$). Note that this particular shape resembles the one predicted by the NE equation

(see for instance, the example illustrated in Figure 1.2).

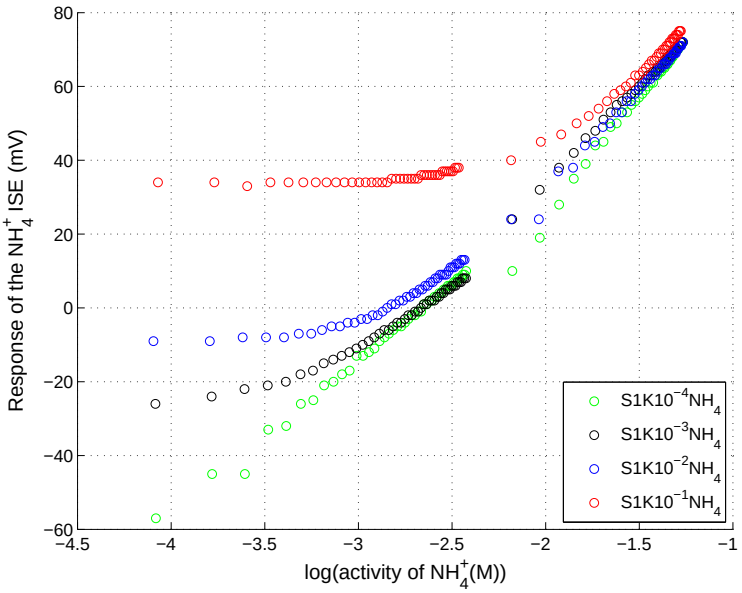


Figure 2.4: First scenario: response of the $NH_4^+$-ISE as a function of the activity of $NH_4^+$ .

The response of the $K^+$-ISE as a function of the potassium ion activity is depicted in Figure 2.5. In this case, one observes a behavior that is not compatible with the NE paradigm since there are some areas in which the response obtained for low activities of interfering ions is greater than the one obtained for high activities[2]. Several hypotheses can be formulated to describe this strange behavior. First, as we have already mentioned, a considerable drift can take place between two experiments. Indeed, if 10mV are subtracted from the results obtained in the experiments S1K10$^{-3}$NH$_4^+$ and S1K10$^{-4}$NH$_4^+$, the shape of resulting figure becomes closer to the one predicted by the NE equation. A second hypothesis would be related to the stabilizing time required by the electrode: perhaps, for the concentration ranges considered in S1K10$^{-3}$NH$_4^+$ and S1K10$^{-4}$NH$_4^+$, the electrode needs a time greater than the period of injection (30s). Finally, there may be indirect interactions between the ions under analysis and the electrodes; for example, we did not consider the effects of the variation of the pH on the ISEs.

#### 2.3.1.1 On the application of alternative models

A very basic principle in data analysis is that nonlinear models should be used only when the linear approximation does not give a well enough description. This is even more evident in the context of source separation since, as discussed in Chapter 1, linear BSS techniques are much simpler than the nonlinear ones. Motivated by that, we studied the implications of considering a model in which the ISE response $E$ is a linear function of the logarithm of the activities $a_j$.

[2]An interesting point here regards the possibility of incorporating into the signal processing block methods able to identify which sensors within the array present a response that deviates from the response predicted by the NE model. Although not treated in the present research, this feature would be quite helpful to practitioners.

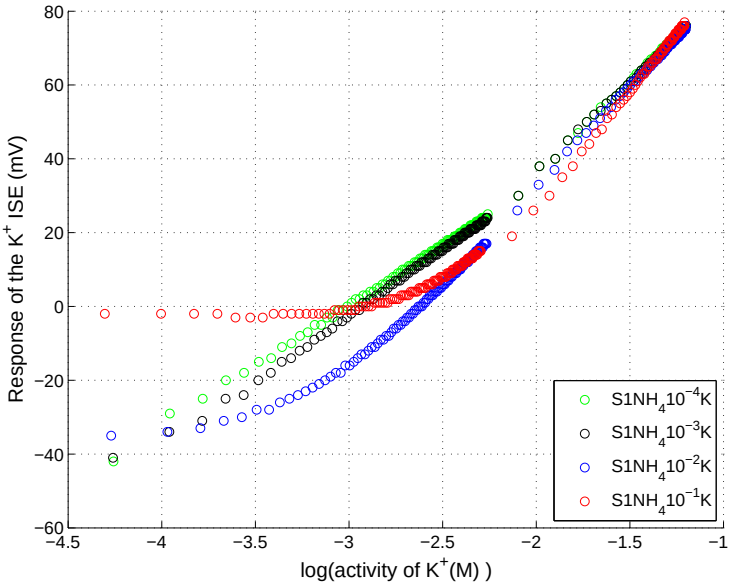


Figure 2.5: First scenario: response of the $K^+$-ISE as a function of the activity of $K^+$ .

When there are only two ions, this model becomes

$$E = c_0 + c_1 \log(a_1) + c_2 \log(a_2), \tag{2.3}$$

where $c_i$ represents the model parameters. Note that linear BSS can be used in this case if one considers the following transformation of variables: $s_i = \log(a_i)$.

The model (2.3) offers a simpler description than that of the NE model. In our study, we also considered a model that is more complex than the NE equation. Indeed, in order to investigate if, as in the case of gas sensors, the presence of cross-product terms may resulted in a better modeling of the studied ISEs, the following extension of the NE equation was defined

$$E = E_0 + d \log\left(a_1 + K_{1,2} a_2 + Q_{1,2} a_1 a_2\right), \tag{2.4}$$

where $E_0$, $d$, $K_{1,2}$ $Q_{1,2}$ correspond to the model parameters. We shall refer to this model as the NE-cross model.

After performing some experiments, we verified that the linear model given in Equation (2.3) only gives a rough description of the ISE device. Indeed, in Tables 2.3 and 2.4, one can note that the linear model gives rather inferior SNR when compared to the NE model. Concerning the NE-cross model, it performs slightly better than the standard NE model. Actually, this is expected because the NE model is a particular case of the NE-cross model. Therefore, the important question here is whether the gains brought by the NE-cross model justify the increase in the model complexity.

A possible way to investigate the trade-off between model complexity and model accuracy can be obtained through the Bayesian information criterion (BIC) [81]. The BIC is a function of the training error and of the number of model parameters. Ideally, the model with lower BIC must be favored. In tables 2.3 and 2.4, we show the BICs for each model. Due to the

large residuals, the linear model presents a much higher BIC than the nonlinear models. Within the nonlinear models, the difference between the estimated BICs was relatively smaller; the NE-cross model was the one with smaller BIC. However, it is important to remark here that, for the BIC's standpoint, the difference between the complexity associated with the NE and the NE-cross models is just given by the number of parameters present in each model —three in the NE model and four NE-cross —and, thus, such a difference is small. On the other hand, for the source separation standpoint, a method tailored for the NE-cross model is much more complex than the one designed to NE equation, and, thus, more susceptible to separability problems and overfitting.

Table 2.3: First scenario: modeling the ammonium electrode.

| | **Linear model** | | **NE model** | | **NE-cross model** | |
|---|---|---|---|---|---|---|
| **Experiment** | SNR (dB) | BIC | SNR (dB) | BIC | SNR (dB) | BIC |
| $S1K10^{-1}NH_4$ | 15.8 | 163.7 | 31.2 | −115.2 | 31.5 | −116.7 |
| $S1K10^{-2}NH_4$ | 13.0 | 361.5 | 30.0 | 5.1 | 30.3 | 2.9 |
| $S1K10^{-3}NH_4$ | 13.0 | 385.6 | 30.1 | 25.6 | 32.6 | −21.7 |
| $S1K10^{-4}NH_4$ | 15.2 | 349.8 | 22.7 | 194.1 | 24.5 | 160.8 |

Table 2.4: First scenario: modeling the potassium electrode.

| | **Linear model** | | **NE model** | | **NE-cross model** | |
|---|---|---|---|---|---|---|
| **Experiment** | SNR (dB) | BIC | SNR (dB) | BIC | SNR (dB) | BIC |
| $S1NH_410^{-1}K$ | 13.4 | 694.4 | 30.3 | −12.6 | 33.1 | −122.8 |
| $S1NH_410^{-2}K$ | 14.0 | 719.4 | 35.7 | −184.4 | 38.7 | −305.8 |
| $S1NH_410^{-3}K$ | 16.5 | 564.8 | 26.5 | 152.68 | 30.9 | −25.7 |
| $S1NH_410^{-4}K$ | 17.3 | 529.1 | 23.8 | 258.2 | 30.0 | −3.3 |

### 2.3.2 Second scenario

In Tables 2.5 and 2.6, we show the regression results for the sodium and potassium electrodes. Again, the NE equation resulted in good SNRs when the experiments were considered separately. Moreover, we observed that the sensitivity of the sodium electrodes toward the potassium ion is high. This interference can be observed in Figure 2.6, in which we plot the responses of the two sodium electrodes within the array as a function of the sodium activity.

The interference of the ion $Na^+$ in the response of the $K^+$-ISE was relative small. This is indicated, for instance, by the small[3] selectivity coefficients obtained in the experiment $S2Na10^{-1}K$.

[3]Note that a good indicator of the interference phenomenon is the selectivity coefficient obtained in the experiment where the activity of the interfering ion is high. However, for small activities of the interference ion, high selectivity coefficients does not necessarily point out a strong interference. Actually, in these cases, the selectivity coefficients are multiplying very low activities and, as consequence, even when they vary in a large range of values, their influence on the regression is small.

Table 2.5: Second scenario: modeling the two sodium electrodes through the NE equation.

| **Experiment** | $E_0$(mV) | | $d$(mV) | | $K_{Na^+,K^+}$ | | SNR(dB) | |
|---|---|---|---|---|---|---|---|---|
| | ISE(1) | ISE(2) | ISE(1) | ISE(2) | ISE(1) | ISE(2) | ISE(1) | ISE(2) |
| S2K10$^{-i}$Na $i = 1, \ldots, 4$ | 207.19 | 185.36 | 60.46 | 51.24 | 0.0410 | 0.0308 | 10.7 | 9.8 |
| S2K10$^{-1}$Na | 382.32 | 390.37 | 206.19 | 226.21 | 0.3162 | 0.3866 | 26.2 | 28.0 |
| S2K10$^{-2}$Na | 287.08 | 260.43 | 115.85 | 103.85 | 0.8273 | 0.7948 | 31.2 | 31.6 |
| S2K10$^{-3}$Na | 264.41 | 241.24 | 96.26 | 85.78 | 3.6122 | 4.8365 | 27.4 | 27.0 |
| S2K10$^{-4}$Na | 250.27 | 226.25 | 82.68 | 71.72 | 10.7876 | 10.1880 | 23.0 | 23.5 |

Table 2.6: Second scenario: modeling the K$^+$-ISE through the NE equation.

| **Experiment** | $E_0$(mV) | $d$(mV) | $K_{K^+,Na^+}$ | SNR(dB) |
|---|---|---|---|---|
| S2Na10$^{-i}$K $i = 1, \ldots, 4$ | 119.47 | 46.06 | 0.0018 | 8.7 |
| S2Na10$^{-1}$K | 153.78 | 62.26 | 0.0008 | 21.5 |
| S2Na10$^{-2}$K | 144.78 | 56.07 | 0.0058 | 19.0 |
| S2Na10$^{-3}$K | 144.55 | 57.67 | 0.6350 | 23.7 |
| S2Na10$^{-4}$K | 131.18 | 52.50 | 7.2332 | 17.5 |

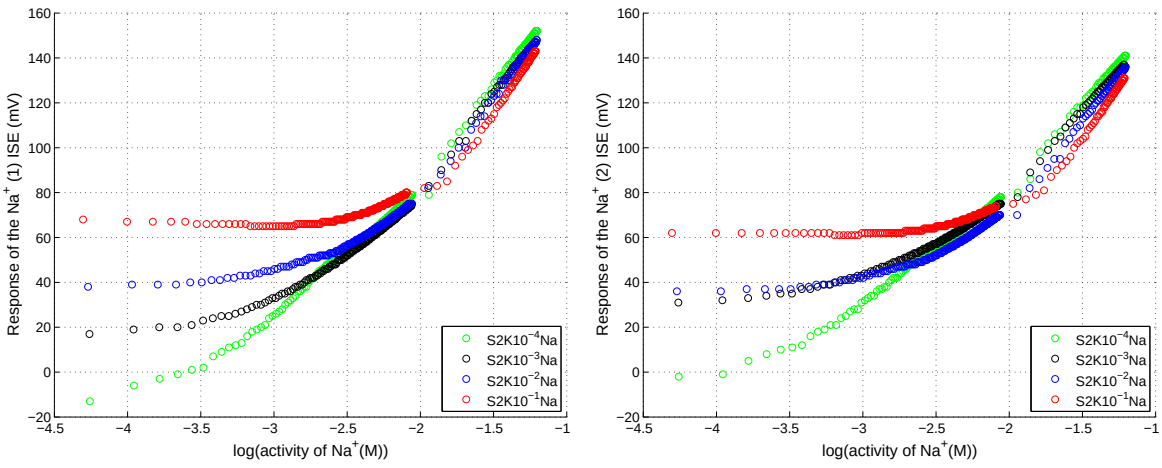


Figure 2.6: Second scenario: responses of the two sodium electrodes within the array as a function of the activity of Na$^+$).

Another worth mentioning point concerning the K$^+$-ISE in this second scenario is that, as can be observed in Figure 2.7, this electrode presented the same irregular behavior as in the first scenario.

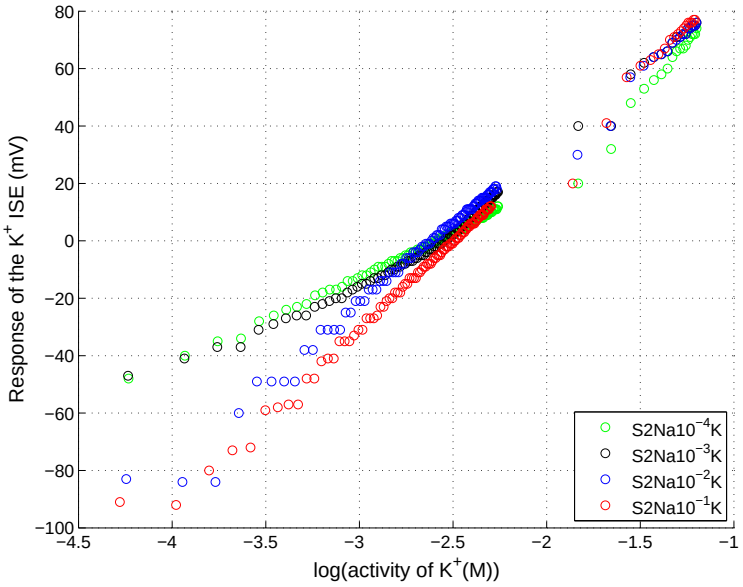


Figure 2.7: Second scenario: response of the $K^+$-ISE as a function of the activity of $K^+$ .

#### 2.3.2.1 The response of the $Cl^-$-ISE

In this subsection, we investigate the response of the $Cl^-$-ISE. As can be verified[4] in Figure 2.8, the $Cl^-$-ISE response is not sensitive to the presence of the $Na^+$ ion. This is in accordance with the great majority of ISEs described in the literature. Indeed, it is rare to find mentions about a possible interference caused by cations in anionic ISEs.

At first glance, in this particular scenario, the fact that the $Cl^-$-ISE does not respond to cations could ease the derivation of a BSS method. In fact, due to the defined injection scheme, the concentration of $Cl^-$ is the sum of the concentrations of $Na^+$ and $K^+$ and, thus, we would end-up with an electrode ($Cl^-$-ISE) that is somehow related to the sum of the sources[5]. Still, this idea is of limited interest because such a relationship of concentrations is not expected to be observed in a real problem.

#### 2.3.2.2 Diversity between sodium electrodes

Finally, we try to check whether the two sodium electrodes present variations that can be useful in BSS[6]. This point can be easily verified by plotting the response of the first $Na^+$-ISE versus the response provided by the second one. This is done in Figure 2.9 for the experiments S2Na10$^{-i}$K, $i = 1, \ldots, 4$. As can be observed in this figure, for all experiments, there is an almost perfect linear relationship between these two electrodes, which means that a very reduced degree of diversity exists. In this particular case, thus, the use of these two sodium electrodes would not

[4] In anionic ISEs, the Nernstian slope is negative, from where the decreasing of the response as the activity grows.

[5] Note, however, that such a relation is only an approximation as the sources actually represent ionic activities.

[6] Note that, in BSS, it is desirable to have a high degree of diversity within the array to avoid sensors with similar responses.

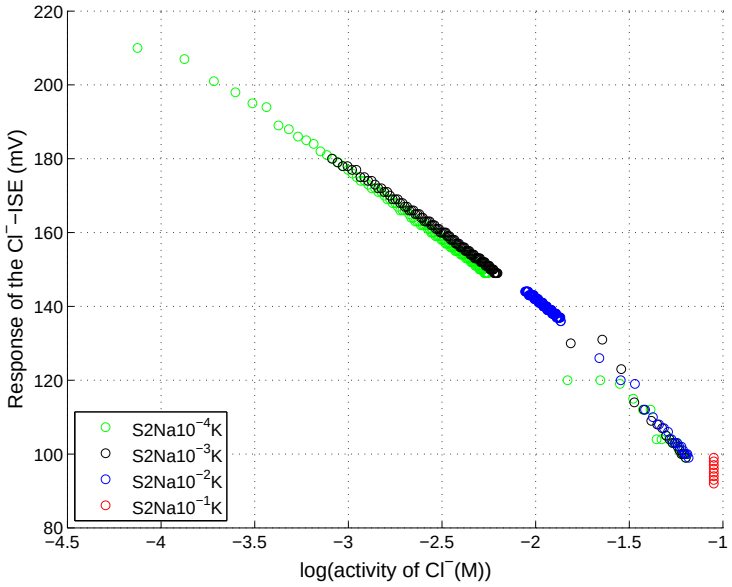


Figure 2.8: Second scenario: response of the $Cl^-$-ISE as a function of the activity of $Cl^-$.

bring any benefit to the development of BSS methods.

### 2.3.3 Third scenario

The results of the regression analysis for this third scenario are shown in Table 2.7 (sodium electrodes) and in Table 2.8 (calcium electrode). Compared to the preceding experiments, the interference level in this third scenario was quite low. This can be verified in Figure 2.10, which depicts responses of the first $Na^+$-ISE and of the $Ca^{2+}$-ISE as a function of the respective activities. Note that, the response of both electrodes are influenced by the activities of the interfering ions only when the activity of the target ion is below 0.001M. Finally, as in the second scenario, a quite reduced diversity is observed within the two sodium electrodes.

Table 2.7: Third scenario: modeling of the two sodium electrodes through the NE equation.

| **Experiment** | $E_0$(mV) | | $d$(mV) | | $K_{Na^+,Ca^{2+}}$ | | SNR(dB) | |
|---|---|---|---|---|---|---|---|---|
| | ISE(1) | ISE(2) | ISE(1) | ISE(2) | ISE(1) | ISE(2) | ISE(1) | ISE(2) |
| S3Ca10$^{-i}$Na $i = 1, \ldots, 4$ | 237.48 | 213.89 | 62.22 | 54.39 | 0.0063 | 0.0039 | 9.3 | 9.4 |
| S3Ca10$^{-1}$Na | 225.71 | 212.95 | 57.54 | 57.11 | 0.0009 | 0.0010 | 32.2 | 32.4 |
| S3Ca10$^{-2}$Na | 227.95 | 215.80 | 63.74 | 62.06 | 0.0063 | 0.0066 | 32.5 | 36.6 |
| S3Ca10$^{-3}$Na | 235.56 | 216.10 | 70.19 | 62.05 | 0.0201 | 0.0159 | 35.9 | 33.6 |
| S3Ca10$^{-4}$Na | 242.42 | 227.39 | 78.61 | 72.87 | 0.0349 | 0.0682 | 30.4 | 30.6 |

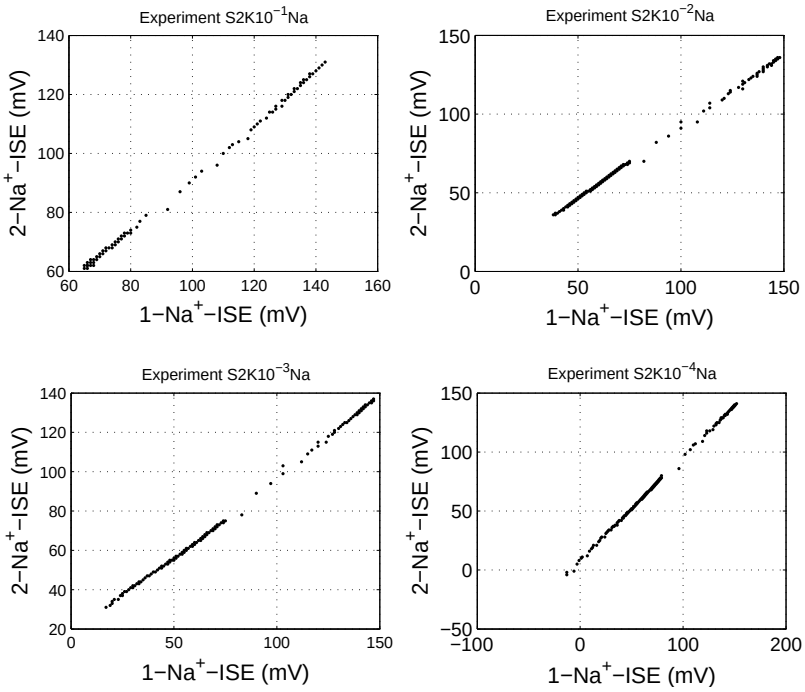


Figure 2.9: Second scenario: analyzing the diversity within the responses of the two sodium electrodes.

Table 2.8: Third scenario: modeling the $Ca^{2+}$-ISE through the NE equation.

| **Experiment** | $E_0$(mV) | $d$(mV) | $K_{Ca^{2+},Na^+}$ | SNR(dB) |
|---|---|---|---|---|
| S3Na10$^{-i}$Ca $i = 1, \ldots, 4$ | 130.55 | 41.84 | 0.0831 | 15.9 |
| S3Na10$^{-1}$Ca | 133.42 | 42.81 | 0.0370 | 23.5 |
| S3Na10$^{-2}$Ca | 150.33 | 50.70 | 3.5737 | 28.0 |
| S3Na10$^{-3}$Ca | 145.27 | 48.37 | 304.65 | 26.1 |
| S3Na10$^{-4}$Ca | 152.60 | 52.53 | 3530.5345 | 21.3 |

## 2.4 Conclusions

In this chapter we described a set of experiments that were conducted with ISE arrays. A nonlinear regression analysis based on the NE was carried out to model the acquired data.

A first point that called our attention was the pronounced lack of repeatability of the ISEs used in the experiments. This characteristic has led to poor regression results when all experiments were considered at the same time. Still, we observed that, within the same experiment, the NE equation gives a good description of the electrode response. Concerning the ISE modeling, we could also check that a linear model provides a very crude approximation of the interference process. Therefore, in the context of source separation, the application of linear techniques would have to face a mixing model corrupted by a large amount of modeling noise, which is not a trivial task.

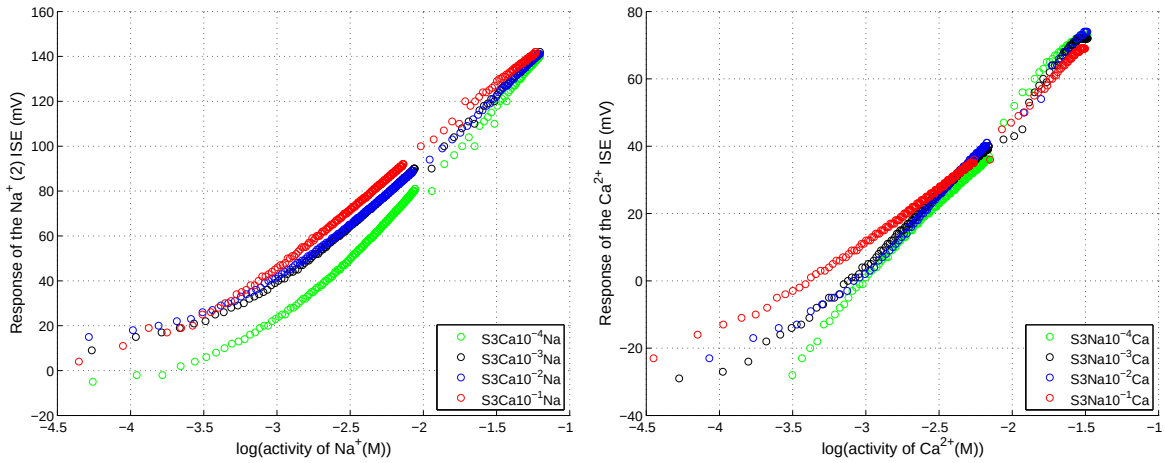


Figure 2.10: Third: response of the first sodium electrode (left) and of the calcium electrode (right).

Still in the context of source separation, the first scenario was the most interesting one. Indeed, in this case, both electrodes within the array were susceptible to interference. Conversely, in the third scenario, the electrodes proved to be more robust to interference from other ions.

Finally, our experiments also allowed us to investigate some points that are important in practice. Firstly, we verified that the two electrodes of the same type used in scenarios 2 and 3 gave too similar responses. Thus, because of this lack of diversity, there is no advantage in using these two electrodes (instead of only one of them) in a source separation context. Secondly, we saw that, in the second scenario, the response of the $Cl^-$-ISE was not influenced by the cationic species and that, because of the relation between the concentrations of the chemical species in the considered experiment, it is related to the sum of the sources.

# Chapter 3

# Methods based on Independent Component Analysis

## 3.1 Introduction

This chapter initiates the second part of the present thesis. We now turn our attention to the investigation of source separation methods tailored for chemical sensor arrays. A first and natural step toward this goal is to focus on ICA methods since they operate with a minimum amount of prior information. As mentioned in Chapter 1, some advances in this direction have already been reported [23, 24]: one can find ICA methods that can be applied to tin oxide gas sensor arrays (LQ model) and to a potentiometric electrode arrays for detecting ions of equal valences (PNL model).

In this chapter, we aim at designing ICA methods for a situation that has not yet been addressed, namely ISE arrays made for analyzing ions of different valences. Depending on the array configuration, this particular case may result in a rather complex mixing model for which it is difficult to define the separating structure and a proper algorithm for adjusting their parameters. To overcome these problems, we consider a recurrent separating system and investigate learning rules based on the ICA framework.

## 3.2 Problem statement: the mixing model

First of all, let us clarify an important point concerning the notation. In this chapter, we will omit the temporal index; the $j$-th source and the $i$-th mixture will be represented by $s_j$ and $x_i$, respectively. This is done because in ICA methods the signals are seen as realizations of i.i.d. random processes[1]. Thus, according to the NE model (see Equation (1.2)), the response $x_i$ of the $i$-th ISE within the array is given by

$$x_i = e_i + d_i \log\Big(s_i + \sum_{j,j\neq i} a_{ij} s_j^{\frac{z_i}{z_j}}\Big). \tag{3.1}$$

[1]More precisely, ICA does not take into account temporal relationship between sucessive samples.

Note that a notation different from Equation (1.2) is used here: now the selectivity coefficients are represented by $a_{ij}$ and the DC level by $e_i$. The terms $z_i$ and $z_j$ denote the valence of the ions $i$ and $j$, respectively.

As discussed in Section 1.4, when the ratio $z_i/z_j$ is equal to 1, the mixing model (3.1) becomes a particular case of the class of PNL models. On the other hand, when the valences are different, the resulting mixing model becomes tougher because a nonlinearity (power term) appears inside the logarithm term.

A possible way to deal with the presence of terms $z_i/z_j \neq 1$ relies on a clever choice of the electrodes composing the array. To illustrate that, let us take as an example the third scenario of the experiments described in Chapter 2. The goal in that case was to estimate the activities of $Ca^{2+}$ and $Na^{+}$. Suppose that such estimation is conducted through two sodium ISEs, instead of considering an array composed of one calcium and one sodium electrode. Therefore, according to Equation (3.1), the mixing model can be written as:

$$x_1^{(ISE_1)} = e_1^{(ISE_1)} + d_1^{(ISE_1)} \log\left(s_1 + a_{12}^{(ISE_1)} s_2^{1/2}\right), \tag{3.2}$$

$$x_1^{(ISE_2)} = e_1^{(ISE_2)} + d_1^{(ISE_2)} \log\left(s_1 + a_{12}^{(ISE_2)} s_2^{1/2}\right), \tag{3.3}$$

where $s_1$ and $s_2$ denote the activities of the sodium and calcium ions, respectively. The key point is that such mixing process, under the simple transformation $s_2^* = s_2^{1/2}$, can be rewritten as a PNL model. Note that a similar result could be obtained through other configurations. For example, if two calcium ISEs were selected, the transformation $s_1^* = s_1^2$ would also culminate in a PNL model.

Whenever possible, the procedure introduced in the last paragraph should be adopted as it permits the application of PNL methods. Nonetheless, a clever choice of the ISEs depends on some practical issues that, in some situations, may be unfavorable. For instance, if the sodium electrodes used in our experiments (see Chapter 2) were considered in the example under discussion, the aforementioned idea would not work. Indeed, as the responses of the sodium electrodes in those experiments were too similar, we would end up with a very ill-conditioned PNL model that cannot be handled without strong prior information on the sources. Therefore, in these cases, electrodes of different types should be used and, thus, there is no way to avoid the power terms in the nonlinear mixing model.

Motivated by that limitation, we shall discuss, in the rest of this chapter, how a BSS scheme can be set for this difficult case.

### 3.2.1 A simplified mixing model

In view of the complexity of the mixing model (3.1), some simplifications are considered hereafter. First, we assume that the valences of the ions under analysis are known in advance. Second, the parameters $d_i$ and $e_i$ are also known in advance. Therefore, before applying the developed method on the acquired data, one should conduct the following pre-processing step to invert the logarithm functions

$$x_i = 10^{\left(\frac{x_i^* - e_i}{d_i}\right)}, \tag{3.4}$$

where $x_i^*$ denotes the actual response provided by $i$-th electrode of the sensor array. The parameter $d_i$ can be set by simply considering the theoretical value predicted by the NE equation. It should be stressed, however, that when the theoretical value strongly deviates from the actual one, the pre-processing step (3.4) may introduce a nonlinear effect not predicted by the simplified mixing model. Fortunately, a discrepancy between the actual value of $e_i$ and the one used in the pre-processing stage is not as important as in the case of the parameter $d_i$. Indeed, when $e_i$ is not exactly known, we can still apply our method but the best one can do is to retrieve each source up to an unknown multiplicative gain (see Appendix A for a more detailed discussion on the ambiguities associated with the NE model).

A last simplification of the mixing model (3.1) concerns the number of sources and sensors. Although the techniques proposed in this chapter can also be extended to high-dimensional scenarios, our development will only consider the case with two sources and two mixtures. This assumption is realistic in many practical situations where there is one interfering ion that is dominant while the others can be neglected. Moreover, this choice makes possible a theoretical analysis and, thus, a better understanding of the elements of our proposals.

Based on the simplifications described in the last paragraphs, the mixing model (3.1) can be written as[2]:

$$\begin{array}{rcl} x_1 & = & s_1 + a_{12} s_2^k \\ x_2 & = & s_2 + a_{21} s_1^{\frac{1}{k}} \end{array} . \tag{3.5}$$

The term $k$ corresponds to $z_1/z_2$ and we assume that $k \in \mathbb{N}$; this is the case, for instance, in the detection of $Ca^{2+}$ and $Na^{+}$ where $k = 2$. It is worth noticing that, since the sources are non-negative in our problem —they represent chemical activities —there is no risk of having complex-value numbers from the term $s_1^{\frac{1}{k}}$. Finally, as we are interested in an ICA solution, it is assumed that the signals $s_1$ and $s_2$ are mutually statistically independent.

## 3.3 Defining a separating structure

### 3.3.1 Invertibility of the mixing model

A very important point to be addressed before defining a separating system concerns the invertibility of the mixing system (3.5). In other words, we should verify if it is possible to restore a given value $s_i$ from the knowledge of $x_i$ and of the coefficients $a_{ij}$. This can be done by resolving equation (3.5) for $s_1$ and $s_2$. By a simple manipulation of this expression, we obtain

$$x_1 = s_1 + a_{12}\Big(x_2 - a_{21} s_1^{(1/k)}\Big)^k. \tag{3.6}$$

After straightforward calculation, including a binomial expansion, (3.6) becomes

$$(1 + a_{12}b_0)s_1 + a_{12}\sum_{i=1}^{k-1} b_i s_1^{1-\frac{i}{k}} + (a_{12}b_k - x_1) = 0, \tag{3.7}$$

where $b_i = \binom{k}{i} x_2^i (-a_{21})^{(k-i)}$, and $\binom{k}{i}$ is defined as $\frac{k!}{i!(k-i)!}$.

[2]In this model, each ISE has a different ion as target.

By considering the transformation $u = s_1^{\frac{1}{k}}$ in Equation (3.7), one can verify that the solution of this expression is equivalent to the determination of the roots of a polynomial of order $k$ and, as a consequence, the number of solutions grows linearly as $k$ increases. A relevant point here concerns the nature of these solutions, i.e. whether they are still nonlinear combinations of $s_1$ and $s_2$. The main problem to conduct such an analysis is that we need to solve Equation (3.7), which is a difficult task for high values of $k$.

In order to gain some insight into Equation (3.7), let us solve it for $k = 2$. After some calculation, we obtain the following two solutions: the expected pair $(\phi_1, \phi_2) = (s_1, s_2)$ and the pair given by

$$\begin{aligned} \phi_1 &= \left( \frac{(2a_{12}a_{21}s_2)+(a_{12}a_{21}^2-1)s_1^{\frac{1}{2}}}{(1+a_{12}a_{21}^2)} \right) \\ \phi_2 &= s_2 + a_{21}s_1^{\frac{1}{2}} - a_{21} \left| \left( \frac{(2a_{12}a_{21}s_2)+(a_{12}a_{21}^2-1)s_1^{\frac{1}{2}}}{(1+a_{12}a_{21}^2)} \right) \right| \end{aligned} . \tag{3.8}$$

Therefore, the simplified mixing model (3.5) is not invertible and, even more problematic, one of the solutions consists of a nonlinear mixture of the sources. Therefore, we must somehow limit the operation of the source separation technique to the regions in which the mixing model is locally invertible. In the sequel, we will describe how this can be done in a systematic way by using a recurrent network as separating system.

#### 3.3.1.1 A nonlinear recurrent separating system

Besides the non-invertibility of the model (3.5), there is another problem that renders difficult the search for a proper separating structure in this case. In fact, unlike the linear model or even the PNL model, it is not possible to define a direct separating structure for the simplified NE model because, as discussed in the last section, the inversion of this model is associated with the resolution of a polynomial model of order $k$. Interestingly enough, this problem is close to the one of LQ mixtures and, therefore, one can follow the strategy proposed in [86]: the use of a recurrent system as separating structure[3].

In our case, we adopt the separating structure shown in Figure 3.1. In mathematical terms, this recursive structure is characterized by the following dynamics

$$\begin{aligned} y_1(n+1) &= x_1 - w_{12}y_2(n)^k \\ y_2(n+1) &= x_2 - w_{21}y_1(n)^{\frac{1}{k}} \end{aligned} , \tag{3.9}$$

where $[w_{12}\ w_{21}]^T$ are the parameters to be adjusted and $[x_1\ x_2]^T$ represents a given sample of the mixtures[4]. In order to understand how this structure works, we must investigate their equilibrium points. At convergence, by setting $y_1(n+1) = y_1(n) = y_1$ and $y_2(n+1) = y_2(n) = y_2$ in (3.9), one can easily check that, when $[w_{12}\ w_{21}]^T = [a_{12}\ a_{21}]^T$, the equilibrium points

[3]Like the LQ model, the simplified NE model is actually a particular case of the class of additive-target mixtures (ATM) which was recently defined by Deville and Hosseini [51]. They provided some examples showing that recurrent separating structures are indeed quite valuable in this particular class of mixture.

[4]Note that each sample of the mixtures demands one execution of the dynamics (3.9).

correspond to the solutions of (3.6). Put differently, the recurrent network is able to perform an implicit inversion of the mixing model.

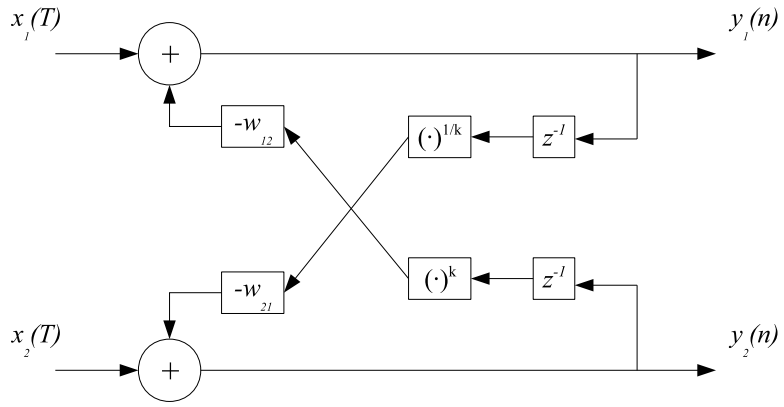


Figure 3.1: A recurrent separating system for the simplified NE mixing model.

Evidently, we saw that the mixing model is not globally invertible and, thus, the recurrent network of Equation (3.9) may converge to points other than the actual sample of the sources, e.g. to (3.8). The next step of our investigation is exactly to verify the conditions to be satisfied so that the equilibrium point associated with the sources is stable and, thus, a potential attractor for the adopted dynamical system.

In view of the difficulty embedded in a global analysis of stability, we consider the study of the local stability in the neighborhood of the equilibrium point $\mathbf{s} = [s_1 \ s_2]^T$ based on the first-order (i.e. linear) approximation of the nonlinear system (3.9). This linearization can be expressed by using a vectorial notation as follows:

$$\mathbf{y}(n+1) \approx \mathbf{c} + \mathbf{J}\Big|_{\mathbf{y}=\mathbf{s}} \mathbf{y}(n), \tag{3.10}$$

where $\mathbf{y}(n) = [y_1(n) \ y_2(n)]^T$, $\mathbf{c}$ is a constant vector. $\mathbf{J}\Big|_{\mathbf{y}=\mathbf{s}}$ is the Jacobian matrix —evaluated at the equilibrium point $\mathbf{y} = \mathbf{s}$ —of the dynamics (3.9), that is:

$$\mathbf{J}\Big|_{\mathbf{y}=\mathbf{s}} = \begin{bmatrix} \frac{\partial y_1(n)}{\partial y_1(n-1)}\Big|_{\mathbf{y}=\mathbf{s}} & \frac{\partial y_1(n)}{\partial y_2(n-1)}\Big|_{\mathbf{y}=\mathbf{s}} \\ \frac{\partial y_2(n)}{\partial y_1(n-1)}\Big|_{\mathbf{y}=\mathbf{s}} & \frac{\partial y_2(n)}{\partial y_2(n-1)}\Big|_{\mathbf{y}=\mathbf{s}} \end{bmatrix} = \begin{bmatrix} 0 & -a_{12} k s_2^{(k-1)} \\ -\frac{1}{k} a_{21} s_1^{(\frac{1}{k}-1)} & 0 \end{bmatrix}. \tag{3.11}$$

A necessary and sufficient condition for local stability of a discrete recurrent system is that the absolute values of the eigenvalues of the Jacobian matrix evaluated at the equilibrium point of interest be smaller than one [85]. Applying this result on (3.11), the local stability of the network for a given realization of the sources is guaranteed when the following condition holds:

$$|a_{12} a_{21} s_1^{(\frac{1}{k}-1)} s_2^{k-1}| < 1. \tag{3.12}$$

This stability condition points out a first constraint of our strategy, given that we are able to separate only the sources lying in this region. In the context of the chemical sensing problem treated in this work, this condition gives the range in which our ISE array can operate properly.

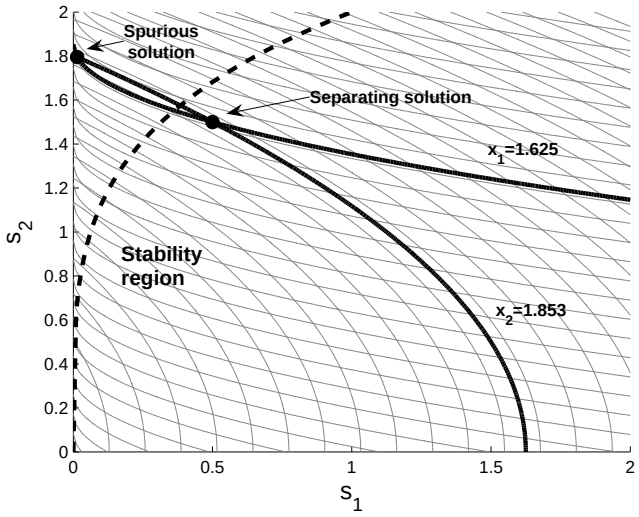


Figure 3.2: Stability boundary (dashed line) and equilibrium points (black dots) of the dynamics (3.9).

Another interesting point related to the stability of the recurrent separating system is that it may provide a systematic way to avoid the convergence to a solution that does not correspond to the actual sources. In order to clarify this idea, let us present an example. Consider the mixing of the sample $\mathbf{s} = [0.5\ 1.5]^T$ in a scenario where the parameters in (3.5) are given by $a_{12} = a_{21} = 0.5$ and $k = 2$. The resulting sample of the mixtures is $\mathbf{x} = [1.625\ 1.853]^T$. In Figure 3.2, we plot the contour lines $x_1 = constant$ and $x_2 = constant$ in the $(s_1, s_2)$ plane. In particular, we highlight the contour lines corresponding to the samples of the mixtures in our examples. The solutions of (3.6), or equally the equilibrium points of (3.9), are given by the intersection of these two contour lines. In this particular example, we found the following solutions: $[0.5\ 1.5]^T$ (as expected) and the spurious solution $[0.01\ 1.79]^T$ (this is the solution given by (3.8)). Still in Figure 3.2, we indicate the region for which the condition (3.12) is met. The key point here is that, while the equilibrium point related to the actual source is within the stability region, the spurious solution lies outside and, as a consequence, will never be a potential attractor for the recurrent network (3.9). Of course, this example is not a proof. However, we observed in our simulations such an approach may indeed be useful to deal with the non-invertibility of the mixing model.

As mentioned before, the stability condition of Equation (3.12) should be satisfied for each sample. Thus, if $s_1$ and $s_2$ are bounded in the intervals $(s_{1_{min}}, s_{1_{max}})$ and $(s_{2_{min}}, s_{2_{max}})$, respectively, then a necessary condition for the stability of all samples can be written as[5]

$$|a_{12}a_{21}s_{1_{min}}^{(\frac{1}{k}-1)}s_{2_{max}}^{k-1}| < 1. \tag{3.13}$$

It is interesting to note that such condition is somewhat related to the degree of nonlinearity of the mixing model given that the point $(s_{1_{min}}, s_{2_{max}})$ is one that suffers the most severe nonlinear

[5]This is simply a worst-case condition.

distortion[6].

The stability condition (3.13) provides an important practical information in the context of ISEs, namely: given the range of the sources, one can trace the stability boundaries in the $(a_{12}, a_{21})$ plane, i.e. one may know for which selectivity coefficients the adopted recurrent network works properly. For example, suppose that we are interested in detecting the ions in the range $0.001\text{M} - 0.5\text{M}$. Then, the adopted recurrent separating will work properly if the ISE array has selectivities coefficients inside the gray regions shown in Figure 3.3(a) (for $k = 2$) and in Figure 3.3(b) (for $k = 3$). Note that the area of the stability region becomes smaller as $k$ grows.

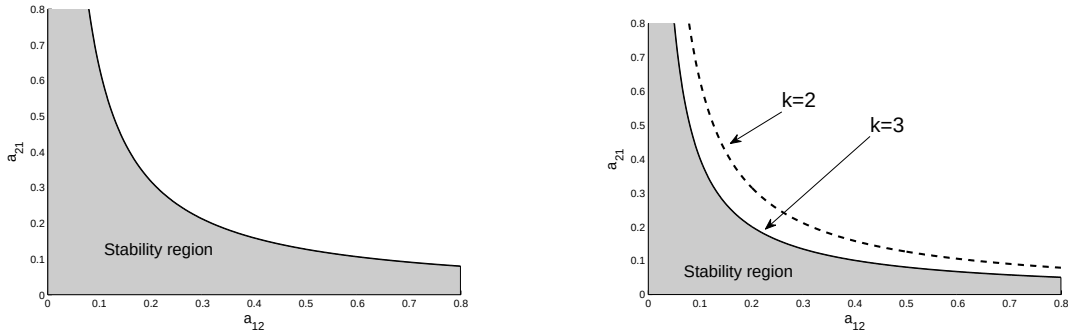


(a) Stability region for $k = 2$.

(b) Stability region for $k = 3$.

Figure 3.3: Stability boundaries in the $(a_{12}, a_{21})$ plane: an example where the ions lie in the range $0.001\text{M} - 0.5\text{M}$.

## 3.4 ICA learning algorithm

Having defined the separating structure, we can now turn our attention to developing ICA-based learning algorithms to adjust the parameters of the chosen separating structure. We begin by studying methods based on higher-order statistics.

### 3.4.1 Approach based on higher-order statistics

An easy route to perform ICA in the linear case is based on the nonlinear decorrelation approach [95, 90]. The motivation behind this idea comes from the following alternative definition of statistical independence: two random variables $y_1$ and $y_2$ are mutually statistically independent if, and only if,

$$E\{f(y_1)g(y_2)\} = E\{f(y_1)\}E\{g(y_2)\} \tag{3.14}$$

for any non-zero continuous functions $f(\cdot)$ and $g(\cdot)$. Evidently, it would be impossible to set a practical algorithm for enforcing such a condition. However, it turns out that in many practical cases the statistical independence can be achieved by assuring condition (3.14) for only one pair

[6]Note that the derivative of $s_1^{1/k}$ increases as $s_1$ decreases whereas the derivative of $s_2^k$ increases as $s_2$ increases.

of functions $f(\cdot)$ and $g(\cdot)$. This approach can be valuable even for some nonlinear mixing models, as demonstrated for the LQ case [86].

In the nonlinear decorrelation approach, a clever choice of the nonlinear functions $f(\cdot)$ and $g(\cdot)$ becomes of paramount importance. A very common approach [90] is to set $f(x) = x^3$ and $g(x) = x$. In our problem, this choice leads to the following learning rule:

$$\begin{array}{rcl} w_{12} & \leftarrow & w_{12} + \mu E\{y_1^3 \bar{y}_2\} \\ w_{21} & \leftarrow & w_{21} + \mu E\{y_2^3 \bar{y}_1\} \end{array}, \tag{3.15}$$

where $\mu$ corresponds to the learning rate and $\bar{y}_i$ to the centered version of $y_i$, i.e. $\bar{y}_i^r = y_i^r - E\{y_i^r\}$. One can check[7] that (3.15) converges when $E\{y_1^3 y_2\} = E\{y_1^3\}E\{y_2\}$ and $E\{y_2^3 y_1\} = E\{y_2^3\}E\{y_1\}$. Obviously, these conditions are only necessary ones for the statistical independence between the sources and, as a consequence, there may be particular sources for which such strategy fails. On the other hand, this strategy provides a less complex algorithm than those that are directly connected with a measure of statistical independence.

#### 3.4.1.1 On the local stability of the learning rule

Several works [69, 148, 48] on linear BSS have studied some convergence issues related to learning rules similar to (3.15). Such an analysis is usually conducted 1) by searching for the equilibrium points of the learning rule—with special attention to possible spurious solutions —and 2) by analyzing the stability conditions for each equilibrium point; in particular, one is usually interested in knowing for which kind of sources the separating solution is a stable fixed point. Following the same guidelines considered in the aforementioned works, a local convergence analysis of (3.15) will be sketched in the following.

According to the ordinary differential equation theory, it is possible to rewrite (3.15) —by assuming that $\mu$ is sufficiently small —as:

$$\begin{array}{rcl} \frac{dw_{12}}{dt} = f_1(w_{12}, w_{21}) & = & E\{y_1^3 \bar{y}_2\} \\ \frac{dw_{21}}{dt} = f_2(w_{12}, w_{21}) & = & E\{y_2^3 \bar{y}_1\}. \end{array} \tag{3.16}$$

A first point to be stressed is that the determination of all equilibrium points of (3.16), which is done by searching for $w_{ij}$ that satisfies $E\{y_i^3 \bar{y}_j\} = 0$, is a rather difficult task. Even for $k = 1$, which corresponds to the linear BSS problem, this calculation demands a great deal of effort [148]. Still, we know that $[w_{12}\ w_{21}]^T = [a_{12}\ a_{21}]^T$ is an equilibrium point given that the outputs $y_1$ and $y_2$ are mutually independent[8] in this case. Therefore, one can, at least, study the conditions of stability for this particular point.

[7] Note that (3.15) converges when $E\{y_i^3 \bar{y}_j\} = E\{y_i^3 y_j\} - E\{y_i^3\}\ E\{y_j\} = 0$.

[8] When we say that $[w_{12}\ w_{21}]^T = [a_{12}\ a_{21}]^T$ is a fixed point of (3.15), we are tacitly assuming that, in such case, $y_1 = s_1$ and $y_2 = s_2$. However, we saw that, even when the parameters of the separating system are well adjusted, the recurrent separating system can converge to points other than the actual sources. Therefore, in our analysis, we are assuming that these spurious points do not met the stability condition (3.12); this was the case in the example presented in Figure 3.2.

As in the case of the separating structure, we can study the local stability of a fixed point of (3.16) through a first-order approximation. In this situation, the Jacobian matrix is given by

$$\mathbf{J} = \begin{bmatrix} \frac{\partial f_1(w_{12},w_{21})}{\partial w_{12}} & \frac{\partial f_1(w_{12},w_{21})}{\partial w_{21}} \\ \frac{\partial f_2(w_{12},w_{21})}{\partial w_{12}} & \frac{\partial f_2(w_{12},w_{21})}{\partial w_{21}} \end{bmatrix}. \tag{3.17}$$

This expression can be rewritten —by simply applying chain rules on Equation (3.16) —as

$$\mathbf{J} = \begin{bmatrix} \left(3E\{y_1^2\bar{y}_2\frac{\partial y_1}{\partial w_{12}}\} + E\{\bar{y}_1^3\frac{\partial y_2}{\partial w_{12}}\}\right) & \left(3E\{y_1^2\bar{y}_2\frac{\partial y_1}{\partial w_{21}}\} + E\{\bar{y}_1^3\frac{\partial y_2}{\partial w_{21}}\}\right) \\ \left(3E\{y_2^2\bar{y}_1\frac{\partial y_2}{\partial w_{12}}\} + E\{\bar{y}_2^3\frac{\partial y_1}{\partial w_{12}}\}\right) & \left(3E\{y_2^2\bar{y}_1\frac{\partial y_2}{\partial w_{21}}\} + E\{\bar{y}_2^3\frac{\partial y_1}{\partial w_{21}}\}\right) \end{bmatrix}. \tag{3.18}$$

As we are now dealing with a continuous dynamics, a given equilibrium point of the learning rule is locally stable when the real parts of all eigenvalues of the Jacobian matrix are negative [85].

The next step of our development is to find the partial derivatives of the entries of the Jacobian matrix. This can be done by applying the chain rule property on (3.9). Indeed, it is easy to check that

$$\frac{\partial y_1}{\partial w_{12}} = -(y_2^k + w_{12}ky_2^{k-1}\frac{\partial y_2}{\partial w_{12}}), \tag{3.19}$$

and also that

$$\frac{\partial y_2}{\partial w_{12}} = -\frac{1}{k}w_{21}y_1^{\frac{1}{k}-1}\frac{\partial y_1}{\partial w_{12}}. \tag{3.20}$$

By inserting this last expression into (3.19), one obtains:

$$\frac{\partial y_1}{\partial w_{12}} = \frac{-y_2^k}{1 - w_{12}w_{21}y_1^{\frac{1}{k}-1}y_2^{k-1}}. \tag{3.21}$$

After similar calculations, the other derivatives can be found:

$$\frac{\partial y_2}{\partial w_{12}} = \frac{w_{21}y_1^{\frac{1}{k}-1}y_2^k}{k(1 - w_{12}w_{21}y_1^{\frac{1}{k}-1}y_2^{k-1})}, \tag{3.22}$$

$$\frac{\partial y_1}{\partial w_{21}} = \frac{kw_{12}y_1^{\frac{1}{k}}y_2^{k-1}}{1 - w_{12}w_{21}y_1^{\frac{1}{k}-1}y_2^{k-1}}, \tag{3.23}$$

$$\frac{\partial y_2}{\partial w_{21}} = \frac{-y_1^{\frac{1}{k}}}{1 - w_{12}w_{21}y_1^{\frac{1}{k}-1}y_2^{k-1}}. \tag{3.24}$$

Since we are interested in the stability of the separating point, it is necessary to find the eigenvalues of (3.18) for $\mathbf{w} = \mathbf{a}$ and $\mathbf{y} = \mathbf{s}$. By conducting this substitution to the case $k = 1$ —which corresponds to the linear case —one can check that the terms

$$E\left\{\bar{y}_1^3\frac{\partial y_2}{\partial w_{12}}\right\}\Big|_{\mathbf{w}=\mathbf{a},\mathbf{y}=\mathbf{s}}, E\left\{y_1^2\bar{y}_2\frac{\partial y_1}{\partial w_{21}}\right\}\Big|_{\mathbf{w}=\mathbf{a},\mathbf{y}=\mathbf{s}}, E\left\{\bar{y}_2^3\frac{\partial y_1}{\partial w_{21}}\right\}\Big|_{\mathbf{w}=\mathbf{a},\mathbf{y}=\mathbf{s}}, E\left\{y_2^2\bar{y}_1\frac{\partial y_2}{\partial w_{12}}\right\}\Big|_{\mathbf{w}=\mathbf{a},\mathbf{y}=\mathbf{s}}$$

become null. Furthermore, the denominators of the derivatives become $1 - w_{12}w_{21}$. These simplifications allowed [148, 69] to express the stability conditions for the solution $\mathbf{w} = \mathbf{a}$ as a function of only some statistics of the sources. For $k \neq 1$, however, this seems impossible; the presence of nonlinear terms in the denominators of the derivatives makes difficult the separation of the contributions of $a_{ij}$ and $s_i$. Consequently, the best one can do in this case is to obtain a condition that is also a function of the mixing parameters, which is of limited interest in a blind scenario.

*Stability of the learning rule (3.15): a practical example*

In order to illustrate the local stability condition derived from Equation (3.18), we conduct simulations considering the following two cases: 1) sources distributed according to a uniform random variable and 2) sources following an exponential distribution. In both cases, the number of samples is 10000 and the mixing parameters are given by $a_{12} = a_{21} = 0.5$. Moreover, the sources lie in the interval $[0.1, 1]$. This configuration assures, for both examples, the local stability of the recurrent separating system (Equation (3.12)).

Concerning the stability of the nonlinear decorrelation learning rule (3.15), we calculated for both situations the eigenvalues of the Jacobian matrix (3.18) at the separating point $w_{12} = a_{12}$ and $w_{21} = a_{21}$. For uniform sources, the real parts of the eigenvalues were negative and, thus, the separating point is a potential attractor for the learning rule. On the other hand, in the case of exponential sources, one of the eigenvalues had a positive real part, thus violating the condition of local stability.

To check if the stability analysis of the last paragraph is confirmed in practice, we executed the learning rule (3.18) for both types of sources mentioned before. We considered 20000 iterations and a small step $\mu = 0.0001$. The initial condition for $[w_{12}\ w_{21}]^T$ was given by the separating point $[a_{12} = 0.5\ a_{21} = 0.5]^T$ added to a small random perturbation. In Figure 3.4 (left), we plot the trajectory in the plane $[w_{12}\ w_{21}]^T$ during the learning rule for the uniform sources. Note that the dynamics remains in the neighborhood of the separating solution. However, as can be seen in the right side of Figure 3.4, for the exponential distributed sources, the dynamics diverges despite the initial condition close to the separating point.

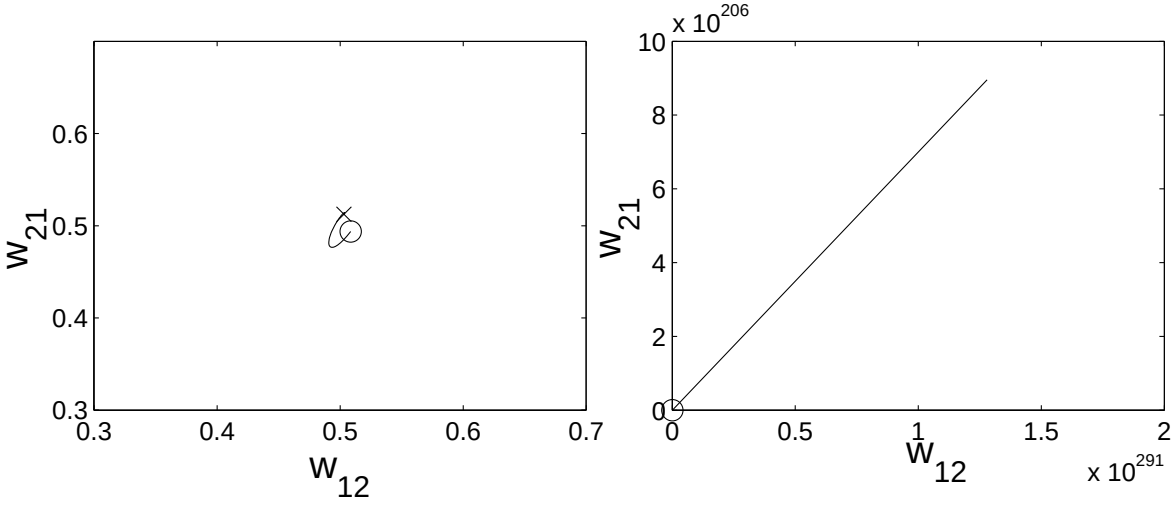


Figure 3.4: Trajectories in the $(w_{12}, w21)$ plane. Left: uniform distributed sources. Right: exponential distributed sources. The symbol $\circ$ represents the initial condition and the symbol $\times$ the equilibrium point.

Table 3.1: Nonlinear decorrelation algorithm: average SIR results over 100 experiments and standard deviation (STD).

| | $\mathrm{SIR}_1(\,\mathrm{dB})$ | $\mathrm{SIR}_2(\,\mathrm{dB})$ | $\mathrm{SIR}(\,\mathrm{dB})$ | $STD(\mathrm{SIR})$ |
|---|---|---|---|---|
| $k = 2$ (Situation 1) | 37.18 | 33.05 | 35.12 | 8.90 |
| $k = 2$ (Situation 2) | 18.07 | 15.46 | 16.77 | 0.975 |
| $k = 2$ (Situation 3) | 36.49 | 31.84 | 34.17 | 4.92 |
| $k = 3$ (Situation 1) | 22.46 | 21.04 | 21.75 | 5.02 |

#### 3.4.1.2 Results

To assess the performance of the recurrent separation system (3.9) trained by the learning rule (3.15), we conducted some experiments for the cases $k = 2$ and $k = 3$. Here, and throughout this thesis, the performance of the separation technique is quantified according to the following index:

$$\mathrm{SIR}_i = 10 \log \left( \frac{E\{s_i^2\}}{E\{(s_i - \hat{s}_i)^2\}} \right), \tag{3.25}$$

where $s_i$ denotes the actual source and $\hat{s}_i$ its respective estimation (after correct scaling). A global index is defined as $\mathrm{SIR} = 1/n_s \sum_{i=1}^{n_s} \mathrm{SIR}_i$.

*Case of $k = 2$.*

In a first scenario, we consider the separation of two sources uniformly distributed between $[0.1, 1.1]$. The mixing parameters were given by $a_{12} = 0.5$ and $a_{21} = 0.5$; $n_d = 3000$ samples were considered and the number of iterations regarding the learning algorithm (3.15) was 3500 with a learning step of $\mu = 0.05$. The initial conditions of the dynamics (3.9) were chosen as $[y_1(1)\ y_2(1)]^T = [0\ 0]^T$. The results of this first case are expressed in the first row of Table 3.1. In Figure 3.5, the joint distributions of the mixtures and of the retrieved signals are depicted for a typical case ($\mathrm{SIR} = 35\,\mathrm{dB}$). Note that the outputs of the separating system are almost uniformly distributed, which indicates that the separation task was fulfilled. Also, we performed experiments by considering on each sensor an additive white Gaussian noise with of $\mathrm{SNR} = 15\,\mathrm{dB}$. The results for this second scenario are depicted in the second row of Table 3.1.

A third scenario was composed by a uniformly distributed source between $[0.3, 1.3]$ and a sinusoidal source varying in the range $[0.2, 1.2]$. In this case, the mixing parameters were given by $a_{12} = 0.6$ and $a_{21} = 0.6$ and the parameters related to the separating system were adjusted as in the first experiment. Again, the satisfactory SIRs presented in the third row of Table 3.1 indicate that our method was able to separate the source in this case.

*Case of $k = 3$.*

The problem becomes more tricky when $k = 3$. Firstly, we observed through simulations that, even for a separating point $[w_{12}\ w_{21}]^T = [a_{12}\ a_{21}]^T$ that satisfies the equilibrium condition (3.12), the structure (3.9) does not guarantee source separation, since there may be another

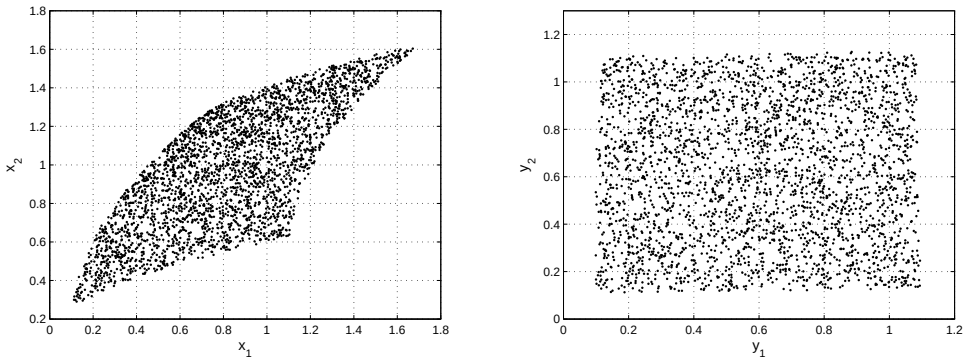


(a) Mixed signals. (b) Retrieved signals.

Figure 3.5: Nonlinear decorrelation algorithm: first situation (separation of uniformly distributed sources) - $k = 2$.

stable equilibrium solution that has no relation with the sources. In this particular case, we observed, after performing some simulations, that the adopted network may be attracted by a stable limit cycle and, also, that it is possible to overcome this problem by changing the initial conditions of (3.9) when a periodic equilibrium solution occurs.

A second problem in this case is related to the convergence of the learning rule. Some simulations suggested the existence of spurious minima in this case. These two problems result in a performance degradation of the method when compared to the case $k = 2$, as can be seen in the last row of Table 3.1. In this case, we considered a scenario with two sources uniformly distributed between $[0.3, 1.3]$ and mixing parameters given by $a_{12} = 0.5$ and $a_{21} = 0.5$. The initial conditions of (3.9) were defined as $[0.5\ 0.5]^T$. Also, we considered $n_d = 3000$ samples and 10000 iterations of the learning algorithm with $\mu = 0.01$.

### 3.4.2 Approach based on mutual information

If, on the one hand, Equation (3.15) results in a simple learning rule demanding only the estimation of some higher-order statistics, on the other hand, we saw that it presents some convergence problems which may be exacerbated especially if the sources are close to the stability boundary of the recurrent separating network (this was the case for $k = 3$). Therefore, aiming to obtain a more robust learning algorithm, we investigate whether it is possible to set an alternative algorithm based on the mutual information minimization.

#### 3.4.2.1 Minimizing the mutual information: a first idea

For a 2-D random vector constituted of two random variables $y_1$ and $y_2$, the mutual information is defined as

$$I(\mathbf{y}) = H(y_1) + H(y_2) - H(y_1, y_2). \tag{3.26}$$

As discussed in Section 1.3, a common trick to avoid the estimation of the joint entropy $H(y_1, y_2)$ consists in expressing it as a function of the joint entropy of the mixtures. Thus, considering

that the mapping provided by (3.26) after the convergence is invertible in the region containing the mixed signals and applying the entropy transformation law [130, 90], one obtains:

$$I(\mathbf{y}) = H(y_1) + H(y_2) - H(\mathbf{x}) - E\{\ln(|\det \mathbf{J}|)\}, \tag{3.27}$$

where $\mathbf{J}$ is the Jacobian matrix associated with the separating system mapping. Since the term $H(\mathbf{x})$ does not depend on $\mathbf{w}$, the minimization of (3.27) becomes equivalent to minimizing

$$C(\mathbf{y}) = H(y_1) + H(y_2) - E\{\ln(|\det \mathbf{J}|)\}. \tag{3.28}$$

We conducted some tests with a gradient-based algorithm to optimize (3.28). We checked that the resulting algorithm was quite dependent on a good estimation of the score functions; a numerical example can be found in [60]. This limitation motivated us to consider an approach based on the notion of the mutual information differential, described in Section 3.4.2.2. However, as shown by Yannick Deville and collaborators in a recent[9] technical report [53], there is, in [60], an error in the calculation of the gradient of (3.28); more precisely in the Jacobian term[10]. Therefore, instead of attributing this bad performance to the estimation of the score functions, it could be simply a result of the calculation errors. However, this question seems tricky. Indeed, we observed, in preliminary simulations, that even when the correct calculation is considered, the gradient-based algorithm to optimize (3.28) works only when a very accurate estimation of the score functions is available. We intend to continue our investigation to clarify this point in future works.

#### 3.4.2.2 Minimizing the mutual information: an approach based on the notion of the mutual information differential

We develop in this section an alternative learning rule for minimizing the mutual information. Motivated by the difficulties in working with Equation (3.28), we consider the direct minimization of (3.27). In fact, although equivalent from a theoretical standpoint, expressions (3.27) and (3.28) may lead, in a nonlinear context, to different practical algorithms. Moreover, due to the estimator errors, the performance of these two algorithms is not the same. This can be explained by the different statistical properties of the estimators considered in both approaches, as demonstrated in [2] for the case of PNL models.

The direct minimization of (3.27) can be carried out by considering the notion of the differential of the mutual information, introduced in [18]. In this work, it was shown that a small variation $\Delta\mathbf{y}$ of a given random vector $\mathbf{y}$ results, up to higher-order terms (expressed by $o(\Delta\mathbf{y})$), in the following variation of the mutual information

$$I(\mathbf{y} + \Delta\mathbf{y}) - I(\mathbf{y}) = E\{\Delta\mathbf{y}^T \beta_{\mathbf{y}}(\mathbf{y})\} + o(\Delta\mathbf{y}), \tag{3.29}$$

[9] This error was showed to the author by Prof. Deville during the evaluation of the present work.

[10] One must take into account the indirect terms given by the total derivative. These terms come from the recurrent terms of the separating system.

where $\beta_{\mathbf{y}}(\mathbf{y})$ is the score function difference vector associated with the random vector $\mathbf{y}$. This result allows one to interpret $\beta_{\mathbf{y}}(\mathbf{y})$ as the gradient[11] of the mutual information with respect to $\mathbf{y}$. In mathematical terms, the $i$-th element of $\beta_{\mathbf{y}}(\mathbf{y})$ is given by

$$\beta_{y_i}(\mathbf{y}) = \left(-\frac{d \ln p(y_i)}{dy_i}\right) - \left(-\frac{\partial \ln p(\mathbf{y})}{\partial y_i}\right), \tag{3.30}$$

where $-\frac{\partial \ln p(\mathbf{y})}{\partial y_i}$ denotes the $i$-th component of the joint score function of $\mathbf{y}$ and $-\frac{d \ln p(y_i)}{dy_i}$ the marginal score function of $y_i$. It can be proved [18] that $\mathbf{y}$ have independent components if, and only if, $\beta_{y_i}(\mathbf{y}) = 0$ for every $i$.

The result expressed in (3.29) provides the guidelines for setting a learning algorithm according to the minimum mutual information idea. However, as we are interested in the gradient of (3.27) with respect to $\mathbf{w}$, we must find how a small variation of the separating system parameters $\mathbf{w}$, denoted $\Delta\mathbf{w}$, affects the small variation $\Delta\mathbf{y}$. This can be done by considering the linearized version of the separating system (3.9), that is

$$\begin{bmatrix} \Delta y_1 \\ \Delta y_2 \end{bmatrix} = \frac{\partial \mathbf{y}}{\partial \mathbf{w}} \Delta\mathbf{w} = \begin{bmatrix} \frac{\partial y_1}{\partial w_{12}} & \frac{\partial y_1}{\partial w_{21}} \\ \frac{\partial y_2}{\partial w_{12}} & \frac{\partial y_2}{\partial w_{21}} \end{bmatrix} \begin{bmatrix} \Delta w_{12} \\ \Delta w_{21} \end{bmatrix}. \tag{3.31}$$

The elements of $\frac{\partial \mathbf{y}}{\partial \mathbf{w}}$ were already calculated in this chapter and are given by Equations (3.21), (3.22), (3.23) and (3.24).

Finally, by substituting (3.31) into (3.29) one readily obtains:

$$I(\mathbf{y} + \Delta\mathbf{y}) - I(\mathbf{y}) = E\left\{\Delta\mathbf{w}^T \frac{\partial \mathbf{y}}{\partial \mathbf{w}}^T \beta_{\mathbf{y}}(\mathbf{y})\right\} + o(\Delta\mathbf{y}). \tag{3.32}$$

This expression allows one to establish the gradient of the mutual information with respect to the parameters $\mathbf{w}$:

$$\frac{\partial I(\mathbf{y})}{\partial \mathbf{w}} = E\left\{\frac{\partial \mathbf{y}}{\partial \mathbf{w}}^T \beta_{\mathbf{y}}(\mathbf{y})\right\}. \tag{3.33}$$

Therefore, it is expected that the following learning rule minimizes the mutual information between the reconstructed sources

$$\mathbf{w} \leftarrow \mathbf{w} - \mu E\left\{\frac{\partial \mathbf{y}}{\partial \mathbf{w}}^T \beta_{\mathbf{y}}(\mathbf{y})\right\}, \tag{3.34}$$

where $\mu$ denotes the learning rate.

Concerning the estimation of the score function difference vector $\beta_{\mathbf{y}}(\mathbf{y})$ in (3.34), we considered the method proposed in [134]. In short, this is a kernel-based method which differs from the classical approaches in two points: the estimation is done over a regular grid and a

[11] As pointed out in [18], an intuitive way to understand this result is to consider a N-dimensional (and deterministic) function $f(\mathbf{y})$. Indeed, for a small perturbation $\boldsymbol{\epsilon}_{\mathbf{y}}$, we can write

$$f(\mathbf{y} + \boldsymbol{\epsilon}_{\mathbf{y}}) - f(\mathbf{y}) = \boldsymbol{\epsilon}_{\mathbf{y}}^T \frac{\partial f(\mathbf{y})}{\partial \mathbf{y}} + o(\boldsymbol{\epsilon}_{\mathbf{y}}^2);$$

where $\frac{\partial f(\mathbf{y})}{\partial \mathbf{y}} = [\frac{\partial f(\mathbf{y})}{\partial y_1} \cdots \frac{\partial f(\mathbf{y})}{\partial y_N}]^T$ corresponds to the gradient of $f(\mathbf{y})$ with respect to $\mathbf{y}$. That said, an analogy between this expression and (3.29) suggests that $\frac{\partial I(\mathbf{y})}{\partial \mathbf{y}} = \beta_{\mathbf{y}}(\mathbf{y})$.

cardinal spline is used as kernel function. As a consequence, one obtains a faster algorithm than the classical kernel method. As remarked in [15], although originally developed for estimating conditional score functions, this method can also be used for estimating $\beta_{\mathbf{y}}(\mathbf{y})$.

#### 3.4.2.3 Results

This section is devoted to assess the learning rule (3.34). We consider the detection of $Ca^{2+}$ and $Na^{+}$ ($k = 2$). The sources in our experiments were artificially generated, but the mixtures were obtained using the selectivity coefficients (shown in the first row of Table 3.2) extracted from the experiments S3Na10$^{-4}$Ca and S3Na10$^{-1}$Ca, described in Chapter 2. The responses of the electrodes in these experiments are plotted in Figure. 3.6, which also depicts the predicted responses provided by the NE model.

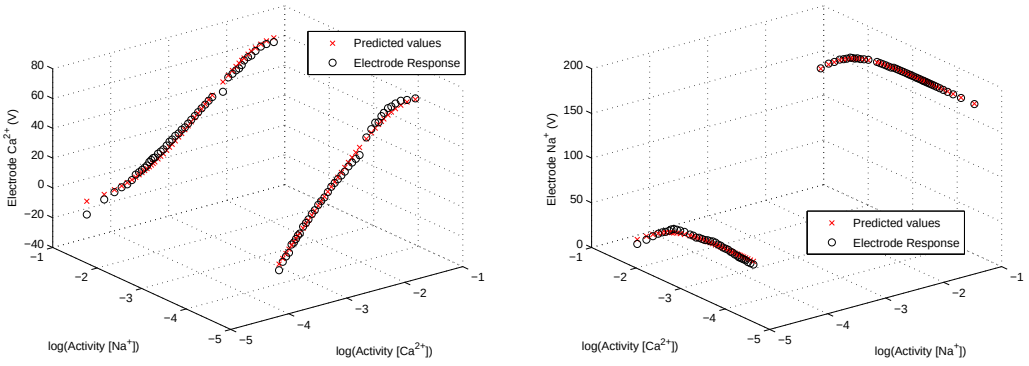


(a) $Ca^{2+}$ electrode response. (b) $Na^{+}$ electrode response.

Figure 3.6: Electrodes responses in the experiments S3Na10$^{-4}$Ca and S3Na10$^{-1}$Ca .

We also consider a second scenario where the selectivity coefficients are higher than the ones of the first case. Actually, this will permit us to assess the performance of the BSS method in a situation where the interference takes place in the two electrodes. In this case, the values of the selectivity coefficients, which are presented in the second row of Table 3.2, were taken from [152].

Table 3.2: Selectivity coefficients considered in the experiments

| | $a_{12}$ | $a_{21}$ |
|---|---|---|
| First scenario (from experiments of Chapter 2) | 0.0589 | 0.0001 |
| Second scenario (from [152]) | 0.1995 | 0.3981 |

*Performance of the source separation method*

For the first scenario, we consider a situation in which the activity of the ion $Ca^{2+}$ lies in the interval $[10^{-4}, 10^{-3}]$M, whereas the activity of $Na^{+}$ varies between $[10^{-4}, 10^{-1}]$M. In Figure 3.7, we present the artificial sources generated for this case and also the mixtures generated by (3.5).

A set of $n_d = 500$ samples of the mixtures was considered. The learning rate was set $\mu = 0.003$ and the initial conditions of the recurrent network were $[y_1(1)\ y_2(1)]^T = [0\ 0]^T$. In this situation, the learning algorithm converged after 8500 iterations. The results of this first case are expressed in the first row of Table 3.3. Our method was able to separate the sources, as can be seen in Figure 3.7. For matter of comparison, we also show in the second row of Table 3.3, the results obtained with the nonlinear decorrelation method presented in Section 3.4.1.

Table 3.3: Obtained SIR for both scenarios.

| | $SIR_1$ (dB) | $SIR_2$ (dB) | SIR (dB) |
|---|---|---|---|
| First scenario (mutual information algorithm) | 56.90 | 56.35 | 56.62 |
| First scenario (nonlinear decorrelation algorithm) | 33.78 | 30.54 | 32.16 |
| Second scenario (mutual information algorithm) | 43.77 | 35.70 | 39.74 |
| Second scenario (nonlinear decorrelation algorithm) | 36.96 | 40.78 | 38.87 |

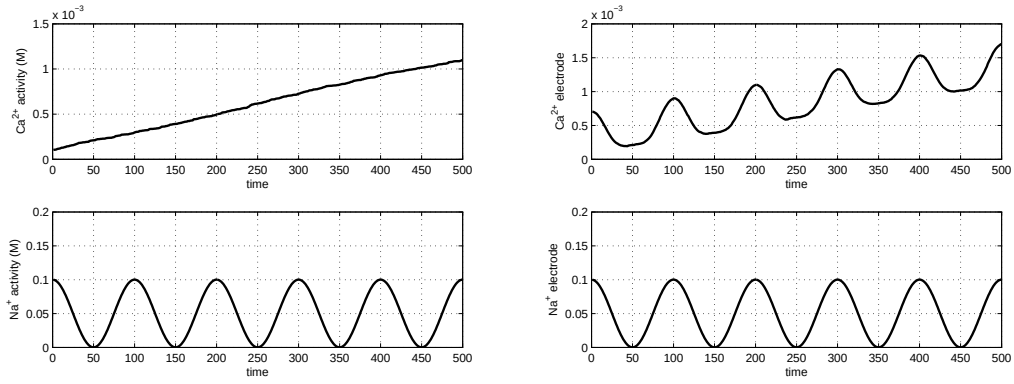


(a) Sources.




(b) Mixtures.

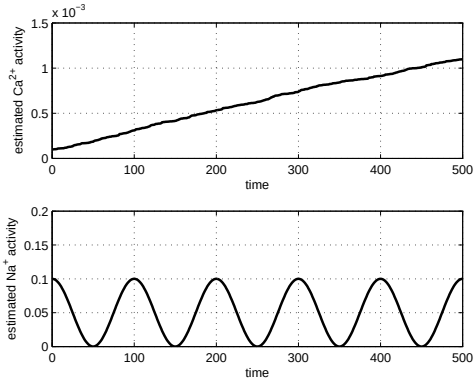


(c) Retrieved sources after 8500 iterations.

Figure 3.7: Mutual information minimization algorithm: sources, mixtures and estimated sources for the first scenario.

For the second scenario, the $Ca^{2+}$ ion activity varies in $[10^{-4}, 10^{-2}]$M while the $Na^+$ activity is varying in $[10^{-4}, 10^{-1}]$M. The sources and the associated mixtures are depicted in Figure 3.8. Note that in this situation, the interference is clear in both electrodes. Again, the number of

available samples was $n_d = 500$. The convergence was observed after 600 iterations while the learning rate in this case was set $\mu = 0.01$. As can be checked in the third row of Table 3.3, our proposal was able to provide good source estimations and performed better than the method introduced in Section 3.4.1 (fourth row of Table 3.3). This is illustrated in Figure 3.8, where we show the retrieved sources in a typical situation. Finally, we present in Figure 3.9, the evolution of the $[w_{12}\ w_{21}]^T$ during the learning algorithm. Note that these parameters indeed converge to the ideal values which are given by selectivity coefficients $a_{12}$ and $a_{21}$.

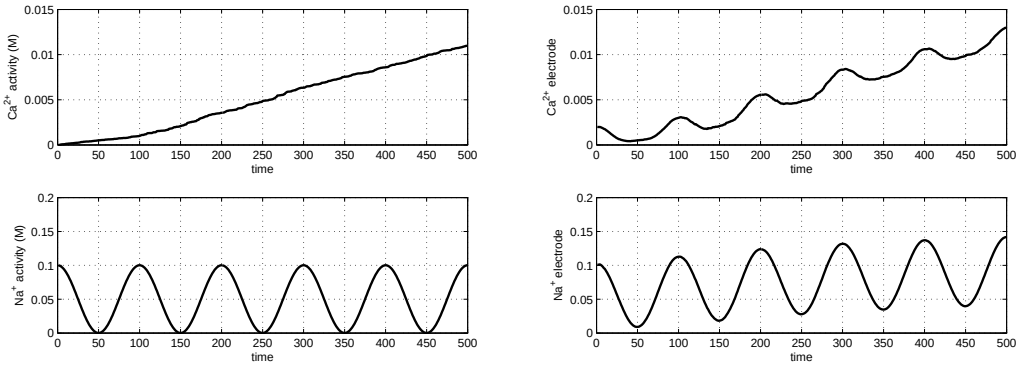


(a) Sources.




(b) Mixtures.

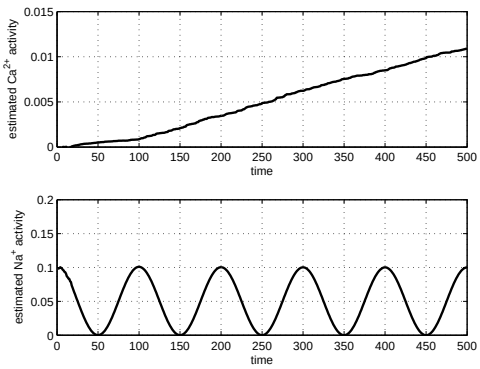


(c) Retrieved sources after 600 iterations.

Figure 3.8: Mutual information minimization algorithm: sources, mixtures and sources estimates for the second scenario.

*Sensitivity to noise*

As discussed in Chapter 1, the NE model, although widely used, has some limitations and, in some cases, gives only an approximate description. Motivated by that, we here conduct some experiments with the aim of investigating how sensitive to noise the proposed method is. The following two situations were considered:

1. Additive white Gaussian noise (AWGN), represented by $n_i$, inside the logarithm of the NE

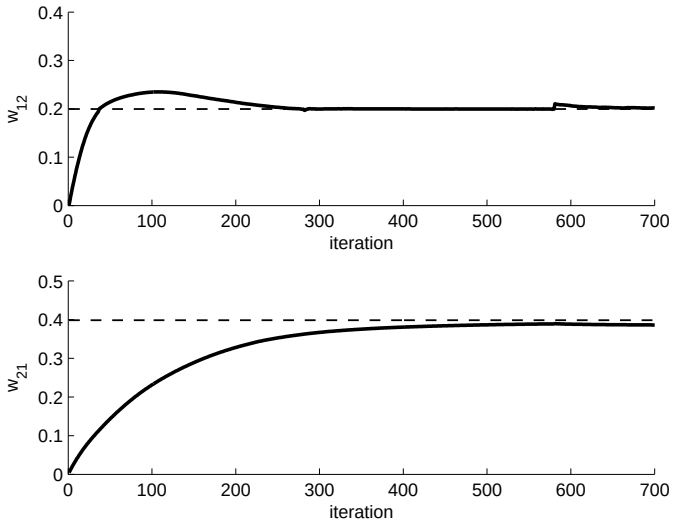


Figure 3.9: Mutual information minimization algorithm: evolution of the separating system parameters (solid) and the selectivity coefficients (dashed)

equation, which, for the simplified NE model (3.5), becomes

$$x_i = s_i + a_{ij} s_j^{z_i/z_j} + n_i. \tag{3.35}$$

This noise here is associated with model error due to the missing interfering ions and will be called "internal" noise.

2. AWGN, represented by $n_i$, outside the logarithm of the NE equation, that is

$$x_i^* = e_i + d_i \log(s_i + a_{ij} s_j^{z_i/z_j}) + n_i. \tag{3.36}$$

This noise will be called "external" noise. In view of Equation (3.4), the external noise model is equivalent to a multiplicative noise in the simplified NE model (3.5):

$$x_i = 10^{\frac{e_i + d_i \log(s_i + a_{ij} s_j^{z_i/z_j}) + n_i - e_i}{d_i}} = \left(s_i + a_{ij} s_j^{z_i/z_j}\right) 10^{\frac{n_i}{d_i}}. \tag{3.37}$$

We investigated these noise models in the separation of sources uniformly distributed between $[0.1, 1.1]$ with $k = 2$. In Figure 3.10, which represents the average of 30 experiments, we plot the performance index SIR as a function of the SNR for both noise models. Note that, for a same SNR, the noise model (3.36) culminates in a larger performance degradation when compared to the model (3.35). In fact, this can be attributed to the noise amplification introduced by power term in Equation (3.4) —as discussed before, this preprocessing stage results in the presence of a multiplicative noise in the simplified NE model. Finally, we remark that the proposed method can provide good SIR for SNR equivalent to the SNR obtained in the regressions with real data presented in Chapter 2.

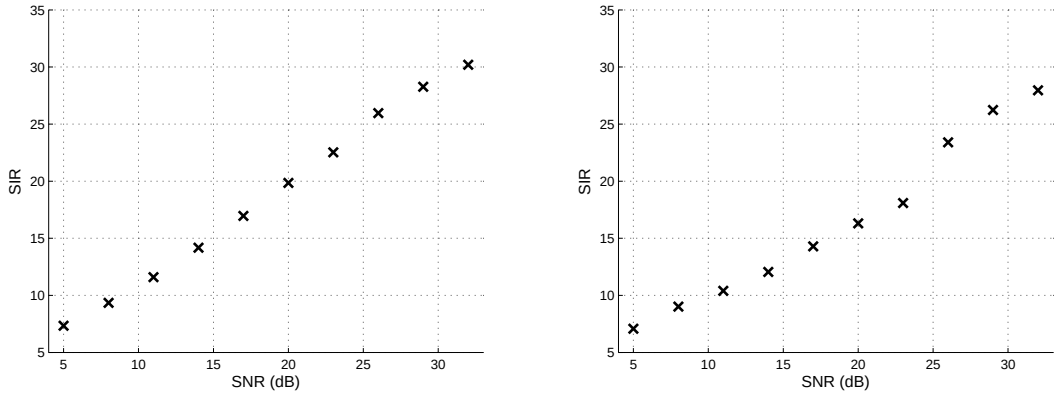


(a) Output SIR versus "internal" noise SNR. Model (3.35) (AWGN inside the logarithm).

(b) Output SIR versus "external" noise SNR. Model (3.36) (AWGN outside the logarithm).

Figure 3.10: Mutual information minimization algorithm: influence of noise.

*Influence of the number of samples*

We also investigated the performance degradation of our method as the number of available samples decreases. Our motivation for this analysis comes from the fact that in the envisaged chemical sensing application the number of samples is usually small. In this study, we consider a scenario with sources uniformly distributed and $k = 2$. We checked through simulations that good estimations are provided for SIR higher than 20 dB. Therefore, as we can see in Figure 3.11, where each result represents the average of 20 experiments, the proposed algorithm works properly with a number of samples equal to or greater than $n_d = 400$. This large number is necessary for properly estimating the score function difference vector present in (3.18).

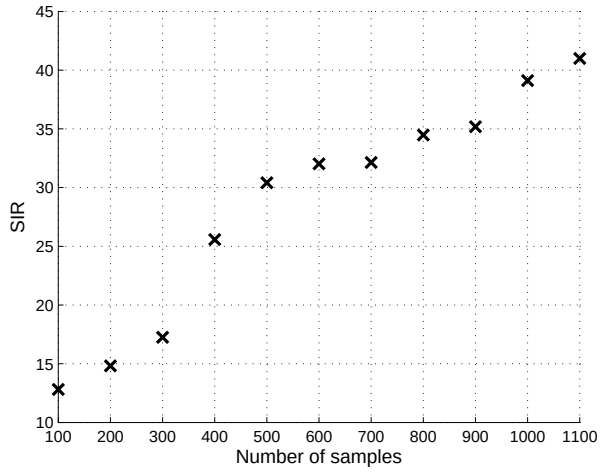


Figure 3.11: Mutual information minimization algorithm: influence of the number of samples.

*An example of source separation for the case $k = 3$*

In this section, we investigate the performance of the ICA method for the case $k = 3$. For that, the separation of two sources uniformly distributed between $[0.2, 1.2]$ is considered. The mixing parameters are given by $a_{12} = a_{21} = 0.5$ and the learning step by $\mu = 0.008$. In this situation, there are a few samples of the sources that do not satisfy the stability condition (3.12). Thus, the adopted separating system will never converge to these samples which means that they cannot be retrieved. Also, these samples act as a kind of noise in the adaptation stage, in the sense that even for an ideal separating system, there are outputs that are still mixtures of the sources which may disturb the separating criteria.

Regardless the problem discussed above, our proposal performs well in this scenario: we obtained $\mathrm{SIR}_1 = 39.41\,\mathrm{dB}$ and $\mathrm{SIR}_2 = 36.4\,\mathrm{dB}$ (average of 50 simulations). However, we observed that the algorithm did not converge in 2 among the 50 experiments. In Figure 3.12, the joint distributions of the mixtures and of the retrieved signals are depicted for a typical case. Note that the outputs of the separating system are almost uniformly distributed, which indicates that the separation task was accomplished.

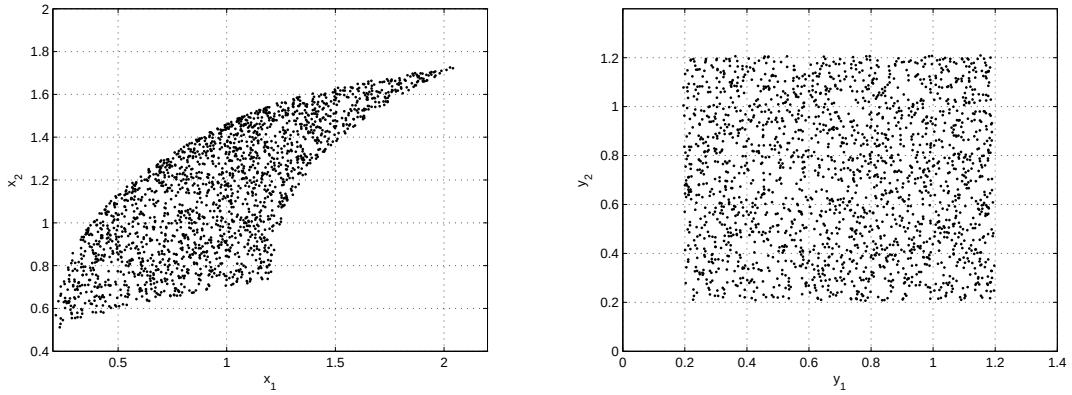


(a) Mixed signals. (b) Retrieved signals.

Figure 3.12: Mutual information minimization algorithm: example of source separation when $k = 3$.

### 3.4.3 Separability issues

In our experiments, we did not observe any solution that gave independent components which were still mixed versions of the sources. In other words, no counterexample to the separability of the mixing model (3.5) was found. Of course, this observation is by no means a proof[12] but, at least, it validates, in a certain extent, an ICA formulation for this class of mixing model.

A possible way to gain some insight into the separability of the model (3.5) can be achieved

[12]Proving the separability of (3.5) seems to be a difficult task. Indeed, unlike the PNL model, it is not possible to prove the separability of (3.5) based on the separability of the linear model. Moreover, the model (3.5) does not satisfy the addition theorem [64], which guarantees separability.

by analyzing the mutual information between the retrieved signals $y_1$ and $y_2$ as a function of separating system parameters. In this spirit let us consider an example where the sources are uniformly distributed in $[0.1, 1.1]$ and the mixing coefficients are given by $a_{12} = a_{21} = 0.5$. In Figure 3.13, we plot the logarithm of the mutual information[13] $I(y_1, y_2)$ as function of $w_{12}$ and $w_{21}$, the parameters of the separating system (3.9). Note that the global minimum is indeed located near the point $w_{12} = w_{21} = 0.5$, which corresponds to the ideal solution in terms of source separation.

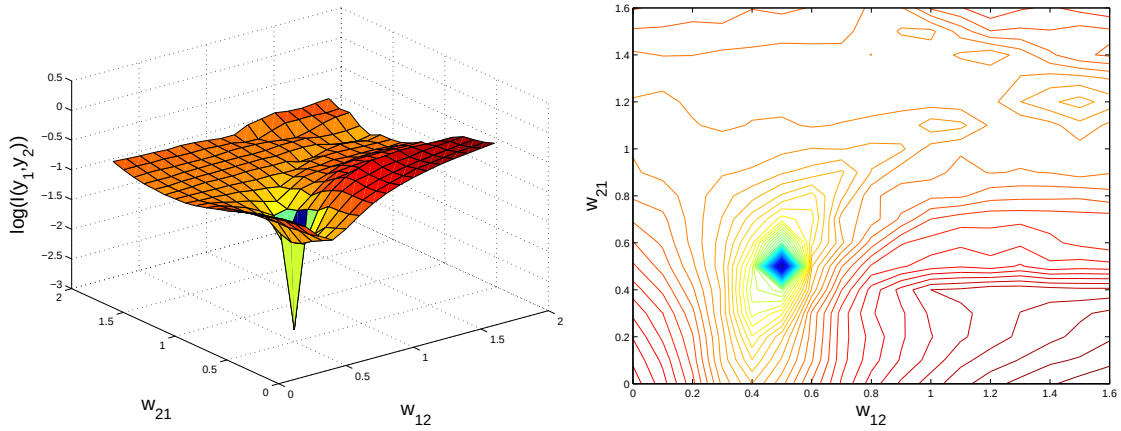


Figure 3.13: Logarithm of the mutual information between $y_1$ and $y_2$ as a function of the separating system parameters $w_{12}$ and $w_{21}$. Left: surface. Right: contour.

## 3.5 Toward a complete solution

Before closing this chapter, let us discuss some issues related to an ICA solution for the situation in which the slopes $d_i$ considerably deviates from the value predicted by the NE model. In these cases, as discussed before, the methods developed for the simplified model (3.5) are useless and, therefore, it becomes necessary to set a strategy for estimating $d_i$. Of course, a first idea in this spirit is to extend the ICA approach to the "complete" NE model (Equation (3.1)). The separating system in this case is similar to the one considered for PNL mixtures (see Figure 1.6). However, we must replace the linear separating stage by the recurrent network defined for the simplified NE model (Equation (3.9)).

A first problem in developing an ICA method for the mixing model (3.1) is related to the stability of the recurrent network. Actually, there is an enormous risk of instability when the parameters $d_i$ and the parameters of the recurrent network are adjusted at the same time; we could observe this problem in practice during our attempts to build an ICA solution based on a gradient-descent minimization.

Besides this practical problem, the separability of the complete NE model is also a relevant open problem. In the last section, we saw that even for the simplified model (3.5), although we did not find counter examples, there is no result assuring separability in this case.

[13] In this example, the mutual information was estimated through the method proposed in [118].

Regardless of those problems, it is still possible to investigate whether an ICA solution is, at least, feasible in such a case. In this spirit, let us consider a situation with $n_s = 2$ uniformly distributed sources, $n_m = 2$ mixtures and $n_d = 2000$ samples. The mixing coefficients in this example are given by: $a_{12} = 0.5$, $a_{21} = 0.5$, $d_1 = 0.59$ and $d_2 = 0.59$.

To set an ICA method in this case, one must resolve the following optimization problem:

$$\min_{w_{12},w_{21},d_1,d_2} I(y_1, y_2). \tag{3.38}$$

To cope with the instability problem, we consider the evolutionary technique described in Appendix B to optimize (3.38). This algorithm requires estimating $I(y_1, y_2)$, which was done according to the method presented in [46]. The optimization of (3.38) has led to estimations ($\hat{w}_{12} = 0.46$, $\hat{w}_{21} = 0.45$, $\hat{d}_1 = 0.61$ and $\hat{d}_2 = 0.58$) close to the actual values, which means that the separating system was able to retrieve good estimations of the sources. This can be confirmed in Figure 3.14 which depicts the scatter plots of the sources, the mixtures and the recovered sources.

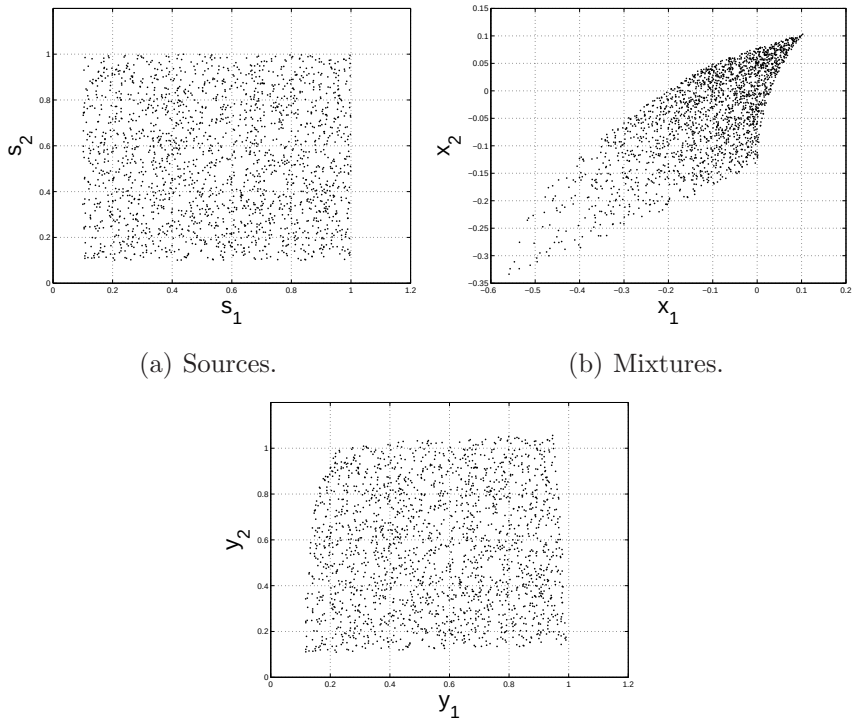


(a) Sources. (b) Mixtures.

(c) Recovered sources.

Figure 3.14: Applying ICA to the complete NE model: scatter plots.

Despite these good results, this example serves only to illustrate the applicability of ICA methods to the NE model. In fact, the approach adopted in this section suffers from several drawbacks that may limit its application to a real problem. Firstly, we observed that it does not work when the number of samples is smaller than 1000. Moreover, the conjunction evolutionary method/mutual information estimator results in a rather time-demanding algorithm even when only two sources are considered.

## 3.6 Conclusion

In this chapter, we investigated source separation methods for potentiometric arrays designed for analyzing ions of different valences. We considered a recurrent separating system that was able to perform a sort of implicit inversion of the mixing system. We showed that the stability of this recurrent network depends on the range of the sources and on selectivity coefficients.

Concerning the learning rule, an ICA approach based on nonlinear decorrelation criterion was studied in a first moment. Then, in order to obtain a more robust method, we investigated ICA methods based on the minimum mutual information principle. We considered an approach based on the notion of the differential of the mutual information. Simulation results indicated the efficacy of our proposal but, on the other hand, showed that it requires a relative large number of samples to achieve good estimations for the sources. Moreover, the application of the methods developed in the present chapter to the actual data described in Chapter 2 is not possible. Actually, the sources in the performed experiments were clearly dependent, thus violating the fundamental assumption of statistical independence considered in the ICA formulation of the present chapter.

Finally, we discussed the difficulties in developing an ICA method for the complete NE model. Motivated by these limitations, we will show in the next chapter how the incorporation of prior information can simplify the derivation of source separation algorithms.

# Chapter 4

# Source separation methods incorporating prior information

## 4.1 Introduction

Originally, the study on source separation focused on scenarios where a minimum amount of prior information is available. In ICA methods, for instance, only the independence between the sources is assumed. More recently, however, there is a clear trend toward methods in which some additional prior information is taken into account. The reason for that is simple: in many problems, additional information appears in a very natural way and, very often, by considering it, one obtains a better performance or a simpler algorithm or both.

In this chapter, we investigate the use of prior information in the context of the nonlinear mixing models associated with chemical sensor arrays. More precisely, we describe two contributions showing that, based on additional prior information, it becomes possible to estimate the component-wise nonlinear functions present in the NE model. In a first moment (Section 4.2), we address the same case studied in the last chapter: ISE arrays for detecting ions of different valences. Then, in a second moment (Section 4.3), we turn our attention to the PNL model, which, as discussed before, is related to the detection of ions of equal valences.

## 4.2 Incorporating prior information through a geometric approach

In this section, we consider the same problem treated in Chapter 3: the detection of two ions having different valences through an array composed of different ISEs. According to the NE model, this situation is given by[1]

$$\begin{aligned} x_1(t) &= d_1 \log\Big(p_1(t)\Big) = d_1 \log\Big(s_1(t) + a_{12} s_2(t)^k\Big) \\ x_2(t) &= d_2 \log\Big(p_2(t)\Big) = d_2 \log\Big(s_2(t) + a_{21} s_1(t)^{\frac{1}{k}}\Big) \end{aligned} , \tag{4.1}$$

[1]The offset terms $e_i$ present in NE equation are not considered here because they only introduce a scale ambiguity.

where $k = z_1/z_2$.

In the last chapter we developed an ICA method for Equation (4.1) assuming that the parameters $d_i$ are known in advance. As discussed in Section 3.5, there are some problems in the design of a complete source separation method for the model (4.1), e.g. the risk of instability. A possible way to overcome these limitations is to consider a two-stage approach where the parameters $d_i$ are firstly estimated. Then, in a second moment, the recurrent system is adjusted. The difficulty in such an approach resides in the definition of a criterion for dealing with the first stage of (4.1). To cope with this problem, we consider, in addition to the assumptions considered in Chapter 3, the following assumption

**Assumption 1** *There is, at least, a period of time where one, and only one, of the sources takes a constant value different from zero.*

In other words, we are assuming something similar to a silent period in which the activity of one of the ions is constant. This kind of hypothesis is very common in problems involving speech separation. In the context of chemical sources this hypothesis also seems valid in some applications as can be seen in the waveforms presented in [78].

### 4.2.1 Inversion of the NE model component-wise functions

The following parametric model can be considered to invert the first stage of (4.1)

$$\begin{array}{rcl} e_1(t) & = & 10^{\frac{x_1(t)}{d_1^*}} \\ e_2(t) & = & 10^{\frac{x_2(t)}{d_2^*}} \end{array} , \tag{4.2}$$

where $d_i^*$ denotes the unknown parameters. In the sequel, we will show how these parameters can be adjusted with the aid of Assumption 1.

Let us consider a time window where $s_1(t)$ takes a constant value $S_1 \neq 0$. During this time window, according to (4.1), it asserts that

$$\begin{array}{rcl} p_1(t) & = & S_1 + a_{12} s_2(t)^k \\ p_2(t) & = & s_2(t) + a_{21} S_1^{\frac{1}{k}} \end{array} . \tag{4.3}$$

From this expression, it is not difficult to see that

$$p_1(t) = S_1 + a_{12}(p_2(t) - a_{21} S_1^{\frac{1}{k}})^k. \tag{4.4}$$

Hence, under such an assumption, (4.4) is a polynomial of order $k$ in the $(p_1, p_2)$ plane[2].

The next step of our development is to check how the polynomial in the $(p_1, p_2)$ plane is propagated in the $(e_1, e_2)$ plane. By considering (4.1), one can rewrite (4.2) as:

$$\begin{array}{rcl} e_1(t) & = & 10^{\frac{d_1 \log(p_1(t))}{d_1^*}} = p_1(t)^{\frac{d_1}{d_1^*}} \\ e_2(t) & = & 10^{\frac{d_2 \log(p_2(t))}{d_2^*}} = p_2(t)^{\frac{d_2}{d_2^*}} \end{array} . \tag{4.5}$$

[2]Note that such property also holds when $s_2(t)$ takes a constant value and, thus, the same development can also be done for this case.

The polynomial in Equation (4.4) can be expressed by

$$p_1(t) = \sum_{i=0}^{k} \varphi_i p_2(t)^i, \tag{4.6}$$

where the coefficients $\varphi_i$ can be determined by the binomial expansion of (4.4). Therefore, after a straightforward development considering (4.6) and (4.5), the following expression is obtained:

$$e_1(t) = \left[ \sum_{i=0}^{k} \varphi_i e_2(t)^{\frac{d_2^*}{d_2} i} \right]^{\frac{d_1}{d_1^*}}. \tag{4.7}$$

To sum up, we had a polynomial in the $(p_1, p_2)$ plane that was lost in the $(x_1, x_2)$ plane because of the logarithm functions. Based on this observation, the inversion of these functions can be driven by the recovery of a polynomial in the $(e_1, e_2)$ plane (see illustration in Figure 4.1). More precisely, we search for $d_1^*$ and $d_2^*$ that result in a polynomial of order $k$ in the $(e_1, e_2)$ plane. In fact, it is clear that when the optimum solution $(d_1^* = d_1, d_2^* = d_2)$ is achieved, the expression (4.7) is a polynomial of order $k$. Evidently, the reverse question must be investigated: does a polynomial in the $(e_1, e_2)$ plane result necessarily in the solution $(d_1^* = d_1, d_2^* = d_2)$?

A simple inspection of (4.7) reveals a negative answer for the question posed in the last paragraph; there is a particular situation in which a polynomial is obtained although the mapping (4.5) is still nonlinear. In fact, when $S_1$ is null, then all the coefficients except $\varphi_k$ in (4.6) are null. In this situation, expression (4.7) becomes

$$e_1(t) = \left[ \varphi_k e_2(t)^{\frac{d_2^*}{d_2} k} \right]^{\frac{d_1}{d_1^*}},$$

and, thus, the solution $(d_1^* = Dd_1, d_2^* = Dd_2)$, where $D$ is a constant, also gives a polynomial of order $k$ although does not correspond to our desired solution. This explains why it was necessary to consider that $S_1 \neq 0$ in Assumption 1. Although the idea cannot be applied for time windows where $S_1 = 0$, it is noteworthy that one can distinguish between this situation and the case when $S_1 \neq 0$ (the "good case"); if, and only if, $S_1 = 0$, than the obtained polynomial passes through the origin.

Let us now discuss how the idea introduced in the last paragraphs can be implemented. First, we must define a way to check if a set of points in the $(e_1, e_2)$ plane corresponds to a polynomial of order $k$. This can be done by assuming, as a cost function, the mean square of the residuals resulting from the regression of the set of samples $\{(e_1(t), e_2(t))\}_{t=1}^{N}$ (where $N$ is the number of samples) through a polynomial of order $k$. In this context, the following optimization problem can be formulated:

$$\min_{d_1^*, d_2^*} J = \sum_t \left( e_1(t) - \sum_{i=0}^{k} \alpha_i \left( e_2(t) \right)^i \right)^2, \tag{4.8}$$

where $\alpha_i$ corresponds to the $i$-th regression coefficient. In order to gain more insight, let us

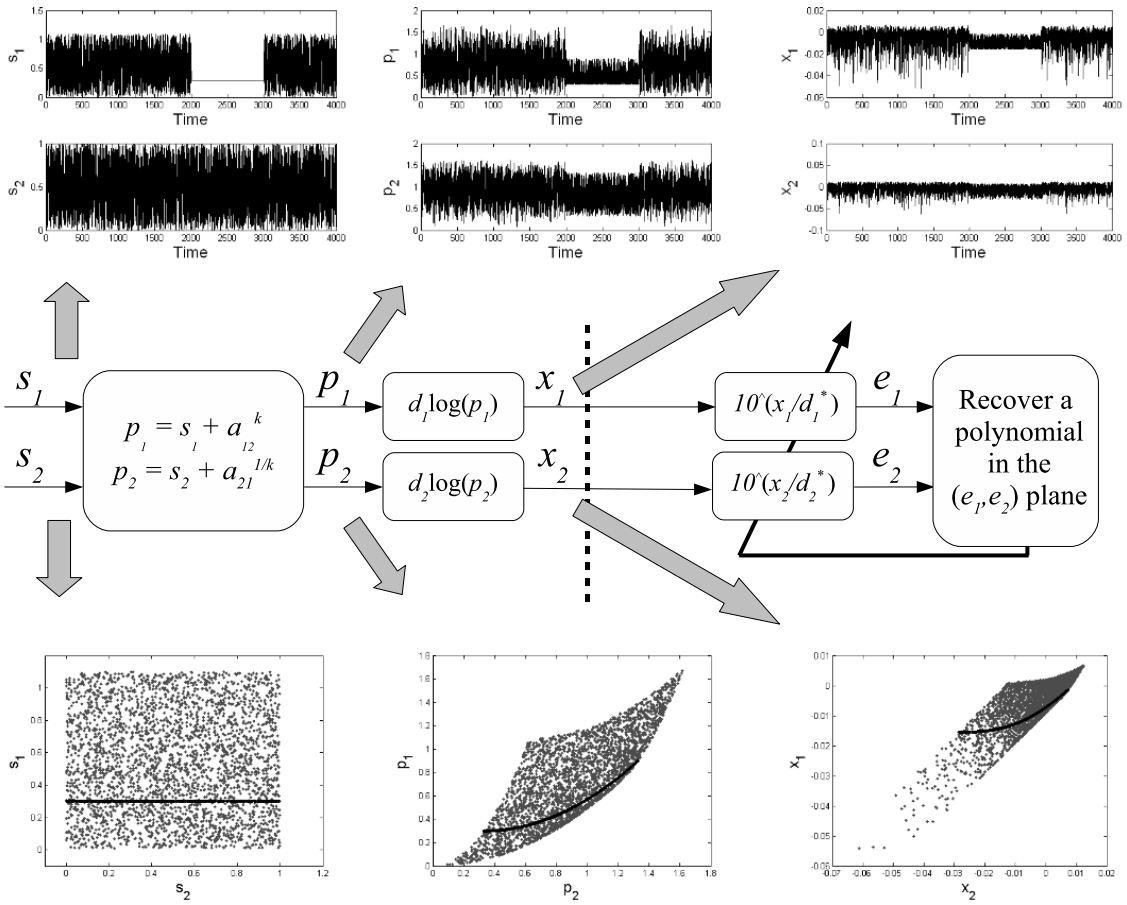


Figure 4.1: Illustration of the proposed idea. Top: signals in time. Bottom: scatter plots of the signals. The time window in which the source $s_1$ has zero-variance is highlighted in the scatter plots. This period results in a polynomial of order $k$ in the $(p_1, p_2)$ plane, which is lost after the logarithm functions. The idea is to adapt $d_1^*$ and $d_2^*$ to restore a polynomial in the $(e_1, e_2)$ plane.

substitute (4.7) into (4.8), which gives

$$\min_{d_1^*,d_2^*} \sum_t \left( \left[ \sum_{i=0}^{k} \varphi_i(e_2(t))^{\frac{d_2^*}{d_2} i} \right]^{\frac{d_1}{d_1^*}} - \sum_{i=0}^{k} \alpha_i \left(e_2(t)\right)^i \right)^2 . \tag{4.9}$$

One may note that this expression is a nonlinear function with respect to the parameters $\{d_1^*, d_2^*\}$. Moreover, in view of Equation (4.7), for a given sample at time $t$ there is an underlying relation between $e_1(t)$ and $e_2(t)$, which in turn makes the regression coefficients $\alpha_i$ nonlinearly dependent on the parameters to be optimized. As a consequence, it becomes difficult to obtain the derivatives of this function. Furthermore, such a cost function may present suboptimum local minima. These problems may pose some problems to the development of gradient-based optimization methods.

### 4.2.2 Detection of silent periods

The idea described in the last section works under the assumption that there is a time window in which one of the sources does not vary. Evidently, if a blind scenario is envisaged, then one should be able to detect this "silent period". A possible way to perform this task is to consider the problem from a geometric standpoint. Given that the mixing model is invertible and the sources are supposed bounded, the borders of the distribution in the $(x_1, x_2)$ plane corresponds to the situation in which one of the source is constant. Therefore, at least in an ideal situation, we could detect the silent periods by estimating the borders of the distribution of the mixtures, in the same way as performed[3] in [17]. Note that this strategy works even when the Assumption 1 is not met. However, this procedure is difficult to implement in practice since it demands a very accurate estimate of the borders, which may be difficult to achieve when the number of samples is small.

A second approach to search the silent periods is based on the fact that when one of the sources is constant, each sensor response corresponds to a deterministic function of the same random variable, i.e. $x_1 = g_1(s_2)$ and $x_2 = g_2(s_2)$. Therefore, such situation is the one with maximum (complete) dependence between the sensors and, thus, we may try to identify the silent periods by searching time windows for which a measure of dependence is maximized[4]. This idea has already been developed for linear source separation in [52] where the silent periods are found by observing the second-order correlation measure. In our case, however, we deal with a nonlinear model and, as consequence, it is more prudent[5] to employ a measure able to detect nonlinear dependences. A natural candidate in this case is the mutual information.

The mutual information of two continuous random variables lies on the interval $0 \leq I(x_1, x_2) < +\infty$, being zero when $x_1$ and $x_2$ are statistically independent, and tending to infinity when there is a deterministic relation between these variables. Therefore, we can find the silent periods by looking at the time windows for which the mutual information is maximized. In fact, it is more practical to maximize a normalized version of the mutual information [45] defined as

$$\varsigma(x_1, x_2) = \sqrt{1 - \exp(-2I(x_1, x_2))},$$

where $I(x_1, x_2)$ corresponds to the mutual information between $x_1$ and $x_2$. It is easy to verify that $\varsigma(x_1, x_2) \in [0, 1]$ and its maximum value is attained when there is a deterministic relationship between $x_1$ and $x_2$.

To illustrate the idea of the last paragraph, we present in Figure 4.2 the evolution of the normalized mutual information between the sensors response (estimated through a time window of length $W = 151$) and the respective sources. Note that the maximum of the mutual information occurs exactly for time windows containing a constant source.

[3] This work considers the PNL case, i.e. when $k = 1$ in Equation (4.1).

[4] If one is not sure about the existence of, at least, one silent period, then one must compare the normalized mutual information with a threshold close to one.

[5] Note however that [49] employed a method based on a second-order correlation measure to deal with a related problem in the context of LQ mixtures.

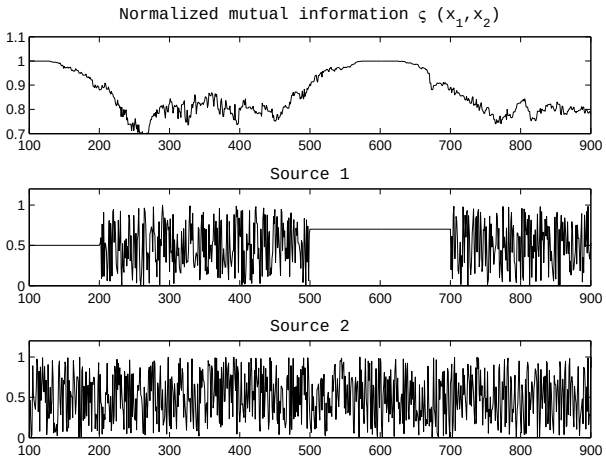


Figure 4.2: Top: Mutual information between the mixtures. Center and bottom: the corresponding sources.

### 4.2.3 Description of a complete source separation method for the NE model

The idea introduced in the preceding sections allows us to set a complete algorithm, which is described in Table 4.1, for the NE mixing model. In the first step (detection of silent periods), we adopted the mutual information estimator proposed in [46]. As already discussed, it is difficult to set a gradient-descent algorithm for optimizing (4.8) in the second stage. In view of this limitation, we consider an optimization based on the opt-aiNet algorithm [47]. This evolutionary method has been proved to be efficient in signal processing applications (see [12], for instance). In addition to its robustness to local minima, the opt-aiNet only needs zero-order information of the cost function, which, as discussed before, is a very interesting feature for our problem. The technical details of this method can be found in Appendix B.

Having counterbalanced the logarithm functions, the final step is to apply the method introduced in Chapter 3 to deal with the second stage of the NE model.

### 4.2.4 Results

To assess the performance of the algorithm described in Table 4.1, we simulated the problem of detecting the ions $Ca^{2+}$ and $Na^{+}$ through an array of two sensors (each one has a different ion as target). For that, we consider the parameters $a_{12} = 0.79$ and $a_{21} = 0.40$, which were taken from [152]. Also, we have assumed that both sensors have a perfect Nerstian response, i.e., $d_1 = 0.029$ and $d_2 = 0.059$.

Concerning the parameters of the algorithm, a set of $n_d = 1000$ samples was considered. The detection of the silent periods was performed by estimating the mutual information for a window of a length of $W = 151$ samples. Actually, we observed that it is difficult to achieve a reliable estimation of the mutual information with a smaller number of samples. Finally, the number of iterations considered in the training of the recurrent network was 1500 and the learning rate was $\mu = 0.02$.

Table 4.1: Complete source separation method for the NE model

1. Detection of silent periods
   - Estimate the mutual information between the mixtures $x_1$ and $x_2$ for a moving-time window of length $W$.
   - Select the time window in which the mutual information is maximum.
2. Estimation of the component-wise functions.
   - For the selected time window, minimize expression (4.8) with respect to $d_1^*$ and $d_2^*$.
3. Application of the recurrent network proposed in Chapter 3.
   - Determine the parameters $w_{ij}$ of (3.9) through the learning rule (3.34). The inputs of the recurrent network are $e_i$.

Under the described scenario and with the two sources shown in Figure 4.3, our method has achieved the following performance indexes $\mathrm{SIR}_1 = 40.52\,\mathrm{dB}$, $\mathrm{SIR}_2 = 38.27\,\mathrm{dB}$ and $\mathrm{SIR} = 39.39\,\mathrm{dB}$, which means that our proposal did well in this case, as can be confirmed by looking at the mixed signals and at the retrieved sources in Figure 4.3.

### 4.2.5 Discussion

Notwithstanding the good results presented in the preceding section, there is a significant performance degradation when the algorithm of Table 4.1 is applied in noisy scenarios. More precisely, we observed that a proper operation of our method needs, at least, a signal-to-noise ratio of $\mathrm{SNR} = 40\,\mathrm{dB}$. This limitation can be attributed to the two following causes. First, as already discussed in Section 3.4.2.3, there is a noise amplification phenomenon in the separating structure due to the exponential functions used for inverting the logarithm functions. Second, as (4.8) is basically the error regression from a polynomial regression, this cost function is sensitive to noise. This becomes even more problematic given that the size of zero-variance periods is usually small, which means that only a small number of samples is considered in the evaluation (4.8).

## 4.3 Separation of PNL mixtures: incorporating prior information in the frequency domain

We now turn our attention to the source separation problem related to potentiometric electrode arrays designed for detecting ions of equal valences. As discussed in Chapter 1, this case results in a PNL mixing model, which is basically composed of a linear mixing stage followed by a set of component-wise functions (see Figure 1.6). We also mentioned in Chapter 1 that some of the PNL methods work in a two-stage basis, in which the nonlinear and linear stages of the PNL

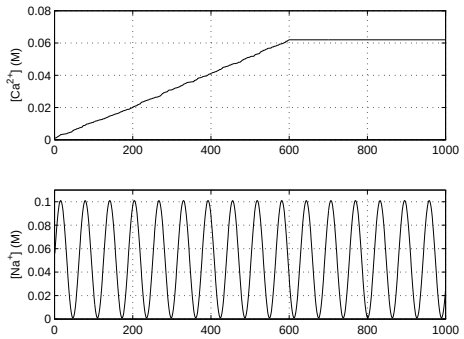


(a) Sources.

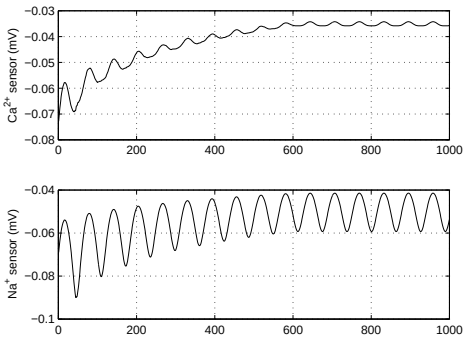


(b) Mixtures.

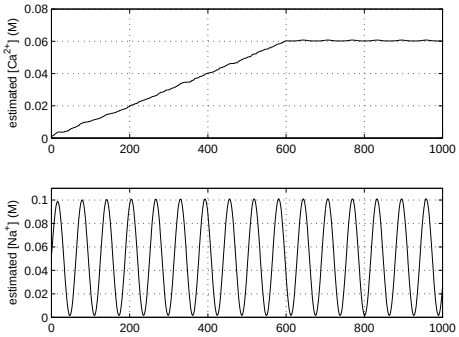


(c) Retrieved sources.

Figure 4.3: Application of the algorithm described in Table 4.1: sources, mixtures and recovered.

model are treated separately. Indeed, if the nonlinear effects introduced in a PNL model can be counterbalanced in a first stage, then the remaining task becomes essentially of linear nature and, thus, can be accomplished in a very efficient way by linear source separation methods.

The main difficulty in the design of a PNL two-stage solution is how to find a criterion for correctly adjust the functions $\mathbf{g}(\cdot) = [g_1(\cdot) \dots g_{n_m}(\cdot)]$ so they can invert the effects introduced by $\mathbf{f}(\cdot) = [f_1(\cdot) \dots f_{n_m}(\cdot)]$. Actually, unlike the linear stage, the non-linear stage $\mathbf{f}(\cdot)$ has a diagonal Jacobian and, thus, does not affect the level of independence between the input signals[6]. This fact eliminates all the possibilities of working with criteria based on independence measurements and, thus, points out that two-stage methods require prior information other than the statistical independence between the sources.

In the context of the application treated in thesis, a first idea would be to develop a two-stage PNL solution based on the same prior information considered in the preceding section (silent periods). In fact, as discussed in Section 4.2.2, this idea is strongly related to the geometrical PNL method proposed in [17], which basically enforces the scatter plots of the signals $q_i(t) = g_i(x_i(t))$ to have linear borders[7]. The main limitation of this method is that its extension to scenarios with more than two sources is complicated. Moreover, as we discussed before, a

[6]We are assuming here $f_i(\cdot)$ is an invertible function

[7]This procedure results in the same idea presented in Section 4.2 when $k = 1$.

geometric approach has the inconvenient of being too sensitive to noise.

In this section we will show that an alternative PNL two-stage solution can be developed by considering that the sources are smooth signals, an assumption which is also realistic in the context of chemical sensors. We shall detail this idea in the sequel.

### 4.3.1 From smooth signals to baseband signals

Before introducing the proposed method, let us discuss some points concerning smooth signals. First of all, it is noteworthy that the definition of a smooth signal is not unique. For example, one can borrow from mathematics the concept of smoothness to characterize a smooth signal as a function that has derivatives of all orders. Alternatively, a smooth signal can be defined as any signal that presents a very slow temporal variation or, equivalently, any signal whose spectral content is concentrated in the low-frequency bands. In this work, we consider this last definition.

Although more representative in practice, defining a smooth signal as a slowly-varying signal is still too broad and, thus, a more rigorous description should be done if one is interested in exploiting this characteristic. In this context, several works [117, 31] consider that the smoothness/slowness of a discrete-time $x(n)$ can be evaluated by

$$\rho = E\{(x(n) - x(n-1))^2\}. \tag{4.10}$$

This quantity, which is nothing but the variance of the first derivative of $x(n)$, is indeed in accordance with the practical notion behind a smooth signals. To illustrate that, we show in Figure 4.4 three different signals (all having the same variance) and the estimated $\rho$ for each case.

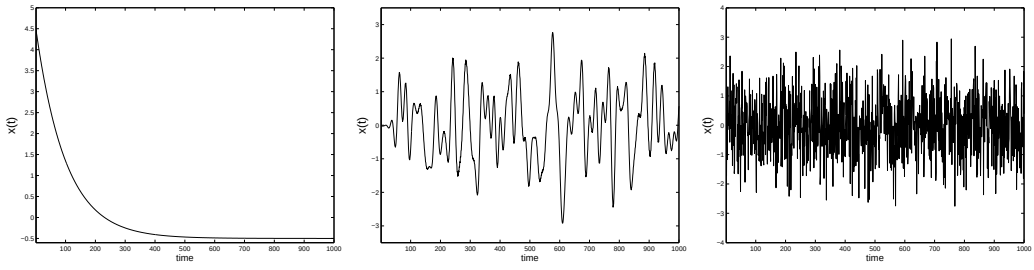


(a) $\rho = 0.0001$ (b) $\rho = 0.0250$ (c) $\rho = 1.9795$

Figure 4.4: Three signals and their respective measure $\rho$, defined in (4.10).

As the derivative operator is associated with high-pass filtering in the frequency domain, expression (4.10) can be equally seen as a measure of the energy associated with the high-frequency components of $x(t)$. This interpretation is helpful in that it points out a close relationship between the rationale behind (4.10) and the concept of a baseband signal. Indeed, a baseband signal is defined as a signal whose energy beyond a given frequency (bandwidth) is null. Note, however, that one can easily find a baseband signal having a high $\rho$; that is, the concept of baseband signal is wider than the definition of smoothness based on (4.10).

In the rest of this chapter, we will focus on the assumption that the sources are baseband signals. As discussed in the preceding paragraph, baseband signals are related to slowly-varying signal, which is a typical characteristic of chemical signals. Moreover, the notion of a baseband signal is somewhat more precise[8] than classifying a signal as smooth according (4.10).

### 4.3.2 Preliminaries: mixing model and assumptions

In our development, we will consider the notation shown in Figure 1.6, where $z_i(t)$ and $q_i(t)$ denote the $i$-th output of the linear mixing stage and the $i$-th output of the nonlinear separating stage, respectively. Our goal in this section will be to define a strategy for adjusting the nonlinear functions $\mathbf{g}(\cdot) = [g_1(\cdot), g_2(\cdot), \ldots, g_{n_m}(\cdot)]^T$ to invert $\mathbf{f}(\cdot) = [f_1(\cdot), f_2(\cdot), \ldots, f_{n_m}(\cdot)]^T$. After canceling these nonlinear functions, the second stage of the separating system is reduced to a linear BSS problem.

The proposed strategy for inverting $\mathbf{f}(\cdot)$ only requires the following assumption

**Assumption 2** *Each source $s_i(t)$ is a baseband signal with maximum frequency given by $B_{s_i}$.*

Note, however, since the inversion of the component-wise function $\mathbf{f}(\cdot)$ is only a step in a BSS context, there may be necessary to consider additional assumptions. For instance, the application of an ICA method to the linear stage requires that the sources be independent, whereas the application of second-order methods (like SOBI) requires that $B_{s_1} \neq B_{s_2} \neq \ldots B_{s_{n_s}}$.

### 4.3.3 Spectral spreading due to nonlinear distortion: application to the PNL model.

In view of Assumption (2), the signals $z_i(t)$ are also bandlimited signals with maximum frequency given by $B_{z_i(t)} = \max(B_{s_1(t)}, \cdots, B_{s_n(t)})$. However, based on an important result from the nonlinear signal processing theory (see [103, 115, 55] for instance), we know that if the bandlimited signal $z_i(t)$ is submitted to a monotonic nonlinear function $f(\cdot)$, then the spectrum of the observed signal $x_i(t) = f(z_i(t))$ will be wider than the spectrum of the original signal.

In order to show why spectral spreading takes place in nonlinear systems, let us assume that $f_i(\cdot)$ admits a power series expansion, i.e.

$$x_i(t) = f_i\left(z_i(t)\right) = \sum_{k=1}^{\infty} f_i^{(k)} z_i(t)^k. \tag{4.11}$$

Denoting by $Z_i(\omega)$ the Fourier transform of $z_i(t)$, the Fourier transform of (4.11) is given by

$$X_i(\omega) = f_i^{(1)} Z_i(\omega) + f_i^{(2)} Z_i(\omega) * Z_i(\omega) + f_i^{(3)} Z_i(\omega) * Z_i(\omega) * Z_i(\omega) + \cdots, \tag{4.12}$$

where the symbol '$*$' stands for the convolution operator. A basic property of the convolution states that if $R_1(\omega)$ and $R_2(\omega)$ denote the Fourier transform of two signals bandlimited to $B_1$ and $B_2$, respectively, then $R_1(\omega) * R_2(\omega)$ is bandlimited to $B_1 + B_2$ [128]. Therefore, in

[8] Indeed, while the concept of a baseband signal is binary, the classification of smooth signals through (4.10) requires the arbitrary definition of a threshold.

Equation (4.12), since $Z_i(\omega)$ is bandlimited to $B_{z_i(t)}$, then $Z_i(\omega) * Z_i(\omega)$ will be bandlimited to $2B_{z_i(t)}$, $Z_i(\omega) * Z_i(\omega) * Z_i(\omega)$ to $3B_{z_i(t)}$, and so forth. As a consequence, it is expected that the maximum frequency of $X_i(\omega)$ be larger than $B_{z_i(t)}$. This phenomenon is illustrated in Figure 4.5 which shows the effects in the frequency domain of a nonlinear transformation.

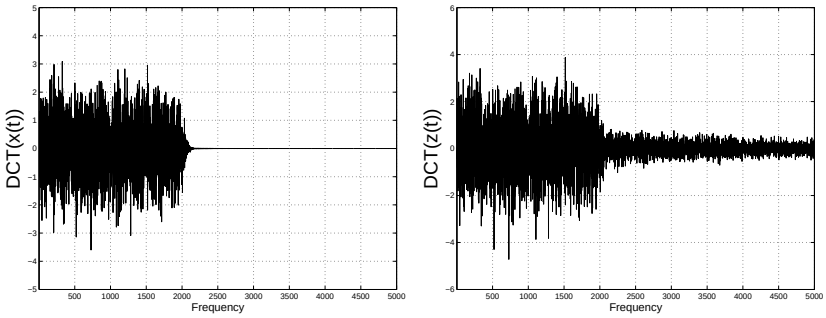


(a) DCT of $x(t)$. (b) DCT of $z(t) = \tanh(x(t))$.

Figure 4.5: Illustration of the spectral spreading caused by a nonlinear distortion: the DCTs of a baseband signal $x(t)$ and of the distorted version $z(t) = \tanh(x(t))$.

The spectral spreading phenomenon described above suggests a natural way to counterbalance the nonlinear effects introduced by $f_i(\cdot)$. The idea here is to adjust $g_i(\cdot)$ so that it gives a signal $q_i(t) = g_i(x_i(t))$ that is bandlimited to the original bandwidth of the input signal $z_i(t)$. Indeed, in view of Equation (4.12), this condition is satisfied when $q_i(t) = g_i(f_i(z_i(t))) = \alpha z_i(t) + \beta$, where $\alpha, \beta \in \mathbb{R}$, that is, when the composition of the two functions is a linear function, which is exactly the desired solution. This idea has also been exploited in several works [55, 56] for the case of SISO systems. Yet, to the best of our knowledge, this strategy has never been exploited in the context of BSS.

### 4.3.4 Implementation issues

We here discuss how the idea introduced in the last section can be put into practice. In mathematical terms, we should find a criterion to estimate the function $g_i(\cdot, \mathbf{b}_i)$, which is parametrized by $\mathbf{b}_i$. Since we are searching for a signal $q_i(t) = g_i(x_i, \mathbf{b}_i)$ whose energy beyond the frequency $B_{z_i(t)}$ is as low as possible, a first and natural way for adjusting $\mathbf{b}_i$ is expressed by the following minimization problem

$$\min_{\mathbf{b}_i} J_1(\mathbf{b}_i) = \frac{E_{q_i(t)}^{f > B_{z_i(t)}}}{E_{q_i(t)}}, \tag{4.13}$$

where $E_{q_i(t)}$ denotes the total energy of $q_i(t)$ and $E_{q_i(t)}^{f > B_{z_i(t)}}$ the energy associated with the frequency components greater than $B_{z_i(t)}$. The purpose of the term $E_{q_i(t)}$ is to avoid a trivial solution where the signal $q_i(t)$ has null energy.

The cost function defined in (4.13), which is the basis of the approach developed in [55], works with the strong assumption that $B_{z_i(t)}$ is known in advance. As a consequence, its application is not possible in a blind source separation context, as such an information is usually not available. Yet, it would be possible to extend $J_1(\mathbf{b}_i)$ to a complete blind scenario with unknown $B_{z_i(t)}$. In

fact, we could replace, in (4.13), $B_{z_i(t)}$ by a value $\hat{B}_{z_i(t)}$ that satisfies the condition $\hat{B}_{z_i(t)} > B_{z_i(t)}$ (for instance, this can be achieved by selecting $\hat{B}_{z_i(t)}$ close to one[9]). In this new situation, we are thus trying to minimize the spectral spreading in the band $[\hat{B}_{z_i(t)} > B_{z_i(t)}, 1]$. Evidently, since this is only a necessary condition, there is no theoretical guarantee that such a procedure will lead to a proper compensation of $f_i(\cdot)$. On the other hand, this procedure usually performs well in practice, at least in noiseless situations.

When the mixtures are corrupted by noise, it turns out that the complete blind strategy described in the last paragraph may become rather suboptimal. For example, suppose that $\hat{B}_{z_i(t)} >> B_{z_i(t)}$, i.e. our guess is much higher that the actual bandwidth of $z_i(t)$. Then, the criterion (4.13) will consider only a few high-frequency components, whereas all the information available in the band $[B_{z_i(t)}, \hat{B}_{z_i(t)}]$ will be discarded. As a consequence, the resulting estimator in this case will be much less robust to noise than the estimator considering the actual value $B_{z_i(t)}$. This is particularly undesirable in our problem given that even a low-power noise can become significant after the nonlinear functions.

In view of the limitations associated with the blind extension of the paradigm introduced by Equation (4.13), a more reasonable approach is to define a cost function in which $B_{z_i(t)}$ is also considered as an unknown parameter. In this spirit, we propose the following cost function

$$\min_{\mathbf{b}, \hat{B}_{z_i(t)}} J_2(\mathbf{b}, \hat{B}_{z_i(t)}) = \frac{E_{q_i(t)}^{f>\hat{B}_{z_i(t)}}}{E_{q_i(t)}^{f>\hat{B}_{z_i(t)}-\phi}}, \tag{4.14}$$

where the parameter $\phi$ lies inside $]0, 1[$ and should be assigned in advance. Later, we will discuss how this can be done.

Given that (4.14) is simply the ratio between the energies of $q_i(t)$ in the bands $[\hat{B}_{z_i(t)}, 1]$ and $[\hat{B}_{z_i(t)} - \phi, 1]$, this cost function attains a small value whenever the energy in the band $[\hat{B}_{z_i(t)}, 1]$ is much smaller than the energy in the band $[\hat{B}_{z_i(t)} - \phi, 1]$. The key point here is that such a situation is expected for the desired solution to our problem, i.e. for the situation in which $(\mathbf{b} = \mathbf{b}_d, \hat{B}_{z_i(t)} = B_{z_i(t)})$, where $\mathbf{b}_d$ represents the parameters that provide the inversion of $f_i(\cdot)$. To gain more insight into this question, let us rewrite (4.14) as the following maximization problem

$$\max_{\mathbf{b}_i, \hat{B}_{z_i(t)}} J_2(\mathbf{b}_i, \hat{B}_{z_i(t)}) = \frac{E_{q_i(t)}^{f>\hat{B}_{z_i(t)}-\phi}}{E_{q_i(t)}^{f>\hat{B}_{z_i(t)}}}, \tag{4.15}$$

The term $E_{q_i(t)}^{f>\hat{B}_{z_i(t)}-\phi}$ is given by the sum of the terms $E_{q_i(t)}^{f>B_{z_i(t)}}$ and $E_{q_i(t)}^{B_{z_i(t)}-\phi<f<B_{z_i(t)}}$. Therefore, (4.15) can rewritten as

$$\max_{\mathbf{b}_i, \hat{B}_{z_i(t)}} J_2(\mathbf{b}_i, \hat{B}_{z_i(t)}) = 1 + \frac{E_{q_i(t)}^{B_{z_i(t)}\phi<f<B_{z_i(t)}}}{E_{q_i(t)}^{f>\hat{B}_{z_i(t)}}} \equiv \max_{\mathbf{b}_i, \hat{B}_{z_i(t)}} J_2(\mathbf{b}_i, \hat{B}_{z_i(t)}) = \frac{E_{q_i(t)}^{B_{z_i(t)}-\phi<f<B_{z_i(t)}}}{E_{q_i(t)}^{f>\hat{B}_{z_i(t)}}}. \tag{4.16}$$

[9] In this work, we consider that the signals are already in a discrete-time representation. Given that, we always refer to the normalized frequency, where $B = 1$ corresponds, in the analog domain, to $F_s/2$, where $F_s$ is the sampling frequency.

In the desired solution, $g_i \circ f_i$ is approximately linear and, thus, $q_i(t)$ is bandlimited in $B_{z_i(t)}$. Therefore, in this situation, a very low energy $E_{q_i(t)}^{f>B_{z_i(t)}}$ is expected. On the other hand, the term $E_{q_i(t)}^{B_{z_i(t)}-\phi<f<B_{z_i(t)}}$ lies within the bandwidth of $z_i(t)$, and, as a consequence, is expected to be much larger than $E_{q_i(t)}^{f>B_{z_i(t)}}$, which thus explains the rationale behind the maximization of (4.16).

It is worth noting that significant variations between $E_{q_i(t)}^{f>\hat{B}_{z_i(t)}}$ and $E_{q_i(t)}^{f>\hat{B}_{z_i(t)}-\phi}$ may also happen if the spectrum of $q_i(t)$ presents energy variations as, for instance, an attenuated band. As a consequence, the cost function (4.14) tends to present local modes around the points $\hat{B}_{z_i(t)}$ where these variations occur. A practical consequence of this observation regards the definition of the optimization algorithm: as $J_2(\mathbf{b}, \hat{B}_{z_i(t)})$ may be multimodal, the application of methods based only on local search mechanisms, such as the pure gradient-based techniques, is not recommended since they may converge to local minima.

Another important practical point regards the role of $\phi$ in $J_2(\mathbf{b}, \hat{B}_{z_i(t)})$. This parameter acts as a sort of frequency resolution. For example, if the input signal is periodic (pure harmonics), then $\phi$ should be small as the energy variations are high concentrated in the spectrum. Conversely, for aperiodic signals, the energy is less concentrated in the spectrum and, thus, a greater value for $\phi$ must be defined. In practice, we observed that a good rule of thumb is to select $\phi = 0.01$ for periodic signals and $\phi = 0.1$ for aperiodic signals.

### 4.3.5 A complete algorithm for PNL source separation

Having discussed how the nonlinear inversion of $f_i(\cdot)$ can be carried out, the complete algorithm for PNL source separation can be summarized as follows:

1. **First stage**. For each mixture $x_i(t)$, find $g_i(x_i(t), \mathbf{b}_i)$ by minimizing the cost function $J_2(\mathbf{b}_i, \hat{B}_{z_i(t)})$ (Equation (4.16));

2. **Second stage**. The estimated sources $y_i(t)$ are obtained by applying a linear source separation or extraction method to the signals $q_i(t) = g_i(x_i(t))$.

As it was discussed before, due to the existence of local optima in $J_2(\mathbf{b}_i, \hat{B}_{z_i(t)})$, the adopted optimization method should be robust to sub-optimal convergence. In this work, we resort to the opt-aiNet (see Appendix B for more details). The optimization of (4.16) through the opt-aiNet requires the evaluation of the energy of $q_i(t)$ in a given frequency band. This can be done by calculating the frequency content of $q_i(t)$ via, for instance, the discrete cosine transform (DCT)[10]. Then, the energy is given by the Euclidean norm of the DCT coefficients associated with the desired band.

Concerning the second stage, any linear BSS method can be applied. Evidently, it is important to assure that the selected method is appropriate for the considered set of sources. For

[10]We could equally adopt the discrete Fourier transform (DFT). However, the DCT has the advantage of being a real-valued transform. Furthermore, we checked through preliminary simulations that the DCT gives better results for aperiodic signals.

example, in the case of Gaussian sources, ICA methods based on higher-order statistics cannot be applied. A last remark about this issue regards the assumption of baseband sources. We developed a linear source extraction method that explicitly makes use of this information. The details of this method, which is denoted SOFI (second-order frequency identification) algorithm, are given in Appendix C.

### 4.3.6 Results

We present in this section a set of simulations performed in order to check the effectiveness of the proposed two-stage PNL method. In a first moment, we study the problem of compensating the component-wise functions. Then, we present an example that shows the usefulness of our proposal in a complete PNL source separation framework. Finally, we discuss the application of the developed method to actual data.

#### 4.3.6.1 Inversion of the nonlinear stage

In order to illustrate the applicability of the cost function (4.16), let us consider an example of PNL mixing model with $n_s = 2$ sources and $n_m = 2$ mixtures. The two sources, whose bandwidths are given by $B_{s_1(t)} = 0.2$ and $B_{s_2(t)} = 0.5$, were obtained from low-pass FIR filters (100 taps) driven by white Gaussian noise. The linear part of the PNL mixing system is given by the matrix $\mathbf{A} = [1\ 0.5; 0.6\ 1]$. Concerning the nonlinear component-wise functions $f_i(\cdot)$, our analysis encompassed two cases: the NE model ($f_i(z_i) = d_i \log(z_i)$) and the situation where the inverting functions $g_i(\cdot)$ are polynomials.

*Nicolsky-Eisenman model (ions with equal valences)*

In this case the inversion of the nonlinear stage can be achieved by means of the following functions

$$q_i(t) = g_i(x_i(t), \hat{d}_i) = 10^{\left(\frac{x_i(t)}{\hat{d}_i}\right)} = z_i(t)^{\frac{d_i}{\hat{d}_i}}. \tag{4.17}$$

If, and only if, $\hat{d}_i = d_i$, the composition $g_i \circ f_i$ is linear and, thus, this situation corresponds to the desired solution.

Since the function $g_i(x_i(t), \hat{d}_i)$ is parametrized by just one parameter, it becomes possible to visualize the shape of the cost function (4.16) in this case. For example, in a noiseless situation in which $d_1 = 0.059$ and $d_2 = 0.040$, the cost functions for both $g_1(\cdot)$ and $g_2(\cdot)$ are shown in Figure 4.6. Note that the values $\hat{d}_i$ that minimize $J_2(\hat{d}_i, \hat{B}_{z_i(t)})$ coincide with the actual values of $d_i$. Moreover, the proposed criterion is minimized for both cases when $\hat{B}_{z_i(t)} = 0.54$, which is close to the bandwidth of the linear mixtures ($B_{z_i(t)} = 0.5$).

As discussed in Section 4.3.4, there may exist locally optimal models if there are energy variations in the spectrum of $z_i(t)$. This phenomenon is clear in Figure 4.6(a) where one can observe a local mode around the frequency $\hat{B}_{z_i(t)} = 0.2$. In this case, the energy variation around this frequency takes place because $z_i(t)$ is a linear combination of two bandlimited signals, one of them having a bandwidth equal to $B_{s_1(t)} = 0.2$.

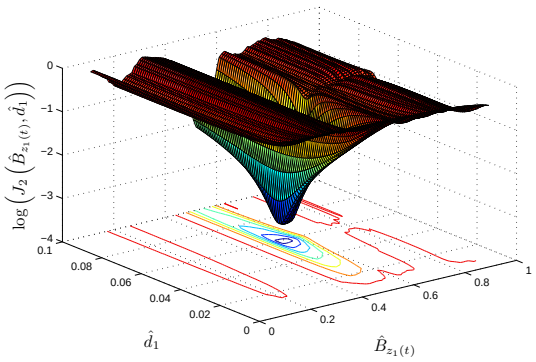


(a) $J_2(\hat{d}_1, \hat{B}_{z_1(t)})$.

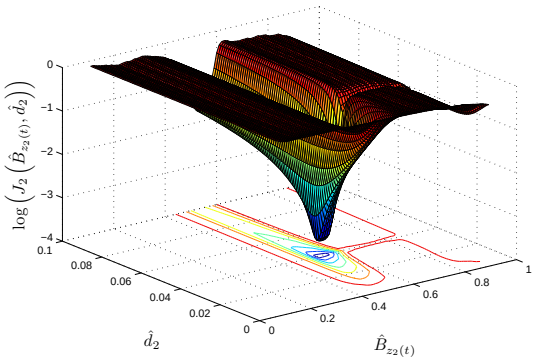


(b) $J_2(\hat{d}_2, \hat{B}_{z_2(t)})$.

Figure 4.6: Cost functions $J_2(\hat{d}_i, \hat{B}_{z_i(t)})$ for the NE model.

A relevant point in nonlinear systems like the NE model regards the effect of the noise. As we mentioned in Section 3.4.2.3, the exponential function $g_i(\cdot)$ amplifies the effects of the noise. Given that, we conducted a set of simulations to investigate these effects on the estimations of $d_2$ obtained by the following approaches: 1) the estimator associated with $J_2(\hat{d}_2, \hat{B}_{z_2(t)})$, 2) the estimator associated with $J_1(\hat{d}_2)$ assuming the knowledge of the bandwidth $B_{z_2(t)}$ (semi-blind case), 3) the same cost function $J_1(\hat{d}_2)$ but now in a complete blind situation, in which $B_{z_2(t)}$ is defined beforehand (we set $\hat{B}_{z_2(t)} = 0.8$). In Table 4.2, which represents the average of 100 experiments, one can note that, in a noiseless scenario, the three estimators give values closer to the actual one ($d_2 = 0.040$). When there is noise, the blind version of $J_1(\hat{d}_2)$ gives poor estimations for $d_2$, whereas $J_1(\hat{d}_2)$ and $J_2(\hat{d}_2, \hat{B}_{z_2(t)})$ still work properly. However, while $J_1(\hat{d}_2)$ assumes the knowledge of the actual bandwidth of the input signal, our cost function $J_2(\hat{d}_2, \hat{B}_{z_2(t)})$ operates in a completely blind fashion.

*Polynomial model*

It is noteworthy that our proposal is by no means restricted to the NE model. To illustrate that, we consider a second situation in which the nonlinear mixing functions are given by

Table 4.2: Effects of noise on the estimation of $d_2$.

| | $\hat{d}_2$ (SNR = 18 dB) | $\hat{d}_2$ (SNR = 20 dB) | $\hat{d}_2$ (noise free) |
|---|---|---|---|
| $J_1(\hat{d}_2)$ (semi-blind) | 0.0515 | 0.0455 | 0.0395 |
| $J_1(\hat{d}_2, \hat{B}_{z_2(t)})$ (blind) | 0.3336 | 0.1085 | 0.0398 |
| $J_2(\hat{d}_2, \hat{B}_{z_2(t)})$ | 0.0490 | 0.0457 | 0.0396 |

$f_i(z_i(t)) = \sqrt[3]{z_i(t)}$. To invert them, we make use of polynomial functions given by:

$$q_i(t) = g_i(x_i(t), \mathbf{w}_i) = a_i x_i^5(t) + b_i x_i^3(t) + c_i x_i(t). \tag{4.18}$$

The expected solution (in a noiseless case) is thus given by $a_i = c_i = 0$ and $b_i = \delta$, where $\delta \in \mathbb{R}$. Note that in this case one can fix, without loss of generality, $b_i = 1$.

In order to check if the cost function (4.16) succeeds in discriminating the desired solution, we plot in Figure 4.7 the shapes of this cost function for the two mixtures of our example. Since this function depends on three parameters ($a_i$, $c_i$ and $\hat{B}_{z_i(t)}$), we had to fix $\hat{B}_{z_i(t)}$ to the value that minimizes (4.16); $\hat{B}_{z_i(t)} = 0.52$ in this case. By looking at the resulting shapes, one can note that the proposed cost function is indeed minimized by the expected solutions of our problem.

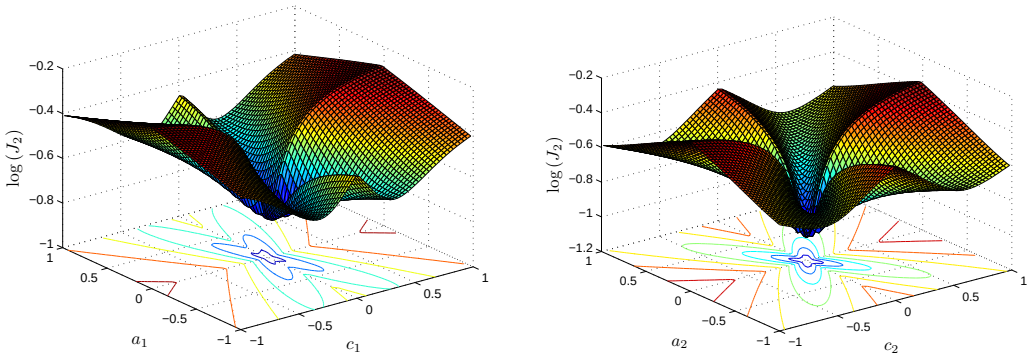


(a) $J_2(a_1, c_1, \hat{B}_{z_1(t)})$. (b) $J_2(a_2, c_2, \hat{B}_{z_2(t)})$.

Figure 4.7: Cost functions $J_2(a_i, c_i, \hat{B}_{z_i(t)})$ for the polynomial model.

#### 4.3.6.2 Example of PNL source separation

We now present an example where the complete procedure, described in Section 4.3.5, is applied to a PNL mixture with 3 sources and 3 sensors. The first source is a sine wave of frequency $B_{s_1(t)} = 0.01$, while the two others are aperiodic signals with bandwidth $B_{s_2(t)} = 0.5$ and $B_{s_3(t)} = 0.8$ —these signals are depicted in Figure 4.9(a) and the resulting mixtures in Figure 4.9(b). The linear part of the mixing system is given by the matrix $\mathbf{A} = [1\ 0.5\ 0.5; 0.4\ 1\ 0.6; 0.3\ 0.6\ 1]$, and the nonlinear functions followed the NE model, i.e., $f_i(x_i) = d_i \log(x_i)$ where $d_1 = 0.050$, $d_2 = 0.060$ and $d_3 = 0.045$. The number of available samples in this situation was 1000, and an AWG noise of SNR = 20 dB was defined in each sensor.

The application of the proposed method provided the following estimations: $\hat{d}_1 = 0.048$, $\hat{d}_2 = 0.070$ and $\hat{d}_3 = 0.044$. As can be seen in Figure 4.8, the resulting mappings between $z_i(t)$ and $q_i(t)$ are close to linear functions, which indicates that the task of inverting the nonlinearities was satisfactorily accomplished. Yet, it is clear in this figure the noise amplification phenomenon; note that the noise effect grows as the input value grows.

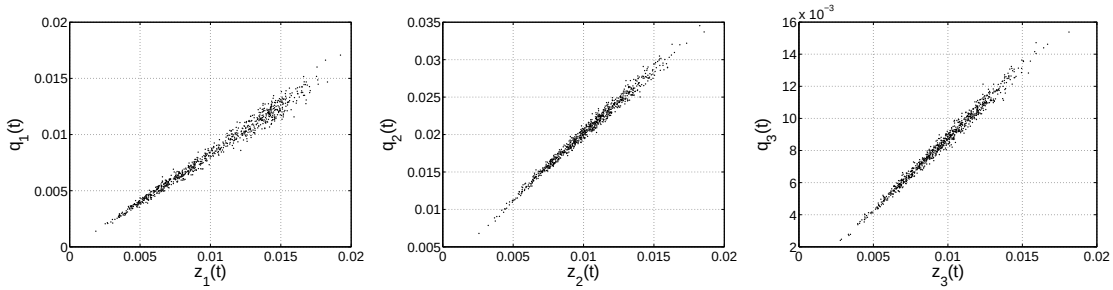


(a) $q_1(t) = g_1(z_1(t))$. (b) $q_2(t) = g_2(z_2(t))$. (c) $q_3(t) = g_3(z_3(t))$.

Figure 4.8: Mappings between $z_i(t)$ and $q_i(t)$ for each channel.

Having dealt with the nonlinear functions, we applied the SOBI algorithm [26] on the signals $q_i(t)$. As can be seen in Figure 4.9(c), this method provided good estimations of the actual sources. The obtained performance indices were $\text{SIR}_1 = 17.75\,\text{dB}$ for the sine wave, and $\text{SIR}_2 = 16.58\,\text{dB}$ $\text{SIR}_3 = 13.18\,\text{dB}$ for the aperiodic signals. We also considered the SOFI algorithm (see Appendix C) for extracting the sinusoidal signal (the smoothest one). As shown in Figure 4.10, a good estimation of the sine wave was obtained; the performance index was $\text{SIR}_1 = 19.39\,\text{dB}$. Note that, due to effect of noise amplification mentioned before, the estimation error is more evident when the signal attains high values. For matter of comparison, we calculated the performance obtained when the original coefficients $d_i$ and the original mixing matrix $\mathbf{A}$ are considered. In this situation, the performance indices were $\text{SIR}_1 = 15.43\,\text{dB}$ for the sine wave, and $\text{SIR}_2 = 10.01\,\text{dB}$ $\text{SIR}_3 = 11.69\,\text{dB}$ for the aperiodic signals. Note that, due to noise, the solutions provided by the original parameters become suboptimal.

#### 4.3.6.3 Application to the actual data

In a last experiment, we check whether our proposal is able to estimate the logarithm functions in the case of actual data. For that, we consider the data of the experiments S1K10$^{-1}$NH$_4$ and S1K10$^{-4}$NH$_4$ (see Chapter 2). Despite the quite reduced number of samples ($n_d = 170$), our method provided fair estimations for the Nernstian slopes ($\hat{d}_1 = 0.031$ and $\hat{d}_2 = 0.056$); for matter of comparison, a MSE regression provided the following values $\hat{d}_1 = 0.039$ and $\hat{d}_2 = 0.050$. To check if the obtained parameters indeed results in a linear mixing model, the signals $q_i(t)$ were modeled as a linear combination of the sources. The resulting signal-to-noise ratios were given by $\text{SNR}_1 = 16.91\text{dB}$ and $\text{SNR}_2 = 22.05\text{dB}$.

A last remark concerns the application of linear BSS methods to the second stage in this case. Neither SOBI nor SOFI were able to separate the linear mixtures in this experiment. Actually, as illustrated in Figure 2.3, the sources obtained in the experiments described in Chapter 2 were

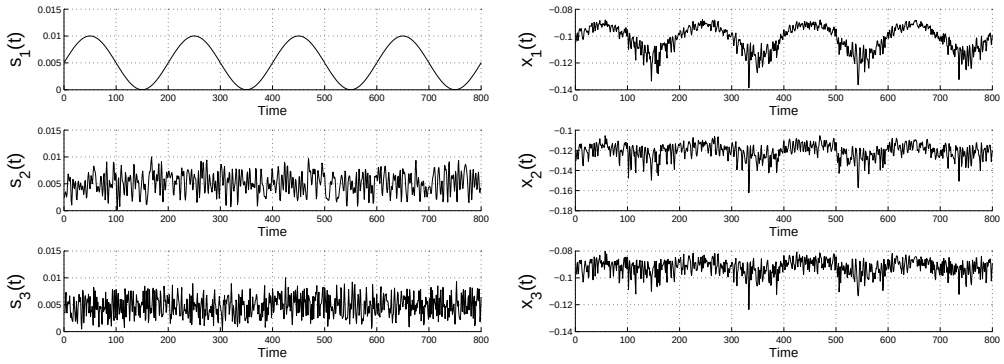


(a) Sources. (b) Noisy mixtures.

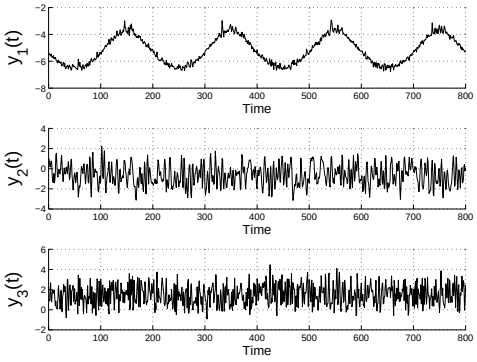


(c) Recovered sources.

Figure 4.9: Application of the complete PNL method (the SOBI algorithm was considered in the linear stage).

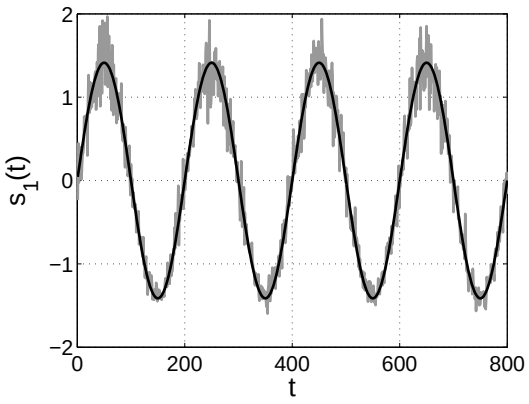


Figure 4.10: Extraction of the smoothest source through the SOFI algorithm. Actual source $s_1(t)$ (black) and estimated source $y_1(t)$ (gray).

highly correlated, thus explaining the poor performance of these two methods.

## 4.4 Conclusion

In this chapter, we introduced two contributions that make use of prior information for estimating the nonlinear component-wise functions that appear in the NE model. In the first one, we considered the nonlinear mixing model associated with the case in which the ions under analysis had different valences. In this situation, we set a geometric approach that was based on the assumption that one of the sources does not vary in a certain time-window. The obtained results confirmed that such an approach can simplify the development of the complete NE model. Yet, the main limitation of the proposed geometrical method resides in its high sensitivity to noise.

Although we focused on the NE model (logarithm functions), the geometrical approach described in the first part of this chapter can be extended to other nonlinear functions.

The second part of this chapter was devoted to the description of a PNL two-stage approach based on the assumption that the sources are baseband signals. We saw that such an assumption is related to slowly-varying signals which in turn are usually observed in chemical sensing applications. Based on a classical result that associates nonlinear functions with spectral spreading, we propose a novel criterion for compensating the effects introduced by the nonlinear section of the PNL model. The novelty of our approach is that it does not require the knowledge of the bandwidths of the sources. Experiments with artificial and actual data demonstrated the effectiveness of our proposal.

We can cite several perspectives involving the contribution described in the second part of this chapter. A first one concerns its extension to more general nonlinear functions. Indeed, we only considered matched situations in the sense that nonlinear separating functions were able to perfectly invert the mixing functions. Although this is quite natural in the application in mind, there may be other applications where no parametric information about the mixing functions is available. In these cases, more general structures (polynomials, neural networks etc) are considered as separating functions and, thus, only an approximate compensation of $f_i$ can be achieved in these cases. In this context, it would be interesting to investigate the behavior of the cost function (4.16) for such cases.

Another interesting perspective related to the proposed cost function (4.16) is that it may be useful in nonlinear source separation problems other than the PNL one. To illustrate that, let us consider the following mixing model

$$x_i(t) = a_{i1}s_1(t) + a_{i2}s_2(t) + b_{i1}\sqrt{s_1(t)} + b_{i2}\sqrt{s_2(t)}. \tag{4.19}$$

Suppose that four mixtures are available. In this case, it is expected that the application of linear ICA-BSS methods provides the following two signals[11]: $y_1(t) = c_{11}s_1(t) + c_{12}\sqrt{s_1(t)}$ and $y_2(t) = c_{21}s_2(t) + c_{22}\sqrt{s_2(t)}$. Given that $y_i(t)$ is not bandlimited, we could apply[12], based on the assumption that the source $s_i(t)$ is bandlimited, the same idea developed in the second part of

[11] Note that such situation is equivalent to a linear BSS problem in which the sources are given by $s_1(t)$, $s_2(t)$, $\sqrt{s_1(t)}$ and $\sqrt{s_2(t)}$. Since there are dependent sources in this case, the best ICA can do is to retrieve linear combinations (subspaces) of the dependent sources.

[12] One way to implement this idea could be achieved by resorting to SISO recurrent networks, similar to the ones proposed in [86] and in Chapter 3.

this chapter to extract $s_i$ from $y_i(t)$. Such an approach would allow one to deal with nonlinear mixing models through linear algorithms followed by a post-processing stage whose goal would be to extract $s_i(t)$ from nonlinear combinations of this signal.

# Chapter 5

# Bayesian approach

## 5.1 Introduction

In this chapter, we continue our investigation on how to take advantage of prior information that is typical of chemical signals. However, while prior information has been used so far as a stratagem for simplifying the mixing model, we now turn our attention to a Bayesian approach, in which prior information appears as a central element. One of the motivations behind this approach is related to some prior information whose incorporation is easier in a probabilistic framework, e.g. the non-negativity of the sources.

In a first part of this chapter, we provide a brief introduction to the Bayesian estimation principle. Then, in Section 5.3, we present a Bayesian source separation method tailored for ISE arrays. The basis of this approach is the use of log-normal distributions to model the sources. Finally, in section 5.4, we introduce a novel Bayesian method aimed at linear and linear-quadratic models. The developed method can be used either in the linear stage of the NE model or in arrays composed of tin-oxide electrodes. Our development in this case follows a model based on truncated Gaussian distributions.

## 5.2 Bayesian source separation

Bayesian estimation [139] has been studied in many domains, from biology to engineering applications. The advent of the so-called Markov Chain Monte Carlo (MCMC) [72] methods and of the variational approximation [146] has allowed the application of Bayesian techniques even in complex and high-dimensional systems.

The central idea in Bayesian estimation is to incorporate some available information about the unknown variables into the likelihood function. This is accomplished through a probabilistic formulation in which the available information are expressed by defining *a priori* distributions, or simply priors, for each unknown parameter. Very often, the use of prior information results in more accurate estimators [98].

The development of Bayesian methods to source separation was addressed in many works [99, 116, 154, 160] —see [100, 119] for an introduction. Moreover, the applicability of Bayesian

source separation methods has been demonstrated in several domains including audio source separation [68], spectroscopy data analysis [122], hyperspectral images [21] and astronomical data processing [159, 54].

In source separation, the unknown parameters comprise the sources but also the coefficients related to the mixing process. Moreover, as it will become clear later, it is usual to assume a hierarchical model in which the parameters of the prior distributions are also seen as unknown parameters; this strategy results in a more flexible modeling. Henceforth, all these unknown parameters will be denoted by the vector $\boldsymbol{\theta}$. Also, the observations of our problem, the mixed signals, will be represented by the matrix $\mathbf{X} \in \mathbb{R}^{n_m \times n_d}$ in which each row contains the response (in time) of a given sensor in the array.

In Bayesian estimation, the available information about $\boldsymbol{\theta}$ is taken into account through a probabilistic modeling. In this spirit, a first step in a Bayesian framework is to assign a prior distribution for each element of $\boldsymbol{\theta}$. This set of priors, which will be represented by $p(\boldsymbol{\theta})$, must somehow be related to the available information at hand. For example, one of the information that we will exploit in the sequel is the non-negativity of the sources; given that the sources represent ionic activities in our problem, it is natural to consider prior distributions whose support lies in $[0, +\infty)$.

Another important element in a Bayesian formulation is the likelihood function, which will be represented by $p(\mathbf{X}|\boldsymbol{\theta})$. Intuitively speaking, while the priors serve to model the unknown parameters, the likelihood function provides a probabilistic model for the relation between the unknown parameters and the observed data. Therefore, in the context of source separation, $p(\mathbf{X}|\boldsymbol{\theta})$ will be directly related to the assumed mixing model. It is noteworthy that the likelihood function by itself can be used to derive source separation methods. As briefly discussed in Chapter 1, many methods assuming a noise-free linear mixing model can be understood in the light of a likelihood formulation [35]. Furthermore, the likelihood principle can be applied even when the noise is explicitly considered in the mixing model description [122, 30].

With the concepts of prior distribution and likelihood function in mind, one can easily understand the rationale behind Bayesian estimation. Indeed, the key element in this approach is the so-called posterior distribution which, according to the Bayes' rule, is given by

$$p(\boldsymbol{\theta}|\mathbf{X}) = \frac{p(\mathbf{X}|\boldsymbol{\theta})p(\boldsymbol{\theta})}{p(\mathbf{X})}. \tag{5.1}$$

Because $p(\mathbf{X})$ is not a function of the unknown parameters $\boldsymbol{\theta}$, the shape of the posterior distribution can be obtained by solely means of the priors and the likelihood function, that is

$$p(\boldsymbol{\theta}|\mathbf{X}) \propto p(\mathbf{X}|\boldsymbol{\theta})p(\boldsymbol{\theta}). \tag{5.2}$$

From expression (5.2), the posterior distribution can be interpreted as an updated version of the prior information brought by the likelihood function, that is, one had an initial belief that was refined after observing the data. An interesting point here is that the contribution of the likelihood term to the shape of $p(\boldsymbol{\theta}|\mathbf{X})$ is implicitly defined in a quite natural manner. For example, when the observations are strongly corrupted by noise, the likelihood term becomes

flat and, as a result, the posterior distribution is mostly influenced by the priors distribution. Conversely, if a great number of observations is available, then the likelihood term becomes sharper and, thus, tends to dominate the posterior distribution.

A last step in the Bayesian approach is to extract an estimation $\hat{\boldsymbol{\theta}}$ of the unknown parameters from the posterior distribution. A first (and natural) solution to this problem can be achieved by considering the values that maximize the posterior distribution, i.e. by resolving the following optimization problem

$$\hat{\boldsymbol{\theta}}_{MAP} = \arg\max_{\boldsymbol{\theta}} p(\mathbf{X}|\boldsymbol{\theta})p(\boldsymbol{\theta}). \tag{5.3}$$

This strategy is known as maximum *a posteriori* (MAP) estimation. Very often, the derivation of the MAP estimator is done for the logarithm of the posterior distribution (note that, as the logarithm is a monotonic function, the solutions of the logarithm of the MAP and of the MAP estimators coincide).

Another popular way to provide an estimation $\hat{\boldsymbol{\theta}}$ from $p(\mathbf{X}|\boldsymbol{\theta})$ is based on the Bayesian minimum mean square error (MMSE) estimation. In this case, the estimations are given by the posterior mean, that is

$$\hat{\boldsymbol{\theta}}_{MMSE} = E\{\boldsymbol{\theta}|\mathbf{X}\} = \int \boldsymbol{\theta}\, p(\boldsymbol{\theta}|\mathbf{X}) d\boldsymbol{\theta}. \tag{5.4}$$

It can be shown [98] that this estimator, which is also known as conditional mean estimator, minimizes $E\{(\hat{\boldsymbol{\theta}} - \boldsymbol{\theta})^2\}$. In some cases, e.g. when the posterior distribution is Gaussian, the MAP and Bayesian MMSE estimators coincide.

### 5.2.1 A simple example

In order to gain more intuition on the Bayesian approach in source separation, let us consider a simple example in which the mixtures are given

$$\mathbf{x}(t) = \mathbf{f}(\mathbf{A}, \mathbf{s}(t)) + \mathbf{n}(t), \tag{5.5}$$

where $\mathbf{A}$ contains all the mixing coefficients and each element of $\mathbf{n}(t)$ corresponds to a zero mean additive white Gaussian noise (AWGN) whose variance, which is assumed known in this example, is given by $\sigma_i^2$. Therefore, the unknown parameters in this case are $\boldsymbol{\theta} = [\mathbf{s}(1), \ldots, \mathbf{s}(n_d), \mathbf{A}]$.

As discussed before, a first step toward a Bayesian estimation is to assign prior distributions for $\boldsymbol{\theta}$. For example, suppose that we know that the sources as well as the mixing coefficients lie in the interval $[0, 1]$. Thus, in this case, a simple way to take into account this information is to assign priors uniformly distributed in $[0, 1]$, i.e.

$$p(s_i(t)) \propto \mathbb{1}_{[0,1]}(s_i(t))$$

and

$$p(a_{ij}) \propto \mathbb{1}_{[0,1]}(a_{ij})$$

where $\mathbb{1}_A(x)$ is the indicator function, which is defined as follows

$$\mathbb{1}_A(x) = \begin{cases} 1 & \text{if } x \in A \\ 0 & \text{if } x \notin A. \end{cases} \tag{5.6}$$

We consider that the sources are white signals and mutually statistically independent (the same for the mixing coefficients). Moreover, we assume that the noise terms are both spatially and temporally uncorrelated. Based on these assumptions, the posterior distribution can be written as follows

$$p(\boldsymbol{\theta}|\mathbf{X}) \propto \prod_{i=1}^{n_m}\prod_{t=1}^{n_d} \exp\left(-\frac{(x_i(t) - f_i(\mathbf{A}, \mathbf{s}(t)))^2}{2\sigma_i^2}\right) \times \prod_{j=1}^{n_s}\prod_{t=1}^{n_d} \mathbb{1}_{[0,1]}(s_j(t)) \times \prod_{i=1}^{n_m}\prod_{j=1}^{n_s} \mathbb{1}_{[0,1]}(a_{ij}). \quad (5.7)$$

According to our previous discussion, the MAP estimator in this case will search for a $\boldsymbol{\theta} = [\mathbf{s}(1), \ldots, \mathbf{s}(n_d), \mathbf{A}]$ that maximizes (5.7) or, equivalently, the logarithm of this expression, that is

$$\hat{\boldsymbol{\theta}}_{MAP} = \arg\max_{\boldsymbol{\theta}} \ln p(\boldsymbol{\theta}|\mathbf{X}) = \\ -\sum_{i=1}^{n_m}\sum_{t=1}^{n_d} \frac{(x_i(t) - f_i(\mathbf{A}, \mathbf{s}(t)))^2}{2\sigma_i^2} + \sum_{j=1}^{n_s}\sum_{t=1}^{n_d} \ln(\mathbb{1}_{[0,1]}(s_j(t))) + \sum_{i=1}^{n_m}\sum_{j=1}^{n_s} \ln(\mathbb{1}_{[0,1]}(a_{ij})). \quad (5.8)$$

Equation (5.8) is helpful in that it illustrates the very idea of Bayesian source separation. For instance, one can note that the term associated with the likelihood function (the first one) is actually trying to fit the observed data to the considered mixing model. This is achieved by minimizing the square error between the data and the representation provided by the assumed model. In this context, the noise variance acts as a sort of a regularization term in that it defines the weight of the likelihood term in (5.8). That is, the higher is the noise variance the smaller is the influence of the likelihood function on the posterior distribution and vice versa.

Concerning the other terms in (5.8), the ones related to the priors, they are avoiding solutions that do not lie in the expected interval. Indeed, if any element of $\boldsymbol{\theta}$ is not in the interval $[0, 1]$, then there are indicator functions that take zero and, as a consequence, Equation (5.8) goes to $-\infty$. That is, the chosen priors in this example are constraining the search space considered in the inference.

Finally, a last step concerns the resolution of (5.8). In this case, as in many other real problems, it is not possible to find an analytical solution to (5.8). In view of this difficulty, this optimization problem is usually carried out by considering iterative methods.

## 5.3 A Bayesian source separation method for the NE model

We now turn our attention to the derivation of a Bayesian source separation method tailored for the NE mixing model. However, before getting into the details of our approach, it is important to discuss the motivations that led us to resort to a Bayesian approach. Firstly, as discussed before, this framework allows the incorporation of prior information in a natural manner, which can result in more realistic solutions. Secondly, in contrast to the developed methods so far, the noise is explicitly considered in a Bayesian formulation; this is important because, as discussed in Chapter 2, the NE equation is only an approximate model which means that the mixtures are corrupted by noise. Finally, as pointed out in [122], a Bayesian formulation may provide fair

estimations of the sources even when they present some degree of correlation. This situation happens in chemical sensing when the analytes are coupled, for instance, through a chemical reaction or a biological regulatory process.

The Bayesian algorithm that will be developed in the sequel aims at the following mixing model

$$x_i(t) = y_i(t) + n_i(t) = e_i + d_i \log\left(s_i(t) + \sum_{j=1, j\neq i}^{n_s} a_{ij} s_j^{z_i/z_j}(t)\right) + n_i(t), \tag{5.9}$$

where $n_i(t)$ corresponds to the AWG noise term. The terms $n_i(t), i = 1, \ldots, n_m$ are mutually independent and, thus, the noise covariance matrix is given by $\mathbf{C_n} = \text{diag}(\boldsymbol{\sigma}^2)$, where the variances $\boldsymbol{\sigma}^2 = \sigma_1^2, \ldots, \sigma_{n_m}^2$, are unknown.

The mixing model (5.9) can also be expressed in a matrix notation:

$$\mathbf{X} = \mathbf{Y} + \mathbf{N} = \mathbf{e} \cdot \mathbf{1}_{1\times n_d} + \text{diag}(\mathbf{d}) \log\left(\mathbf{A} \otimes^{\mathbf{z}} \mathbf{S}\right) + \mathbf{N}, \tag{5.10}$$

where $\mathbf{Y} \in \mathbb{R}^{n_m \times n_d}$, $\mathbf{e} = [e_1, \ldots, e_{n_m}]^T$, $\mathbf{d} = [d_1, \ldots, d_{n_m}]^T$, $\mathbf{A} \in \mathbb{R}_+^{n_m \times n_s}$ and $\mathbf{S} \in \mathbb{R}_+^{n_s \times n_d}$. The element $[i, t]$ of $\mathbf{X}$ corresponds to $x_i(t)$ and therefore the $i$-th row of $\mathbf{X}$ corresponds to the time response of the $i$-th ISE within the array. Analogously, the element $[j, t]$ of $\mathbf{S}$ denotes the activity of the $j$-th ion at the instant $t$, i.e. $s_j(t)$. Matrix $\mathbf{A}$ contains the selectivity coefficients. The vector of valences is denoted by $\mathbf{z} = [z_1, \ldots, z_{n_s}]^T$, and the operator $\otimes^{\mathbf{z}}$ describes the nonlinear transformation inside the logarithm function present in the NE model. If the valences $z_i$ are equal, then $\otimes^{\mathbf{z}}$ results in a simple matrix multiplication (as discussed in Chapter 1, this situation is an example of PNL model). Finally, $\mathbf{1}_{1\times n_d}$ corresponds to a vector (dimension $n_d$) with all elements equal to one.

We may now formulate the source separation problem treated in this section: given the array response $\mathbf{X}$ and assuming that the vector of valences $\mathbf{z}$ is known, we aim at estimating the elements of $\mathbf{S}$ (ionic activities). Since we envisage a blind method, the other parameters related to the mixing model (except $\mathbf{z}$) and the noise variance at each electrode are also unknown and, thus, should be estimated. Furthermore, as it will become clear later, there are other unknown parameters, denoted by $\boldsymbol{\phi}$, which are related to the prior distributions assigned to the sources. Henceforth, all the parameters that should be estimated will be represented by the vector $\boldsymbol{\theta} = [\mathbf{S}, \mathbf{A}, \mathbf{d}, \mathbf{e}, \boldsymbol{\sigma}, \boldsymbol{\phi}]$ and we will adopt the following notation: $\boldsymbol{\theta}_{-\theta_q}$ represents the vector containing all elements of $\boldsymbol{\theta}$ except $\theta_q$.

### 5.3.1 Defining the prior distributions

In this section, we describe how the prior distributions were defined in our Bayesian method. However, before discussing this point, let us present a concept that will be fundamental in the sequel: the notion of conjugate prior. Suppose a problem in which one is interested in estimating $X$ from $Y$. As already discussed, the three quantities of interest in a Bayesian approach are the prior distribution, the likelihood function and the posterior distribution which are represented by $p(X)$, $p(Y/X)$ and $p(X/Y) \propto p(Y/X)p(X)$, respectively. When $p(X/Y)$ and $p(X)$ belong to

the same family of probability distributions, then $p(X)$ is said to be conjugate with respect to the likelihood $p(Y/X)$ [139].

As it will be clarified in Section 5.3.4, the implementation of the Bayesian methods developed in this chapter requires the simulation of conditional posterior distributions. This task is simplified when these posterior distributions assume standard form (Gaussian, exponential etc) since the simulation of these distributions is straightforward. Of course, the role of the priors is important here since they determine the posterior distributions. In this spirit, it is always recommended to define standard priors that be conjugated with the likelihood so the resulting posterior distributions also assume the standard forms of the priors. Unfortunately, this is not always possible and, in these cases, another sampling scheme should be adopted; we will discuss this point later.

#### 5.3.1.1 Prior distribution of the sources S

In our problem, the sources are always non-negative since they represent ionic activities. There are many possibilities to take into account the non-negativity of the sources. For example, in [122], this was achieved through Gamma priors. This distribution has a non-negative support and provides a flexible solution as it can model from sparse to almost uniform sources [122]. However there is a practical drawback associated with the use of a Gamma distribution: it is difficult to find a conjugate prior in the estimation of the Gamma distribution parameters. Therefore, according to our previous discussion, the simulation of conditional posterior distributions becomes more complicated in these cases.

Alternatively, one can model the non-negativity of the sources by considering a log-normal distribution. The motivation behind this choice is twofold. Firstly, in contrast to the Gamma distribution, we will check later that it is possible to define a simple conjugate prior in this case. Also, there is a practical argument behind this choice. Ionic activities are expected to have a relative small variation in the logarithmic scale. This can be taken into account by the log-normal distribution, since such a distribution is nothing but a Gaussian distribution in the logarithmic scale. In mathematical terms, the prior assigned to $s_j(t)$ is given by

$$p(s_j(t)|\mu_j,\sigma_j) \propto \frac{1}{s_j(t)} \exp\left(-\frac{(\ln(s_j(t)) - \mu_j)^2}{2\sigma_j^2}\right) \mathbb{1}_{[0,+\infty[}(s_j(t)), \tag{5.11}$$

where $\mu_j$ and $\sigma_j$ are the distribution parameters, and $\mathbb{1}_{[0,+\infty[}(s_j(t))$ is the indicator function. We assume that the samples are independent and identically-distributed (i.i.d) and also that the sources are mutually statistically independent[1], that is

$$p(\mathbf{S}|\boldsymbol{\phi}_j) = \prod_{j=1}^{n_s}\prod_{t=1}^{n_d} p(s_j(t)|\mu_j,\sigma_j),$$

where $\boldsymbol{\phi}_j = [\mu_j\ \sigma_j]$.

[1] If some information concerning a possible dependency between the sources is available, it can be used in the definition of the *a priori* distributions. In this case, however, one goes toward a less general approach that may useful only to the modeled situation. Besides, the resulting inference problem becomes more difficult in this situation.

#### 5.3.1.2 Prior distribution of the sources hyperparameters $\boldsymbol{\phi}$

Since we consider an hierarchical model, the parameters $\boldsymbol{\phi}_j = [\mu_j \ \sigma_j]$ in Equation (5.11) are also unknown in our problem and, thus, we must assign priors for them. In this context, a Gaussian prior distribution was adopted for $\mu_j$, that is:

$$p(\mu_j) = \frac{1}{\sqrt{2\pi\sigma_{\mu_j}^2}} \exp\left(-\frac{\left(\mu_j - \mu_{\mu_j}\right)^2}{2\sigma_{\mu_j}^2}\right), \tag{5.12}$$

where $\mu_{\mu_j}$ and $\sigma_{\mu_j}$ correspond to the hyperparameters. For[2] $r_j = 1/\sigma_j^2$, a Gamma distribution is considered:

$$p(r_j) = \frac{r_j^{\alpha_{r_j}-1}}{\Gamma(\alpha_{r_j})\beta_{r_j}^{\alpha_{r_j}}} \exp\left(\frac{-r_j}{\beta_{r_j}}\right) \mathbb{1}_{[0,+\infty[}(r_j), \tag{5.13}$$

where $\alpha_{r_j}$ and $\beta_{r_j}$ are the hyperparameters. In Section 5.3.4.2, we will show that these two priors lead to conjugate pairs in the estimation of $\mu_j$ and $r_j = 1/\sigma_j^2$.

#### 5.3.1.3 Prior distribution of the selectivity coefficients A

According to the literature in potentiometric sensors (see [66, 152]), the selectivity coefficients are also non-negative. Moreover, it is rare to find a sensor whose response depends more on the interfering ion than on the target one, that is, $a_{ij}$ usually lies in the interval $[0, A_{max}]$ where $A_{max} \in [0, 1]$. Thus, a uniform distribution can be assumed for each[3] $a_{ij}$, that is

$$p(a_{ij}) \propto \mathbb{1}_{[0,A_{max}]}(a_{ij}). \tag{5.14}$$

If no additional information is available, one can set $A_{max} = 1$. However, it is possible to refine this information by using databases such as [152] or by incorporating some information acquired during the fabrication process. Finally, the coefficients of $\mathbf{A}$ are assumed mutually independent, so that we can write:

$$p(\mathbf{A}) = \prod_{i=1}^{n_m} \prod_{j=1}^{n_s} p(a_{ij}).$$

#### 5.3.1.4 Prior distribution of the Nernstian slopes d

As discussed in Section 1.2.3.1, $d_i$ is related to physical parameters and, for a room temperature, it takes approximately $0.059/z_i$. However, due to the sensor fabrication process and aging, a deviation of this theoretical value is usually observed. Furthermore, even the way the solutions are injected may influence $d_i$ [58]. This possible deviation from the Nernstian value can be taken into account by setting a Gaussian prior of mean $\mu_{d_i} = 0.059/z_i$V, i.e.:

$$p(d_i) \propto \exp\left(-\frac{(d_i - \mu_{d_i})^2}{2\sigma_{d_i}^2}\right). \tag{5.15}$$

[2]For the sake of clarity, we consider the estimation of the precision $r_j$ instead of the variance $\sigma_j^2$. This is done because a Gamma prior for the precision is conjugates with the likelihood in this case.

[3]In view of Equation (5.9), we consider $a_{ij} = 1$ when $i = j$.

$\sigma_{d_i}^2$ must be high enough to correctly model the derivations from the theoretical value. For example, for an electrode whose target ion is monovalent, by setting $\sigma_{d_i} = 0.01$ the probability mass of (5.15) is concentrated (99% of the mass) in the interval $[0.03, 0.09]$. Note again that this knowledge could be refined if additional information is available, or if the measurements are conducted in different temperatures. Finally, we assume that the elements of $\mathbf{d}$ are statistically independent, so that

$$p(\mathbf{d}) = \prod_{i=1}^{n_m} p(d_i).$$

#### 5.3.1.5 Prior distribution of the parameters e

In contrast to the parameters $d_i$, there is no theoretical value for $e_i$. On the other hand, as can be observed in [76, 80] and in the experiments of Chapter 2, this parameter usually lies on the interval $[0.05, 0.35]$V. Hence, the following Gaussian prior distribution can be adopted:

$$p(e_i) \propto \exp\left(-\frac{(e_i - \mu_{e_i})^2}{2\sigma_{e_i}^2}\right). \tag{5.16}$$

The mean of this distribution is given by $\mu_{e_i} = 0.20$V whereas $\sigma_{e_i}^2$ must be defined so the resulting prior goes toward a flat prior in the interval $[0.05, 0.35]$. The elements of $\mathbf{e}$ are assumed mutually independent.

#### 5.3.1.6 Prior distribution of the noise variance $\sigma_i^2$

A common approach [59] to assign priors for the noise variances is based on the inverse Gamma distribution, that is, the precision $\gamma_i = 1/\sigma_i^2$ is modeled through a Gamma distribution with parameters $\alpha_{\sigma_i}$ and $\beta_{\sigma_i}$

$$p(\gamma_i) = \frac{\gamma_i^{\alpha_{\sigma_i}-1}}{\Gamma(\alpha_{\sigma_i})\beta_{\sigma_i}^{\alpha_{\sigma_i}}} \exp\left(\frac{-\gamma_i}{\beta_{\sigma_i}}\right) \mathbb{1}_{[0,+\infty[}(\gamma_i). \tag{5.17}$$

The motivation behind this modeling comes from the fact that it results in a conjugate pair. Moreover, it is possible to set $\alpha_{\sigma_i}$ and $\beta_{\sigma_i}$ to obtain a non-informative prior [59].

### 5.3.2 Probabilistic modeling of the mixing process

Having defined the prior distributions, the next step is to obtain the likelihood $p(\mathbf{X}|\boldsymbol{\theta})$. Based on the mixing model (5.9) and on the assumption of i.i.d. Gaussian noise which is also spatially uncorrelated, the likelihood is given by

$$p(\mathbf{X}|\boldsymbol{\theta}) = \prod_{t=1}^{n_d}\prod_{i=1}^{n_m} \mathcal{N}_{x_i(t)}\left(e_i + d_i \log\Big(\sum_{j=1}^{n_s} a_{ij} s_j(t)^{z_i/z_j}\Big), \sigma_i^2\right), \tag{5.18}$$

where $\mathcal{N}_{x_{ik}}(\mu, \sigma^2)$ represents a Gaussian pdf, in $x_{ik}$, with mean $\mu$ and variance $\sigma^2$.

### 5.3.3 Bayesian inference

Based on the priors and on the likelihood function, one can use the Bayes' rule to obtain the posterior distribution $p(\boldsymbol{\theta}|\mathbf{X})$. Given that the unknown variables of our problem are *a priori* mutually independent (except $\mathbf{S}$ and $\boldsymbol{\phi}$), the prior distribution factorizes and, as a consequence, the posterior distribution becomes

$$p(\boldsymbol{\theta}|\mathbf{X}) \propto p(\mathbf{X}|\mathbf{S},\mathbf{A},\mathbf{e},\mathbf{d},\boldsymbol{\sigma})\, p(\mathbf{S}|\boldsymbol{\phi})\, p(\boldsymbol{\phi})\, p(\mathbf{A})\, p(\mathbf{e})\, p(\mathbf{d})\, p(\boldsymbol{\sigma}). \tag{5.19}$$

Concerning the inference scheme, the implementation of a MAP estimator for (5.19) is difficult because it requires the resolution of a complex high-dimensional optimization problem. At first sight, the implementation of the MMSE Bayesian estimation seems also complicated because it requires the analytical evaluation of an integral which is hard in the problem considered here. Yet, a good approximation of (5.4) can be provided by sampling methods. The idea here is to approximate the MMSE estimator using samples obtained from the posterior distribution $p(\boldsymbol{\theta}|\mathbf{X})$. Indeed, let the generated samples be represented by $\boldsymbol{\theta}^{(1)}, \boldsymbol{\theta}^{(2)}, \ldots, \boldsymbol{\theta}^{(M)}$. Then expression (5.4) can be approximated by

$$\widetilde{\boldsymbol{\theta}}_{MMSE} = \frac{1}{M} \sum_{m=1}^{M} \boldsymbol{\theta}^{(m)}. \tag{5.20}$$

According to the law of large numbers, $\widetilde{\boldsymbol{\theta}}_{MMSE} \rightarrow \boldsymbol{\theta}_{MMSE}$ as $M \rightarrow +\infty$. This important result gives the theoretical foundation for the above-described methodology, which is referred as Monte Carlo integration [140].

### 5.3.4 Gibbs sampling scheme

From expression (5.20), one can note that the implementation of the Bayesian MMSE estimator boils down to the task of generating samples from $p(\boldsymbol{\theta}|\mathbf{X})$. In this work, this task is accomplished by the Gibbs' sampler, a Markov Chain Monte Carlo (MCMC) method specially tailored for simulating joint distributions. The idea in MCMC methods is to generate a Markov chain that admits the desired distribution ($p(\boldsymbol{\theta}|\mathbf{X})$ in our case) as stationary distribution. If we assume that $x \sim p(x)$ stands for the sampling operation, i.e. $x$ is a sample obtained from the distribution $p(x)$, then the Gibbs' sampler can be summarized as follows:

1. Set initial samples $\theta_1^{(0)}, \theta_2^{(0)}, \ldots, \theta_N^{(0)}$;
2. For $m = 1$ to $M$, do

$$\begin{aligned}
\theta_1^{(m)} &\sim p(\theta_1|\theta_2^{(m-1)}, \theta_3^{(m-1)}, , \ldots, \theta_N^{(m-1)}, \mathbf{X}) \\
\theta_2^{(m)} &\sim p(\theta_2|\theta_1^{(m)}, \theta_3^{(m-1)}, \ldots, \theta_N^{(m-1)}, \mathbf{X}) \\
&\vdots \\
\theta_N^{(m)} &\sim p(\theta_N|\theta_1^{(m)}, \theta_2^{(m)}, \ldots, \theta_{N-1}^{(m)}, \mathbf{X})
\end{aligned}$$

end.

As the resulting Markov chain of the Gibbs' sampler takes some time to converge to its stationary distribution, it becomes necessary to perform some iterations of the Gibbs' sampler only to achieve the convergence to the stationary distribution of the underlying Markov chain. During this period, which is known as burn-in period, the samples generated by the Gibbs' sampler are not taken into account by the approximated version of MMSE estimator shown in Equation (5.36).

The fundamental feature of the Gibbs' sampler is that it simulates a high-dimensional joint distribution by sequentially sampling from the conditional distribution of each variable. Actually, the Gibbs' sampler requires only the conditional distributions up to a proportional gain. In the sequel, we will derive the conditional distributions for each element of $\boldsymbol{\theta}$. Such a procedure will be accomplished by observing that

$$p(\theta_q|\boldsymbol{\theta}_{-\theta_q}, \mathbf{X}) \propto p(\mathbf{X}|\boldsymbol{\theta})p(\theta_q) \tag{5.21}$$

and by considering the likelihood function (5.18) and the prior distributions (defined in Section 5.3.1).

#### 5.3.4.1 Conditional distributions for the sources

Substituting expressions (5.18) and (5.11) into (5.21), one has

$$p(s_j(t)|\boldsymbol{\theta}_{-s_j(t)}, \mathbf{X}) \propto \exp\left[\sum_{i=1}^{n_m} -\frac{1}{2\sigma_i^2}\left(x_i(t) - e_i - d_i \log\left(a_{ij}s_j(t)^{z_i/z_j} + \sum_{b=1,b\neq j}^{n_s} a_{ib}s_b(t)^{z_i/z_b}\right)\right)^2 - \frac{(\ln(s_j(t)) - \mu_j)^2}{2\sigma_j^2}\right]\frac{1}{s_j(t)}\mathbb{1}_{[0,+\infty[}(s_j(t)). \tag{5.22}$$

#### 5.3.4.2 Conditional distributions for the sources hyperparameters $\boldsymbol{\phi}$

Because $p(\mathbf{X}|\boldsymbol{\theta})$ is not a function of the parameters $\boldsymbol{\phi}_j = [\mu_j \ \sigma_j]$, the conditional density of $\mu_j$ is given by

$$p\left(\mu_j|\sigma_j, \mathbf{S}_{(j,:)}\right) \propto p\left(\mathbf{S}_{(j,:)}|\mu_j, \sigma_j\right) p(\mu_j), \tag{5.23}$$

where $\mathbf{S}_{(j,:)}$ denotes all the elements of the $j$-th row. By substituting (5.11) and (5.12) into (5.23), we obtain:

$$p\left(\mu_j|\sigma_j, \mathbf{S}_{(j,:)}\right) \propto \prod_{t=1}^{n_d}\left[\exp\left(-\frac{(\ln(s_j(t)) - \mu_j)^2}{2\sigma_j^2}\right)\right]\exp\left(-\frac{\left(\mu_j - \mu_{\mu_j}\right)^2}{2\sigma_{\mu_j}^2}\right). \tag{5.24}$$

The first term of (5.24) can be rewritten as a Gaussian function in $\mu_j$, with mean $\mu_{L_{\mu_j}} = 1/n_d \sum_{t=1}^{n_d} \ln(s_j(t))$ and variance $\sigma_{L_{\mu_j}}^2 = \sigma_j^2/n_d$. Thus, (5.24) becomes a product of two Gaussian distributions which is a Gaussian distribution too, i.e.:

$$p\left(\mu_j|\sigma_j, \mathbf{S}_{(j,:)}\right) \propto \exp\left(-\frac{\left(\mu_j - \mu_{Post_{\mu_j}}\right)^2}{2\sigma_{Post_{\mu_j}}^2}\right), \tag{5.25}$$

where[4] $\sigma_{Post_{\mu_j}} = \sigma_{L_{\mu_j}}^2\sigma_{\mu_{\mu_j}}^2/(\sigma_{L_{\mu_j}}^2 + \sigma_{\mu_{\mu_j}}^2)$ and $\mu_{Post_{\mu_j}} = (\mu_{L_{\mu_j}}\sigma_{\mu_{\mu_j}}^2 + \mu_{\mu_{\mu_j}}\sigma_{L_{\mu_j}}^2)/(\sigma_{L_{\mu_j}}^2 + \sigma_{\mu_{\mu_j}}^2)$.

[4]The derivation of the mean and variance of a product of two Gaussian can be found in [98].

Similarly to the case of $\mu_j$, the conditional density of $r_j = 1/\sigma_j^2$ is given by $p\left(r_j|\mu_j, \mathbf{S}_{(j,:)}\right) \propto p\left(\mathbf{S}_{(j,:)}|\mu_j, r_j\right) p(r_j)$. Thus, by considering (5.11) and (5.13), one has

$$p\left(r_j|\mu_j, \mathbf{S}_{(j,:)}\right) \propto \prod_{t=1}^{n_d} \left[\sqrt{r_j} \exp\left(-0.5 r_j \left(\ln(s_j(t)) - \mu_j\right)^2\right)\right] r_j^{\alpha_{r_j}-1} \exp\left(\frac{-r_j}{\beta_{r_j}}\right) \mathbb{1}_{[0,+\infty[}(r_j). \tag{5.26}$$

We can rewrite $p(r_j|\mu_j, \mathbf{S}_{(j,:)})$ as a Gamma distribution, i.e.

$$p\left(r_j|\mu_j, \mathbf{S}_{(j,:)}\right) \propto r_j^{\alpha_{Post_{r_j}}} \exp\left(-\frac{r_j}{\beta_{Post_{r_j}}}\right) \mathbb{1}_{[0,+\infty[}(r_j), \tag{5.27}$$

where $\alpha_{Post_{r_j}} = \alpha_{r_j} + n_d/2$ and $\beta^{-1}_{Post_{r_j}} = \left(\sum_{t=1}^{n_d} \left(\ln(s_j(t)) - \mu_j\right)^2\right)/2\beta_{r_j}$ It is now clear that we obtain a conjugate pair and, thus, we can sample from $p\left(r_j|\mu_j, \mathbf{S}_{(j,:)}\right)$ by sampling from a Gamma distribution.

#### 5.3.4.3 Conditional distribution of $a_{ij}$

The derivation of the conditional distribution of $p(a_{ij}|\boldsymbol{\theta}_{-a_{ij}}, \mathbf{X})$ is close to the one conducted for $s_j(t)$. Indeed, by considering expression (5.18), (5.21), and (5.14), it turns out that

$$p(a_{ij}|\boldsymbol{\theta}_{-a_{ij}}, \mathbf{X}) \propto \exp\left[-\frac{1}{2\sigma_i^2} \sum_{t=1}^{n_d} \left(x_i(t) - e_i - d_i \log\left(a_{ij} s_j(t)^{z_i/z_j} + \sum_{b=1, b\neq j}^{n_s} a_{ib} s_b(t)^{z_i/z_b}\right)\right)^2\right] \mathbb{1}_{[0,1]}(a_{ij}). \tag{5.28}$$

#### 5.3.4.4 Conditional distribution of $d_i$

By using Equations. (5.9) and (5.15), and after some straightforward calculations, $p(d_i|\boldsymbol{\theta}_{-d_i}, \mathbf{X})$ can be written as the following Gaussian distribution

$$p(d_i|\boldsymbol{\theta}_{-d_i}, \mathbf{X}) \propto \exp\left(-\frac{\left(d_i - \mu_{Post_{d_i}}\right)^2}{2\sigma^2_{Post_{d_i}}}\right), \tag{5.29}$$

where $\sigma_{Post_{d_i}} = \sigma^2_{L_{d_i}} \sigma^2_{\mu_{d_i}} / (\sigma^2_{L_{d_i}} + \sigma^2_{\mu_{d_i}})$, $\mu_{Post_{d_i}} = (\mu_{L_{d_i}} \sigma^2_{\mu_{d_i}} + \mu_{\mu_{d_i}} \sigma^2_{L_{d_i}})/(\sigma^2_{L_{d_i}} + \sigma^2_{\mu_{d_i}})$, and

$$\mu_{L_{d_i}} = \frac{\left(\sum_{t=1}^{n_d} \left(x_i(t) - e_i\right)\right) \log\left(\sum_{b=1}^{n_s} a_{ib} s_b(t)^{z_i/z_b}\right)}{\left(\log\left(\sum_{b=1}^{n_s} a_{ib} s_b(t)^{z_i/z_b}\right)\right)^2}, \tag{5.30}$$

$$\sigma^2_{L_{d_i}} = \frac{\sigma^2_{\mu_{d_i}}}{\left(\log\left(\sum_{b=1}^{n_s} a_{ib} s_b(t)^{z_i/z_b}\right)\right)^2}. \tag{5.31}$$

#### 5.3.4.5 Conditional distribution of $e_i$

The development of this expression is similar to the one performed for $d_i$. After some calculations, it is not difficult to show that

$$p(e_i|\boldsymbol{\theta}_{-e_i}, \mathbf{X}) \propto \exp\left(-\frac{\left(e_i - \mu_{Post_{e_i}}\right)^2}{2\sigma^2_{Post_{e_i}}}\right), \tag{5.32}$$

where $\sigma_{Post_{e_i}} = \sigma^2_{L_{e_i}}\sigma^2_{\mu_{e_i}}/(\sigma^2_{L_{e_i}} + \sigma^2_{\mu_{e_i}})$, $\mu_{Post_{e_i}} = (\mu_{L_{e_i}}\sigma^2_{\mu_{e_i}} + \mu_{\mu_{e_i}}\sigma^2_{L_{e_i}})/(\sigma^2_{L_{e_i}} + \sigma^2_{\mu_{e_i}})$, and

$$\mu_{L_{e_i}} = \frac{\sum_{t=1}^{n_d}\left(x_i(t) - d_i \log\left(\sum_{b=1}^{n_s} a_{ib}s_b(t)^{z_i/z_b}\right)\right)}{n_d} \tag{5.33}$$

$$\sigma^2_{L_{e_i}} = \frac{\sigma_{e_i}}{n_d}. \tag{5.34}$$

#### 5.3.4.6 Conditional distribution of the noise variance $\sigma_i^2$

As discussed before, the attribution of a Gamma prior for $\gamma_i = 1/\sigma_i^2$ culminates in a conjugate pair. Indeed, by considering expressions (5.18) and (5.17), one can show that $p(\gamma_i|\boldsymbol{\theta}_{-\gamma_i}, \mathbf{X})$ can be reduced to the following Gamma distribution:

$$p(\gamma_i|\boldsymbol{\theta}_{-\gamma_i}, \mathbf{X}) \propto \gamma_i^{\alpha_{Post_{\sigma_i}}-1} \exp\left(\frac{-\gamma_i}{\beta_{Post_{\sigma_i}}}\right) \mathbb{1}_{[0,+\infty[}, \tag{5.35}$$

where $\alpha_{Post_{\sigma_i}} = \alpha_{\sigma_i} + n_d/2$ and $\beta^{-1}_{Post_{\sigma_i}} = \frac{1}{2}\sum_{t=1}^{n_d}\left(x_i(t) - e_i - d_i \log\left(\sum_{b=1}^{n_s} a_{ib}s_b(t)^{\frac{z_i}{z_b}}\right)\right)^2 + \beta^{-1}_{\sigma_i}$.

### 5.3.5 Algorithm Description

Let us make some remarks on the final algorithm, which is summarized in Table 5.1. In a first step, we must define hyperparameters that lead to non-informative distributions [139]. In the experiments described in Section 5.3.6, this strategy was implemented by setting the following values for the variances of the Gaussian priors: $\sigma^2_{d_i} = 0.01$ and $\sigma^2_{e_i} = 0.03$. Moreover, a high value of the parameter $\sigma^2_{\mu_j}$, which is related to the sources prior, was defined ($\sigma^2_{\mu_j} = 100$).

As discussed before, the resulting Markov chain of the Gibbs' sampler takes some time to converge to its stationary distribution (burn-in period). For determining the burn-in period, a visual inspection of the evolution of some channel states was done.

A last step in our algorithm concerns a post-processing stage for dealing with the scale and translation ambiguities inherent in blind methods. For example, in PNL mixtures, the best we can do is to obtain an estimation $\tilde{s}_{jt}$ given by $\tilde{s}_j(t) = a_j s_j(t) + b_j$, where $a_j$ and $b_j$ are unknown, and $s_j(t)$ is the actual source. Given that this ambiguity in not acceptable in a sensing problem, we are forced to use at least two calibration points in order to retrieve the scale and translation parameters. This can be done by a simple linear regression, i.e. we need to find $a_j$ and $b_j$ that minimize the mean squared error $J = 1/N_{cal}\sum_{n=1}^{N_{cal}}(\tilde{s}_j(n)^{(c)} - s_j(n)^{(c)})^2$, where $s_j(n)^{(c)}$ denotes the calibration points and $\tilde{s}_j(t)^{(c)}$ the corresponding estimations. The calibration procedure will be discussed in more details in Chapter 6.

#### 5.3.5.1 Conditional distributions and Metropolis-Hasting algorithm

The resulting conditional distributions for almost all parameters in Table 5.1 are given by standard distributions (normal and Gamma), which means that sampling is easy in these cases. However, because of the logarithm in the likelihood function, the expressions of $p(s_j(t)|\boldsymbol{\theta}_{-s_j(t)}, \mathbf{X})$ and $p(a_{ij}|\boldsymbol{\theta}_{-a_{ij}}, \mathbf{X})$ do not assume a standard form. Therefore, the simulation of these distributions requires a more sophisticated method. A possible choice here is to resort to the Metropolis-Hasting (MH) algorithm [140] for simulating $p(s_j(t)|\boldsymbol{\theta}_{-s_j(t)}, \mathbf{X})$ and $p(a_{ij}|\boldsymbol{\theta}_{-a_{ij}}, \mathbf{X})$. Strictly speaking, since we are incorporating MH steps into the Gibbs' sampler, the final algorithm should be classified as an hybrid MCMC method [72].

*Metropolis-Hasting algorithm*

The Metropolis-Hasting algorithm is also a MCMC method and, thus, it is based on building a Markov chain whose stationary distribution is given by the distribution to be sampled. To illustrate how the MH works, let us consider the simulation of a given distribution $p(x)$. The first step in the MH method concerns the definition of an instrumental (or proposal) distribution $g(x; y)$; this distribution should be easy to simulate as it will generate the candidate samples. For example, suppose that $x^{(t)}$ represents the current sample of $p(x)$ , then the following iteration is set for obtaining the next sample $x^{(t+1)}$:

1. $x^* \sim g(x; x^{(t)})$ (generation of candidate sample).
2. Calculate $a = \min\left(1, \frac{p(x^*)g(x^{(t)};x^*)}{p(x^{(t)})g(x^*;x^{(t)})}\right)$.
3. $u \leftarrow$ sample from a uniform distribution in $[0, 1]$.
4. if $u \leq a$, $x^{(t+1)} = x^*$ (accept the proposed sample) else $x^{(t+1)} = x^{(t)}$ (reject the proposed sample).

Note that the MH method demands only the simulation of $g(x; y)$ and the evaluation of $g(x; y)$ and $p(x)$. It can be shown [140, 72] that such a procedure indeed results in a Markov chain of stationary distribution $p(x)$.

An important practical question related to the MH algorithm is the definition of the instrumental distribution $g(x; y)$. Actually, in a theoretical standpoint, there are only some mild conditions to be respected by $g(x; y)$ so the Markov chain has $p(x)$ as stationary distribution [140]. However, in practice, the choice of $g(x; y)$ is fundamental because it determines the acceptation rate and how fast the Markov chain converges to $p(x)$ (see [9] for some examples). Moreover, a bad choice of $g(x; y)$ can make the chain to be confined in a local mode of the probability distribution to be sampled.

In the method described in Table 5.1, truncated Gaussian are considered as instrumental distributions in the MH steps. In order to obtain good acceptance rate, we conducted, for each situation, preliminary simulations to adjust the variances of these distributions.

Table 5.1: Proposed Bayesian source separation algorithm

1. Define hyperparameters $\mu_{\mu_j}$,$\sigma^2_{\mu_j}$,$\alpha_{p_j}$,$\beta_{p_j}$,$\alpha_{\sigma_i}$,$\beta_{\sigma_i}$;
2. Random initialization of the current samples $\boldsymbol{\theta}^0$;
3. Run Gibbs sampler
   For $m = 1$ to $M$ do
   - For $j = 1, \cdots, n_s$, $t = 1, \cdots, n_d$
     $s_j(t)^m \sim p(s_j(t)|\boldsymbol{\theta}_{-s_j(t)}, \mathbf{X})$ (Equation (5.22)) (simulation through MH algorithm)
   - For $j = 1, \cdots, n_s$
     $\mu_j^m \sim p(\mu_j|\boldsymbol{\theta}_{-\mu_j}, \mathbf{X})$ (Equation (5.25))
     $\sigma_j^m \sim p(\sigma_j|\boldsymbol{\theta}_{-\sigma_j}, \mathbf{X})$ (Equation (5.27))
   - For $i = 1, \cdots, n_m$, $j = 1, \cdots, n_s$
     $a_{ij}^m \sim p(a_{ij}|\boldsymbol{\theta}_{-a_{ij}}, \mathbf{X})$ (Equation (5.28)) (simulation through MH algorithm)
   - For $i = 1, \cdots, n_m$
     $d_i^m \sim p(d_i|\boldsymbol{\theta}_{-d_i}, \mathbf{X})$ (Equation (5.29))
     $e_i^m \sim p(e_i|\boldsymbol{\theta}_{-e_i}, \mathbf{X})$ (Equation (5.32))
     $\sigma_i^m \sim p(\sigma_i|\boldsymbol{\theta}_{-\sigma_i}, \mathbf{X})$ (Equation (5.35))

   end
4. Infer the sources through the Bayesian MMSE estimation

$$\tilde{s}_j(t) = \frac{1}{M-B} \sum_{m=B+1}^{M} \mathbf{s}_j(t)^m, \forall j, t, \tag{5.36}$$

   where $B$ denotes the number of iterations of the burn-in period.
5. Retrieve the source scale using $N_{cal}$ calibration points ($N_{cal} \geq 2$).

### 5.3.6 Results

To assess the performance of the algorithm described in Table 5.1, we conduct in a first moment a set of experiments considering artificially generated data. Then, in Section 5.3.6.2, we test our proposal with actual data.

#### 5.3.6.1 Experiments with artificial data

Based on the selectivity coefficients database presented in [152], we define the following testing scenarios:

- First scenario ($n_s = 3$ and $n_m = 3$): array of three electrodes (one $K^+$-ISE , one $NH_4^+$-ISE

-ISE and one $Na^+$-ISE ) to estimate $K^+$ , $NH_4^+$ and $Na^+$. Mixing system parameters: $\mathbf{A} = [1\ 0.16\ 0.40; 0.25\ 1\ 0.19; 0.40\ 0.13\ 1]$, $\mathbf{d} = [0.059\ 0.050\ 0.055]^T$ and $\mathbf{e} = [0.095\ 0.105\ 0.110]^T$.

- Second scenario ($n_s = 2$ and $n_m = 2$): array of two electrodes (one $Ca^{2+}$-ISE and one $Na^+$-ISE ) to estimate the activities of $Ca^{2+}$ and $Na^+$. Mixing system parameters: $\mathbf{A} = [1\ 0.39; 1\ 0.20]$, $\mathbf{d} = [0.026\ 0.046]^T$ and $\mathbf{e} = [0.100\ 0.090]^T$.

In the first scenario we have a PNL model as mixing system. In the second one, the mixing system is similar to the class considered in Chapter 3. Finally, we consider noisy mixtures with a signal-to-noise ratio of SNR = 18 dB in both cases.

We tested our method in a situation where the sources are realizations of log-normal distributions (the number of samples was $n_d = 500$). For the first scenario, we considered $P = 50000$ iterations for the Gibbs sampler with a burn-in period of $B = 30000$. The number of calibration points used in the post-processing stage was $N_{cal} = 5$. The performance indices in this situation were $\text{SIR}_1 = 12.83\,\text{dB}$, $\text{SIR}_2 = 19.0\,\text{dB}$, $\text{SIR}_3 = 17.4\,\text{dB}$, and $\text{SIR} = 16.4\,\text{dB}$, which indicates that our proposal was able to achieve a good source separation (to illustrate that, we show in Figure 5.1 the mixed signals, and in Figure 5.2, the actual sources and their respective estimations). For matter of comparison, we estimated the performance when considering the original parameters that originate the mixtures; the following values were obtained: $\text{SIR}_1 = 18.35\,\text{dB}$, $\text{SIR}_2 = 21.11\,\text{dB}$, $\text{SIR}_3 = 19.72\,\text{dB}$.

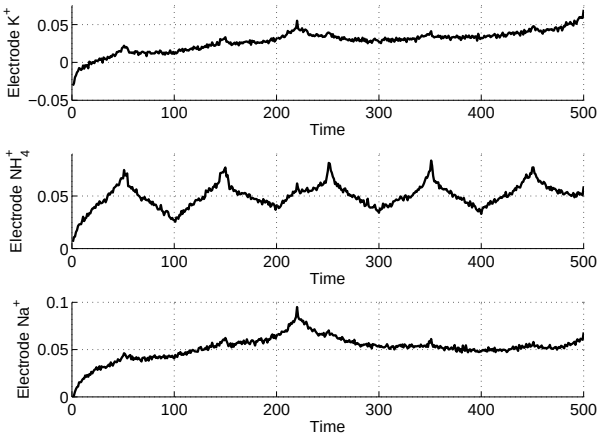


Figure 5.1: Artificial data (first scenario): ISE array outputs (mixtures).

In the second scenario, we considered $P = 25000$ iterations for the Gibbs sampler with a burn-in period of $B = 18000$, and $N_{cal} = 3$ calibration points were used. The performance indices in this case were $\text{SIR}_1 = 17.4\,\text{dB}$, $\text{SIR}_2 = 16.2\,\text{dB}$, and $\text{SIR} = 16.8\,\text{dB}$. As can be observed in Figures 5.3 and 5.4, our method was able to provide fair estimations of the sources.

*Analysis of the Markov Chains*

As we mentioned before, the length of the burn-in period was determined through visual inspection of the Markov chains. In Figure 5.5, we plot the Markov chains for the mixing

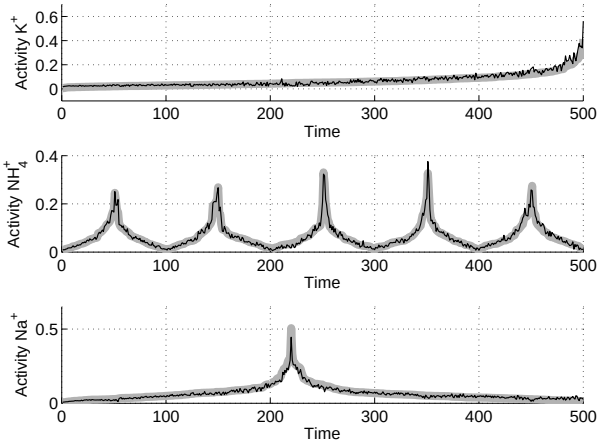


Figure 5.2: Artificial data (first scenario): actual sources (gray) and their estimation (black).

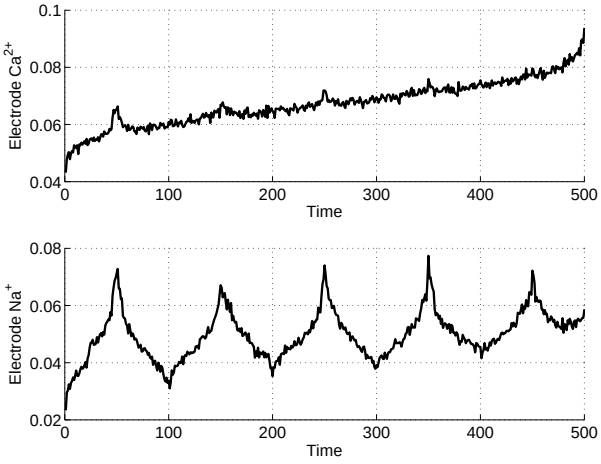


Figure 5.3: Artificial data (second scenario): ISE array outputs (mixtures).

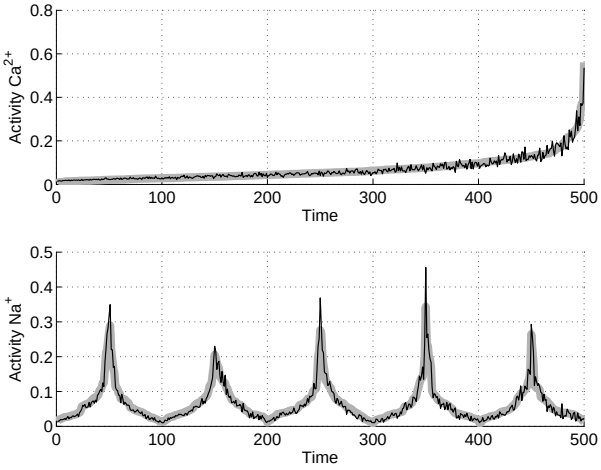


Figure 5.4: Artificial data (second scenario): actual sources (gray) and their estimation (black).

coefficient $a_{12}$ and for the sources at instant $t = 112$ (we considered the first scenario of the last section). Note that, after about 30000 iterations, the chain states indeed converge to values close to the actual ones, which are depicted in gray.

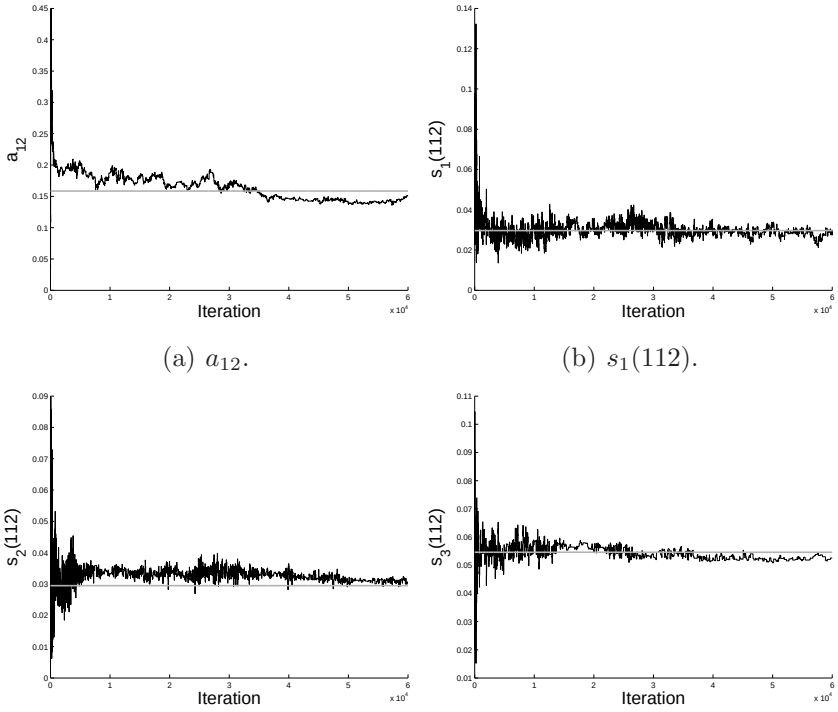


(a) $a_{12}$. (b) $s_1(112)$.

(c) $s_2(112)$. (d) $s_3(112)$.

Figure 5.5: Artificial data (first scenario): Markov chains.

#### 5.3.6.2 Experiments with actual data

In Chapter 2, we saw that the first scenario (detection of ammonium and potassium) was the one with higher level of interference. Motivated by that, we tested our Bayesian method to process the data acquired in the experiments S1NH$_4$10$^{-1}$K and S1NH$_4$10$^{-4}$K. After joining these two experiments in a single dataset, we obtained the sources shown in Figure 5.8. The total number of samples of the two experiments altogether was $n_d = 170$.

In Figure 5.6, we present the responses of the ISE array. Since we have access to the inputs and to the outputs of the electrode array, it is possible to analyze the fitness of the NE model for this case, that is, we can have an idea about the amount of noise in the mixing model. Concerning the potassium electrode, we measured a signal-to-noise ratio of $\mathrm{SNR}_{K^+} = 24\,\mathrm{dB}$. For the ammonium electrode, this value was given by $\mathrm{SNR}_{NH_4^+} = 20\,\mathrm{dB}$. We assumed a Gaussian modeling for the noise in each electrode, and, to have an insight into the pertinence of such assumption, the distribution of the regression errors is plotted in Figure 5.7.

After scale and translation normalization with $N_{cal} = 4$ calibration points, the performance indices (average of 30 experiments) obtained by the Bayesian method in this scenario were $\mathrm{SIR}_1 = 24.0\,\mathrm{dB}$, $\mathrm{SIR}_2 = 22.5\,\mathrm{dB}$ and $\mathrm{SIR} = 23.2\,\mathrm{dB}$. Concerning the parameters of the Gibbs

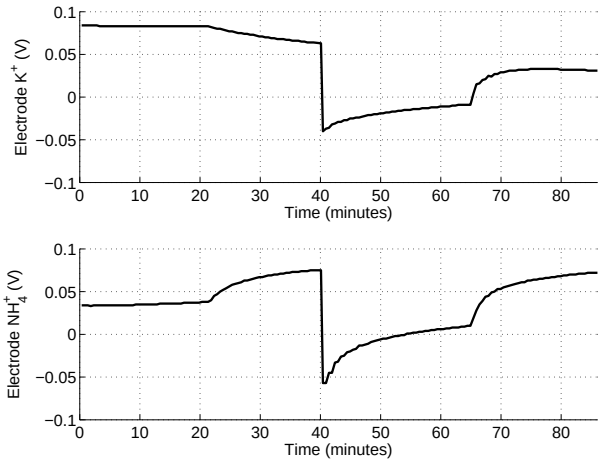


Figure 5.6: Real data: responses provided by the ISE array.

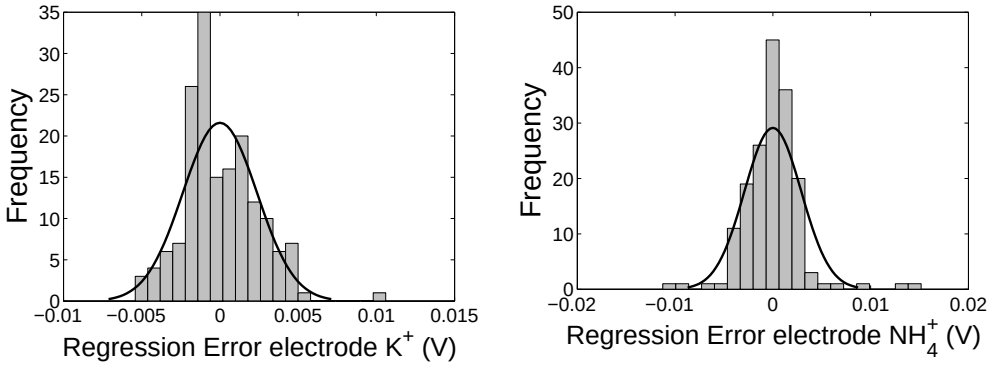


(a) Potassium electrode. (b) Ammonium electrode.

Figure 5.7: Histograms of the regression errors resulting from a fitting with the NE model. The black curves correspond to the fitted Gaussian distribution.

sampler, the number of performed iterations was $P = 10000$ and the burn-in period was $B = 7000$. The obtained signals are shown in Figure 5.8. Despite a small residual interference, mainly for the $K^+$ activity, the method was able to provide good estimations of the sources. On the other hand, the application of a PNL source separation method based on ICA [61] provided poor approximations of the sources ($\mathrm{SIR}_1 = 7.6\,\mathrm{dB}$, $\mathrm{SIR}_2 = -0.3$ and $\mathrm{SIR} = 3.6$).

#### 5.3.6.3 Discussion

The experiments with artificial data showed that the proposal can achieve good estimations even when the valences are different. In the scenario with real data, the Bayesian algorithm achieved a much better performance than the ICA-based PNL algorithm. In fact, in this case the sources were clearly dependent and, thus, they violated the fundamental assumption of any ICA method. Evidently, a scenario with dependent sources also poses a problem to a Bayesian method, since there is no guarantee that the provided data representation is unique in such a case. Nonetheless, in contrast to ICA, a Bayesian method does not optimize a functional associated

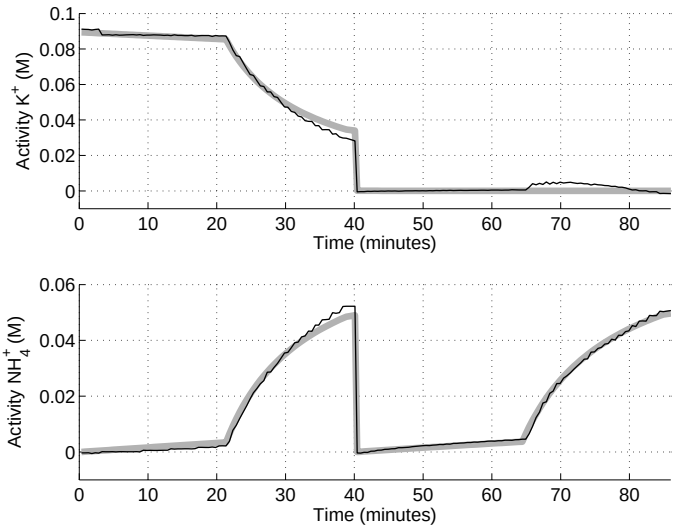


Figure 5.8: Real data: Retrieved signals (black) and actual sources (gray).

with the statistical independence. Rather, it searches for a "good" data representation given a set of prior information. Thus, in the Bayesian approach, the independence should be seen rather as a simplifying assumption, that is, we are just omitting an additional prior information to the inference machine, which may still work.

Concerning the algorithm's convergence, we observed that the Gibbs sampler may get trapped in local minima, thus leading to poor estimations. For the situations with two sources the percentage of poor convergences[5] was 3% for artificial data and 7% for the real case; in the case with three sources, this value attained 17%. Although we do not have access to the source, it is still possible to identify a bad solution: we observed that poor convergence usually implies in a significant mismatch between the representation provided by the Bayesian algorithm and the actual array response.

Another important point concerns the execution time of our method. For the experiments with real data, the MCMC algorithm took about[6] 26s to perform 10000 iterations. Nevertheless, the algorithm took 380s to perform 50000 iterations in the situation with three sources. This points out a well-known drawback of MCMC-based Bayesian methods: their computational burden can become quite large as the number of sources and samples grows.

Finally, let us make a remark concerning the choice of the priors. In this work, we tried to define priors 1) that ease the resulting inference problem and 2) that, based on the available information, limit the range of the unknown parameters. Evidently, there is no guarantee that our choices are optimum and, as we mentioned before, a large dataset of measurements would permit to refine the priors' definition. An interesting issue in this context would be to compare the selected priors with alternative models. Because the possibilities are non-exhaustive, we consider a single example where, instead of log-normal priors for the sources, Gamma distributions

[5]These percentages were obtained through a visual inspection after 30 executions.

[6]The method was implemented in Matlab (Windows XP) and the simulations were performed in a Intel Core 2 duo 3GHz, 2048MB RAM.

are considered.

After applying the solution with the Gamma modeling to process the real data, the obtained performance (average of 30 experiments with $N_{cal} = 4$ calibration points) —$\text{SIR}_1 = 22.4\,\text{dB}$ and $\text{SIR}_2 = 17.5\,\text{dB}$ —was inferior to that of the log-normal prior. Furthermore, as mentioned before, unlike the log-normal case, it is not possible to find a conjugate prior in the estimation of the Gamma distribution parameters. Thus, it becomes necessary to incorporate an additional Metropolis-Hastings algorithm into the Gibbs' sampler, which increases the algorithm's complexity and has the inconvenient of requiring the definition of instrumental distributions, which is not an easy task.

## 5.4 A Bayesian source separation method for linear and linear-quadratic mixtures

In this section, we continue our study on Bayesian methods. However, we now turn our attention to the linear-quadratic model which, as discussed in Chapter 1, is relevant in the context of tin oxide gas sensor arrays. Moreover, as it will be clarified in the sequel, the proposed method can also be applied to linear mixtures.

A first motivation behind a Bayesian source separation method tailored for LQ mixtures is related to the difficulty in defining a proper separating system to this case. In fact, we saw in Chapter 1 that a recurrent separating system was proposed [86, 87] to overcome this problem. Nonetheless, despite its simplicity and its good performance, this approach can operate only when the sources and the mixing parameters lie within the stability region of the recurrent system. Even if the development of more elaborate recurrent networks [51] can extend the stability region, it seems that the resulting training algorithms may be quite complicate in these new situations.

Conversely, in a Bayesian context, the definition of a separating system is not a problem given that BSS is seen rather as a data representation problem and, thus, there is no need to define a separating system in this case. A second fact that motivates the development of a LQ-BSS Bayesian method is related to the possibility of taking into account prior information other than the statistical independence. In our development, we will consider two prior information that are typical in chemical sensing applications, namely: 1) the bounds of the sources and of the mixing coefficient values are known in advance, and 2) the sources have a temporal structure.

Before getting into the details of our proposal, let us recapitulate the LQ mixing model:

$$x_i(t) = \sum_{j=1}^{n_s} a_{ij} s_j(t) + \sum_{1 \leq j < k \leq n_s} b_{ijk} s_j(t) s_k(t) + n_i(t), \quad \forall i \in 1, \ldots, n_m, \forall t \in 1, \ldots, n_d, \tag{5.37}$$

where $a_{ij}$ et $b_{ijk}$ are the mixing parameters and $n_i(t)$ corresponds to the noise term, which is assumed i.i.d. and Gaussian with unknown variance $\sigma_i^2$. In this situation, the unknown parameters are given by $\boldsymbol{\theta} = [s_j(t), a_{ij}, b_{ijk}, \sigma_i^2, \mu_j, p_j]$, where $\mu_j$ and $p_j$ correspond to the parameters related to the sources distributions.

Following the same steps conducted in Section 5.3, we will introduce in the sequel the proposed Bayesian BSS method for the mixing model (5.37).

### 5.4.1 Definition of prior distributions

#### 5.4.1.1 Sources

We here assume a modeling based on truncated Gaussian distributions for the sources. This distribution is interesting when, for instance, the limit values of the sources are known, which is usually the case in the chemical sensing applications considered in this work. In a first moment, the following i.i.d. modeling is considered

$$p(s_j(t)|\mu_j, p_j, s_j^{min}, s_j^{max}) = \frac{\sqrt{\frac{p_j}{2\pi}} \exp\left(-\frac{p_j}{2}\left(s_j(t)-\mu_j\right)^2\right) \mathbb{1}_{[s_j^{min}, s_j^{max}]}(s_j(t))}{\Phi\left(\sqrt{p_j}\left(s_j^{max}-\mu_j\right)\right) - \Phi\left(\sqrt{p_j}\left(s_j^{min}-\mu_j\right)\right)}, \tag{5.38}$$

where $\mu_j, p_j$ are the unknown distribution parameters, and $\Phi(\cdot)$ is the cumulative distribution function of the standard normal distribution. In Figure 5.9, the distribution (5.38) is plotted considering different parameters and bounds.

Very often in real problems, the sources present a temporal structure. Motivated by that, a second prior modeling[7] can be defined by substituting $\mu_j = s_j(t-1)$ in Equation (5.38). The resulting prior is a first-order Markovian model quite similar to the classical AR(1) model driven by Gaussian noise, with the only difference that the recurrence is limited in the interval $[s_j^{min}, s_j^{max}]$. Both in the i.i.d. and in the Markovian modeling, we assume that the sources are mutually independent, i.e. $p(\mathbf{S}) = \prod_{j=1}^{n_s} p(\mathbf{S}_{j,:})$.

#### 5.4.1.2 Sources hyperparameters

For the i.i.d. modeling, uniform priors are assigned for the sources hyperparameters, that is

$$p(\mu_j) \propto \mathbb{1}_{[\mu_j^{min}, \mu_j^{max}]}(\mu_j), \tag{5.39}$$

$$p(p_j) \propto \mathbb{1}_{[p_j^{min}, p_j^{max}]}(p_j), \tag{5.40}$$

where the parameters $\mu_j^{min}$, $\mu_j^{max}$, $p_j^{min}$ and $p_j^{max}$ should be assigned according to the available information. If, for example, the sources are expected to be concentrated near the minimum value, one can set $\mu_j^{min} < \mu_j^{max} < s_j^{min}$. Conversely, if no additional information is available, one must increase the limits of both hyperparameters. Regarding the Markovian modeling, we have only one hyperparameter ($p_j$) and the same prior of Equation (5.40) is assigned for it.

[7] Since the derivation of a Bayesian method is almost the same for the i.i.d. and the Markovian modeling, our calculations will be based in Equation (5.38). Note however that, in the Markovian modeling, there is no need to estimate the term $\mu_j$ that appears in this equation.

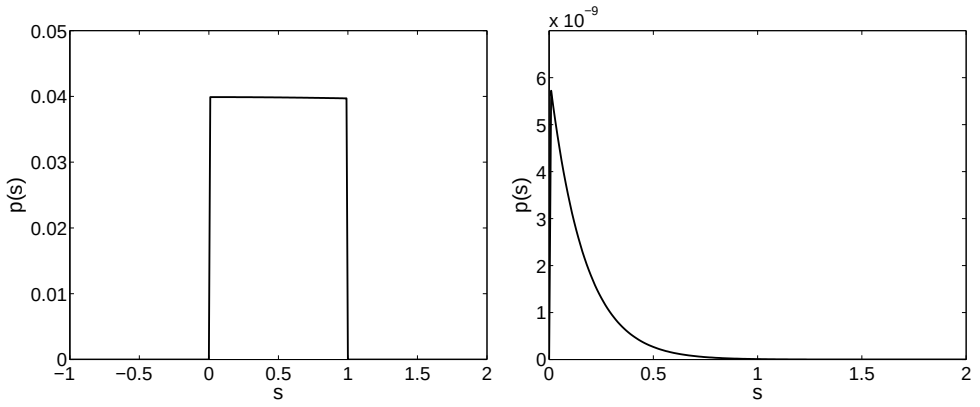


(a) $s_j^{min} = 0$, $s_j^{max} = 1$, $\mu_j = 0$ and $p = 0.01$.

(b) $s_j^{min} = 0$, $s_j^{max} = 100$, $\mu_j = -6$ and $p = 1$.

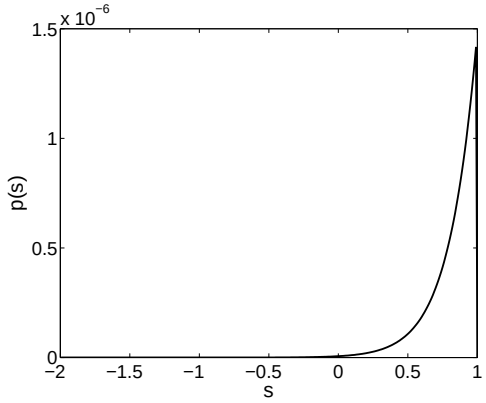


(c) $s_j^{min} = -100$, $s_j^{max} = 1$, $\mu_j = 6$ and $p = 1$.

Figure 5.9: Truncated Gaussian distribution.

#### 5.4.1.3 Mixing parameters

Before assigning priors for the mixing parameters, let us rewrite the LQ mixing model as

$$x_i(t) = \sum_{m=1}^{J} c_{im}\bar{s}_m(t) + n_i(t), \tag{5.41}$$

where $J = n_s + \frac{n_s!}{2(n_s-2)!}$. The vector $\mathbf{c}_i = [c_{i1}, \ldots, c_{iJ}]$ stems from the concatenation of $[a_{i1}, \ldots, a_{in_s}]$ and $[b_{i12}, \ldots, b_{in_s-1n_s}]$; and the vector $\bar{\mathbf{s}}(t) = [\bar{s}_1(t), \ldots, \bar{s}_J(t)]$ denotes the concatenation of the sources $[s_1(t), \ldots, s_{n_s}(t)]$ and the linear quadratic terms $[s_1(t)s_2(t), s_2(t)s_3(t) \ldots, s_{n_s-1}(t)s_{n_s}(t)]$. As it will clarified later, this representation allows us to check that the conditional distributions of $a_{ij}$ and $b_{ijk}$ used in the Gibbs' sampler assume similar expressions. Therefore, for sake of simplicity, both $a_{ij}$ and $b_{ijk}$ will be represented by $c_{im}$.

In our method, the mixing coefficients $c_{im}$ are modeled through uniform priors, i.e.

$$p(c_{im}) \propto \mathbb{1}_{[c_{im}^{min}, c_{im}^{max}]}(c_{im}). \tag{5.42}$$

The distribution bounds should be set based on the available information. An interesting aspect

of this modeling is that it renders possible to perform linear BSS using the same implementation of the LQ case. Indeed, if one sets $c_{in_s+1:J}^{min} = c_{in_s+1:J}^{max} = 0$, then the parameters that multiply the linear-quadratic terms become null and, thus, the resulting model becomes linear. Moreover, if $s_j^{min} = 0$ and $s_j^{max} \to \infty$, our proposal becomes able to model non-negative prior as in non-negative matrix factorization (NMF).

#### 5.4.1.4 Noise variances

Again, we assign Gamma priors for the noise precisions $r_i = 1/\sigma_i^2$, that is

$$p(r_i) \propto r_i^{\alpha_{r_i}-1} \exp\left(\frac{-r_i}{\beta_{r_i}}\right) \mathbb{1}_{[0,+\infty[}(r_i)\,. \tag{5.43}$$

As already discussed before, this choice culminates in a conjugate pair, which eases the sampling step in the Gibbs sampler.

### 5.4.2 Likelihood function

Due to the assumption of white Gaussian noise in the observation model, the likelihood function associated with the mixing model (5.37) is given by

$$p(\mathbf{X}|\boldsymbol{\theta}) = \prod_{t=1}^{n_d}\prod_{i=1}^{n_m} \mathcal{N}_{x_i(t)}\left(\sum_{j=1}^{n_s} a_{ij}s_j(t) + \sum_{1\leq j<k\leq n_s} b_{ijk}s_j(t)s_k(t); \sigma_i^2\right). \tag{5.44}$$

### 5.4.3 Bayesian inference and Gibbs sampler

Since we assume that all elements of $p(\boldsymbol{\theta})$ are statistically independent (except the sources $\mathbf{S}_{j,:}$ and their hyperparameters $\mu_j$ and $p_j$), the posterior distribution $p(\boldsymbol{\theta}|\mathbf{X})$ can be rewritten as

$$p(\boldsymbol{\theta}|\mathbf{X}) \propto p(\mathbf{X}|\boldsymbol{\theta}) \times \prod_{i=1}^{n_m}\prod_{m=1}^{J} p(c_{im}) \times \prod_{n=1}^{n_s} p(\mathbf{S}_{j,:}|\mu_j, p_j) \times \prod_{n=1}^{n_s} p(\mu_j) \times \prod_{n=1}^{n_s} p(p_j) \times \prod_{i=1}^{n_m} p(\sigma_i^2). \tag{5.45}$$

As it was done in Section 5.3.4, we set an inference scheme based on the Bayesian MMSE estimator and on the Gibbs' sampler. In this spirit, we provide in the sequel the expressions of the conditional distributions for each unknown parameter. This will be achieved by considering the expression (5.21) and the priors defined in Section 5.4.1.

#### 5.4.3.1 Conditional distribution: sources

It is not difficult to show that, by substituting expressions (5.21) and (5.38) into (5.21), one has

$$p(s_j(t)|\boldsymbol{\theta}_{-s_j(t)}, \mathbf{X}) \propto \exp\left[-\sum_{i=1}^{n_m}\frac{1}{2\sigma_i^2}\left(\Psi_{ijt}s_j(t) + \Omega_{ijt}\right)^2 - 0.5p_j\left(s_j(t)-\mu_j\right)^2\right]\mathbb{1}_{[s_j^{min}, s_j^{max}]}(s_j(t)), \tag{5.46}$$

where

$$\Omega_{ijt} = x_i(t) - \sum_{g=1, g\neq j}^{n_s} a_{ig} s_g(t) - \sum_{1\leq g<k\leq n_s, g\neq j} b_{igk} s_g(t) s_k(t), \tag{5.47}$$

and

$$\Psi_{ijt} = a_{ij} + \sum_{g=1, g\neq j}^{n_s} b_{ijg} s_g(t). \tag{5.48}$$

After expanding Equation (5.46), one can obtain the expression of the conditional distribution of the sources, given by

$$p(s_j(t)|\boldsymbol{\theta}_{-s_j(t)}, \mathbf{X}) \propto \exp\left(-\frac{\left(s_j(t) - \mu_{Post_j}\right)^2}{2\sigma^2_{Post_j}}\right) \mathbb{1}_{[s_j^{min}, s_j^{max}]}(s_j(t)), \tag{5.49}$$

where $\sigma_{Post_j} = \sigma^2_{L_j}\sigma^2_j/(\sigma^2_{L_j} + \sigma^2_j)$ and $\mu_{Post_j} = (\mu_{L_j}\sigma^2_j + \mu_j\sigma^2_{L_j})/(\sigma^2_{L_j} + \sigma^2_j)$, and

$$\sigma^2_{L_j} = \left(\sum_{i=1}^{n_c} \frac{\Psi^2_{ijt}}{\sigma^2_i}\right)^{-1}, \tag{5.50}$$

$$\mu_{L_j} = \sigma^2_{L_j} \sum_{i=1}^{n_c} \frac{\Omega_{ijt}\Psi_{ijt}}{\sigma^2_i}. \tag{5.51}$$

Expression (5.49) corresponds to a truncated Gaussian distribution and its simulation can be conducted, for instance, by the procedure proposed in [44]. The basic idea of this method is that, by defining a set of latent variables[8], one obtains a very simple method that only requires sampling from uniform distributions.

#### 5.4.3.2 Conditional distribution for the sources hyperparameters

Let us start with the derivation of the conditional distribution of $p_j$. As the likelihood function (5.44) is not a function of $p_j$, it asserts that $p(p_j|\mathbf{S}_{j,:}, \mu_j) \propto p(\mathbf{S}_{j,:}|, p_j, \mu_j)p(p_j)$, that is

$$p(p_j|\mathbf{S}_{j,:}, \mu_j) \propto p_j^{\frac{n_d}{2}} \exp\Big(-0.5p_j \sum_{t=1}^{n_d} (s_j(t) - \mu_j)^2\Big) \times \frac{\mathbb{1}_{[p_j^{min}, p_j^{max}]}(p_j)}{\Phi\left(\sqrt{p_j}\left(s_j^{max} - \mu_j\right)\right) - \Phi\left(\sqrt{p_j}\left(s_j^{min} - \mu_j\right)\right)}. \tag{5.52}$$

This expression does not assume a standard form because of the nonlinearity in the denominator of the second term. This is also true for the distribution $p(\mu_j|s_{j,:}, p_j)$ that appears in the i.i.d. modeling

$$p(\mu_j|\mathbf{S}_{j,:}, p_j) \propto \exp\Big(-0.5p_j \sum_{t=1}^{n_d} (s_j(t) - \mu_j)^2\Big) \times \frac{\mathbb{1}_{[\mu_j^{min}, \mu_j^{max}]}(\mu_j)}{\Phi\left(\sqrt{p_j}\left(s_j^{max} - \mu_j\right)\right) - \Phi\left(\sqrt{p_j}\left(s_j^{min} - \mu_j\right)\right)}. \tag{5.53}$$

[8] In fact, the method proposed in [44] can be regarded as a slice sampling method [72].

The non-standard distributions (5.52) and (5.53) could be simulated through the MH algorithm, as it was done in Section 5.3. However, as discussed before, this kind of solution requires the definition of an instrumental function which is not a trivial task. Besides, the presence of the MH algorithm would increase the complexity of our final solution because the burn-in period is usually bigger when MH stages are considered.

Aiming at a more practical algorithm, we consider an alternative approach based on the use of latent variables. The key idea, which was developed in [75], is based on the following transformation:

$$l_j(t) = \mu_j + p_j^{-1/2} \times \Phi^{-1}\left(\frac{\Phi\left(\sqrt{p_j}\left(s_j(t)-\mu_j\right)\right) - \Phi\left(\sqrt{p_j}\left(s_j^{min}-\mu_j\right)\right)}{\Phi\left(\sqrt{p_j}\left(s_j^{max}-\mu_j\right)\right) - \Phi\left(\sqrt{p_j}\left(s_j^{min}-\mu_j\right)\right)}\right). \tag{5.54}$$

It can be proved [75] that if $s_j(t)$ follows a truncated Gaussian with parameters $\mu_j$ and $p_j$, then $l_j(t)$ is distributed according to a Gaussian distribution of mean $\mu_j$ and precision $p_j$.

From the discussion of the last paragraph, $l_j(t)$ follows a Gaussian distribution, and therefore

$$p(\mathbf{L}_{j,:}|\mu_j, p_j) = \prod_{t=1}^{n_d} \sqrt{\frac{p_j}{2\pi}} \exp\left(-\frac{p_j}{2}\left(l_j(t)-\mu_j\right)^2\right). \tag{5.55}$$

Using this equation and the prior distributions (5.39) and (5.40), one can show that the distributions of $\mu_j$ and $p_j$ conditionally to $l_j(t)$ are given by

$$p(\mu_j|p_j, \mathbf{L}_{j,:}) \propto p(\mu_j)p(\mathbf{L}_{j,:}|\mu_j, p_j) \propto \mathbb{1}_{[\mu_j^{min},\mu_j^{max}]}(\mu_j) \times \exp\left(-\frac{p_j \cdot n_d}{2}\left(\mu_j - \frac{1}{n_s}\sum_{t=1}^{n_d} l_j(t)\right)^2\right) \tag{5.56}$$

$$p(p_j|\mu_j, \mathbf{L}_{j,:}) \propto p(p_j)p(\mathbf{L}_{j,:}|\mu_j, p_j) \propto \mathbb{1}_{[p_j^{min},p_j^{max}]}(p_j) \times p_j^{\frac{n_d}{2}} \exp\left(-p_j \sum_{t=1}^{n_d}\left(l_j(t)-\mu_j\right)^2\right). \tag{5.57}$$

These two distributions reveal an interesting point: if one considers the latent variables $l_j(t)$ instead of the sources $s_j(t)$, then one ends up with tractable distribution, since $p(\mu_j|p_j, \mathbf{L}_{j,:})$ is a truncated Gaussian whereas $p(p_j|\mu_j, \mathbf{L}_{j,:})$ is a truncated Gamma. The simulation of these two distributions can be conducted through the method proposed in [44].

Although originally proposed [75] for i.i.d. models, the procedure described in the last paragraphs can be readily extended for estimating $p_j$ when the Markovian modeling is considered. Indeed, this can be done by observing that the innovation process $s_j(t) - s_j(t-1)$ is distributed according to a truncated Gaussian whose limits depend on the time index. Therefore, the conditional distribution of $p_j$ in this case is obtained by substituting $\mu_j = s_j(t-1)$ in Equation (5.57). Also, the same substitution should be conducted in Equation (5.54) for the calculation of the latent variables $l_j(t)$.

#### 5.4.3.3 Conditional distribution: mixing parameters

The calculation of the conditional distributions can be done by substituting equations (5.42) and (5.44) into Equation (5.21). Therefore, one obtains after some calculations

$$p(c_{im}|\boldsymbol{\theta}_{-c_{im}}, \mathbf{X}) \propto \exp\left( -\frac{\rho_{im}^L}{2}(c_{im} - \nu_{im}^L)^2 \right) \mathbb{1}_{[c_{im}^{min}, c_{im}^{max}]}(c_{im}), \tag{5.58}$$

where

$$\rho_{im}^L = \sigma_i^2 \sum_{t=1}^{n_d} \bar{s}_m(t), \tag{5.59}$$

$$\nu_{im}^L = \frac{\sum_{t=1}^{n_d} \bar{s}_m(t) \left( x_i(t) - \sum_{g=1, g\neq m}^{J} c_{ig} \bar{s}_g(t) \right)}{\sum_{t=1}^{n_d} \bar{s}_m(t)^2}. \tag{5.60}$$

Again, the resulting conditional distribution (Equation (5.58)) is a truncated Gaussian distribution and can be simulated by the technique presented in [44].

#### 5.4.3.4 Conditional distribution: noise variances

The conditional distribution of the noise precision $r_i = 1/\sigma_i^2$ is obtained by substituting (5.43) and (5.44) into Equation (5.21), which gives

$$p(r_i|\boldsymbol{\theta}_{-r_i}, \mathbf{X}) \propto r_i^{\frac{n_d}{2}} \exp\left(-0.5 r_i \Theta_{it}\right) r_i^{\alpha_{r_i}-1} \exp\left(\frac{-r_i}{\beta_{r_i}}\right) \mathbb{1}_{[0,+\infty[}(r_i) \tag{5.61}$$

where $\Theta_{it} = x_i(t) - \sum_{j=1}^{n_s} a_{ij} s_j(t) - \sum_{i,j,k} b_{ijk} s_j(t) s_k(t)$. This equation can be rewritten as

$$p(r_i|\boldsymbol{\theta}_{-r_i}, \mathbf{X}) \propto \exp\left( -r_i \left( 0.5\Theta_{it} + \frac{1}{\beta_{r_i}} \right) \right) r_i^{\frac{n_d}{2} + \alpha_{r_i} - 1} \mathbb{1}_{[0,+\infty[}(r_i), \tag{5.62}$$

which is a Gamma distribution with parameters $\alpha_i = \frac{n_d}{2} + \alpha_{r_i}$ and $\beta_i^{-1} = 0.5\Theta_{it} + \beta_{r_i}^{-1}$.

### 5.4.4 Algorithm Description

In Table 5.2, we summarize the developed Bayesian method for LQ-BSS. A first step in this case concerns the definition of the hyperparameters. As already discussed, information about the bounds of the sources and the mixing coefficients can be taken into account through the hyperparameters $s_j^{min}$, $s_j^{min}$, $c_{im}^{min}$ and $c_{im}^{max}$. For instance, in the context of chemical sources, it is natural to assume $s_j^{min} = 0$. Concerning the sources hyperparameters, if no additional information is available, one must adopt the following strategy: $p_j^{min} = 0$, $p_j^{max} >> 0$, and $\mu_j^{min} << 0$, $\mu_j^{max} >> 0$ (for the i.i.d. case).

### 5.4.5 Results

We here present some experiments to assess the performance of Bayesian solution proposed in the last sections. In a first moment, we test our method in a linear source separation. In this case we consider a toy problem but also a situation with actual data. Then, in Section 5.4.5.2, we address the case of linear-quadratic mixtures.

Table 5.2: Bayesian source separation algorithm for LQ mixtures

1. Define hyperparameters $s_j^{min}$, $s_j^{min}$, $p_j^{min}$, $p_j^{max}$, $c_{im}^{min}$, $c_{im}^{max}$ and, for the i.i.d. case, $\mu_j^{min}$, $\mu_j^{max}$;

2. Random initialization of the current samples $\boldsymbol{\theta}^0$;

3. Run Gibbs sampler
   For $m = 1$ to $M$ do

   - For $j = 1, \cdots, n_s$, $t = 1, \cdots, n_d$
     $s_j(t)^m \sim p(s_j(t)|\boldsymbol{\theta}_{-s_j(t)}, \mathbf{X})$ (Equation (5.49))
   - Define latent variables $l_j(t)$ (Equation 5.54)
   - For $j = 1, \cdots, n_s$
     $\mu_j^m \sim p(\mu_j|\boldsymbol{\theta}_{-\mu_j}, \mathbf{L}_{j,:}, \mathbf{X})$ (Equation (5.56)) (only for the i.i.d. case)
     $p_j^m \sim p(p_j|\boldsymbol{\theta}_{-p_j}, \mathbf{L}_{j,:}, \mathbf{X})$ (Equation (5.57))
   - For $i = 1, \cdots, n_m$, $j = 1, \cdots, J$
     $c_{ij}^m \sim p(c_{ij}|\boldsymbol{\theta}_{-c_{im}}, \mathbf{X})$ (Equation (5.58))
   - For $i = 1, \cdots, n_m$
     $r_i^m \sim p(r_i|\boldsymbol{\theta}_{-r_i}, \mathbf{X})$ (Equation (5.62))

   end

4. Infer the sources through the Bayesian MMSE estimation

$$\tilde{s}_j(t) = \frac{1}{M-B} \sum_{m=B+1}^{M} \mathbf{s}_j(t)^m, \forall j, t, \tag{5.63}$$

   where $B$ denotes the number of iterations of the burn-in period.

5. Retrieve the source scale using $N_{cal}$ calibration points ($N_{cal} \geq 2$).

#### 5.4.5.1 Separation of linear mixtures

*Synthetic Data*

To illustrate the performance of our proposal in a linear case, we tested it in situations where $n_d = 300$, $n_s = 3$, $n_m = 3$; and the mixing matrix is given by $\mathbf{A} = [1\ 0.5\ 0.5\ ;0.6\ 1\ 0.3\ ;0.8\ 0.4\ 1]$ . Three scenarios were considered: 1) the sources are realizations of truncated Gaussian distributions (matched case with our i.i.d. modeling); 2) the sources are realizations of truncated Gaussian Markovian process (matched case with our Markovian modeling); 3) the sources correspond to a sine wave, a ramp function and a sawtooth wave. In all these situations the SNR at each sensor was 20 dB. The total number of iterations of the Gibbs' samples was

$P = 10000$ with a burn-in period of $B = 5000$.

Table 5.3: SIR(dB) for the separation of linear mixtures (synthetic data).

| | Situation 1 (i.i.d. trunc. Gaussian) | Situation 2 (Markovian trunc. Gaussian) | Situation 3 (deterministic sources) |
|---|---|---|---|
| Bayesian method (i.i.d. modeling) | 17.50 | 17.69 | 15.55 |
| Bayesian method (Markovian modeling) | 12.60 | 17.07 | 18.37 |
| FastICA | 20.43 | 17.74 | 11.81 |

The results presented in Table 5.3 represent the mean SIR over 50 experiments. Despite a (not surprisingly) performance degradation when the Markovian prior is used for separating i.i.d. sources, our proposal was able to separate the sources. However, the FastICA algorithm [90] gave us better results in the first scenario and equivalent results in the second one. On the other hand, the application of this method on the third situation did not provide satisfactory results. This was due to the existence of two correlated sources in this scenario. It is worth remembering that, in contrast to the Bayesian approach, the FastICA searches for independent components and, therefore, it may fail when the sources are not independent.

*Actual data*

We also tested the Bayesian solution (linear case) with the data acquired in the experiments S1NH$_4$10$^{-1}$K and S1NH$_4$10$^{-4}$K; this is the same configuration considered in Section 5.3.6.2 and the corresponding outputs of the ISE array are depicted in Figure 5.6. As the Bayesian method considered here is aimed at linear mixtures, we had to set a strategy to invert the logarithm functions present in the NE model. This was done through the method introduced in Section 4.3 (more precisely we considered the results described in Section 4.3.6.3). The hyperparameters were defined as follows: $s_j^{min} = a_{ij}^{min} = 0$, $s_j^{max} = a_{ij}^{max} = 1$. For the Gibbs' sampler, we considered 12000 iterations with a burn-in period of 7000 samples. Finally, to retrieve the sources scales, we make use of the same $N_{cal} = 4$ calibration points considered in Section 5.3.6.2.

In Figures 5.10(a) and 5.10(b), we plot the retrieved sources obtained by the Bayesian method with i.i.d. modeling and Markovian modeling, respectively. The performance indices were quite similar in these two cases: SIR$_1$ = 17.74 dB, SIR$_2$ = 22.13 dB and SIR= 19.94 dB (i.i.d. modeling), and SIR$_1$ = 17.68 dB, SIR$_2$ = 22.11 dB and SIR= 19.90 dB (Markovian modeling). Note that, despite the fair estimations, the combination of the Bayesian linear method with the method introduced in Section 4.3 performed worst than the Bayesian method presented in Section 5.3.6.2 (complete solution). Finally, in Figure 5.10(c), we show the sources obtained by the SOBI algorithm [26]. In this case, while the estimation of the first source is slightly better (SIR$_1$ = 18.45) than the one provided by the Bayesian method, the SOBI algorithm failed to recover the second source (SIR$_2$ = 9.73)

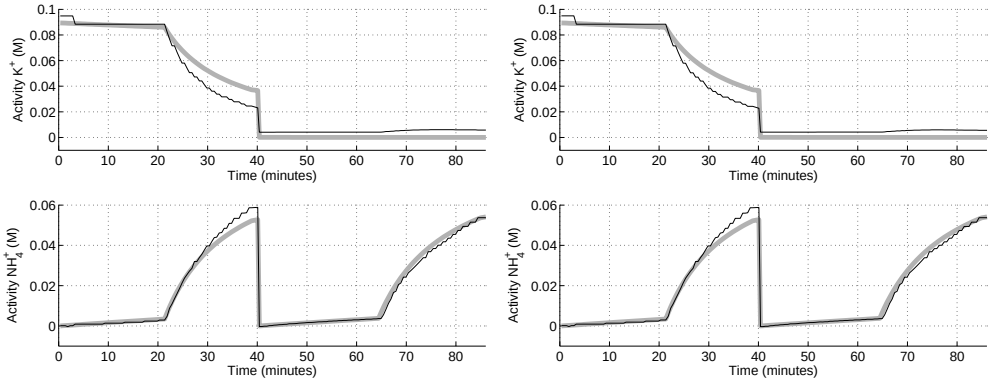


(a) Bayesian method (i.i.d. modeling). (b) Bayesian method (Markovian modeling).

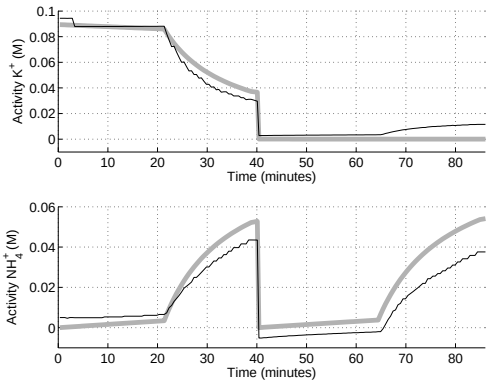


(c) SOBI algorithm.

Figure 5.10: Experiments with actual data: retrieved signals (black) and actual sources (gray).

#### 5.4.5.2 Separation of linear-quadratic mixtures

In a first moment, we considered a situation where $n_d = 500$, $n_s = 2$ and $n_m = 2$. The original sources and the mixtures are presented in Figures. 5.11(a) and 5.11(b), respectively. The mixing parameters were selected $a_{11} = 1$, $a_{12} = 0.5$, $b_{112} = 0.2$, $a_{21} = 0.5$, $a_{22} = 1$, $b_{212} = 0.2$, and the SNR at each sensor was 30 dB. The hyperparameters related to the limit values of the prior distributions were[9] $s_j^{min} = c_{im}^{min} = 0$ and $s_j^{max} = c_{im}^{max} = 1$. Concerning the Gibbs sampler parameters, the total number of iteration was $P = 20000$ with a burn in period of $B = 8000$. In this situation, the obtained performed index were SIR= 26.63 dB for the i.i.d. modeling and SIR= 27.47 dB for the Markovian modeling. We also tested the ICA method proposed in [87] which was able to provide good approximations (SIR= 22.58 dB). Despite the better performance, it worth mentioning that the gains brought by our method comes at the price of a greater computational effort.

We assessed our method in a second scenario similar to the first one with the only difference that the mixing parameters are now given by $a_{11} = 1$, $a_{12} = 0.7$, $b_{112} = 0.6$, $a_{21} = 0.6$, $a_{22} = 1$, $b_{212} = 0.6$. Our method was able to retrieve the sources both for i.i.d. modeling

[9] We set $a_{11}^{min} = a_{22}^{min} = 1$ to avoid scaling ambiguities.

(SIR= 22.17 dB) and for the Markovian modeling (SIR= 23.40 dB). To illustrate that, we showed in Figure 5.11 the retrieved sources for the Markovian modeling (the estimated mixing coefficients were $\hat{a}_{12} = 0.64$, $\hat{b}_{112} = 0.69$, $\hat{a}_{21} = 0.56$, and $\hat{b}_{212} = 0.64$ ). Note that, despite the noise amplification, which is typical in nonlinear systems, the retrieved signals are close to the sources. Conversely, in this new case, the method proposed in [87] failed to separate the sources since the mixing coefficients violate the stability condition of the recurrent separating system.

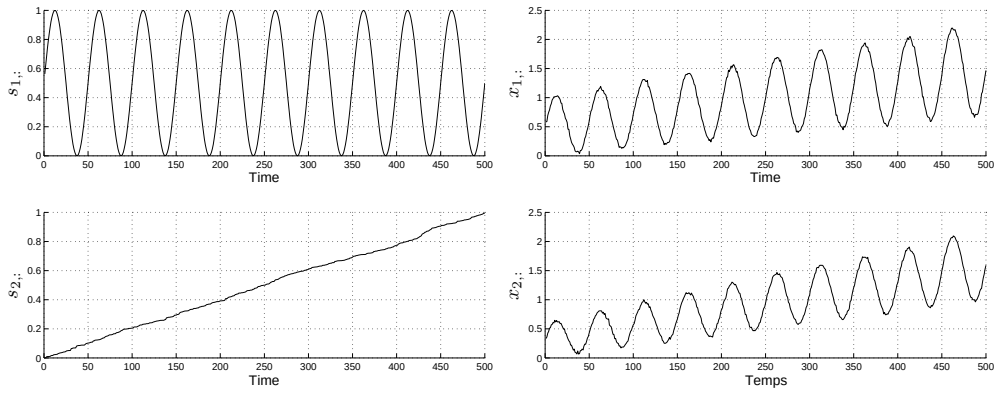


(a) Sources (b) Mixtures

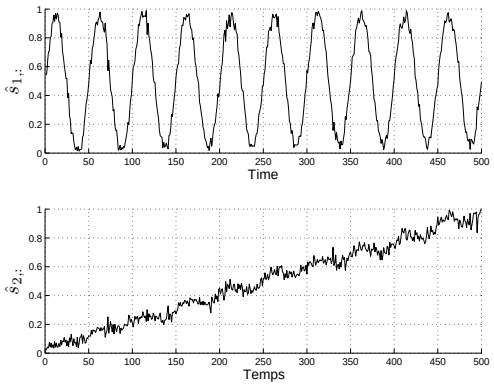


(c) Retrieved sources

Figure 5.11: Separation of LQ mixtures (Markovian modeling): $\text{SIR}_1 = 23.25$ dB and $\text{SIR}_2 = 23.54$ dB.

## 5.5 Conclusion

A first contribution of this chapter was a Bayesian source separation method tailored for the NE model. The implementation of our idea relied on MCMC methods. A set of simulations with synthetic data illustrated the effectiveness of the proposed method in the case when the valences of the ions are equal (PNL model) but also when they are different (mixing model considered in Chapter 3). Moreover, we also tested our proposal considering the experiments of Chapter 2 that present the higher degree of interference. The obtained results showed that the Bayesian algorithm was able to deal with these actual data even under adverse conditions, namely: reduced number of samples and sources with a not negligible degree of correlation.

Conversely, the use of an ICA-based solution failed to separate the sources in this case.

In a second part of this chapter, we considered a Bayesian method aimed at source separation of linear and LQ mixtures. The resulting method was based on truncated Gaussian priors and we considered an i.i.d. as well as a Markovian modeling for the sources[10]. By relying on the definition of latent variables, we could avoid the presence of MH stages, which in turn led to algorithms not requiring the specification of instrumental distributions. The conducted experiments attested to the viability of the proposed method and showed that it is particularly useful in some situations where ICA methods cannot be applied.

A final remark here concerns the computational complexity of the methods introduced in this chapter; this is actually the main drawback of MCMC methods. Indeed, as we could see in the first part of this chapter, the computational burden becomes quite large with increasing number of samples and sources. In this context, there are some perspectives involving the reduction of this complexity. A first one is to consider Hamiltonian MCMC methods to accelerate the sampler's convergence. Also, simplifications regarding the method's implementation could be envisaged. For example, some calculations could be parallelized by considering, for instance, an implementation tailored for a graphics processing unit (GPU). Finally, another approach to obtain a simpler Bayesian implementation could be achieved by defining methods based on the variational approximation [146]. The difficulty here is that such a framework strongly relies on the existence of conjugate priors.

[10]We also investigated the use of Markovian priors in the Bayesian method developed in Section 5.3. However, the resulting algorithm in this case did not work properly.

# Chapter 6

# Practical issues

## 6.1 Introduction

In this brief chapter, we consider some issues that are important in the application of the source separation methods described in the last chapters to real problems. We focus on arrays of ion-selective electrodes. In a first moment, we discuss some questions related to the post-processing stage needed for circumventing the scale ambiguities typical of BSS. Then, we briefly comment on some practical limitations that may pose some problems to the source separation methods, e.g. the time required by ISEs to achieve the steady state.

## 6.2 Circumventing the scale ambiguity

As we mentioned in Chapter 1, the absence of strong prior information in blind source separation methods culminates in permutation and scale ambiguities. Very often, finding the sources up to an unknown permutation does not pose any particular problem. Moreover, in applications in which one is only interested in retrieving the sources waveforms, the scale ambiguity can be accepted. Unfortunately, this is not the case in chemical sensing applications as the main goal is to retrieve the correct value of the concentration and not a scaled version.

Due to the limitation described in the last paragraph, the application of source separation methods to chemical sensor arrays should be followed by a post-processing whose goal is to retrieve the correct scale. This additional stage requires, at least, two calibration points. Evidently, in view of this requirement, we may ask ourselves why not simply use the available calibration points for performing supervised processing. For example, we could define a separating system (inverse of NE model) where the estimate $\hat{s}_j(t)$ is given by

$$\hat{s}_j(t) = \sum_{i=1}^{n_m} a_{ij}^* 10^{\frac{x_i(t)-e_i^*}{d_i^*}}. \tag{6.1}$$

Then, we could estimate $a_{ji}^*$, $d_i^*$, and $e_i^*$ based on a supervised approach, i.e. by minimizing the

following MSE regression criterion

$$J = \sum_{j=1}^{n_s} \sum_{t=1}^{n_d} \left(\hat{s}_j(t) - s_j(t)\right)^2 . \tag{6.2}$$

We will refer to such strategy as the supervised-NE algorithm.

Evidently, the performance of the supervised-NE algorithm depends on the number of available calibration points. To illustrate that, we show Figure 6.1 the resulting SIR as the number of calibrations points $N_{cal}$ grows. In this figure, which represents an average of 100 runs, one can note that supervised-NE method requires $N_{cal} = 20$ for providing a SIR of approximately 20 dB (SIRs bellow this value indicate a poor source separation).

Also in Figure 6.1, we plot the performance of the Bayesian source separation proposed in Section[1] 5.3. It is interesting to note that our Bayesian method only needs $N_{cal} = 3$ to provide an estimation of approximately 20 dB. Of course, this difference[2] between the number of calibration points is achieved because the "real" data processing in our proposal is done by the Bayesian BSS algorithm and the calibration points are only used to circumvent the signal ambiguities.

Figure 6.1 is quite useful in that it clarifies the benefits brought by source separation methods. The first remarkable point is that, when the acquisition of calibration points is not a stringent problem, the employment of supervised method should be favored. Conversely, the application of unsupervised methods becomes attractive when the number of calibration points is relatively small; in our example, for instance, the performance of source separation methods is better than that of the supervised-NE algorithm when there are less than 40 calibration points.

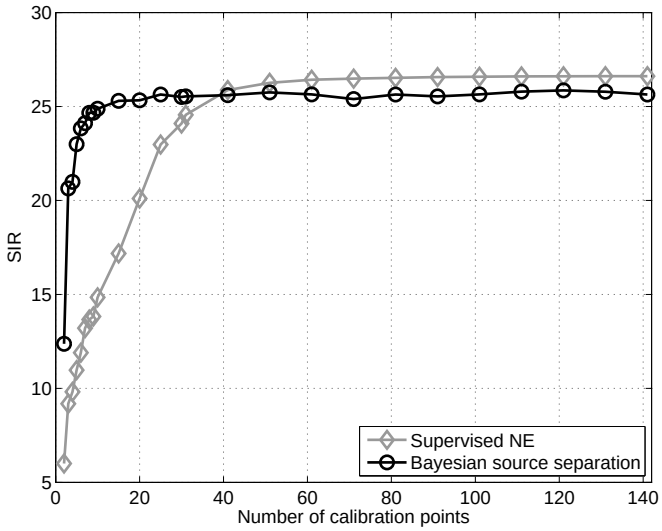


Figure 6.1: Performance index as the number of calibration points grows.

[1] In this case, we considered the scenario with actual described in Section 5.3.6.2.

[2] In Figure 6.1, we plot the training performance of the supervised-NE algorithm. If the test error were plotted, then the difference between the number of calibration points required by the supervised NE method and the one required by the Bayesian method would be slightly bigger.

## 6.3 Difficulties found in practice

In this section, we discuss some practical issues that may hinder the application of source separation methods to ISE arrays.

### 6.3.1 Electrode's dynamics

All along our work, we have assumed that the mixing process that takes in place in an ISE array is instantaneous. However, it is well known [114] that the time taken by an ISE to reach its steady response may not be negligible. The problem here is that, due to the assumption of an instantaneous model, one must wait until the electrode's stabilization to acquire a sample. Of course, this means that the minimum sampling rate that one can consider is limited by the electrode's transition time.

In the experiments that were described in Chapter 2, the injection of solutions took place every 30 seconds while the samples were acquired every 5 seconds. This long period of injection gave some margin to the stabilization of the electrodes. However, if a lower period of injection were considered, we might face some problems given that a new injection could take place before the stabilization of the electrodes regarding the preceding injection. In other words, instantaneous models may not be suitable to fast-varying (high-frequency) signals. An interesting question in this context is the study of dynamical mixing models for these particular cases.

### 6.3.2 Hysteresis

During our experiments, in a test with the a $K^+$-ISE and a $NH_4^+$-ISE, we observed a particular behavior in the response of the $K^+$-ISE that resembled the hysteresis phenomenon. This can be observed in Figure 6.2, which depicts the $K^+$-ISE response as a function of the activity of potassium. It should be noted, however, that the concentration of $NH_4^+$ is also varying in the considered test and, thus, although different responses for the same activity of $K^+$ was obtained, the concentrations of $NH_4^+$ were different. That is, the different responses for the same activity of $K^+$ could be attributed to the interference ion $NH_4^+$-ISE. Nonetheless, it seems that is not the only factor that is influencing the response of the $K^+$-ISE. Indeed, curiously enough, we observed that, for a same activity of $K^+$, the response of the $K^+$-ISE was larger for a smaller activity of $NH_4^+$, which contradicts what we expect from the interference phenomenon. This is the reason why we attribute the strange behavior shown in Figure 6.2 to a phenomenon related to a system memory.

Electrodes presenting hysteresis may pose serious problems to the methods developed in this thesis, given that the adopted mixing model does not take into account such a phenomenon.

### 6.3.3 Estimation of concentration

Because the proposed methods are based on the NE model, the sources correspond to the ionic activities. In some applications, however, the quantity of interest is the concentration. Of course, if one knowns the exact composition of the solution under analysis, then one can

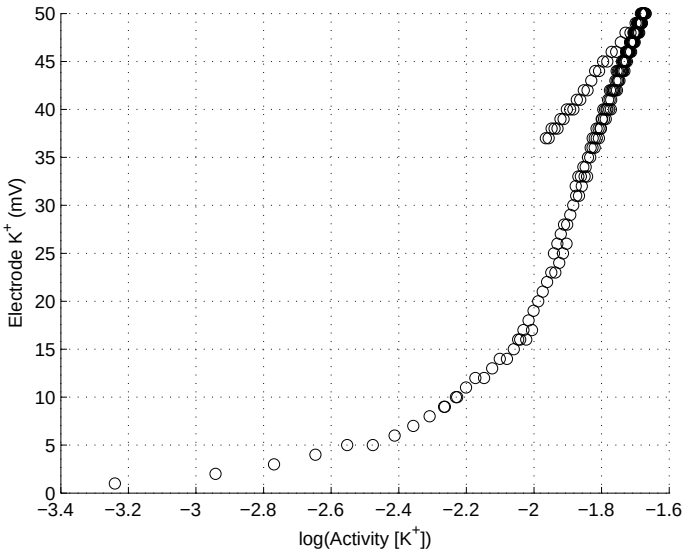


Figure 6.2: Hysteresis in the response of the $K^+$-ISE.

estimate the concentrations from the activities by using the Debye-Hückel equation (see Section 1.2.1). Nonetheless, this procedure cannot be used anymore if there is no information about which ions are in the solution.

## 6.4 Conclusion

In this chapter, we briefly discuss some practical questions related to the application of source separation methods to the design of ISE arrays. By comparing the number of calibration points required by a source separation method and a supervised one to achieve a satisfactory performance, we tried to highlight in which situations the application of the methods developed in this thesis may be interesting. Also, we listed some practical problems that may hamper the application of source separation methods to ISE arrays.

# Conclusions

In this thesis, we considered the development of nonlinear source separation methods designed for mixing models that are related to chemical sensor arrays. The focus of our research was on arrays of ion-selective electrodes. Yet, our achievements may also be useful for the case of arrays of ISFETs, given that such a sensor is often described through the same models used for ISEs. In the present research, we also presented a contribution regarding the linear-quadratic model, which is relevant in the context of arrays of tin oxide gas sensors.

## Summary of contributions

The main contributions of this thesis are related to the development of new algorithms for source separation in nonlinear models originated from the Nicolsky-Eisenman equation. In this context, a first contribution was to address the situation in which the valences of the ions under analysis are different. This case results in a nonlinear model characterized by the presence of a power term. As discussed in Chapter 3, one of the challenges in this type of mixing model was how to define the separating system. Inspired by the solution proposed in [86], we showed that a simple yet efficient way to define the separating system in this case is to resort to recurrent systems. Of course, in such a situation, it became of paramount importance to study the stability of the recurrent separating system so we could have an idea about the range of concentrations and selectivity coefficients within which the proposed method works properly.

Still in Chapter 3, we studied different types of ICA algorithms for adjusting the parameters of the recurrent network set as separating system. In a first moment, we considered an algorithm based on the nonlinear decorrelation principle. Despite its simplicity, we saw that such a method has some performance limitations especially when the sources are close to the stability boundary. Motivated by that, we studied, in a second moment, algorithms based on the minimization of the mutual information between the retrieved sources. In this spirit, we developed a paradigm based on the notion of the differential of the mutual information.

In Chapter 4, we described two contributions based on the use of prior information. In the first one, we developed a way to adjust the Nernstian slopes for the case of the mixing model considered in Chapter 3. The developed method assumes that one of the sources does not vary in a certain time window. This hypothesis allowed us to formulate a criterion founded on geometrical issues.

In a second part of Chapter 4, we turned our attention to the PNL mixing model, which is

relevant for the application considered in this work because the NE equation, for ions of equal valence, becomes an example of PNL model. Based on the assumption that the sources are bandlimited signals, we showed that is possible to define a simple two-stage method, in which the nonlinear stage of the PNL model can be counterbalanced by observing the effects of a nonlinear function on the spectral content of the mixtures. Then, once the nonlinear stage is inverted, the remaining task is of linear natural and, thus, can be dealt with through standard linear source separation.

The data obtained in the experiments described in Chapter 2 shed some light on some difficulties that are often found in real applications. For example, the sources may present a certain degree of correlation and the number of available sample may be quite reduced. Since these facts render difficult the application of ICA methods to our problem (at least to the available data), we investigated, in Chapter 5, the benefits brought by a Bayesian formulation. In a first part of that chapter, we developed a Bayesian source separation for the NE model. We tried to exploit some information that is typical of chemical sensing application, e.g. the fact that the sources are non-negative since they represent concentrations. To implement our Bayesian algorithm, we resorted to an inference scheme based on MCMC methods. The resulting algorithm has led to the most important practical result of the present research: we could perform source separation in a scenario with actual data. It is noteworthy that, to the best of our knowledge, this work was the first one to report results with actual data, thus showing that the application of source separation methods to potentiometric arrays is indeed viable and can pave way for new improvements in chemical sensing system.

Also in Chapter 5, we developed a Bayesian method for the separation of linear-quadratic models. Based on the definition of auxiliary variables, we obtained a method that can be implemented in a simple manner. Moreover, we showed through simulations that the developed method is particularly useful in some cases where ICA methods fail.

Finally, in Chapter 6, we discussed some practical issues that may pose some problems to the application of source separation methods to real problems of chemical sensing.

## Perspectives

The benefits brought by chemical sensor arrays equipped with source separation techniques were highlighted in Chapter 6; we showed, for instance, that such an approach leads to solutions that work even if only a reduced number of samples is available. Of course, in a practical context, this nice feature is quite useful; for instance a less demanding calibration step may ease analysis in the field. Yet, despite the encouraging results obtained in this research, there are still many questions that should be investigated before envisaging the incorporation of source separation blocks into commercial chemical analyzers.

A first important question that must be addressed concerns the number of sources. All along this thesis, we mainly considered that there were two sources and that such an information was known in advance. However, in a practical situation, there might be many sources and, still more problematic, it is not assured that their exact number be known.

A second interesting point to be investigated is related to the underlying mixing process in chemical sensor arrays. In our work, we have considered instantaneous mixing models. However, as discussed in Chapter 6, sensors like ISEs do have a clear dynamical behavior. Besides, several works [109, 155] on gas sensor arrays have shown that the array's dynamics carries some information regarding the mixing process. In view of such observations, it might be interesting to investigate whether we can exploit these dynamical aspects in an unsupervised paradigm by, for instance, formulating a dynamical source separation problem. More generally, we believe that a more precise mixing model could increase the estimation quality, thus permitting the use of source separation methods even in very-high-precision applications.

Finally, another important issue to be considered in future works concerns the definition of more efficient practical algorithms. For instance, all the methods proposed in this thesis operate in an off-line fashion and, thus, cannot be applied in applications requiring real-time operation. Moreover, we also intent to improve the proposed off-line methods. For example, in our Bayesian solution, the inference stage was carried out by means of sampling methods, which often result in time-consuming algorithms when the number of sources and samples is large. One perspective in this context is to investigate Bayesian methods based on the variational approximation [146], since they provide a less complex solution in terms of computational burden.

# Appendix A

# Ambiguities associated with the model (3.1)

In this appendix, we discuss the ambiguities associated with the mixing model (3.1). With that goal in mind, let us consider a situation with two sources and two mixtures. In this case, one has the following mixing model:

$$x_1 = e_1 + d_1 \log(z_1) = e_1 + d_1 \log\Big(s_1 + a_{12} s_2^k\Big), \tag{A.1}$$

$$x_2 = e_2 + d_2 \log(z_2) = e_2 + d_2 \log\Big(s_2 + a_{21} s_2^{1/k}\Big). \tag{A.2}$$

A first point to be addressed concerns the influence of the off-set term $e_i$. In this spirit let us consider the inversion of the nonlinear stage through the following functions:

$$q_1 = 10^{\frac{x_1 - e_1^*}{d_1^*}}, \tag{A.3}$$

$$q_2 = 10^{\frac{x_2 - e_2^*}{d_2^*}}, \tag{A.4}$$

where $e_i^*$ and $d_i^*$ denote the parameters of the separating system. It can be easily verified that

$$q_1 = 10^{\left(\frac{e_1 - e_1^*}{d_1^*}\right)} z_1^{\frac{d_1}{d_1^*}}, \tag{A.5}$$

$$q_2 = 10^{\left(\frac{e_2 - e_2^*}{d_2^*}\right)} z_2^{\frac{d_2}{d_2^*}}. \tag{A.6}$$

From this expression, it becomes clear that the parameter $e_i^*$ only scales $z_i^{d_1/d_1^*}$. As a consequence, it is not possible to retrieve $e_i^*$ by means of ICA methods given that statistical independence is not altered by scaling.

Another interesting point concerns the sources scaling. Actually, when one fixes $a_{11} = a_{22} = 1$ in a linear model with two sources and two mixtures, there is no scale ambiguity in the estimation of the sources. However, this is no longer true for the model (A.2). Indeed, consider the following solution $s_1^* = Ss_1$ and $s_2^* = Ss_2$, where $S$ is a constant representing the scale indeterminacy. To verify if the sources can be scaled, we must check whether it is possible

rewrite (A.2) but now in terms of $s_1^*$ and $s_2^*$. In this spirit, let us assume that $k = 1$ (PNL model). It is not difficult to check that (A.2) can be written as follows

$$x_1 = e_1^* + d_1 \log\left(s_1^* + a_{12} s_2^*\right), \tag{A.7}$$

$$x_2 = e_2^* + d_2 \log\left(s_2^* + a_{21} s_2^*\right), \tag{A.8}$$

where $e_i^* = e_i + d_i^* \log(S)$. This expression points out that the solutions $s_i^* = S s_i$ are valid, which in turn confirms that there is a scale ambiguity in the analyzed case.

# Appendix B

# Optimization via the opt-aiNet algorithm

In this appendix, we describe the opt-aiNet[1] algorithm [47], which was used for accomplishing optimization tasks in Chapters 3 and 4. The opt-aiNet algorithm was inspired by the modus operandi of the immunological system. The applicability of the opt-aiNet to signal processing problems was firstly studied by Attux [11]. In this work, it has been shown that the opt-aiNet is particularly interesting to overcome the following difficulties: 1) existence of bad local minima, 2) impossibility to calculate the derivatives of the cost-function and 3) risk of instability during the learning phase.

The opt-aiNet can be classified as an evolutionary algorithm. A fundamental notion in such class of algorithms is the concept of population, which comprises a set of individuals, each of them representing a candidate solution for the considered optimization problem. Another important concept in evolutionary algorithms is the fitness of each individual. The fitness of an individual is related to the cost function evaluated at the solution represented by that individual. Since the opt-aiNet maximizes the fitness of the population during the iterative procedure, for maximization problems, the fitness can be simply defined as $f = J$, where $J$ corresponds to cost function. Conversely, for minimization problems, the fitness is given by $f = 1/(1 + J)$.

The robustness of the opt-aiNet to suboptimal convergence is due to the existence of a mechanism that guarantees diversity within the individuals of the population, thus minimizing the risk of having candidate solutions converging to a same local mode of the cost function. Another interesting aspect of the opt-aiNet is the presence of a mechanism to automatically control the size of the population. This characteristic is not found in more classical evolutionary techniques such as the genetic algorithms.

In Table B.1, we present the opt-aiNet algorithm. Briefly speaking, there are two main stages in this method: the first one concerns the step 2 in Table B.1 and is related to a local search procedure whose goal is to improve the fitness of the population through cloning, mutation and selection operators. Step 3 is related to the mechanism responsible for controlling the size of the population and for keeping a satisfactory level of diversity. This is done by suppressing similar

[1] Opt-aiNet is an acronym for Artificial Immune Network for Optimization.

Table B.1: The opt-aiNet algorithm.

1. Initialization: randomly create a population;
2. Local searching: while stopping criterion is not met, do:
   (a) Clonal expansion: for each individual, determine its fitness $f_i$. Generate a set of $Nc$ clones, which are the exact copies of their parent individuals;
   (b) Mutation: mutate each clone $c_i^*$ with a rate that is inversely proportional to the fitness $f_i$ of its parent individual $c_i$, which itself is kept unmutated:

$$c_i^* = c_i + \alpha N(0,1), \text{ with } \alpha = \beta^{-1} \exp\left(-f_i^*\right), \tag{B.1}$$

   where $N(0,1)$ corresponds to the realization of a normal variable; $\beta$ is a free parameter that controls the decay of the inverse exponential function.
   (c) Selection: for each group composed of the parent individual and of their mutated clones, select the individual with highest fitness and calculate the average fitness of the selected individuals.
   (d) Local convergence: if the average fitness of the population does not vary significantly from one iteration to the other, go to the next step; else, return to Step 2;
3. Interactions in the population;
   (a) Individual interactions: determine the similarity between each pair of individuals in the population ;
   (b) Individual suppression: eliminate all but one of the individual whose affinity (similarity calculated by the Euclidean distance) with each other is lower than a pre-specified threshold $\sigma_s$, and determine the size of the population;
   (c) Diversity: introduce a number of new randomly generated individual into the population and return to Step 2.

individuals.

In the opt-aiNet algorithm, there are some parameters that should be defined, notably the number of clones per individual $N_c$, the suppression threshold $\sigma_s$ and the parameter $\beta$ which is related to the mutation. There is no systematic way to adjust all these parameters and, very often, they are adjusted based on preliminary simulations. Concerning the initial size of the population, its definition does not pose a problem since there is an automatic mechanism to control this parameter.

# Appendix C

# Blind extraction of smooth signals through the SOFI algorithm

## C.1 Introduction

In this appendix, we describe a novel linear source separation method for retrieving baseband signals having different bandwidths. Such a configuration is characterized by the existence of inactive bands in the frequency domain. By exploiting the eigenstructure of the mixtures covariance matrix calculated in these inactive bands, we develop a simple yet efficient extraction procedure that works in an ordered fashion, in which the sources are extracted according to their degree of smoothness. Numerical results attest the viability of the proposal.

The work presented in this appendix was done in cooperation with professor Bertrand Rivet.

## C.2 Mixing model and assumptions

We consider a linear mixing model, i.e. the vector $\mathbf{x}(t) = [x_1(t) \dots x_M(t)]^T$ containing the $M$ mixtures is given by

$$\mathbf{x}(t) = \mathbf{A}\mathbf{s}(t), \tag{C.1}$$

where $\mathbf{s}(t) = [s_1(t) \dots s_N(t)]^T$ represents the $N$ sources, and $\mathbf{A} \in \mathbb{R}^{M \times N}$ is the mixing matrix. The $i$-th column of $\mathbf{A}$ is represented by $\mathbf{a}_i$, i.e. $\mathbf{A} = [\mathbf{a}_1 \dots \ \mathbf{a}_N]$.

The following hypotheses are considered:

H1) $M \geq N$, i.e. the number of mixtures is greater or equal to the number of sources, which is assumed to be known.

H2) The sources covariance matrix is given by $R_{\mathbf{s}} = E\{\mathbf{s}(t)\mathbf{s}(t)^T\} = \text{diag}(\sigma_{s_1}^2, \dots, \sigma_{s_N}^2)$, where $\sigma_{s_i}^2$ denotes the variance of the $i$-th source.

H3) Each source $s_i(t)$ is a baseband signal with maximum frequency given by $B_{s_i}$, where $B_{s_1} \neq B_{s_2} \neq \dots \neq B_{s_N}$.

Concerning the hypothesis H1, if $M > N$ then a dimensional reduction, e.g. via principal component analysis (PCA), should be done to obtain $M = N$. Hypothesis H2 assures uncorrelated sources. Finally, hypothesis H3 guarantees sources with different spectral contents, which is a necessary condition for identifiability in methods based on second-order statistics. For the sake of clarity, we also assume that $B_{s_1} < B_{s_2} < \ldots < B_{s_N}$. In view of the permutation ambiguity, there is no loss of generality in this additional assumption, and our method works no matter the original order of the sources.

## C.3 The covariance matrix eigenstructure in inactive bands

Equation. (C.1) also holds in the frequency domain[1], i.e.

$$\mathbf{x}(f) = \mathbf{A}\mathbf{s}(f). \tag{C.2}$$

In view of assumption H3, the baseband sources are inactive in certain frequency bands. For instance, the spectrum of the signal having smaller bandwidth, $s_1(f)$, is inactive beyond the frequency $B_{s_1}$.

Sources having inactive bands can be detected through second-order statistics [138, 149]. Indeed, let us consider a frequency band, represented by $\gamma$, where $K$ signals are inactive, i.e. for $f \in \gamma, \exists \kappa_1, \ldots, \kappa_K \ / \ s_{\kappa_1}(f) = \ldots = s_{\kappa_K}(f) = 0$. In this case, the mixing model becomes overdetermined ($N$ mixtures and $N-K$ sources) and, thus, the covariance matrix of the mixtures in the band[2] $\gamma$, $R_{\mathbf{x}}(\gamma)$, becomes rank deficient. The key point here is that the number of null eigenvalues corresponds to the number of inactive sources, i.e. it is possible to search, in a blind fashion, all the inactive bands by analyzing the profile of the eigenvalues of $R_{\mathbf{x}}(f)$ for all frequencies. This is illustrated in Figure C.1 which shows the DCT of three baseband sources[3] and the eigenvalues of $R_{\mathbf{x}}(f)$.

In practice, the identification of inactive bands is done by searching for the eigenvalues that are smaller than a pre-defined threshold $\phi$. However, suppose that one of the sources, say $s_1$, is much less powerful than the other ones. In this case, even when all the sources are active, the eigenvalue of $R_{\mathbf{x}}(f)$ associated with $s_1$ is much smaller than the other eigenvalues, which may lead to an incorrect inactive period detection. As shown in [149, 138], this problem can be mitigated by replacing the ordinary eigenvalue decomposition by the generalized eigenvector decomposition (GEVD) of the matrices $(R_{\mathbf{x}}(f), R_{\mathbf{x}}([0,1]))$. As a corollary of the result shown in [149], the number of null generalized eigenvalues associated with the GEVD of $(R_{\mathbf{x}}(f), R_{\mathbf{x}}([0,1]))$ also gives the number of inactive sources in the frequency window (size $W$) centered at $f$.

[1] We considered the discrete cosine transform (DCT) to obtain a frequency domain representation. The DCT has the advantage of being a real-valued transform.

[2] The following notation is adopted: given a vector $\mathbf{x}(f)$ of signals in a frequency representation, $R_{\mathbf{x}}([B_{x_1}, B_{x_2}])$ and $R_{\mathbf{x}}(f)$ denote, respectively, the covariance matrix of $\mathbf{x}(f)$ calculated in the band $[B_{x_1}, B_{x_2}]$ and in a frequency window of size $W$ centered at $f$.

[3] We consider the normalized frequency where $B = 1$ corresponds, in the analog domain, to $F_s/2$ ($F_s$ being the sampling frequency).

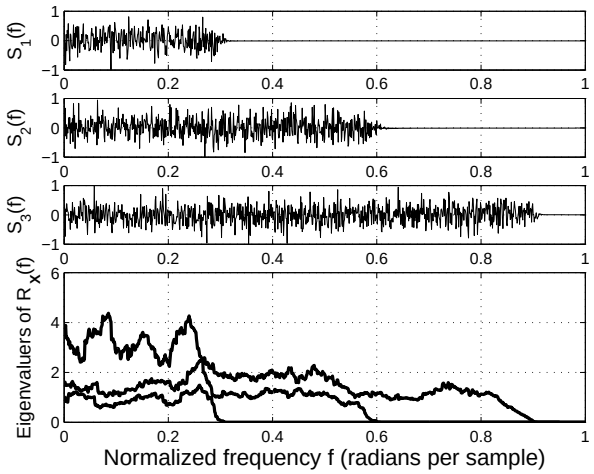


Figure C.1: DCTs of sources (first three signals) and the eigenvalues of $R_{\mathbf{x}}(f)$. The number of null eigenvalues indicates the number of inactive bands.

## C.4 SOFI algorithm

In this section, we discuss how the SOFI algorithm makes use of the particular eigenstructure of $R_{\mathbf{x}}(f)$ for sequentially extracting the sources. A first step in this context is to estimate, through a sliding-window of size $W$, the covariance matrix $R_{\mathbf{x}}(f)$ for all frequencies. Then, as discussed before, the generalized eigenvalues of $(R_{\mathbf{x}}(f), R_{\mathbf{x}}([0,1]))$ can be used to identify the inactive frequency bands. In practical terms, this is done by comparing the generalized eigenvalues at a given frequency $f$ with a pre-established threshold $\phi$.

Based on the information brought by the generalized eigenvalues, one can identify, for instance, the frequency interval $f \in [B_{s_1}, B_{s_2}]$, in which only $s_1(f)$ is inactive. The key point here is that the generalized eigenvector $\mathbf{v}_1$ associated with the unique null generalized eigenvalue of $(R_{\mathbf{x}}([B_{s_1}, B_{s_2}]), R_{\mathbf{x}}([0,1]))$ is orthogonal to all the columns of $\mathbf{A}$ except $\mathbf{a}_1$. Indeed, in this situation one has

$$R_{\mathbf{x}}([B_{s_1}, B_{s_2}])\mathbf{v}_1 = \mathbf{0}. \tag{C.3}$$

As the sources are uncorrelated (H2) and $s_1(f)$ is inactive in the interval $[B_{s_1}, B_{s_2}]$ (H3), one can write[4]

$$R_{\mathbf{x}}([B_{s_1}, B_{s_2}]) = \mathbf{A}R_{\mathbf{s}}([B_{s_1}, B_{s_2}])\mathbf{A}^T = [\mathbf{a}_2 \dots \mathbf{a}_N]\mathrm{diag}(\sigma^2_{s_2(f)}, \dots, \sigma^2_{s_N(f)})[\mathbf{a}_2 \dots \mathbf{a}_N]^T. \tag{C.4}$$

By substituting Equation (C.4) into Equation (C.3), one readily obtains $\mathbf{v}_1^T\mathbf{A} = [\alpha\ 0 \dots 0]$, where $\alpha \neq 0$, which means that $\mathbf{v}_1$ can be used to extract the smoothest source $s_1(f)$.

Even though the idea described above aims at the extraction of the smoothest source, i.e. the one having bandlimited in $B_{s_1}$, it can also be used for recovering the remaining sources. This can be achieved through a deflation procedure (see [163] for instance), in which the goal is

[4]Without loss of generality, $s_2(f), \dots, s_N(f)$ are supposed centered here.

to eliminate the contribution of the estimated source $\hat{s}_1(f) = \mathbf{v}_1^T \mathbf{x}(f)$ to $\mathbf{x}(f)$. In mathematical terms, this procedure is given by

$$\mathbf{x}(f) \leftarrow \mathbf{x}(f) - \mathbf{h}_1 \hat{s}_1(f) \tag{C.5}$$

where $\mathbf{h}_1 = E\{\mathbf{x}(f)\hat{s}_1(f)\}/E\{\hat{s}_1^2(f)\}$ (this vector minimizes $E\{(\mathbf{x}(f) - \mathbf{h}_1\hat{s}_1(f))^2\}$).

As the outcome of the first deflation is a BSS problem with $N$ mixtures and $N-1$ sources, we reduce the dimension of $\mathbf{x}(f)$ via PCA to obtain a $(N-1) \times (N-1)$ model. After that, we retrieve a similar scenario to the one that we had before the first GEVD, but now $s_2(f)$ appears as the smoothest source. Therefore, this signal can be estimated through the GEVD of $R_{\mathbf{x}}([B_{s_2}, B_{s_3}])$ and $R_{\mathbf{x}}([0,1])$. Finally the remaining sources can be extracted by repeating the same steps described so far, as detailed in Algorithm 1.

**Algorithm 1** SOFI algorithm

1: **if** $M > N$, reduce the dimension of $\mathbf{x}(t)$ to $N$ via PCA **end if**
2: Calculate a frequency representation of the mixtures $\Rightarrow x_i(f) = DCT(x_i(t))$, for $i = 1, \ldots, N$
3: For all frequencies $f$, estimate $R_{\mathbf{x}}(f)$ (covariance matrix calculated in a frequency window of size $W$ and centered in $f$) and compute the GEVD of $(R_{\mathbf{x}}(f), R_{\mathbf{x}}([0,1]))$
4: Based on the number of generalized eigenvalues smaller than $\phi$ for each frequency, identify the frequency bands $[0, B_{s_1}]$,$[B_{s_1}, B_{s_2}]$, ...,$[B_{s_N}, 1]$
5: **for** $i = 1$ to $N-1$ **do**
6: Compute GEVD($R_{\mathbf{x}}([B_{s_i}, B_{s_{i+1}}])$,$R_{\mathbf{x}}([0,1])$) $\Rightarrow \mathbf{v}_i$ is the generalized eigenvector associated with the smallest generalized eigenvalue.
7: Estimation of $s_i(f) \Rightarrow \hat{s}_i(f) = \mathbf{v}_i^T \mathbf{x}(f)$
8: Deflation step $\Rightarrow$ Equation (C.5)
9: Reduce the dimension of $\mathbf{x}(f)$ to $N - i$ through PCA
10: **end for**

Some remarks on the SOFI algorithm. First, if the extraction of only a few smooth sources is envisaged, then there is no need to estimate the eigenvalues profile for all frequencies: one may stop when the number of inactive bands is equal to the number of sources to be extracted. Second, even when H3 is only approximated, the SOFI algorithm can recover all the sources except those having the same bandwidth.

## C.5 Experiments

Before describing the experiments, let us discuss the selection of $W$ and $\phi$. $W$ acts as a sort of frequency resolution in the sense that a small $W$ allows the separation of sources having close bandwidths. Of course, too small a $W$ means that only few samples are used in the estimation of $R_{\mathbf{x}}(f)$, i.e. there is a tradeoff between frequency resolution and estimation accuracy. In the experiments provided in this section, we checked that a good empirical strategy to set $W$ is to consider about 5% of the total number of samples.

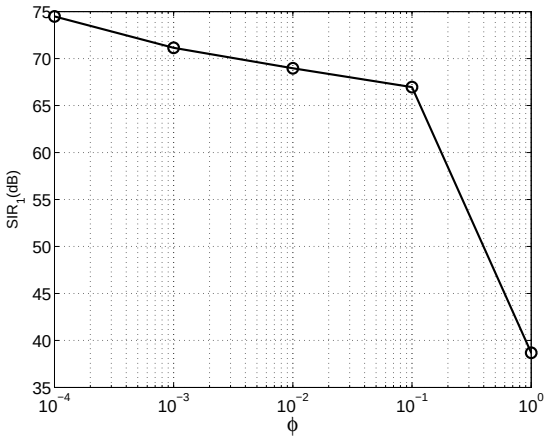


Figure C.2: Performance as a function of the threshold $\phi$.

Ideally, the smaller the threshold $\phi$, the better the silent periods detection is and, consequently, the better the performance is. This was actually observed in experiments with noiseless models. For example, in Figure C.2, we plot the index $\mathrm{SIR}_1$ as a function of $\phi$ (we considered here the extraction of one source from three mixtures). Note, however, that the influence of $\phi$ is minimal when $\phi < 0.1$. In noisy scenarios, the definition of $\phi$ is more tricky and requires a visual inspection of the eigenvalues profile.

### C.5.1 Source Separation

We here consider the separation of the sources shown in the first column of Figure C.3: an exponential signal and three signals obtained from low-pass filtering of white Gaussian noise; the respective bandwidths are given by $B_{s_1} = 0.2$, $B_{s_2} = 0.5$, and $B_{s_3} = 0.8$. The mixtures are shown in the second column of Figure C.3 (2000 samples were considered). The third column of Figure C.3 presents the signals recovered by the SOFI algorithm ($W = 71$ and $\phi = 0.001$). The original order of extraction is kept in Figure C.3; note that SOFI indeed ranks the components according to their smoothness. The performance indices in this case were: $\mathrm{SIR}_1 = 63\,\mathrm{dB}$, $\mathrm{SIR}_2 = 30\,\mathrm{dB}$, $\mathrm{SIR}_3 = 30\,\mathrm{dB}$, and $\mathrm{SIR}_4 = 27\,\mathrm{dB}$. Note that the SIR decreases as the extraction procedure progresses; this is typical in deflation-based approaches and is due to the accumulation of errors from the precedent iterations.

### C.5.2 Extraction of a smooth signal from a large number of mixtures

We consider the extraction of an exponential signal from $N$ mixtures of $N$ sources having bandwidths between 0.4 and 0.9. As shown in Table C.1, the SOFI algorithm (with $\phi = 0.0001$ and $W = 101$) has led to high SIRs, even for a large $N$. We also show in this table the performances achieved by the SOBI [26] and FastICA [90] algorithms[5]. As these two methods

[5]The FastICA did not converge for $N = 50$ and $N = 70$.

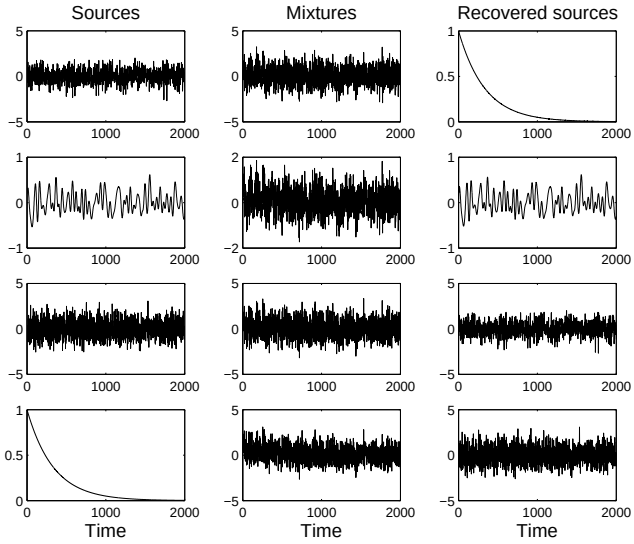


Figure C.3: Example of source separation: sources (first column), mixtures (second column) and retrieved signals (third column).

Table C.1: Extraction of the smoothest signal: SIR ( dB) for different number of sources $N$ (average over 50 experiments).

| | $N = 2$ | $N = 10$ | $N = 20$ | $N = 50$ | $N = 70$ |
|---|---|---|---|---|---|
| SOFI | 86.7 | 72.5 | 68.7 | 63.2 | 55.5 |
| SOBI | 61.0 | 43.7 | 40.4 | 36.3 | 34.9 |
| FastICA | 39.2 | 23.7 | 19.6 | – | – |

do not rank the sources, the exponential source was obtained by analyzing each retrieved signal[6].

### C.5.3 Source extraction in a noisy situation

We here consider the extraction of the exponential depicted in Figure C.4 (first row third column) from $M = 10$ mixtures (first two columns of Figure C.4) of $N = 5$ sources (signals of bandwidths $B_{s_2} = 0.4$, $B_{s_3} = 0.6$, $B_{s_4} = 0.8$ and $B_{s_5} = 0.9$). Each mixture was corrupted by additive white Gaussian noise of signal-to-noise ratio (SNR) equal to 15 dB. Regardless of noise, it is still possible[7] to identify the inactive bands; by inspecting Figure C.5 it is clear that the inactive bands can be identified by looking at the eigenvalues lower than approximately 0.1 (this value is thus attributed to the threshold $\phi$). The first inactive band is thus the one in which there is only one eigenvalue lower than $\phi$ ($\hat{B}_{s_1} = 0.03$ and $\hat{B}_{s_2} 0.43$ in this case). The SOFI algorithm ($W = 301$) provided the second signal ($\text{SIR}_1 = 10.4\,\text{dB}$) of the third column in Figure C.4.

[6] [117] proposed a method to extract smooth sources based on the FastICA. As the idea was to force the first component to be the smoothest one, the performance of this constrained FastICA approach is equivalent to that of the ordinary FastICA (symmetric orthogonalization version).

[7] This is due to the GEVD; if the ordinary EVD were considered, the noise terms would be taken as inactive sources.

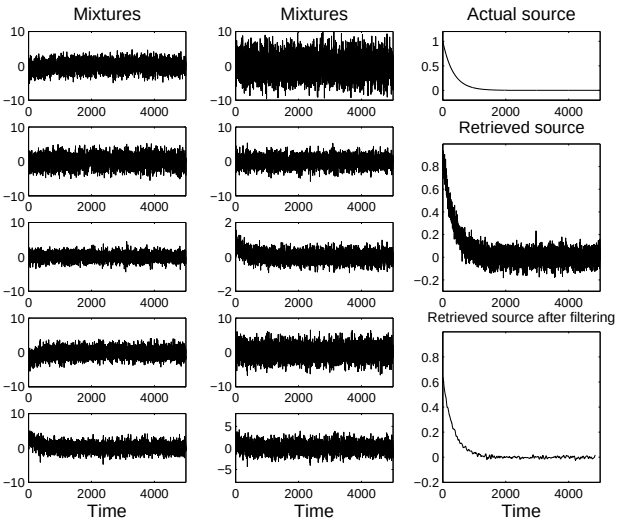


Figure C.4: Source extraction: mixtures (first and second columns). Third column contains: actual source, its estimation, and a filtered version of this estimation.

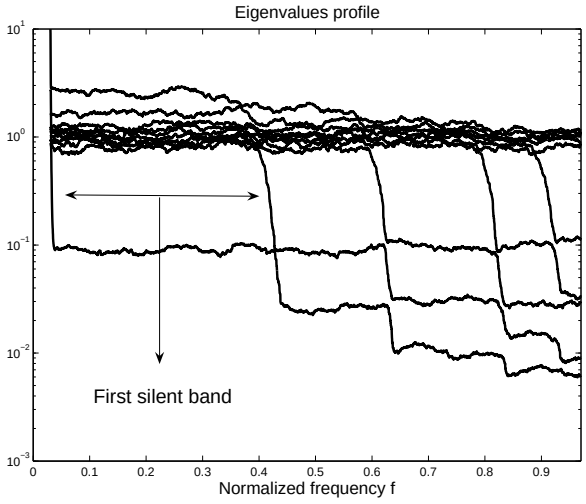


Figure C.5: Generalized eigenvalues of $(R_{\mathbf{x}}(f), R_{\mathbf{x}}([0,1]))$ in a noisy scenario.

Note that the estimated bandwidths can be used to improve the extracted source. Indeed, after low-pass filtering (stopband at $\hat{B}_{s_1} = 0.03$), we obtained $\mathrm{SIR}_1 = 23.9\,\mathrm{dB}$ (see the third column, last row of Figure C.4). For matter of comparison, the performance of the SOBI algorithm was $\mathrm{SIR}_1 = 10.4\,\mathrm{dB}$.

Finally, we consider the same situation described above but now with a noise of $\mathrm{SNR} = 10\,\mathrm{dB}$. Again, based on a visual inspection of the eigenvalues profile, we set $\phi = 0.4$. The performance obtained by the SOFI algorithm was $\mathrm{SIR}_1 = 6.0\,\mathrm{dB}$, and $\mathrm{SIR}_1 = 22.6\,\mathrm{dB}$ after low-pass filtering at the estimated $\hat{B}_{s_1} = 0.013$. A similar performance of the SOBI algorithm was obtained ($\mathrm{SIR}_1 = 6.0\,\mathrm{dB}$).

## C.6 Conclusion

We introduced in this appendix the SOFI algorithm, a BSS method designed to separate baseband signals. By exploiting the existence of inactive bands, we developed a simple algorithm that is based on second-order statistics and on a deflation procedure. As it could be checked in simulations, the proposed method performs well even in the presence of noise; moreover, it outperformed standard BSS algorithms in the problem of extracting a smooth signal from a great number of mixtures. Future works include the derivation of an automatic strategy for adjusting the parameter $\phi$ in noisy scenarios.

# Appendix D

# List of publications

## Journals

1. L. T. Duarte, C. Jutten and S. Moussaoui, A Bayesian Nonlinear Source Separation Method for Smart Ion-selective Electrode Arrays, *IEEE Sensors Journal*, vol. 9, no. 12, pp. 1763-1771, Dec. 2009

2. L. T. Duarte, B. Rivet and C. Jutten, Blind Extraction of Smooth Signals based on a Second-Order Frequency Identification Algorithm, *IEEE Signal Processing Letters*, vol. 17, no. 1, pp. 79-82, Jan. 2010

## Conferences

1. L. T. Duarte and C. Jutten, Blind Source Separation of a Class of Nonlinear Mixtures, *Proc. of the 7th International Workshop on Independent Component Analysis and Signal Separation (ICA 2007)*, 2007.

2. L. T. Duarte and C. Jutten, A Mutual Information Minimization Approach for a Class of Nonlinear Recurrent Separating Systems, *Proc. of the IEEE Workshop on Machine Learning for Signal Processing (MLSP 2007)*, 2007.

3. L. T. Duarte and C. Jutten, A Nonlinear Source Separation Approach to the Nicolsky-Eisenman Model, *Proc. of of the 16th European Signal Processing Conference (EUSIPCO 2008)*, 2008.

4. L. T. Duarte, C. Jutten and S. Moussaoui, Ion-selective Electrode Array based on a Bayesian Nonlinear Source Separation Method, *Proc. of the 8th International Workshop on Independent Component Analysis and Signal Separation (ICA 2009)*, 2009.

5. L. T. Duarte, C. Jutten and S. Moussaoui, Bayesian Source Separation of Linear-quadratic and Linear Mixtures through a MCMC Method, *Proc. of the IEEE Workshop on Machine Learning for Signal Processing (MLSP 2009)*, 2009.

6. L. T. Duarte, R. Suyama, R. R. F. Attux, B. Rivet, C. Jutten and J. M. T. Romano, Source Separation of Baseband Signals in Post-nonlinear Mixtures, *Proc. of the IEEE Workshop on Machine Learning for Signal Processing (MLSP 2009)*, 2009.

7. L. T. Duarte, C. Jutten and S. Moussaoui, Séparation de Sources dans le cas de Mélanges Linéaires-quadratiques et Linéaires par une Approche Bayésienne, *Proc. of the Colloque du GRETSI*, 2009.

# Bibliography


[1] K. Abed-Meraim, A. Belouchiani, and Y. Hua, "Blind identification of a linear-quadratic mixture of independent components based on joint diagonalization procedure," in *Proceedings of the IEEE International Conference on Acoustics, Speech, and Signal Processing (ICASSP)*, vol. 5, 7-10 May 1996, pp. 2718–2721.

[2] S. Achard and C. Jutten, "Identifiability of post-nonlinear mixtures," *IEEE Signal Processing Letters*, vol. 12, no. 5, pp. 423–426, May 2005.

[3] S. Achard, D.-T. Pham, and C. Jutten, "Quadratic dependence measure for nonlinear blind source separation," in *Proceedings of the Fourth International Workshop on Independent Component Analysis and Blind Signal Separation (ICA)*, 2003.

[4] ——, "Criteria based on mutual information minimization for blind source separation in post nonlinear mixtures," *Signal Processing*, vol. 85, pp. 965–974, 2005.

[5] K. J. Albert, N. S. Lewis, C. L. Schauer, G. A. Sotzing, S. E. Stitzel, T. P. Vaid, and D. R. Walt, "Cross-reactive chemical sensor arrays," *Chemical Reviews*, vol. 100, pp. 2595–2626, 2000.

[6] S. Alegret and A. Merkoci, Eds., *Comprehensive analytical chemistry: electrochemical sensor analysis*. Elsevier, 2007.

[7] L. B. Almeida, *Nonlinear source separation*. Morgan & Claypool Publishers, 2006.

[8] S.-I. Amari, "Natural gradient works efficiently in learning," *Neural Computational*, vol. 10, no. 2, pp. 251–276, 1998.

[9] C. Andrieu, N. de Freitas, A. Doucet, and M. I. Jordan, "An introduction to MCMC for machine learning," *Machine Learning*, vol. 50, pp. 5–43, 2003.

[10] M. Attari, M. Heniche, and F. Boudjema, "A two dimensional intelligent calibration of an ion sensor," in *Proceedings of the IEEE Instrumentation and Measurement Technology Conference, IMTC 1996*, vol. 2, 1996, pp. 788–791 vol.2.

[11] R. R. F. Attux, "Novos paradigmas para equalização e identificação de canais baseados em estruturas não-lineares e algoritmos evolutivos," Ph.D. dissertation, University of Campinas (UNICAMP), 2005, in Portuguese.

[12] R. R. F. Attux, M. Loiola, R. Suyama, L. N. de Castro, F. V. Zuben, and J. M. T. Romano, "Blind search for optimal wiener equalizers using an artificial immune network model," *EURASIP Journal on Applied Signal Processing*, vol. 2003, pp. 740–747, 2003.

[13] R. R. F. Attux, A. Neves, L. T. Duarte, R. Suyama, C. Junqueira, L. Rangel, T. M. Dias, and J. M. T. Romano, "On the relationships between blind equalization and blind source separation — part i: foundations," *Journal of Communication and Information Systems (JCIS)*, vol. 22, pp. 41–52, 2007.

[14] ——, "On the relationships between blind equalization and blind source separation — part ii: relationships," *Journal of Communication and Information Systems (JCIS)*, vol. 22, pp. 53–61, 2007.

[15] M. Babaie-Zadeh, "On blind source separation in convolutive and nonlinear mixtures," Ph.D. dissertation, Institut National Polytechnique de Grenoble, 2002.

[16] M. Babaie-Zadeh and C. Jutten, "A general approach for mutual information minimization and its application to blind source separation," *Signal Processing*, vol. 85, pp. 975–995, 2005.

[17] M. Babaie-Zadeh, C. Jutten, and K. Nayebi, "A geometric approach for separating post non-linear mixtures," in *Proceedings of the XI European Signal Processing Conference (EUSIPCO)*, 2002.

[18] ——, "Differential of the mutual information," *IEEE Signal Processing Letters*, vol. 11, no. 1, pp. 48–51, January 2004.

[19] E. Bakker, "Electrochemical sensors," *Analytical Chemistry*, vol. 76, pp. 3285–3298, 2004.

[20] E. Bakker, R. K. Meruva, E. Pretsch, and E. Meyerhoff, "Selectivity of polymer membrane-based ion-selective electrodes: self-consistent model describing the potentiometric reponse in mixed ion solutions of different charge," *Analytical Chemistry*, vol. 66, pp. 3021–3030, 1994.

[21] N. Bali and A. Mohammad-Djafari, "Bayesian approach with hidden Markov modeling and mean field approximation for hyperspectral data analysis," *IEEE Transactions on Image Processing*, vol. 17, no. 2, pp. 217–225, 2008.

[22] M. Baret, D. L. Massart, P. Fabry, F. Conesa, C. Eichner, and C. Menardo, "Application of neural network calibrations to an halide ISE array," *Talanta*, vol. 51, pp. 863–877, 2000.

[23] G. Bedoya, "Nonlinear blind signal separation for chemical solid-state sensor arrays," Ph.D. dissertation, Universitat Politecnica de Catalunya, 2006.

[24] G. Bedoya, C. Jutten, S. Bermejo, and J. Cabestany, "Improving semiconductor-based chemical sensor arrays using advanced algorithms for blind source separation," in *Sensors for Industry Conference (SIcon)*, 2004, pp. 149–154.

[25] A. J. Bell and T. J. Sejnowski, "An information-maximization approach to blind separation and blind deconvolution," *Neural Computation*, vol. 7, no. 6, pp. 1129–1159, 1995.

[26] A. Belouchrani, K. Abed-Meraim, J.-F. Cardoso, and E. Moulines, "A blind source separation technique using second-order statistics," *IEEE Transactions on Signal Processing*, vol. 45, no. 2, pp. 434–444, Feb. 1997.

[27] A. Belouchrani and M. G. Amin, "Blind source separation based on time-frequency signal representations," *IEEE Transactions on Signal Processing*, vol. 46, no. 11, pp. 2888–2897, Nov. 1998.

[28] S. Bermejo, C. Jutten, and J. Cabestany, "ISFET source separation: foundations and techniques," *Sensors and Actuators B*, vol. 113, pp. 222–233, 2006.

[29] S. Bermejo and J. Solé-Casals, "Blind source separation for solid-state chemical sensor arrays," in *Proceedings of the IEEE Sensor Array and Multichannel Signal Processing Workshop (SAM)*, 18-21 July 2004, pp. 437–440.

[30] O. Bermond and J.-F. Cardoso, "Approximate likelihood for noisy mixtures," in *Proceedings of the First International Workshop on Independent Component Analysis and Blind Signal Separation (ICA)*, 1999.

[31] T. Blaschke, P. Berkes, and L. Wiskott, "What is the relation between slow feature analysis and independent component analysis?" *Neural Computation*, vol. 18, pp. 2495–2508, 2006.

[32] R. Blatt, A. Bonarini, E. Calabro, M. D. Torre, M. Matteucci, and U. Pastorino, "Lung cancer identification by an electronic nose based on an array of mos sensors," in *Proceedings of International Joint Conference on Neural Networks (IJCNN)*, 12–17 Aug. 2007, pp. 1423–1428.

[33] G. Burel, "Réseaux de neurones en traitement d'images : des modèles théoriques aux applications industrielles," Ph.D. dissertation, Université de Bretagne occidentale, 1991.

[34] S. Capone, A. Forleo, L. Francioso, R. Rella, P. Siciliano, J. Spadavecchia, and D. S. Presicce, "Solid state gas sensors: state of the art and future activities," *Journal of Optoelectronics and Advanced Materials*, vol. 5, no. 5, pp. 1335–1348, 2003.

[35] J.-F. Cardoso, "Blind signal separation: statistical principles," *Proceedings of the IEEE*, vol. 86, no. 10, pp. 2009–2025, Oct. 1998.

[36] J.-F. Cardoso and B. H. Laheld, "Equivariant adaptive source separation," *IEEE Transactions on Signal Processing*, vol. 44, no. 12, pp. 3017–3030, Dec. 1996.

[37] J.-F. Cardoso and A. Souloumiac, "Blind beamforming for non-gaussian signals," *IEE Proceedings-F Radar and Signal Processing*, vol. 140, no. 6, pp. 362–370, 1993.

[38] M. S. Castilho and N. R. Stradiotto, "Determination of potassium ions in biodiesel using a nickel(ii) hexacyanoferrate-modified electrode," *Talanta*, vol. 74, pp. 1630–1634, 2008.

[39] P. Comon, "Independent component analysis, a new concept?" *Signal Processing*, vol. 36, pp. 287–314, 1994.

[40] P. Comon and C. Jutten, Eds., *Séparation de sources 1 : concepts de base et analyse en composantes indépendantes.* Hermès Science Publications, 2007, in French.

[41] T. M. Cover and J. A. Thomas, *Elements of information theory.* Wiley-Interscience, 1991.

[42] M. Cretin and P. Fabry, "Detection and selectivity properties of Li+-ion-selective electrodes based on NASICON-type ceramics," *Analytica Chimica Acta*, vol. 354, pp. 291–299, 1997.

[43] A. D'Amico and C. D. Natale, "A contribution on some basic definitions of sensors properties," *IEEE Sensors Journal*, vol. 1, no. 3, pp. 183–190, 2001.

[44] P. Damien and S. G. Walker, "Sampling truncated normal, beta, and gamma densities," *Journal of Computational and Graphical Statistics*, vol. 10, pp. 206—215, 2001.

[45] G. A. Darbellay, "The mutual information as a measure of statistical dependence," in *Proceedings of the IEEE International Symposium on Information Theory*, 29 June-4 July 1997, p. 405.

[46] G. A. Darbellay and I. Vajda, "Estimation of the information by an adaptive partitioning of the observation space," *IEEE Transactions on Information Theory*, vol. 45, no. 4, pp. 1315–1321, May 1999.

[47] L. N. de Castro and F. J. V. Zuben, "Learning and optimization using the clonal selection principle," *IEEE Transactions on Evolutionary Computation*, vol. 6, pp. 239–251, 2002.

[48] Y. Deville, "Analysis of the convergence properties of self-normalized source separation networks," *IEEE Transactions on Signal Processing*, vol. 47, no. 5, pp. 1272–1287, 1999.

[49] Y. Deville and S. Hosseini, "Blind identification and separation methods for linear-quadratic mixtures and/or linearly independent non-stationary signals," in *Proceedings of the 9th International Symposium on Signal Processing and its Application (ISSPA)*, 2007.

[50] ——, "Stable higher-order recurrent neural network structures for nonlinear blind source separation," in *Proceedings of the Seventh International Workshop on Independent Component Analysis and Blind Signal Separation (ICA)*, 2007, pp. 161–168.

[51] ——, "Recurrent networks for separating extractable-target nonlinear mixtures. part i: Non-blind configurations," *Signal Processing*, vol. 89, pp. 378–393, 2009.

[52] Y. Deville and M. Puigt, "Temporal and time-frequency correlation-based blind source separation methods. part i: Determined and underdetermined linear instantaneous mixtures," *Signal Processing*, vol. 87, pp. 374–407, 2007.

[53] Y. Deville, A. Deville, and S. Hosseini, "Effect of indirect dependencies on "A mutual information minimization approach for a class of nonlinear recurrent separating systems"," 2009. [Online]. Available: http://arxiv.org/abs/0910.4558

[54] N. Dobigeon, "Modèles bayésiens hiérarchiques pour le traitement multi-capteur," Ph.D. dissertation, Institut National Polytechnique de Toulouse, 2007.

[55] K. Dogancay, "Blind compensation of nonlinear distortion for bandlimited signals," *IEEE Transactions on Circuits and Systems I: Regular Papers*, vol. 52, no. 9, pp. 1872–1882, 2005.

[56] ——, "Adaptive pre-distortion of nonlinear systems using out-of-band energy minimization," in *Proceedings of the IEEE International Symposium on Circuits and Systems (ISCAS)*, 2007, pp. 277–280.

[57] D. Donoho and V. Stodden, "When does non-negative matrix factorization give correct decomposition into parts?" in *Proceedings of the NIPS 2003*, 2003.

[58] S. A. Dorneanu, V. Coman, I. C. Popescu, and P. Fabry, "Computer-controlled system for ises automatic calibration," *Sensons and Actuators B*, vol. 105, p. 521–531, 2005.

[59] A. Doucet and X. Wang, "Monte Carlo methods for signal processing," *IEEE Signal Processing Magazine*, vol. 22, pp. 152–170, 2005.

[60] L. T. Duarte and C. Jutten, "A mutual information minimization approach for a class of nonlinear recurrent separating systems," in *Proceedings of the IEEE Workshop on Machine Learning for Signal Processing (MLSP)*, 2007.

[61] L. T. Duarte, R. Suyama, R. R. F. Attux, F. J. V. Zuben, and J. M. T. Romano, "Blind source separation of post-nonlinear mixtures using evolutionary computation and order statistics," in *Proceedings of the 6th International Workshop on Independent Component Analysis and Signal Separation (ICA)*, 2006.

[62] R. O. Duda, P. E. Hart, and D. G. Stork, *Pattern classification*, 2nd ed. Wiley-Interscience, 2000.

[63] A. T. Duong and M. A. Ryan, "Space invariant independent component analysis and enose for detection of selective chemicals in an unknown environment," California Institute of Technology, Tech. Rep., 2005.

[64] J. Eriksson and V. Koivunen, "Blind identifiability of class of nonlinear instantaneous ica models," in *Proceedings of the XI European Signal Processing Conference (EUSIPCO)*, 2002, pp. 7–10.

[65] ——, "Identifiability, separability, and uniqueness of linear ICA models," *IEEE Signal Processing Letters*, vol. 11, no. 7, pp. 601–604, July 2004.

[66] P. Fabry and J. Fouletier, Eds., *Microcapteurs chimiques et biologiques : application en milieu liquide.* Lavoisier, 2003, in French.

[67] M. Falasconi, M. Pardo, M. Vezzoli, and G. Sberveglieri, "Cluster validation for electronic nose data," *Sensons and Actuators B*, vol. 125, pp. 596–606, 2007.

[68] C. Févotte and S. J. Godsill, "A Bayesian approach for blind separation of sparse sources," *IEEE Transactions on Audio, Speech and Language Processing*, vol. 14, pp. 2174–2188, 2006.

[69] J.-C. Fort, "Stabilité de l'algorithme de séparation de sources de jutten et hérault," *Traitement du Signal*, vol. 8, no. 1, pp. 35–42, 1991.

[70] J. Gallardo, S. Alegret, and M. del Valle, "Application of a potentiometric electronic tongue as a classification tool in food analysis," *Talanta*, vol. 66, pp. 1303–1309, 2005.

[71] P. Georgiev, F. Theis, A. Cichocki, and H. Bakardjian, *Data Mining in Biomedicine.* Springer, 2005, ch. Sparse component analysis: a new tool for data mining, pp. 91–116.

[72] W. R. Gilks, S. Richardson, and D. Spiegelhalter, Eds., *Markov chain Monte Carlo in practice.* Chapman & Hall, 1995.

[73] R. Gribonval, *Séparation de sources 2 : au dela de l'aveugle, et applications.* Hermes Science Publications, 2007, ch. Parcimonie.

[74] R. Gribonval and S. Lesage, "A survey of sparse component analysis for blind source separation: principles, perspectives, and new challenges," in *Proceedings of the European Symposium on Artificial Neural Networks (ESANN)*, 2006.

[75] W. Griffiths, "A Gibbs' sampler for a truncated multivariate normal distribution," University of Melbourne, Tech. Rep., 2002.

[76] P. Gründler, *Chemical sensors: an introduction for scientists and engineers.* Springer, 2007.

[77] O. Gualdron, J. Brezmes, E. Llobet, A. Amari, X. Vilanova, B. Bouchikhi, and X. Correig, "Variable selection for support vector machine based multisensor systems," *Sensors and Actuators B*, vol. 122, pp. 259–268, 2007.

[78] M. Gutiérrez, S. Alegret, R. Cáceres, J. Casadesús, and O. M. M. del Valle, "Nutrient solution monitoring in greenhouse cultivation employing a potentiometric electronic tongue," *Journal of Agricultural and Food Chemistry*, vol. 56, pp. 1810—-1817, 2008.

[79] R. Gutierrez-Osuna, "Pattern analysis for machine olfaction: a review," *IEEE Sensors Journal*, vol. 2, no. 3, pp. 189–202, June 2002.

[80] M. Hartnett and D. Diamond, "Potentometric nonlinear multivariate calibration with genetic algorithm and simplex optmization," *Analytical Chemistry*, vol. 69, pp. 1909–1918, 1997.

[81] T. Hastie, R. Tibshirani, and J. Friedman, *The elements of statistical learning*, 2nd ed. Springer, 2009.

[82] S. Haykin, Ed., *Blind deconvolution*. Prentice-Hall, 1994.

[83] S. Haykin and Z. Chen, "The cocktail party problem," *Neural Computation*, vol. 17, pp. 1875–1902, 2005.

[84] J. Hérault, C. Jutten, and B. Ans, "Détection de grandeurs primitives dans un message composite par une architecture de calcul neuromimétique en apprentissage non supervisé," in *Proceedings of the GRETSI*, 1985, pp. 1017–1022.

[85] R. C. Hilborn, *Chaos and nonlinear dynamics: an introduction for scientists and engineers*, Second, Ed. Oxford University Press, 2000.

[86] S. Hosseini and Y. Deville, "Blind separation of linear-quadratic mixtures of real sources using a recurrent structure," in *Proceedings of the 7th International Work-conference on Artificial And Natural Neural Networks (IWANN)*, 2003, pp. 289–296.

[87] ——, "Blind maximum likelihood separation of a linear-quadratic mixture," in *Proceedings of the Fifth International Workshop on Independent Component Analysis and Blind Signal Separation (ICA)*, 2004, pp. 694–701.

[88] P. O. Hoyer, "Non-negative matrix factorization with sparseness constraints," *Journal of Machine Learning Research*, vol. 5, pp. 1457–1469, 2004.

[89] A. Hulanicki, S. Glab, and F. Ingman, "Chemical sensors definitions and classification," *Pure and Applied Chemistry*, vol. 63, pp. 1247–1250, 1991.

[90] A. Hyvärinen, J. Karhunen, and E. Oja, *Independent component analysis*. John Wiley & Sons, 2001.

[91] A. Hyvärinen and P. Pajunen, "Nonlinear independent component analysis: existence and uniqueness results," *Neural Networks*, vol. 12, pp. 429–439, 1999.

[92] A. Jerger, H. Kohler, F. Becker, H. B. Keller, and R. Seifert, "New applications of tin oxide gas sensors ii. Intelligent sensor system for reliable monitoring of ammonia leakages," *Sensons and Actuators B*, vol. 81, pp. 301–307, 2002.

[93] C. Jutten, "Calcul neuromimétique et traitement du signal : analyse en composantes indépendantes," *Thèse d'État*, 1987, in French.

[94] C. Jutten and P. Comon, Eds., *Séparation de sources 2 : au dela de l'aveugle, et applications*. Hermès Science Publications, 2007, in French.

[95] C. Jutten and J. Hérault, "Blind separation of sources, part 1: an adpative algorithm based on neuromimetic architecture," *Signal Processing*, vol. 24, pp. 1–10, 1991.

[96] C. Jutten and J. Karhunen, "Advances in blind source separation (BSS) and independent component analysis (ICA) for nonlinear mixtures," *International Journal of Neural Systems*, vol. 14, pp. 267–292, 2004.

[97] J. Karhunen, P. Pajunen, and E. Oja, "The nonlinear PCA criterion in blind source separation: relations with other approaches," *Neurocomputing*, vol. 22, pp. 5–20, 1998.

[98] S. M. Kay, *Fundamentals of statistical signal processing: estimation theory.* Prentice-Hall, 1993.

[99] K. H. Knuth, "A bayesian approach to source separation," in *Proceedings of the First International Workshop on Independent Component Analysis and Blind Signal Separation, ICA 1999*, 1999.

[100] ——, "Informed source separation: A bayesian tutorial," in *Proceedings of the 13th European Signal Processing Conference (EUSIPCO)*, 2005.

[101] M. Krob and M. Benidir, "Blind identification of a linear-quadratic model using higher-order statistics," in *Proceedings of the IEEE International Conference on Acoustics, Speech, and Signal Processing (ICASSP)*, vol. 4, 27-30 April 1993, pp. 440–443vol.4.

[102] J.-L. Lacoume, P.-O. Amblard, and P. Comon, *Statistique d'ordre superior pour le traitment de signal.* Masson, 2003.

[103] H. J. Landau and W. L. Miranker, "The recovery of distorted band-limited signals," *Journal of Mathematical Analysis and Applications*, vol. 2, pp. 97–104, 1961.

[104] D. D. Lee and H. S. Seung, "Algorithms for non-negative matrix factorization," *Advances in Neural Information Processing Systems*, vol. 13, pp. 556–562, 2001.

[105] J. A. Lee, C. Jutten, and M. Verleysen, "Non-linear ica by using isometric dimensionality reduction," in *Proceedings of the 5th International Workshop on Independent Component Analysis and Signal Separation (ICA)*, 2004.

[106] T.-W. Lee, M. Girolami, A. J. Bell, and T. J. Sejnowski, "A unifying information-theoretic framework for independent component analysis," *Computers & Mathematics with Applications*, vol. 39, pp. 1–21, 2000.

[107] A. Legin, A. Rudnitskaya, Y. Vlasov, C. D. Natale, E. Mazzone, and A. D'Amico, "Application of electronic tongue for quantitative analysis of mineral water and wine," *Electroanalysis*, vol. 11, pp. 814–820, 1999.

[108] H. Li, T. Adali, W. Wang, and D. Emge, "Non-negative matrix factorization with orthogonality constraints and its application to raman spectroscopy," *Journal of VLSI Signal Processing*, vol. 48, pp. 83–97, 2007.

[109] E. Llobet, J. Brezmes, X. Vilanova, J. E. Sueiras, and X. Correig, "Qualitative and quantitative analysis of volatile organic compounds using transient and steady-state responses of a thick-film tin oxide gas sensor array," *Sensors and Actuators B*, vol. 41, pp. 13–21, 1997.

[110] E. Llobet, X. Vilanova, J. Brezmes, D. Lopez, and X. Correig, "Electrical equivalent models of semiconductor gas sensors using pspice," *Sensors and Actuators B*, vol. 77, pp. 275–280, 2001.

[111] E. Llobet, X. Vilanova, J. Brezmes, J. E. Sueiras, R. Alcubilla, and X. Correiga, "Steady-state and transient behavior of thick-film tin oxide," *Journal of The Electrochemical Society*, vol. 145, no. 5, pp. 1772–1779, 1998.

[112] W. Lu and J. C. Rajapakse, "Approach and applications of constrained ica," *IEEE Transactions on Neural Networks*, vol. 16, no. 1, pp. 203–212, 2005.

[113] L. Lvova, E. Martinelli, F. Dini, A. Bergamini, R. Paolesse, C. D. Natale, and A. D'Amico, "Clinical analysis of human urine by means of potentiometric electronic tongue," *Talanta*, vol. 77, pp. 1097—-1104, 2009.

[114] C. Maccà, "Response time of ion-selective electrodes: Current usage versus IUPAC recommendations," *Analytica Chimica Acta*, vol. 512, pp. 183–190, 2004.

[115] E. Masry, "The recovery of distorted band-limited stochastic processes," *IEEE Transactions on Information Theory*, vol. 19, no. 4, pp. 398–403, Jul 1973.

[116] J. W. Miskin, "Ensemble learning for independent component analysis," Ph.D. dissertation, University of Cambridge, 2000.

[117] N. Mitianoudis, T. Stathaki, and A. G. Constantinides, "Smooth signal extraction from instantaneous mixtures," *IEEE Signal Processing Letters*, vol. 14, pp. 271–274, 2007.

[118] R. Moddemeijer, "On estimation of entropy and mutual information of continuous distributions," *Signal Processing*, vol. 16, pp. 233–248, 1989.

[119] A. Mohammad-Djafari, *Séparation de sources 2 : au dela de l'aveugle, et applications*. Hermes Science Publications, 2007, ch. Approche bayésienne en séparation de sources, pp. 483–517.

[120] W. E. Morf, M. Badertscher, T. Zwickl, N. F. de Rooij, and E. Pretsch, "Effects of ion transport on the potential response of ionophosfore-based membrane electrodes: a theorectical approach," *Journal of physical chemistry B*, vol. 103, pp. 11 346–11 356, 1999.

[121] P. T. Mosley, "Solid state gas sensors," *Measurement Science and Technology*, vol. 8, pp. 223—-237, 1997.

[122] S. Moussaoui, "Séparation de sources non-négatives. application au traitement des signaux de spectroscopie," Ph.D. dissertation, Université Henri Poincaré, Nancy 1, 2005.

[123] S. Moussaoui, D. Brie, and J. Idier, "Non-negative source separation: range of admissible solutions and conditions for the uniqueness of the solution," in *Proceedings of the IEEE International Conference on Acoustics, Speech, and Signal Processing (ICASSP)*, vol. 5, 18-23 March 2005, pp. v/289–v/292Vol.5.

[124] M. Nägele, E. Bakker, and E. Pretsch, "General description of the simultaneous response of potentiometric ionophore-based sensors to ions of different charges," *Analytical Chemistry*, vol. 71, pp. 1041–1048, 1999.

[125] H. Nagle, R. Gutierrez-Osuna, and S. S. Schiffman, "The how and why of electronic noses," *IEEE Spectrum*, vol. 35, no. 9, pp. 22–31, Sept. 1998.

[126] U. Oesch, D. Ammann, and W. Simon, "Ion-selective membrane electrodes for clinical use," *Clinical Chemistry*, vol. 32, pp. 1448–1459, 1986.

[127] T. Ogunfunmi, *Adaptive nonlinear system identification: the Volterra and Wiener model approaches*. Springer, 2007.

[128] A. V. Oppenheim, R. W. Schafer, and J. R. Buck, *Discrete-time signal processing*, 2nd ed. Prentice-Hall, 1999.

[129] P. Paatero and U. Tapper, "Positive matrix factorization: A non-negative factor model with optimal utilization of error estimates of data values," *Environmetrics*, vol. 5, pp. 111–126, 1994.

[130] A. Papoulis and U. Pillai, *Probability, random variables, and stochastic processes*, Fourth, Ed. McGraw-Hill, 2004.

[131] M. Pardo and G. Sberveglieri, "Remarks on the use of multilayer perceptrons for the analysis of chemical sensor array data," *IEEE Sensors Journal*, vol. 4, no. 3, pp. 355–363, June 2004.

[132] ——, "Classification of electronic nose data with support vector machines," *Sensons and Actuators B*, vol. 107, pp. 730—737, 2005.

[133] F. Parret, P. Menini, A. Martinez, K. Soulantica, A. Maisonnat, and B. Chaudret, "Improvement of micromachined $SnO_2$ gas sensors selectivity by optimised dynamic temperature operating mode," *Sensors and Actuators B*, vol. 118, pp. 276–282, 2006.

[134] D.-T. Pham, "Fast algorithms for mutual information based independent component analysis," *IEEE Transactions on Signal Processing*, vol. 52, no. 10, pp. 2690–2700, Oct. 2004.

[135] ——, "Flexible parametrization of postnonlinear mixtures model in blind sources separation," *IEEE Signal Processing Letters*, vol. 11, no. 6, pp. 533–536, June 2004.

[136] D.-T. Pham and J.-F. Cardoso, "Blind separation of instantaneous mixtures of nonstationary sources," *IEEE Transactions on Signal Processing*, vol. 49, no. 9, pp. 1837–1848, 2001.

[137] D.-T. Pham and P. Garat, "Blind separation of mixture of independent sources through a quasi-maximum likelihood approach," *IEEE Transactions on Signal Processing*, vol. 45, pp. 1712–1725, 1997.

[138] B. Rivet, "Blind non-stationnary sources separation by sparsity in a linear instantaneous mixture," in *Proceedings of the 8th International Conference on Independent Component Analysis and Signal Separation (ICA)*, 2009.

[139] C. P. Robert, *The Bayesian Choice*. Springer, 2007.

[140] C. P. Robert and G. Casela, *Monte Carlo Statistical Methods*, 2nd ed. Springer, 2004.

[141] A. Rudnitskaya and A. Legin, "Sensor systems, electronic tongues and electronic noses, for the monitoring of biotechnological processes," *Journal of Industrial Microbiology and Biotechnology*, vol. 35, pp. 443—-451, 2008.

[142] H. Sakai, S. Iiyama, and K. Toko, "Evaluation of water quality and pollution using multichannel sensors," *Sensons and Actuators B*, vol. 66, pp. 25–255, 2000.

[143] R. Sameni, "Extraction of fetal cardiac signals from an array of maternal abdominal recordings," Ph.D. dissertation, Institut Polytechnique de Grenoble, 2008.

[144] J. Saurina, E. López-Aviles, A. L. Moal, and S. Hernández-Cassou, "Determination of calcium and total hardness in natural waters using a potentiometric sensor array," *Analytica Chimica Acta*, vol. 464, pp. 89–98, 2002.

[145] D. A. Skoog, D. M. West, F. J. Holler, and S. R. Crouch, *Fundamentals of analytical chemistry*. Brooks Cole, 2003.

[146] V. Smidl and A. Quinn, *The variational Bayes method in signal processing*. Springer, 2005.

[147] J. Solé-Casals, M. Babaie-Zadeh, C. Jutten, and D.-T. Pham, "Improving algorithm speed in post nonlinear mixtures and wiener systems inversion," in *Proceedings of the Fourth International Conference on Independent Component Analysis and Blind Signal Separation*, Nara, Japan, April 2003, pp. 639–644.

[148] E. Sorouchyari, "Blind separation of sources, part iii: Stability analysis," *Signal Processing*, vol. 24, pp. 21–29, 1991.

[149] A. Souloumiac, "Blind source detection and separation using second order nonstationarity," in *Proceedings of the IEEE International Conference on Acoustics, Speech, and Signal Processing (ICASSP)*, vol. 3, 1995, pp. 1912–1915 vol.3.

[150] A. Taleb and C. Jutten, "Source separation in post-nonlinear mixtures," *IEEE Transactions on Signal Processing*, vol. 47, no. 10, pp. 2807–2820, Oct. 1999.

[151] L. Tong, R.-W. Liu, V. C. Soon, and Y.-F. Huang, "Indeterminacy and identifiability of blind identification," *IEEE Transactions on Circuits and Systems*, vol. 38, no. 5, pp. 499–509, 1991.

[152] Y. Umezawa, P. Bühlmann, K. Umezawa, K. Tohda, and S. Amemiya, "Potentiometric selectivity coefficients of ion-selective electrodes," *Pure and Applied Chemistry*, vol. 72, pp. 1851–2082, 2000.

[153] Y. Umezawa, K. Umezawa, and H. Sato, "Selectivity coefficients for ion-selective electrodes: recommended methods for reporting K values," *Pure and Applied Chemistry*, vol. 67, pp. 507–518, 1995.

[154] H. Valpola, "Bayesian ensemble learning for nonlinear factor analysis," Ph.D. dissertation, Helsinki University of Technology, 2000.

[155] A. Vergara, E. Llobet, E. Martinelli, N. D. Corrado, A. D'Amico, and X. Correig, "Feature extraction of metal oxide gas sensors using dynamic moments," *Sensors and Actuators B*, vol. 122, pp. 219–226, 2007.

[156] Y. Vlason, A. Legin, A. Rudnitskaya, C. D. Natalte, and A. D'Amico, "Nonspecific sensor arrays ("electronic ") for chemical analysis of liquids," *Pure and Applied Chemistry*, vol. 77, pp. 1965—-1983, 2005.

[157] Y. G. Vlasov, A. V. Legin, and A. M. Rudnitskaya, "Electronic tongue: chemical sensor systems for analysis of aquatic media," *Russian Journal of General Chemistry*, vol. 78, pp. 2532—-2544, 2008.

[158] J. Watson, K. Ihokura, and G. S. V. Coles, "The tin dioxide gas sensor," *Measurement Science and Technology*, vol. 4, pp. 711–719, 1993.

[159] S. P. Wilson, E. E. Kuruoglu, and E. Salerno, "Fully Bayesian source separation of astrophysical images modelled by mixture of Gaussians," *IEEE Journal of Selected Topics in Signal Processing*, vol. 2, no. 5, pp. 685–696, Oct. 2008.

[160] O. Winther and K. B. Petersen, "Bayesian independent component analysis: variational methods and non-negative decompositions," *Digital Signal Processing*, 2007.

[161] N. Yamazoe, G. Sakai, and K. Shimanoe, "Oxide semiconductor gas sensors," *Catalysis Surveys from Asia*, vol. 7, no. 1, pp. 63–75, 2003.

[162] N. Yamazoe and K. Shimanoe, "Theory of power laws for semiconductor gas sensors," *Sensons and Actuators B*, vol. 128, pp. 566–573, 2008.

[163] V. Zarzoso, P. Comon, and M. Kallel, "How fast is FastICA?" in *Proceedings of the European Signal Processing Conference (EUSIPCO)*, 2006.

[164] R. Zdunek and A. Cichocki, "Gibbs regularized nonnegative matrix factorization for blind separation of locally smooth signals," in *Proceedings of the 15th IEEE International Workshop on Nonlinear Dynamics of Electronic Systems (NDES07)*, 2007.

[165] A. Ziehe, M. Kawanabe, S. Harmeling, and K.-R. Müller, "Blind separation of post-nonlinear mixtures using gaussianizing transformations and temporal decorrelation," *Journal of Machine Learning Research*, vol. 4, pp. 1319–1338, 2003.

# Conception de réseaux de capteurs chimiques intelligents : une approche fondée sur les méthodes de séparation de sources

Leonardo Tomazeli Duarte

Thèse pour obtenir le grade de Docteur de l'Institut Polytechnique de Grenoble
Spécialité : Signal, Image, Parole, Télécoms
Soutenue publiquement le 17 novembre 2009

**JURY**

Prof. Jacques FOULETIER, Président
Prof. Yannick DEVILLE, Rapporteur
Dr. Ali MOHAMMAD-DJAFARI, Rapporteur
Prof. Christian JUTTEN, Directeur de thèse
Dr. Saïd MOUSSAOUI, Examinateur
Dr. Pierre TEMPLE-BOYER, Examinateur

**Résumé**

Dans ce document, nous présentons un résumé des travaux réalisés pendant la thèse de doctorat de Leonardo Tomazeli Duarte. Une description plus détaillée de ces travaux est présentée dans la version originale (en anglais) du manuscrit [1].

## 1 Introduction

L'une des principales difficultés dans l'utilisation de capteurs chimiques concerne le manque de sélectivité inhérent à ces dispositifs. La stratégie classique pour faire face à ce problème est fondée sur le développement de nouvelles membranes qui conduisent à des capteurs plus sélectifs. Toutefois, plus récemment, on a démontré que ce problème peut également être traité par une autre approche, dans laquelle l'acquisition de données est effectuée par un réseau de capteurs qui ne sont pas forcément sélectifs. Ainsi, après l'acquisition, les informations pertinentes sont récupérées à l'aide des outils de traitement de signal. L'un des bénéfices le plus remarquable dans cette démarche concerne la flexibilité et l'adaptabilité du système de mesure. Compte tenu de ces deux caractéristiques, l'idée décrite ci-dessus, et illustrée à la figure 1, est couramment appelée ≪réseau de capteurs chimiques intelligent ≫.

La méthode de traitement du signal utilisée dans un réseau de capteurs chimiques intelligent dépend 1) du type d'analyse souhaitée (*quantitative* ou *qualitative*) et 2) du paradigme d'adaptation de la technique

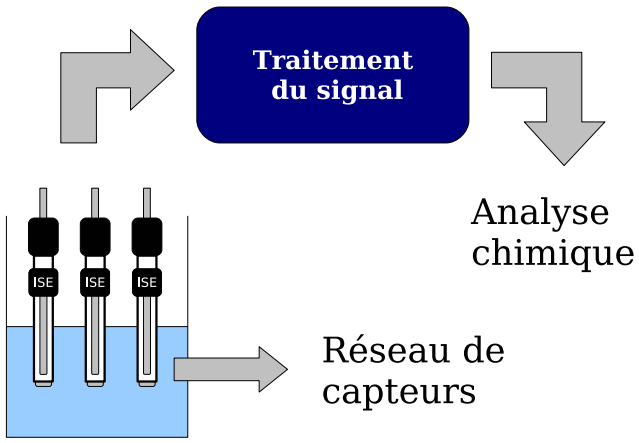


FIGURE 1 – Réseau de capteurs chimiques intelligent.

choisie ; les techniques dites *supervisées* ont besoin d'un jeu d'échantillons d'étalonnage pour l'adaptation, tandis que les techniques *non-supervisées* n'utilisent que les réponses fournies par le capteurs. La combinaison de ces deux caractéristiques conduit à des problèmes différents de traitement du signal, comme le montre le tableau 1.

TABLE 1 – Réseaux de capteurs intelligents : les différents types de méthode de traitement du signal.

| | **Analyse qualitative** | **Analyse quantitative** |
|---|---|---|
| **Supervisé** | Classification supervisée | Régression multivariée |
| **Non-supervisé** | Clustering | **Séparation aveugle des sources** |

Dans cette thèse, nous nous plaçons dans le contexte de l'analyse quantitative non-supervisée. Cette situation peut être formulée comme un problème de séparation aveugle de sources (SAS). En effet, les méthodes de séparation aveugle de sources (SAS) ont pour but retrouver un ensemble de signaux inconnus (appelés sources) en n'utilisant qu'un ensemble de mélanges, c'est-à-dire des observations obtenues en mélangeant les sources. Dans l'application envisagée, les sources représentent les activités chimiques des espèces en cours d'analyse tandis que les mélanges comprennent les réponses de chaque capteur dans le réseau. Le principal avantage dans l'utilisation des méthodes de SAS concerne la réduction, voire l'élimination, de l'étape d'étalonnage.

Puisque les capteurs chimiques considérés dans cette recherche, *les électrodes ioniques sélectives* (ISE), présentent des réponses non linéaires, le processus de mélange sous-jacent au réseau de capteurs est non linéaire, ce qui rend le problème difficile. En effet, quoique le problème de séparation de mélanges linéaires et ses solutions reposent désormais sur de solides bases théoriques [2, 3], l'instance non linéaire de la SAS présente encore des défis théoriques et pratiques [4].

Les principales contributions de cette recherche sont liées justement au développement de méthodes de séparation dans des mélanges non-linéaires à partir de mesures réalisées sur des réseaux d'électrodes

sélectives potentiométriques. Plus précisément, nous considérons le processus de mélange engendré par l'équation de Nicolsky-Eisenman (NE) [5, 6], d'après laquelle la réponse du $i$-ème capteur du réseau, représentée par $x_i(t)$, s'écrit :

$$x_i(t) = e_i + d_i \log\Big(s_i(t) + \sum_{j,j\neq i} a_{ij} s_j(t)^{\frac{z_i}{z_j}}\Big), \tag{1}$$

où $s_i(t)$ et $s_j(t)$ correspondent respectivement aux activités chimiques de l'ion «cible » et des ions «interférants ». Les paramètres $e_i$ et $d_i$ sont des paramètres inconnus à valeur constant. Finalement, la quantité $z_k$, qui est supposée connue dans ce travail, correspond à la valence de l'ion $k$.

Ce résumé est organisé comme suit : dans la partie 2, nous commentons les expériences que nous avons conduit afin d'obtenir un ensemble de données réels pour valider les modèles considérés ainsi que les méthodes proposées. Ensuite, nous décrivons les techniques proposées, à commencer, dans la partie 3, par celles fondées sur l'analyse en composantes indépendantes (ACI). Dans la partie 4, nous montrons deux stratégies pour simplifier le problème de SAS à partir de la prise en compte des informations a priori typiques de l'application traitée. Dans la partie 5, nous continuons notre investigation sur la prise en compte des informations a priori, mais maintenant en nous appuyant sur une approche bayésienne. Enfin, nous présentons nos conclusions et des perspectives dans la partie 6.

## 2 Expériences avec des électrodes sélectives

L'objectif des expériences réalisées a été d'acquérir un ensemble de données avec les mesures suivantes : 1) évolution temporelle de l'activité des ions en cours d'analyse (sources) et 2) la réponse de chaque ISE dans le réseau (mélanges). Ces expériences ont été conduites au Laboratoire d'Analyse et d'Architecture des Systèmes (LAAS-CNRS, Toulouse) dans le cadre d'une collaboration avec le Dr Pierre Temple-Boyer et son équipe. Les données obtenues sont publiquement disponibles sur le site www.gipsa-lab.inpg.fr/isea.

Nous avons considéré les scénarios suivants (chaque scénario était composé de 8 expériences.) :

1. Analyse d'une solution contenant $NH_4Cl$ et KCl en utilisant une $NH_4^+$-ISE et une $K^+$-ISE ;
2. Analyse d'une solution contenant NaCl et KCl en utilisant une $Na^+$-ISE, une $K^+$-ISE et une $Cl^-$-ISE ;
3. Analyse d'une solution contenant NaCl et $CaCl_2$ en utilisant une $Ca^{2+}$-ISE, deux $Na^+$-ISEs et une $Cl^-$-ISE ;

Le premier scénario est un exemple bien connu d'interférence dans le contexte des électrodes sélectives : les ions potassium et ammonium. Par exemple, ce cas est pertinent dans les applications telles que la surveillance de la qualité de l'eau. Dans le deuxième scénario, nous considérons aussi l'analyse de deux ions monovalents (sodium et potassium), mais maintenant avec un réseau de capteurs composé de quatre électrodes, dont une électrode de sodium supplémentaire. La motivation pour effectuer ce deuxième scénario consistait à vérifier si une éventuelle variabilité entre deux capteurs du même type pourrait être exploitée par une méthode de SAS. Enfin, dans le troisième scénario, nous analysons la situation dans laquelle les ions ont des valences différentes (calcium et sodium). D'après l'équation de NE, cette situation conduit à un modèle de mélange qui présente des termes de puissances.

Dans la figure 2, nous montrons le dispositif expérimental. En bref, il y avait deux burettes automatiques qui injectaient des solutions salines afin de faire varier les concentrations, et donc les activités, des ions analysés. La configuration des burettes et l'acquisition des données ont été faites à l'aide d'un logiciel développé par les chercheurs du LAAS.

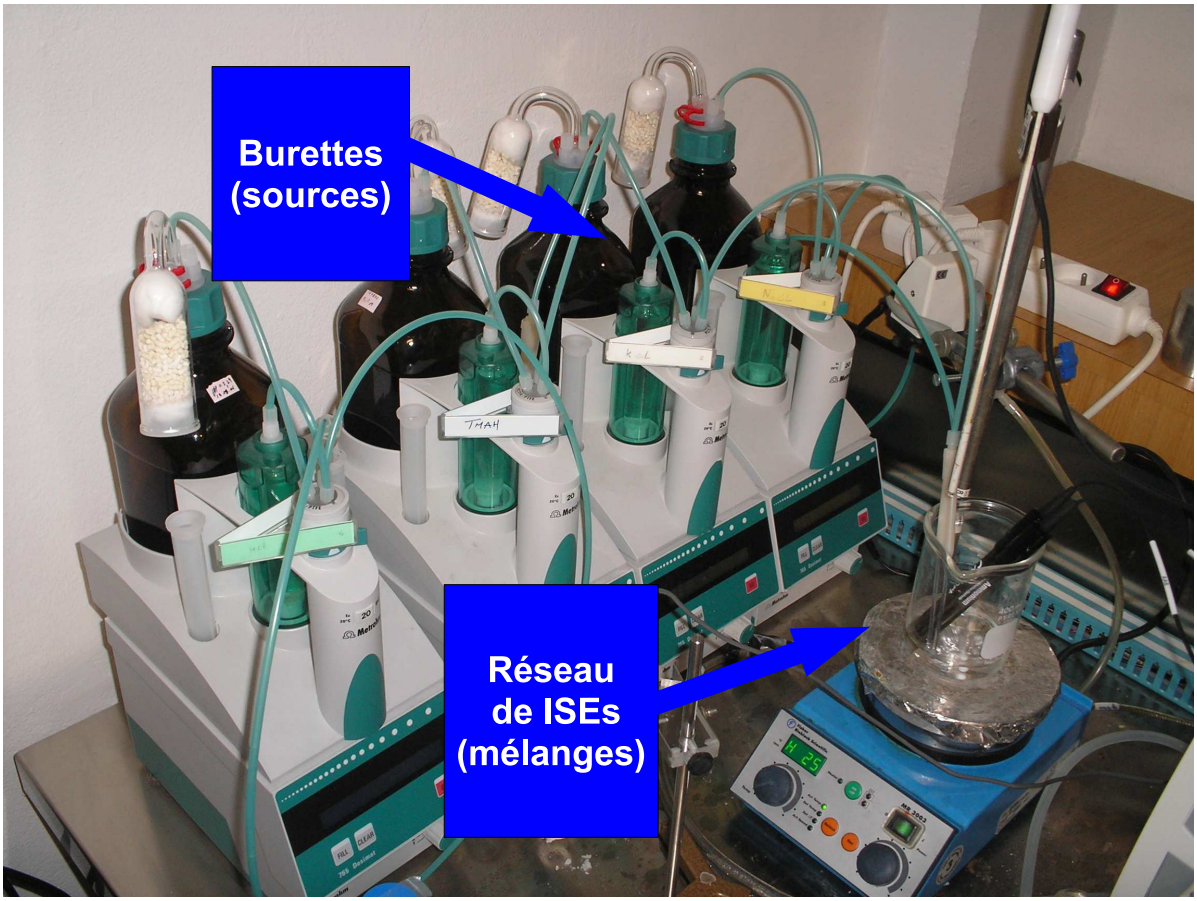


FIGURE 2 – Le dispositif expérimental.

Quant à l'analyse de données, nous avons considéré une approche fondée sur des régressions non-linéaires par moindres carrés. En général, le modèle de NE a fourni des bonnes explications pour les données d'une même expérience. Toutefois, à cause du manque de répétabilité dans les réponses des ISEs, il s'est avéré difficile de modéliser ensemble toutes les expériences d'un même scénario. Curieusement, alors que cette absence de répétabilité pose des problèmes dans un contexte supervisé (il peut en résulter des modèles avec une capacité de généralisation faible), il sert comme un argument pour les approches non supervisé.

D'après notre analyse de données, le scénario 1 a été le plus intéressant pour l'étude des méthodes de SAS. En effet, dans ce cas, nous avons observé un niveau d'interférence important dans les électrodes de potassium et ammonium. Une autre observation importante de notre analyse est que les deux capteurs de sodium utilisés dans le scénario 2 présentaient des réponses très similaires, ce qui rend très difficile, au moins dans ce cas particulier, la conception de méthodes de séparation pour des réseaux composés de

capteurs du même type.

# 3 Méthodes fondées sur l'analyse en composantes indépendantes (ACI)

Une première étape naturelle pour développer des méthodes de SAS est de se concentrer sur les techniques d'analyse en composantes indépendantes (ACI), puisqu'elles fonctionnent avec un minimum d'information préalable : uniquement le fait que les sources sont statistiquement indépendantes. Récemment, quelques résultats dans cette direction ont été rapportés. En particulier, Bedoya [7] a analysé l'application des méthodes d'ACI pour la détection des ions de même valence. Dans cette situation, le modèle de NE devient un cas particulier de la classe de modèles de mélanges post non linéaires (PNL) pour laquelle il existe de nombreuses solutions [8, 9, 10].

Dans cette thèse, nous étudions les méthodes d'ACI pour une situation qui n'a pas encore été abordée, à savoir : des réseaux de ISEs conçus pour analyser des ions de valences différentes. En fonction de la configuration du réseau, ce cas particulier peut engendrer un modèle de mélange assez complexe. Face à cette difficulté, nous avons considéré, dans un premier moment, une version simplifiée du modèle de NE, où les paramètres $d_i$ et $e_i$ sont supposés connus par avance. De plus, nous traitons l'analyse de deux ions (donc deux sources) à partir d'un réseau de deux électrodes, chacun ayant un ion différent comme cible. Dans cette situation, le modèle (1) s'écrit

$$\begin{array}{rcl} x_1 & = & s_1 + a_{12} s_2^k \\ x_2 & = & s_2 + a_{21} s_1^{\frac{1}{k}} \end{array} , \tag{2}$$

où le terme $k$ correspond au rapport des valences $z_1/z_2$ ; nous supposons que $k \in \mathbb{N}$, ce qui est le cas, par exemple, dans le scénario 2 (détection des ions sodium et calcium) de nos expériences.

Une première difficulté dans la conception d'une méthode de séparation pour le modèle (2) concerne le choix d'un système apte à inverser les processus de mélange. En effet, puisque le modèle (2) n'est pas inversible, il s'avère difficile de définir un système d'inversion direct. Afin de surmonter ce problème, nous avons proposé comme système d'inversion la structure récurrente illustrée par la figure 3. L'une des motivations pour un tel choix a été les bons résultats obtenus par des systèmes d'inversion récurrents dans le contexte de mélanges linéaires-quadratiques (LQ) [11, 12].

On peut montrer que, étant donné un échantillon des mélanges $[x_1(T)\ x_2(T)]^T$, l'échantillon des sources qui a généré ces mélanges, $[s_1(T)\ s_2(T)]^T$, est un point fixe du système montré dans la figure 3 lorsque ses paramètres sont égaux aux paramètres du système mélangeant. Autrement dit, la structure récurrente adoptée est capable de procéder à une inversion implicite du processus mélangeant. Évidemment, il devient important dans ce cas de vérifier si le point fixe séparant est stable. Dans ce contexte, nous avons mené une étude de la stabilité locale du système séparant récurrent, ce qui nous a fourni des conditions nécessaires pour le bon fonctionnement de notre méthode.

Quant à adaptation de la structure récurrente adoptée, nous avons considéré, dans un premier temps, une méthode basée sur la décorrelation non linéaire. Cette approche fournit une règle d'apprentissage simple qui ne demande que l'estimation de quelques statistiques d'ordre supérieur. Néanmoins, nous avons

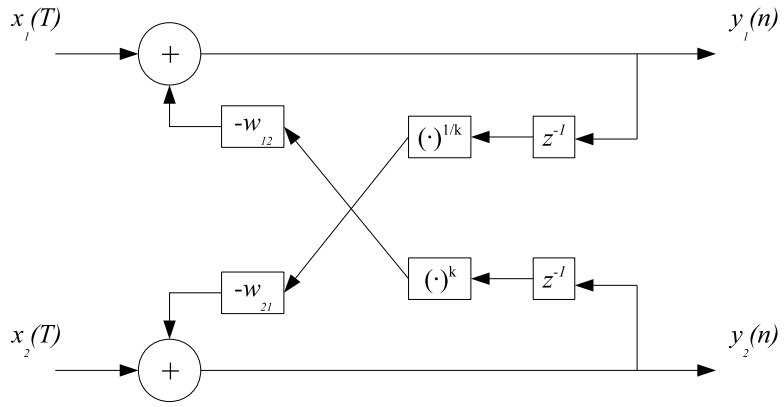


FIGURE 3 – La structure récurrent adoptée comme système separant.

vérifié, à partir d'une étude de stabilité, que la règle d'adaptation obtenue ne peut être appliquée que pour quelques classes de sources. Face à cette difficulté, nous avons considéré d'autres types de méthodes ACI qui sont fondées sur une mesure plus précise d'indépendance : l'information mutuelle.

La dérivation d'un algorithme ACI suivant la minimisation de l'information mutuelle a été effectuée à l'aide du théorème proposé en [13]. Cela nous a permis d'obtenir un algorithme dont l'implémentation est assez simple. Néanmoins, malgré les bons résultats obtenus dans quelques scénarios artificiels, la méthode proposée présente quelques limitations qui ont empêché son application sur des données réelles. D'abord, puisqu'il s'agit d'une méthode ACI, les sources sont supposées indépendantes, ce qui n'a pas été le cas pour les données réelles. De plus, la méthode développée demande un grand nombre d'échantillons pour fournir une bonne estimation des sources.

# 4 Utilisation des informations a priori

À l'origine, l'étude sur la séparation à la source était concentrée sur des situations très générales, où un minimum d'information sur les sources était pris en compte. Dans les méthodes de l'ACI, par exemple, on ne considère que l'hypothèse d'indépendance entre les sources. Néanmoins, plus récemment, il y a une tendance claire vers des méthodes qui prennent en compte des informations supplémentaires. La raison en est simple : dans de nombreux problèmes, les informations supplémentaires apparaissent très naturellement. De plus, en s'appuyant sur ces informations, on peut obtenir une meilleure performance et des algorithmes plus efficaces, et souvent plus simples.

Dans cette thèse, nous avons étudié l'utilisation des informations a priori qui sont souvent disponibles dans l'application traitée. Dans un premier temps (voir paragraphe 4.1), nous avons considéré la même situation décrite dans la section précédent, à savoir : l'analyse d'ions de valences différentes. Ensuite, nous avons considéré l'utilisation des informations a priori pour définir une nouvelle méthode de séparation de mélanges PNL, qui, rappelons-le, sont liés à la détection d'ions de valences égales.

## 4.1 Utilisation d'informations a priori : approche géométrique

Dans la proposition décrite dans la partie 3, nous avons supposé que les paramètres $d_i$ étaient connus par avance. A priori, on pourrait étendre la méthode proposée pour estimer ces paramètres. Cependant, dans ce cas, le risque d'instabilité de la structure récurrente devient important. En outre, la séparabilité du système de mélange n'est pas assurée dans ce cas. Autrement dit, on n'est pas sûr que l'application du principe de l'ACI soit suffisante pour assurer la séparation des sources.

C'est dans le contexte décrit au paragraphe précédent que la prise en compte des informations a priori s'avère intéressante. En effet, en supposant comme hypothèse additionnelle que l'une des sources reste constante pendant un période de temps, nous avons proposé un algorithme pour estimer les paramètres $d_i$ dans une étape qui précède l'application de la méthode décrite dans la partie 3. En bref, l'estimation des paramètres $d_i$ est conduite en prenant en compte les courbes engendrées dans le plan conjoint des signaux pendant la période d'inactivité. Afin d'illustrer la performance de la méthode proposée, nous montrons, dans la figure 4, les sources, les mélanges et les sources estimées par l'algorithme dans un scénario synthétique. Notons que la méthode a réussi à séparer les sources. Cependant, le besoin d'un grand nombre d'échantillons est toujours présent dans ce cas.

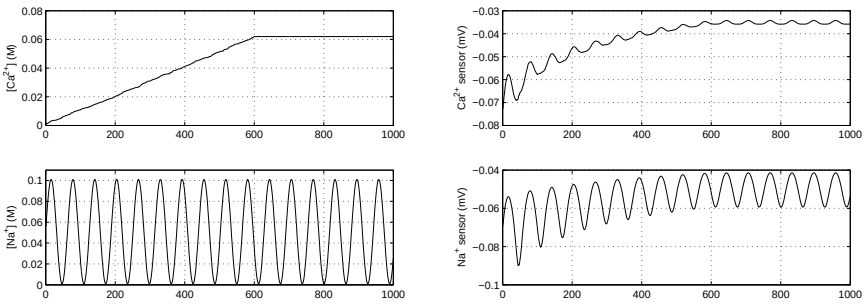


(a) Sources (b) Mélanges

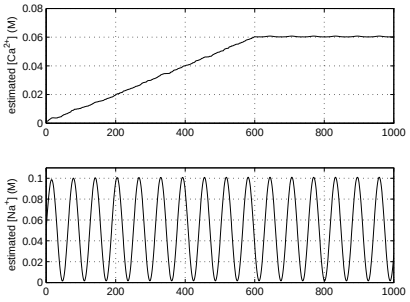


(c) Sources estimées

FIGURE 4 – Application de la méthode géométrique.

## 4.2 Utilisation d'informations a priori : approche fréquentielle

Dans le contexte de mélanges PNL, nous avons proposé une nouvelle méthode en deux étapes, fondée sur l'hypothèse que les sources sont des signaux à bande limitée. Ceci est souvent le cas pour les signaux

chimiques puisqu'ils sont à variation très lente. Compte tenu de cette hypothèse, les signaux issus de la première partie du système mélangeant sont toujours des signaux à bande limitée, puisqu'ils sont des combinaisons linéaires des sources. Néanmoins, à cause de l'étalement spectral introduit par les fonctions non linéaires, les mélanges PNL sont des signaux ayant un spectre plus large que celui des sources.

Afin d'inverser les effets introduits par les fonctions non linéaires de mélanges, nous avons proposé une nouvelle méthode où on ajuste les fonctions non linéaires de séparation de sorte que leurs sorties soient à nouveau des signaux à bande limitée. Ainsi, une fois cette première étape est achevée, on peut utiliser les méthodes de SAS linéaire pour retrouver les sources originelles. L'application de la méthode proposée, qui est illustrée à la figure (5), s'est avérée très efficace dans les scénarios synthétiques et aussi dans le premier scénario de nos expériences.

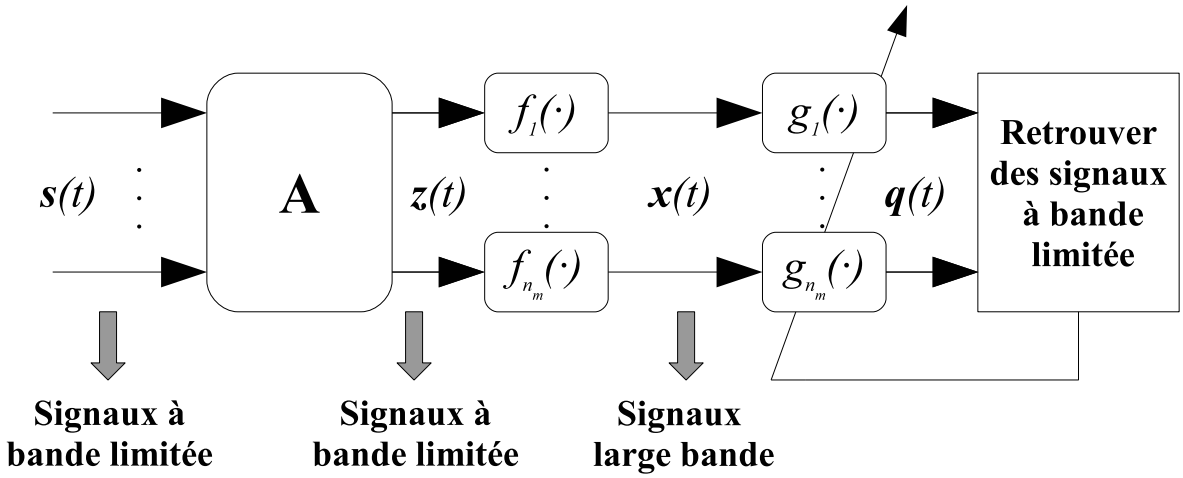


FIGURE 5 – Schéma de séparation de sources à bande limitée dans des mélanges PNL.

## 5 Approche bayésienne

Les méthodes présentées dans la partie précédente utilisent les informations a priori plutôt comme une stratégie pour simplifier le modèle de mélange. Une autre façon de prendre en compte des informations a priori typiques de signaux chimiques peut être obtenue à partir d'une formulation bayésienne, où les informations préalables apparaissent maintenant comme un élément central. L'une des motivations derrière cette approche est liée à certaines informations a priori dont la prise en compte est plus facile dans un cadre probabiliste, comme par exemple la non-négativité des sources [1] ou le caractère bruité des mesures.

Essentiellement, il y a trois étapes dans la formulation d'une méthode bayésienne de séparation de sources [14]. Tout d'abord, il faut définir des lois a priori pour chaque paramètre inconnu. C'est dans cette étape qu'on incorpore les informations disponibles du problème traité. Par exemple, nous avons défini des lois log-normales afin de prendre en compte la non-négativité des sources.

1. Cette information découle du fait que les sources représentent des activités ioniques.

La deuxième étape concerne l'obtention de la loi a posteriori. Pour cela, il faut trouver la fonction de vraisemblance des paramètres inconnus, ce qui dépend du modèle de mélange supposé ainsi que du modèle du bruit. Ensuite, on obtient les expressions de la loi a posteriori en appliquant la règle de Bayes. Enfin, il faut définir un schéma d'inférence des paramètres inconnus à partir de la loi a posteriori trouvée. Par exemple, on peut considérer l'estimateur bayésien avec un coût quadratique. Cependant, dans notre problème, cet estimateur ne peut pas être calculé de façon analytique compte de tenu de la complexité de la loi a posteriori, aussi nous avons considéré des approximations fondées sur les méthodes d'échantillonnage. Plus précisément, cette tâche a été réalisée en employant les méthodes de Monte Carlo par chaînes de Markov (MCMC).

Nous avons évalué la méthode bayésienne proposée avec les données réelles du premier scénario de nos expériences (voir partie 2). Dans la figure 6, nous présentons les réponses fournies par le réseau de capteurs. Notons que le problème d'interférence est évident dans ce cas particulier. Le nombre d'échantillons disponibles était de 170. Dans la figure 7, nous montrons les sources estimées par la méthode bayésienne. Malgré une interférence résiduelle, notamment pour l'électrode de potassium, celle-ci est faible et la méthode a été capable de fournir des bonnes estimations des sources. Cela est corroboré par les rapports signal-sur-interférence obtenus dans ce cas : $RSI_1 = 24$ dB et $RSI_2 = 22,5$ dB. A titre de comparaison, une méthode fondée sur l'ACI [15] a échoué dans l'estimation des sources : $RSI_1 = 7,6$ dB et $RSI_2 = -0,3$ dB. Cette mauvaise performance est due au fait que, dans cette expérience, les sources sont fortement corrélées, ne respectant donc pas l'hypothèse fondamentale de l'ACI.

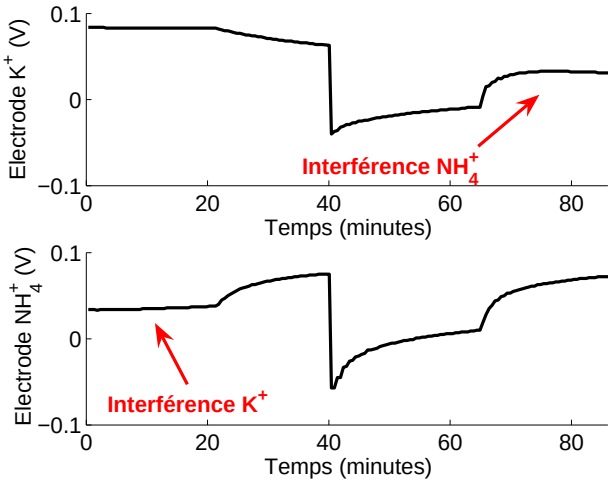


FIGURE 6 – Évaluation de la méthode bayésienne avec les données réelles du premier scénario : les mélanges.

# 6 Conclusions

Le thème central de cette thèse a été le développement de méthodes de séparation sources conçues pour les réseaux de capteurs d'électrodes ioniques sélectives. Le résultat le plus important de la présente

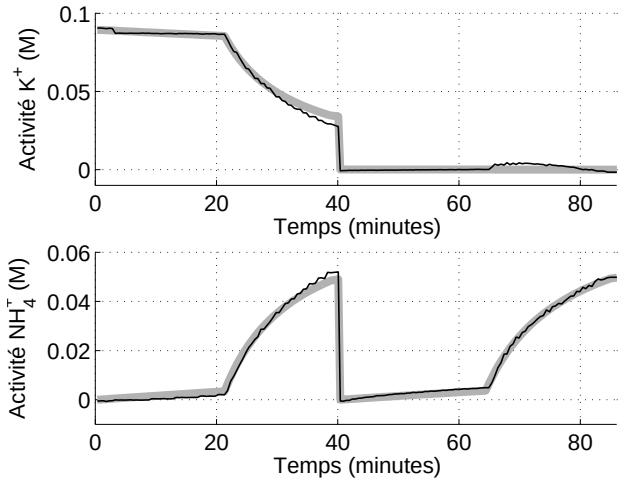


FIGURE 7 – Évaluation de la méthode bayésienne avec les données réelles du premier scénario : les sources (gris) et les sources estimées (noir).

recherche a été obtenu par la méthode bayésienne, qui a été capable de retrouver des bonnes estimations des sources même face à des conditions défavorables (sources corrélées et faible nombre d'échantillons).

Il est à noter que, au meilleur de notre connaissance, ce travail est le premier à rapporter des résultats avec des données réelles, montrant ainsi que l'utilisation de réseaux de capteurs chimiques équipés avec des méthodes de séparation de sources est effectivement viable et peut ouvrir la voie à des nouveaux types de systèmes d'analyse chimique. Toutefois, malgré les résultats encourageants obtenus dans cette recherche, il existe encore de nombreuses questions qui doivent être examinées avant d'envisager l'application industrielle des méthodes proposées.

Tout d'abord, une première question importante qui doit être examinée concerne le nombre de sources. Tout au long de cette thèse, nous avons considéré qu'il n'y avait que deux sources et qu'on disposait de cette information. Toutefois, dans de nombreuses situations pratiques, il peut y avoir beaucoup plus de sources et, de plus, il n'est pas certain que leur nombre exact soit connu.

Un deuxième point intéressant à étudier est liée au processus de mélange sous-jacent au réseau d'électrodes. Dans notre travail, nous avons considéré des modèles de mélange instantané. Toutefois, les capteurs de type ISE présentent un comportement dynamique qui n'est pas négligeable. Compte tenu de cette observation, il pourrait être intéressant de vérifier les bénéfices apportés par une formulation dynamique du modèle de mélange. Enfin, une autre question importante à considérer concerne la conception d'algorithmes plus efficaces. Par exemple, il serait intéressant de développer des méthodes capables d'opérer en temps réel, ou proche du temps réel, notamment dans le cadre bayésien.

# Références

[1] L. T. Duarte. *Design of smart chemical sensor arrays : an approach based on source separation methods.* PhD thesis, Institut Polytechnique de Grenoble, 2009.

[2] P. Comon and C. Jutten, editors. *Séparation de sources 1 : concepts de base et analyse en composantes indépendantes*. Hermès Science Publications, 2007.

[3] A. Hyvärinen, J. Karhunen, and E. Oja. *Independent component analysis*. John Wiley & Sons, 2001.

[4] C. Jutten and J. Karhunen. Advances in blind source separation (BSS) and independent component analysis (ICA) for nonlinear mixtures. *International Journal of Neural Systems*, 14 :267–292, 2004.

[5] P. Fabry and J. Fouletier, editors. *Microcapteurs chimiques et biologiques : application en milieu liquide*. Lavoisier, 2003.

[6] P. Gründler. *Chemical sensors : an introduction for scientists and engineers*. Springer, 2007.

[7] G. Bedoya. *Nonlinear blind signal separation for chemical solid-state sensor arrays*. PhD thesis, Universitat Politecnica de Catalunya, 2006.

[8] M. Babaie-Zadeh. *On blind source separation in convolutive and nonlinear mixtures*. PhD thesis, Institut National Polytechnique de Grenoble, 2002.

[9] S. Achard, D.-T. Pham, and C. Jutten. Criteria based on mutual information minimization for blind source separation in post nonlinear mixtures. *Signal Processing*, 85 :965–974, 2005.

[10] A. Taleb and C. Jutten. Source separation in post-nonlinear mixtures. *IEEE Transactions on Signal Processing*, 47(10) :2807–2820, Oct. 1999.

[11] S. Hosseini and Y. Deville. Blind separation of linear-quadratic mixtures of real sources using a recurrent structure. In *Proceedings of the 7th International Work-conference on Artificial And Natural Neural Networks (IWANN)*, pages 289–296, 2003.

[12] S. Hosseini and Y. Deville. Blind maximum likelihood separation of a linear-quadratic mixture. In *Proceedings of the Fifth International Workshop on Independent Component Analysis and Blind Signal Separation (ICA)*, pages 694–701, 2004.

[13] M. Babaie-Zadeh, C. Jutten, and K. Nayebi. Differential of the mutual information. *IEEE Signal Processing Letters*, 11(1) :48–51, January 2004.

[14] A. Mohammad-Djafari. *Séparation de sources 2 : au dela de l'aveugle, et applications*, chapter Approche bayésienne en séparation de sources, pages 483–517. Hermes Science Publications, 2007.

[15] L. T. Duarte, R. Suyama, R. R. F. Attux, F. J. Von Zuben, and J. M. T. Romano. Blind source separation of post-nonlinear mixtures using evolutionary computation and order statistics. In *Proceedings of the 6th International Workshop on Independent Component Analysis and Signal Separation (ICA)*, 2006.